

Sustainable Aviation

T. Hikmet Karakoc
Emre Özbek *Editors*

Unmanned Aerial Vehicle Design and Technology

 **SARES**
INTERNATIONAL SUSTAINABLE AVIATION
AND ENERGY RESEARCH SOCIETY


 Springer

Sustainable Aviation

Series Editors

T. Hikmet Karakoc , Eskisehir Technical University, Eskisehir, Türkiye

C. Ozgur Colpan , Department of Mechanical Engineering, Dokuz Eylül University, Buca, Izmir, Türkiye

Alper Dalkiran , School of Aviation, Süleyman Demirel University, Isparta, Türkiye

The Sustainable Aviation book series focuses on sustainability in aviation, considering all aspects of the field. The books are developed in partnership with the International Sustainable Aviation Research Society (SARES). They include contributed volumes comprising select contributions to international symposiums and conferences, monographs, and professional books focused on all aspects of sustainable aviation. The series aims at publishing state-of-the-art research and development in areas including, but not limited to:

- Green and renewable energy resources and aviation technologies
- Aircraft engine, control systems, production, storage, efficiency, and planning
- Exploring the potential of integrating renewables within airports
- Sustainable infrastructure development under a changing climate
- Training and awareness facilities with aviation sector and social levels
- Teaching and professional development in renewable energy technologies and sustainability


T. Hikmet Karakoc • Emre Özbek
Editors


Unmanned Aerial Vehicle Design and Technology

 Springer

 **SARES**
INTERNATIONAL SUSTAINABLE AVIATION
AND ENERGY RESEARCH SOCIETY

Editors

T. Hikmet Karakoc 
Faculty of Aeronautics and Astronautics
Eskisehir Technical University
Eskisehir, Türkiye

Emre Özbek 
UAV Technology and Operatorship Program
Eskisehir Technical University
Eskisehir, Türkiye

Information Technology Research
and Application Center
Istanbul Ticaret University
Istanbul, Türkiye

ISSN 2730-7778

ISSN 2730-7786 (electronic)

Sustainable Aviation

ISBN 978-3-031-45320-5

ISBN 978-3-031-45321-2 (eBook)

<https://doi.org/10.1007/978-3-031-45321-2>

© The Editor(s) (if applicable) and The Author(s), under exclusive license to Springer Nature Switzerland AG 2024

This work is subject to copyright. All rights are solely and exclusively licensed by the Publisher, whether the whole or part of the material is concerned, specifically the rights of translation, reprinting, reuse of illustrations, recitation, broadcasting, reproduction on microfilms or in any other physical way, and transmission or information storage and retrieval, electronic adaptation, computer software, or by similar or dissimilar methodology now known or hereafter developed.

The use of general descriptive names, registered names, trademarks, service marks, etc. in this publication does not imply, even in the absence of a specific statement, that such names are exempt from the relevant protective laws and regulations and therefore free for general use.

The publisher, the authors, and the editors are safe to assume that the advice and information in this book are believed to be true and accurate at the date of publication. Neither the publisher nor the authors or the editors give a warranty, expressed or implied, with respect to the material contained herein or for any errors or omissions that may have been made. The publisher remains neutral with regard to jurisdictional claims in published maps and institutional affiliations.

This Springer imprint is published by the registered company Springer Nature Switzerland AG
The registered company address is: Gewerbestrasse 11, 6330 Cham, Switzerland

Paper in this product is recyclable.

Preface

The field of unmanned aerial systems (UAS) has rapidly evolved in recent years, becoming a trending research topic across the globe. The increasing availability of electronic components and low project costs have made UAS platforms more popular than ever before, and they are being applied in diverse areas of civil life and military operations. As such, the need for a comprehensive guide to UAS system design, components, control, operations, and regulations has become paramount.

This book, titled *Unmanned Aerial Vehicle Design and Technology*, aims to fill this gap by providing readers with a well-rounded and detailed index of the technology. The book is intended for a wide range of audiences, including researchers, aero/mech engineering students, hobby enthusiasts, and civil aviation organization officials.

The book covers a range of topics, from the basics of UAS technology to the most advanced concepts and applications. Readers will gain valuable insights into UAS system design, including the various components that make up a UAS, their control systems, and their operational capabilities.

The book is the result of extensive research and collaboration among a group of experts in the field of UAS technology. Their collective expertise and insights are reflected in the various chapters of the book. We are confident that this book will prove to be a valuable resource for anyone seeking to gain a comprehensive understanding of UAS technology and its various applications.

We hope that this book will inspire new ideas and innovations in the field of UAS technology, and that it will contribute to the continued evolution and growth of this exciting field.

We would like to thank Springer's editorial team for their support towards the preparation of this book and the chapter authors and reviewers for their outstanding efforts.

Eskisehir, Türkiye

T. Hikmet Karakoc
Emre Özbek

Contents

1	A Review on Trending Topics on the Civilian Drones in the Second Century of Aviation: Current Status, Challenges, and Research Opportunities	1
	T. Hikmet Karakoc and Emre Özbek	
2	Systems Engineering Approach on UAS Design	15
	Emre Özbek, Selcuk Ekici, and T. Hikmet Karakoc	
3	Aerodynamic Analysis of Short Landing Solar-Powered UAV for Environmental Monitoring Applications	31
	Chinnapat Thipyopas and Nattapong Warin	
4	Onboard Trajectory Coordination of Multiple Unmanned Air Vehicles	53
	James Sease, Stephen Warwick, and Afzal Suleman	
5	Applications of Drones in the Health Industry	69
	Kursat Alp Yigit, Alper Dalkiran, and T. Hikmet Karakoc	
6	An Evaluation of the Current Status and Trends in All Electric Urban Air Mobility UAVs	95
	Emre Özbek, Alper Dalkiran, Evren Yilmaz Yakin, Selcuk Ekici, and T. Hikmet Karakoc	
7	Aerodynamic Shape Optimization and the Effect of Morphing Winglet-Induced Tip Vortex Structure on the UAS-S45	111
	Musavir Bashir, Simon Longtin-Martel, Ruxandra Mihaela Botez, and Tony Wong	
8	Observer-based Feedback Linearization Control of a Quadrotor Subjected to Sensor Noise	135
	Ahmet Ermeýdan and Aziz Kaba	

9 An Evaluation on Landing Gear Configurations of Fixed-Wing, Rotary-Wing, and Hybrid UAVs 153
Emre Özbek, Selcuk Ekici, and T. Hikmet Karakoc

10 Non-linear System Identification for UAS Adaptive Control 167
Sean Bazzocchi and Afzal Suleman

11 Use of Unmanned Aerial Vehicles for Imaging and Remote Sensing 179
Alpaslan Durmuş and Erol Duymaz

Index 193

About the Editors

T. Hikmet Karakoc Ph.D., graduated from the Department of Mechanical Engineering, Anadolu University. He received his M.Sc. degree in Mechanical Engineering from the Yildiz Technical University. He received his Ph.D. from Anadolu University, where he started his full-time teaching and received his Full Professorship. He is currently researching at the Eskisehir Technical University. He has a wide range of research interests, including sustainable aviation, aircraft propulsion systems, insulation, heating, ventilating, and air conditioning (HVAC), indoor air quality, gas turbines, cogeneration systems, renewable energy, energy economics, fuels, and combustion. He has participated in numerous industrial projects on these topics as a researcher, consultant, and project manager for over 30 projects and corporations. He also started a contest on special insulation applications among university students. He served as an Editor-in-Chief, guest editor, and editorial board member for international scientific journals. He published national and international papers in over 300 journals and 40 books. Professor Karakoc actively follows membership positions for the Chamber of Mechanical Engineers and many sectorial associations, international scientific organizations, and societies. He is an active Board of Directors member of the International Association for Green Energy. He is currently holding the presidency of the SARES organization, which is actively supporting scientists and students in the area of sustainable aviation. He also organizes four symposiums on aviation subject areas as a Founding Chair.

Emre Özbek Ph.D., is a distinguished Full Lecturer in the Unmanned Aircraft Technology and Operations Program at Eskisehir Technical University. He holds an M.Sc. and B.Sc. in Aircraft Airframe and Powerplant Maintenance from the same institution and has recently completed his Ph.D. His doctoral research focused on the design and successful flight of a Rear Spar Articulated Morphing Wing UAV, a pioneering fixed-wing UAV operating without controlled surfaces. Dr. Özbek's expertise extends to the design of various electrical unmanned aerial vehicles (UAVs) for international competitions and projects, spanning both fixed and rotary wing categories. He has led the Anatolia Aero Design UAV design team at Eskisehir

Technical University for seven years, serving as team captain and chief designer. In addition to his academic pursuits, he has applied his knowledge in the industry as an aircraft engineer. He has worked remotely with Dronee, contributing to the design of vertical take-off and landing UAVs for aerial mapping. Before this, he was the chief aircraft designer of multirotor UAVs at Huma Technology. His research interests are broad and innovative, encompassing UAV design, manufacturing, structural analysis, RANS aircraft analysis, and low fidelity analysis methods such as 3D panels and vortex-lattice method. He is also deeply interested in UAV autonomous flight, alternative energy sources, fuel cell technology, sustainability in aviation, and additive manufacturing methods. His contributions to the field have been recognized with two patents, further establishing his position as a leader in UAV technology and design.

Chapter 1

A Review on Trending Topics on the Civilian Drones in the Second Century of Aviation: Current Status, Challenges, and Research Opportunities



T. Hikmet Karakoc  and Emre Özbek 

Acronyms

UAV Unmanned aerial vehicle
UAS Unmanned aerial system
VTOL Vertical take-off and landing

1.1 Introduction

Unmanned aerial vehicles have been a current research topic for the last two decades. Today, we can easily say that this sector continues to experience a boom in scientific research and technological development (Tiwari and Dixit 2015). The development of microelectromechanical units, frequently used in unmanned aerial vehicles, developments in propulsion systems such as batteries and electric motors, and developments in production technologies such as three-dimensional (3D) printing methods have been the fuel of progress in the unmanned aerial vehicle sector. At the end of this process, unmanned aerial vehicles became accessible and usable to many

T. H. Karakoc
Faculty of Aeronautics and Astronautics, Eskisehir Technical University, Eskisehir, Türkiye
Information Technology Research and Application Center, Istanbul Ticaret University, Istanbul,
Türkiye
e-mail: hkarakoc@eskisehir.edu.tr; thkarakoc@ticaret.edu.tr

E. Özbek (✉)
UAV Technology and Operatorship Program, Eskisehir Technical University, Eskisehir,
Türkiye
e-mail: emreozbek@eskisehir.edu.tr

researchers or individuals. Today, an unmanned aerial vehicle can be easily obtained and flown thanks to the developed control systems.

Many missions carried out by manned aircraft in the past are now being performed by unmanned aerial vehicles (DeGarmo and Nelson 2004). In manned operations, costs are higher, and human factors such as fatigue and stress can cause operational problems (Venus 2021). The fact that unmanned aerial vehicles can perform repetitive or prolonged tasks at a meager cost without any loss of performance has ensured their integration into many sectors (Yinka-Banjo and Ajayi 2019). Unmanned aerial vehicles are now involved in processes in many areas, especially in areas such as agriculture, mining, public works investigations, forest fires, filming, and mapping.

The first century of aviation began with the Wright brothers' flight. Within the developments during the first century, our primary focus as humanity was to keep aircraft airworthy. At the end of the first century, an aviation industry with a low accident rate and social acceptance was established, which completed all flight phases, especially take-off, flight, and landing, without any problems.

In the second century of aviation, our primary focus is now sustainability. In addition to its benefits, such as globalization and time savings, aviation creates undesirable outputs, such as greenhouse gas emissions and noise emissions (Niedzielski et al. 2021). Topics such as increasing the aerodynamic efficiency of aircraft designs, using alternative fuel sources, developing green engine concepts, and increasing electric usage, reducing fossil fuel usage are the changes researchers and industry want to establish in the aircraft industry. So, the second century of aviation focuses on making our existing fleets of aircraft more sustainable with improvements in several disciplines.

On the other hand, the Unmanned aerial vehicle (UAV) industry started this new century of aviation with considerable increases in the number of civil unmanned aerial vehicles (Chang 2015). Before the 2000s, the unmanned aerial vehicle industry was mainly composed of unmanned aerial vehicles used for military purposes, but today, the amount of civilian unmanned aerial vehicles is quite dominant.

The unmanned aerial vehicle sector continues to grow, especially with the driving force of the civil services sector. UAVs have been integrated into many sectors with their low cost and advantages. While some roles were previously played by manned aircraft, some were created by drones. Nowadays, integration with different sectors is constantly developing, and new use areas can be derived almost daily.

1.2 An Overlook of the Civilian UAV Industry

Today, unmanned aerial vehicles are the least costly option to raise a camera to a certain altitude. As a result of this cost advantage, it is possible to identify more than 100 areas of use for civil unmanned aerial vehicles in various industries. In this section, some usage areas will be presented in detail. These detailed usage areas have been selected according to their market volumes. The selection basis was Business

Insider's "Commercial Unmanned Aerial Vehicle (UAV) Market Analysis – Industry Trends, Forecasts and Companies" report (Business Insider 2022).

1.2.1 Agricultural UAVs

It would be best if we start by asking the question What is an agricultural UAV? Agricultural UAV is the name given to UAVs used in any mission in the field of agriculture. UAVs are often referred to the mission for which they are customized in this way.

The most used task of agricultural UAVs is the spraying of crops against agricultural pests. So why prefer spraying pesticides with agricultural UAVs? Spraying with unmanned aerial vehicles reduces the amount of pesticides used. Minimizing pesticide usage is vital for cost minimization and prevention of ecological and environmental damage. Precision agriculture is an important concept that includes the targeted use of resources; in this perspective, the role of unmanned aerial vehicles is crucial (Velusamy et al. 2021).

Land vehicles or manned spraying aircraft are used in pesticide spraying as conventional methods. Airplanes are costly, and farmers have difficulty accessing this service. For this reason, pesticides are applied in the fields with tractor-like vehicles. But making way for these vehicles in areas where farmers can plant their crops that will make money is a process that reduces the productivity of their fields. UAVs do not need such roads and do not harm cultivated crops.

Assessment of water stress is another agricultural task that UAVs perform. Separating the yellowed areas that indicate irrigation problems from the green areas in densely planted fields can be easily achieved with aerial images. This work can be done with image processing techniques, or a user can manually achieve the process through quality photos. Carrying out these inspections in the fields provides the opportunity to detect irrigation problems early and intervene before the crops deteriorate (del Cerro et al. 2021). Similarly, crop diseases and the nutrition status of the crops can also be monitored using UAVs (Hafeez et al. 2022).

Yield estimation is another agricultural mission accomplished by agricultural UAVs. Thanks to these techniques, farmers can learn the number of plants cultivated in the field (Duan et al. 2021). The estimation of yield expected after the harvest and the returns that will be obtained can be modeled. These tasks make it easier for farmers to manage their economic situation, including the storage demands and crop insurance policies (Xu et al. 2021). At the same time, yield estimation can be seen as an analysis of the effect of techniques applied to the crops.

1.2.2 *Infrastructure UAVs*

Getting a camera to a specific altitude cost efficiently developed a sector for structures that must be inspected at certain times. Tasks in the infrastructure header are generally inspection and monitoring-based tasks. While these tasks can be performed routinely, needs such as inspection of damage arise after natural disasters.

Checking the integrity of train tracks or railroads from time to time is an essential task for freight and passenger transportation. Especially situations such as landslides cause problems that can result in accidents and breakdowns of trains. Image processing methods are often sufficient to carry out inspections in this area. Machine learning techniques are also integrated into unmanned aerial systems to make the analysis more accurate (Saini et al. 2022).

Inspection of highways can be carried out similarly with unmanned aerial systems. Since these areas are sparse, especially in terms of people and structures, it is possible to make navigation and examination in these areas. Landslides on highways, asphalt deterioration, and wreck inspection after accidents can be carried out with unmanned air systems. Using machine learning techniques, examinations are carried out on the images obtained, and cracks formed on the highways can be examined (Moon and Lee 2022).

Pipeline and power line inspections, another area of infrastructure, are another key driver of this task group. Providing energy for cities and industrial zones continuously is essential in terms of quality of life and economic life. Controls of power lines can be carried out both routinely and after disasters. Unmanned systems also provide significant cost advantages in this area when compared to manned systems. In pipeline control, leak investigations can be carried out using infrared cameras. In industries such as oil and gas pipelines, situations that can create considerable costs in an outage are monitored at low cost by unmanned aerial vehicles (Alharam et al. 2020).

There are also various inspection areas on renewable energy. In solar power plants, the panels' temperatures must be equal to each other. Thermal images obtained by unmanned aerial vehicles are of great importance for the detection of panels that do not work or cause problems. Identification of malfunctioning of solar panels with thermographic images increases the efficiency of solar power plants (Higuchi and Babasaki 2018). In wind turbines, fatigue and stress cracks may occur, primarily due to dynamic loads. Periodic examination of these cracks and taking precautions are essential for these facilities. It is crucial to detect these problems accurately, especially since the organization of maintenance operations in offshore turbines is very costly. Image analysis is performed using deep learning-supported systems on wind turbine blades, and discontinuities on the surface can be detected (Shihavuddin et al. 2019).

Inspecting the discontinuities on the surface of essential structures constitutes another sector. Using unmanned aerial systems, the legs and decks of vital structures such as bridges and viaducts can be examined. Also, inspections are carried out

using unmanned aerial systems in important infrastructure areas, such as the outer walls of offshore oil rigs and liquefied natural gas tanks (Sudevan et al. 2018).

1.2.3 Transport UAVs

Unmanned aerial vehicles have begun to occupy an important area in freight transportation. The importance of an unmanned cargo delivery system has been seen in processes such as minimizing human interaction and quarantine, especially in the Covid-19 pandemic that peaked between 2019 and 2021.

Many companies are working on delivering the cargo they receive from a center with unmanned aerial vehicles to the end user. In this regard, cargo up to 2.3 kg can be transported with the Amazon Prime Air drone delivery program (Chalupníčková et al. 2014). Deutsch Post (DHL) is also working on delivering the cargo to the last parcel with its Parcelcopter project (Chitta and Jain 2017). Drone station designs also come to the fore to realize this type of cargo delivery.

The transportation of humanitarian aid and health-related materials also stands out as one of the areas where unmanned aerial vehicles are integrated. Unmanned aerial vehicles come to the fore, especially in rural areas or regions where land transportation is difficult seasonally, for rapid transportation of medicines, serum, blood units, test results, and vaccines. Drone medical delivery by Zipline company in Rwanda has been one of the leading applications in this regard (Ackerman and Koziol 2019). Unmanned aerial vehicles have started to offer a reliable and cost-effective option for important missions involving a race against time, such as organ transplantation (Scalea et al. 2019).

Through its Wing drones, Alphabet uses delivery drones to provide innovative services. They have tested a system to conveniently transport coffee and food in Australian districts (Roca-Riu and Menendez 2019). The ability to distribute daily necessities such as food and beverage with unmanned aerial vehicles within the automation framework will support human interaction and approaches that reduce costs.

Transporting people also comes to the forefront as another task to be done in the future with unmanned aerial vehicles. In this research area, known as urban air mobility, autonomous vehicles carry people as cargo but perform their duties between various stations. China's EHang company is developing this type of autonomous unmanned aerial vehicle (Gunady et al. 2022). These vehicles can also be defined as air taxis or electric vertical take-off and landing (eVTOL) vehicles. eVTOL defines these vehicles with a combination of electric and vertical take-off and landing features.

1.2.4 Security UAVs

In addition to their use in homeland security and country defense, unmanned aerial vehicles are also used in law enforcement or individual security applications. Facility perimeter control is a popular option among users for this purpose. As a safety and security measure, unmanned aerial vehicles are used around factories, important facilities, and warehouses. In addition to the cameras fixed at a certain point, the blind spots that may occur can be monitored with drones, thus increasing the facility's safety (Teixidó et al. 2021).

Traffic surveillance is used for the identification of vehicles around facilities, campuses, and extensive infrastructure. Detection and tracking of foreign vehicles can be performed using UAVs. These applications are essential for increasing the security of a region. Also, traffic monitoring is used by law enforcement to assess driver behavior and speed limit obedience in many countries.

Border patrol and customs in many countries, including the United States and European Union, also started employing UAVs. Illegal immigration is one of the biggest problems of our time. Illegal immigrants bring mostly smuggled drugs, weapons, and valuable products into countries without going through customs. This situation causes significant problems in terms of public health and safety (Kosłowski and Schulzke 2018).

In terms of the security of homes and gardens, individual consumers have started creating demand for security systems using unmanned aerial vehicles. With the integration of UAVs into conventional processes such as guards, safety cameras, and vibration sensors, real-time information and safety can be provided with higher reliability. A surveillance drone can perform sensing, analyzing, and control in these integrated internet-of-things-based security systems (Deebak and Al-Turjman 2020).

1.2.5 Media and Entertainment UAVs

The low cost of unmanned aerial vehicles has enabled the inclusion of aerial shooting scenes in many movies and TV shows. In the past, scenes such as the vehicle chase scenes we saw in movies were shot with helicopters. However, these were quite costly shots. Today, there is little need for helicopters anymore. Many scenes can be shot with drones. In the radio and television industry, large equipment was transported, set up for the set, and then filmed in order to shoot scenes with cameras moving on a rail. Now it is possible to perform these only with the maneuvers of an unmanned aerial vehicle.

One of the UAVs used for entertainment purposes is light shows. Hundreds of unmanned aerial vehicles performing light shows together became a special show that started to take its place in important events (Waibel et al. 2017). Unmanned aerial vehicles that perform these light shows autonomously have begun to replace night-time events such as fireworks displays.

Drone racing is emerging as another source of entertainment with unmanned aerial vehicles. First-person view pilot goggles are used on these flights, providing pilots with a smooth experience as if they were playing a computer game. Maneuvers are carried out on various tracks using the agile maneuvers of multicopter vehicles, aiming to complete the track in a short time. National and international tournaments and leagues began to be organized in the field of drone racing (Standaert 2021). This led to the creation of a large hobby industry.

1.2.6 A Master List for Civilian Usage of UAVs

The list of civilian jobs using drones is based on the authors' experience and their knowledge from various sources. Here, tasks in various sectors with unmanned aerial vehicles are listed in Table 1.1.

1.3 Current Bottlenecks and Challenges of the Civilian UAV Industry

Although unmanned aerial vehicles are already integrated into many sectors, as assessed in the previous section, some problems prevent them from appearing in more sectors and creating bottlenecks for the industry. Endurance, noise, navigation, insurance, technical education inadequacy, and harsh regulations are pointed out as bottlenecks in this section.

1.3.1 Endurance Problem

Airtime or endurance, considered among the technical performance criteria in unmanned aerial vehicle design, limits the effects of multirotor-type electric unmanned aerial vehicles. Most of the areas of use of unmanned aerial vehicles presented in the second part are carried out with multirotor-type unmanned aerial vehicles due to ease of piloting, maneuverability, and cost. In these vehicles, the use of electric motors is almost restricted due to their response time requirements for control.

The motors used in multirotor unmanned aerial vehicles are generally brushless direct current (BLDC) motor-type electric motors combined with lithium ion polymer (LiPo) batteries (Borikar et al. 2022). In addition to LiPo batteries, Li-Ion batteries are also used in unmanned aerial vehicles. However, the main problem of both lithium-based electrochemistry is their low energy density compared to fuels.

Table 1.1 Civilian use cases for drones master list

A master list of civilian use cases for drones	
3D Building Mapping	Advertising
Aerial Photography	Agr. Disease Identification
Agr. Spraying	Agr. Yield Monitoring
Air Quality Monitoring	Airline Aircraft Inspection
Ambulance Drone	Analysis of Wildlife Damage
Airport Bird Chasing	Archeological Field Exploration
Construction Site Monitoring	Disaster Relief
Drone Flight Training	Drone Racing
Emission Inspection	Erosion Inspections on Riverbeds
Event Filming	Fertilization Monitoring
Irrigation Monitoring	Filmmaking
Fire Extinguishing	Fire Monitoring
Forest Health Monitoring	Gas Pipe Inspection
Glacier Monitoring	Healthcare
Herd Control	Hotel Promotion Filming
Human Transport	Humanitarian Aid Delivery
Indoor Modelling for Museums	Industrial Jet Wash
Infrastructure Building	Insurance Inspections
Journalism	Land Vehicle Promotion Filming
Landfill Management	Light Shows
Magnetic Mapping	Marine Conservation
Maritime Emission Control	Maritime Operations
Meteorological Survey	Mineral Exploration
Mining Site Security Inspections	Morphological Inspections
Nature Conservation	Offshore Platform Inspection
Online Food Delivery	Parcel Package Delivery
Pipelines Inspection	Power Line Cleaning/Firethrowing
Power Lines Inspection	Radiation Detection
Railroad Inspections	Reforestation Planning
Real Estate Advertising	Retail Cargo Delivery
Road Inspection	Rooftop Inspection
Search and Rescue	Site Surveillance
Soil Assessment	Solar Panel Monitoring
Space Applications	Thermal Insulation Inspection
Telecommunications Relay	Topographical Survey
Traffic Monitoring	Urban Planning
Volcano Inspection	Warehouse Operations
Waste Management	WiFi Hotspot
Wildfire Detection	Wildlife Monitoring
Wind Turbine Inspection	Yacht Promotion Filming

More endurance is advantageous for the user in every task that can be done with unmanned aerial vehicles. If the battery is replaced after landing, the task can be continued if there is a full-state spare battery. However, if there is only one battery, the charge cycles increase the task's duration. It is crucial to perform the task without landing, especially in tasks such as surveillance and monitoring.

1.3.2 Noise Problem

The noise of unmanned aerial vehicles poses problems, especially in multirotor or multirotor hybrid vehicles. Even the lightest classes of unmanned aerial vehicles can cause noises above 90 decibels that might permanently damage the eardrum (Miljković 2018). The effects of unmanned aerial vehicles on the health of people and the stress of pets in their missions in the city are serious research topics. In addition, the effects on the stress of farm animals in farming areas should be investigated.

The current noise emissions of unmanned aerial vehicles cause problems in social acceptance (Eißfeldt 2020). For them to be more integrated into daily life, it is necessary to go down to lower decibel amounts. With the reduction of noise emissions, the fields for unmanned aerial vehicles in indoor missions will expand.

1.3.3 Mid-Air Collision and Navigation Problems

The ability of unmanned aerial vehicles to perform risk-free navigation in areas where there are too many obstacles in the city will enable them to become widespread in these missions. Today, with the development of sensor systems, great progress has been made in obstacle detection and avoidance. However, the problems with obstacles such as electrical wires or nets or the risks of collision with other drones in the air have not been minimized.

The development and spread of concepts such as urban air mobility will be possible by overcoming this bottleneck. Increasing environmental awareness of unmanned aerial vehicles will make their flights safer. The creation of three-dimensional models and maps of cities, as well as satellite-based navigation systems, may allow an important step forward. The use of 5G lines will provide significant advantages for unmanned aerial vehicles to communicate with each other and with other aircraft (Xue et al. 2020).

1.3.4 Insurance Problems

Third-party damages that may occur while performing commercial missions with unmanned aerial vehicles are generally the responsibility of the pilot and operator. The laws may differ according to the civil aviation regulations to which the countries are subject. However, while there are insurance policies for the damages we can give to someone else, there is not a sufficient service sector to find an insurance policy for the damage we can cause to our own drone.

Kwon and Cheung published a recent study on this subject that identifies the industry's situation (Kwon and Cheung 2022). However, the sector needs more experts and researchers who will work in a multidisciplinary manner on the necessary factors and technical information in order to carry out risk analysis.

Not having an insurance policy for the damages they may cause to their own unmanned aerial vehicle poses a significant obstacle, especially for entrepreneurs. The loss of unmanned aerial vehicles as a result of hardware problems or piloting errors that entrepreneurs who set up their businesses with mostly financial loans and investments can put them out of service. The existence of these hesitations slows the growth of the civil drone industry. As more entrepreneurs in more countries access these policies and operate safely, the industry will grow faster.

1.3.5 Technical Education Requirement

Organizations that provide piloting and operator training on unmanned aerial vehicles have become widespread. However, organizations that provide technical support and repair in case of malfunctions are generally electronic maintenance organizations that have the approval of unmanned aerial vehicle companies.

Increasing the technical literacy of individual users is essential for developing the drone industry. Creating more resources on this subject and starting to give associate degree technician training will accelerate the development.

In addition to repairing off-the-shelf unmanned aerial vehicles, the ability of the users to perform the payload conversion among the tasks of the unmanned aerial vehicles that can be customized for some missions will add flexibility to the service industry.

1.4 Research Trends Topics for Civilian UAVs

Trending research topics often address the bottlenecks outlined in the previous section. These are the issues that researchers and industrial stakeholders attach importance to. Hybrid powertrains occupy an important place among these trending topics addressing the endurance problem. Alternative fuel solutions such as fuel cell

batteries and solar panel batteries are applied to unmanned aerial vehicles to increase flight times (Bahari et al. 2022). Ultracapacitors are also integrated into these powertrains (Sagaria et al. 2021). In addition to alternative energy hybrid systems, there are also multirotor systems carrying a generator and gasoline tank (Nurrohaman et al. 2019).

Wireless charging techniques are also being tried to be applied to unmanned aerial vehicles. The laser beaming technique is used in a variety of military missions. It is realized by sending a concentrated and continuous light beam to the photovoltaic surface placed under it to extend unmanned aerial vehicles' flight time (Chittoor et al. 2021).

Fixed-wing unmanned aerial vehicles have higher airtime compared to multirotors. They gain this advantage thanks to reciprocating engines and their long wings. However, the fact that they need an area for take-off and landing creates operational inefficiency. Hybrid VTOL systems can perform vertical take-off and landing with electric motors, while internal combustion engines can provide the thrust in horizontal flight. This type of system is one of the solutions that increase endurance. Platforms called tail-sitter unmanned aerial vehicles are more efficient systems that can land and take off on their tails. The control architecture of these systems is more complex, but they can perform efficient and long flights. Hybridization methods and vertical landing and take-off capability to fixed-wing unmanned aerial vehicles remain important research topics (Saeed et al. 2018).

Tethered unmanned systems are connected to the ground station with a cable, and power and data are transferred with this cable called the tether (Belmekki and Alouini 2020). Tether provides an unlimited flight time, in theory. However, the main problem with this type of unmanned aerial vehicle is that it cannot get too far from the ground station. However, using such UAVs in surveillance-based missions such as border security and coastguarding constitutes a current research topic.

The use of passive and active noise reduction techniques and the development of new techniques have an important place in reducing noise emissions. Propellers in unmanned aerial vehicles are the most significant contributor to noise emissions. Passive methods, such as using ducted fans, can reduce noise emissions. Active methods can be advanced with the use of technologies such as magnetically excited blades. Also, combining passive and active noise reduction methods to achieve more significant noise reduction may be feasible (Miljković 2018).

Fail-safe and adaptive fail-tolerant control approaches are vital for the performance of a safe mission. Fault-adaptive architectures, such as detecting sensor errors or misreadings with other sensors, and maintaining the operation by disabling the faulty sensor are valuable research topics (Abbaspour et al. 2018). Models and experimental studies in this area are very important for the safe use of unmanned aerial vehicles in residential areas.

Bio-inspired systems and component designs are approaches that increase the efficiency and capacity of unmanned aerial vehicles. Morphing wing technology aims to make the wings of fixed-wing unmanned aerial vehicles or helicopters more efficient by actively changing their shape, just like the wings of birds (Min et al.

2010). With the morphing wing technology, the wing areas, camber ratios, thickness distributions, and aspect ratios of the wings can be changed during the flight.

Gesture control is another trending technology that enables unmanned aerial vehicles to coordinate with hand movements without requiring control. It can be thought that it can be useful for entertainment and educational purposes. They can also be used as guide units to support the indoor navigation of disadvantaged individuals, such as visually impaired individuals (Al Zayer et al. 2016).

Cyber security is another important area for unmanned aerial vehicles. Hijacking and hacking pose vital concerns for drone users (Hartmann and Giles 2016). In these cases, unsafe situations may occur in which unmanned aerial vehicles are involved. The cryptography of the data link of the unmanned aerial vehicle with the ground station has an important place in the prevention efforts. It may also be effective to limit personal use of the ground station computer or tablet used in an unmanned aerial vehicle to protect against situations such as hacking of the ground station.

Counter-drone measures have become a concern with the growth of the unmanned aerial vehicle industry. The widespread use of unmanned aerial vehicles also allows for malicious use. Measures such as signal spoofing have begun to be taken for airspaces to be protected from unmanned aerial vehicles (Ferreira et al. 2022). The development and testing of new counter-drone measures are trending research topics.

Air traffic integration of UAVs is an issue that aviation authorities are actively working on. With studies in this area, authorities try to determine unmanned aerial vehicles' flight zones and control them without overloading the air traffic management systems. Modeling and simulation studies have an important place in integrating unmanned aerial vehicles into air traffic (Zhao et al. 2019).

References

- Abbaspour A, Yen KK, Forouzaneshad P, Sargolzaei A (2018) A neural adaptive approach for active fault-tolerant control design in UAV. *IEEE Trans Syst Man Cyber Syst* 50(9):3401–3411
- Ackerman E, Koziol M (2019) The blood is here: Zipline's medical delivery drones are changing the game in Rwanda. *IEEE Spectr* 56(5):24–31
- Al Zayer M, Tregillus S, Bhandari J, Feil-Seifer D, Folmer E (2016) Exploring the use of a drone to guide blind runners. In: *Proceedings of the 18th international ACM SIGACCESS conference on computers and accessibility*. ACM, pp 263–264
- Alharam A, Almansoori E, Elmadeny W, Alnoiami H (2020) Real time AI-based pipeline inspection using drone for oil and gas industries in Bahrain. In: *2020 international conference on innovation and intelligence for informatics, computing and technologies (3ICT)*. IEEE, pp 1–5
- Bahari M, Rostami M, Entezari A, Ghahremani S, Etminan M (2022) Performance evaluation and multi-objective optimization of a novel UAV propulsion system based on PEM fuel cell. *Fuel* 311:122554
- Belmekki BEY, Alouini MS (2020) Unleashing the potential of networked tethered flying platforms for B5G/6G: prospects, challenges, and applications. *arXiv preprint arXiv:2010.13509*
- Borikar GP, Gharat C, Deshmukh SR (2022) Application of drone Systems for spraying pesticides in advanced agriculture: a review. *IOP Conf Ser Mater Sci Eng* 1259(1):012015. IOP Publishing

- Business Insider (2022) Commercial UAV market analysis. Accessed 20 Oct 2022, from <https://www.businessinsider.com/commercial-uav-market-analysis>
- Chalupníčková H, Bahenský P, Sýkora V, Heralová D (2014) The use of drones in air cargo transportation. *Econ Soc Environ* 4509:1–6
- Chang T (2015) Regulatory environment and structural change of UAV industry. *J Aerosp Syst Eng* 9(3):17–22
- Chitta S, Jain RK (2017) Last mile delivery using drones. In: *Technology convergence, innovation & decision sciences*. Springer, pp 1–5
- Chittoor PK, Chokkalingam B, Mihet-Popa L (2021) A review on UAV wireless charging: fundamentals, applications, charging techniques and standards. *IEEE Access* 9:69235–69266
- Deebak BD, Al-Turjman F (2020) Drone of IoT in 6G wireless communications: technology, challenges, and future aspects. In: Li C et al (eds) *Unmanned aerial vehicles in smart cities*. Springer, pp 153–165
- DeGarmo M, Nelson G (2004, Sept) Prospective unmanned aerial vehicle operations in the future national airspace system. Paper presented at AIAA 4th Aviation Technology, Integration and Operations (ATIO) Forum, Providence, Rhode Island
- del Cerro J, Cruz Ulloa C, Barrientos A, de León Rivas J (2021) Unmanned aerial vehicles in agriculture: a survey. *Agronomy* 11(2):203
- Duan B, Fang S, Gong Y, Peng Y, Wu X, Zhu R (2021) Remote estimation of grain yield based on UAV data in different rice cultivars under contrasting climatic zone. *Field Crop Res* 267:108148
- Eißfeldt H (2020, Oct) Acceptance of drone delivery is limited (not only) by noise concerns. Paper presented at first international conference on quiet drones, Flensburg, Germany
- Ferreira R, Gaspar J, Sebastião P, Souto N (2022) A software defined radio based anti-UAV Mobile system with jamming and spoofing capabilities. *Sensors* 22(4):1487
- Gunady N, Wright E, Mudumba S, Sells BE, Chao H, DeLaurentis DA (2022) Evaluating demand of emerging urban air mobility vehicles with changing cost. Paper presented at AIAA SCITECH 2022 Forum, San Diego, California
- Hafeez A, Husain MA, Singh SP, Chauhan A, Khan MT, Kumar N et al (2022) Implementation of drone technology for farm monitoring & pesticide spraying: a review. *Inf Process Agric* 9(1): 3–15
- Hartmann K, Giles K (2016, May) UAV exploitation: a new domain for cyber power. Paper presented at 2016 8th international conference on cyber conflict (CyCon), Tallinn, Estonia
- Higuchi Y, Babasaki T (2018, Oct) Failure detection of solar panels using thermographic images captured by drone. Paper presented at 2018 7th international conference on renewable energy research and applications (ICRERA), Paris, France
- Koslowski R, Schulzke M (2018) Drones along borders: border security UAVs in the United States and the European Union. *Int Stud Perspect* 19(4):305–324
- Kwon WJ, Cheung ND (2022) Drone risks and drone insurance market: focusing on US coverages. *SSRN*
- Miljković D (2018) Methods for attenuation of unmanned aerial vehicle noise. In: 41st international convention on information and communication technology, electronics and microelectronics (MIPRO). IEEE, pp 0914–0919
- Min Z, Kien VK, Richard LJ (2010) Aircraft morphing wing concepts with radical geometry change. *IES J A Civil Struct Eng* 3(3):188–195
- Moon B, Lee H (2022) Drone-image based fast crack analysis algorithm using machine learning for highway pavements. *Eng Proc* 17(1):15
- Niedzielski P, Ziolo M, Kozuba J, Kuzionko-Ochrymiuk E, Drop N (2021) Analysis of the relationship of the degree of aviation sector development with greenhouse gas emissions and measures of economic development in the European Union countries. *Energies* 14(13):3801
- Nurrohman MF, Titalim BA, Utama TH, Adiprawita W (2019) Design and implementation of on-board hybrid generator for rotary wing drone. In: *International conference on electrical engineering and informatics (ICEEI)*. IEEE, pp 310–314

- Roca-Riu M, Menendez M (2019) Logistic deliveries with drones: state of the art of practice and research. In: 19th Swiss transport research conference (STRC 2019), STRC
- Saeed AS, Younes AB, Cai C, Cai G (2018) A survey of hybrid unmanned aerial vehicles. *Prog Aersp Sci* 98:91–105
- Sagaria S, Neto RC, Baptista P (2021) Assessing the performance of vehicles powered by battery, fuel cell and ultra-capacitor: application to light-duty vehicles and buses. *Energy Convers Manag* 229:113767
- Saini A, Kishore KG, Sriram KSS, Singh D, Singh KP (2022) Machine learning approach for detection of track assets for railroad health monitoring with drone images. In: IGARSS 2022-2022 IEEE international geoscience and remote sensing symposium. IEEE, pp 4891–4894
- Scalea JR, Restaino S, Scassero M, Bartlett ST, Wereley N (2019) The final frontier? Exploring organ transportation by drone. *Am J Transplant* 19(3):962–964
- Shihavuddin ASM, Chen X, Fedorov V, Nymark Christensen A, Andre Brogaard Riis N, Branner K et al (2019) Wind turbine surface damage detection by deep learning aided drone inspection analysis. *Energies* 12(4):676
- Standaert W (2021) Digital growth strategies at drone racing league. *J Inf Technol Teach Cases* 11(1):2–7
- Sudevan V, Shukla A, Karki H (2018, October) Current and future research focus on inspection of vertical structures in oil and gas industry. In: Proceedings of the 18th international conference on control, automation and systems (ICCAS). IEEE, pp 144–149
- Teixidó P, Gómez-Galán JA, Caballero R, Pérez-Grau FJ, Hinojo-Montero JM, Muñoz-Chavero F, Aponte J (2021) Secured perimeter with electromagnetic detection and tracking with drone embedded and static cameras. *Sensors* 21(21):7379
- Tiwari A, Dixit A (2015) Unmanned aerial vehicle and geospatial technology pushing the limits of development. *Am J Eng Res* 4:16–21
- Velusamy P, Rajendran S, Mahendran RK, Naseer S, Shafiq M, Choi JG (2021) Unmanned Aerial Vehicles (UAV) in precision agriculture: applications and challenges. *Energies* 15(1):217
- Venus M (2021) How duty rosters and stress relate to sleep problems and fatigue of international pilots. *Int J Aviat Aeronaut Aersp* 8(3):5
- Waibel M, Keays B, Augugliaro F (2017) Drone shows: creative potential and best practices. ETH Zurich
- Xu W, Chen P, Zhan Y, Chen S, Zhang L, Lan Y (2021) Cotton yield estimation model based on machine learning using time series UAV remote sensing data. *Int J Appl Earth Obs Geoinf* 104:102511
- Xue F, Yeh SP, Bai J, Talwar S (2020) Connected aeriels. In: Gill SS, Talwar S (eds) *5G verticals: customizing applications, technologies and deployment techniques*. Springer, pp 211–233
- Yinka-Banjo C, Ajayi O (2019) Sky-farmers: applications of unmanned aerial vehicles (UAV) in agriculture. *Auton Veh* 1:107–128
- Zhao Z, Luo C, Zhao J, Qiu Q, Gursoy MC, Caicedo C, Basti F (2019, April) A simulation framework for fast design space exploration of unmanned air system traffic management policies. In: Proceedings of the integrated communications, navigation and surveillance conference (ICNS). IEEE, pp 1–10

Chapter 2

Systems Engineering Approach on UAS Design



Emre Özbek , Selcuk Ekici, and T. Hikmet Karakoc 

Acronyms

UAV Unmanned aerial vehicle
UAS Unmanned aerial system
VTOL Vertical take-off and landing

2.1 Systems Engineering Approach

The systems engineering approach is a decision-making process that facilitates the acquisition and use of complex systems. The systems engineering approach is actually an approach that can be applied to any process in life. However, when analysed on a product basis, it is generally used in design and production processes that require a multidisciplinary working environment. The systems engineering approach adopts the analysis and understanding of a whole product by breaking it down into parts. This segmentation is done from the most comprehensive section to

E. Özbek (✉)

UAV Technology and Operatorship Program, Eskisehir Technical University, Eskisehir, Türkiye

e-mail: emreozbek@eskisehir.edu.tr

S. Ekici

Igdir University, Igdir, Türkiye

T. H. Karakoc

Faculty of Aeronautics and Astronautics, Eskisehir Technical University, Eskisehir, Türkiye

Information Technology Research and Application Center, Istanbul Ticaret University, Istanbul, Türkiye

e-mail: hkarakoc@eskisehir.edu.tr; thkarakoc@ticaret.edu.tr

the simplest section. For example, in an airplane, the platform itself constitutes the system level, while a bolt connecting the engine to the fuselage is considered at the part level.

Segmentation of a complex system into sub-levels with a systems engineering approach brings many advantages through the life cycle of any product. For example, combining teams from different disciplines that will develop subsystems in a system framework in the design process prevents the complexity of relationships between subsystems that may arise in the future. Systems engineering facilitates not only the design but also the usage processes, which are a part of the product's life cycle and their maintenance during this process. Thanks to this approach, which has been used in airline aircraft for many years, processes are facilitated by using subsystem and component codes in maintenance. Processes such as part replacement and orders can also be managed with less complexity.

If we continue to evaluate the design processes, which is the main subject of the chapter, the first step is to determine the characteristics of the product or system that will emerge at the end of the process while starting the design application with the systems engineering approach. One of the important features of the systems engineering approach is that all subsystems contain the properties of the system (Frank 2006). If exemplified in terms of unmanned aerial vehicles, the propulsion subsystem of an electric unmanned aerial system is also expected to be electric. In the electric propulsion subsystem, the motor will be an electric motor, and the energy source will be a battery. That is, all segments are related to each other. If the expectations that the product will meet are answered with some features throughout the system, these properties will be implemented in all subsystems.

The success of any system depends on how well it meets the design requirements (Ramesh et al. 1997). The diversity of unmanned aerial vehicle configurations can create a lot of question marks in this regard. Fixed wing, rotary wing, hybrid, helicopter, multi-copter, biplane, tail sitter, amphibious, lighter than air. . . The reason why all these configuration types have a place in unmanned aviation is that they arise in meeting the requirements of different applications. For example, in applications where imaging is required from a certain point in the air, the hover capability brings multi-copters to the fore (Quan 2017). Traffic inspections are one of these applications, and in these applications, we often encounter unmanned aerial vehicles in this configuration (Garcia-Aunon et al. 2019). In applications such as spraying pesticides from the air, it is more advantageous to use helicopter-type platforms that can carry more payload (Tran et al. 2019). As can be seen from the examples, the extent to which a system design meets expectations directly reveals the performance of the system. Considering that all subsystems of a system are focused on performing the task of the system, the performance of the subsystems can be directly related to the success of the system.

When we evaluate the performance of a system consisting of many subsystems, one of the features we will encounter is that the subsystems work like links of a chain. The relationship between subsystems can be dependent or independent. Ultimately, all subsystems affect the success of the entire system. From this, we can deduce that the success of a system can be at least as much as the success of the successful subsystem. Although the range and endurance characteristics of an

unmanned aerial vehicle used to observe the activity of volcanoes can be met by the platform's propulsion subsystem and power subsystem, if the imaging subsystem selected for its mission is insufficient in terms of image quality, this will reduce the performance of the system.

2.2 Levels of Systems Engineering Approach for UAS

Systems engineering is the process of examining a product from the top to its foundations. In this context, it is important to understand what levels the systems engineering perspective is divided into. These levels can be expressed as a system of systems, systems, subsystems, components and part levels.

The system of systems level is the level formed by systems coming together. Each of the systems that brings the system of systems together is operational sub-parts with individual job descriptions and their own subsystems. Two specific examples of system of systems level are airspace control and an airport. Here, the systems perform different operations and work in conjunction with each other within the system of systems. When the air traffic control process is considered, air traffic towers, controllers, radar systems, aircraft in the air, unmanned aerial vehicles and pilots are actual systems individually, but they work together within a system of systems to perform an organized air traffic control.

Contrary to popular belief, when the abbreviation UAS is used, it describes a system of systems, not a system. As Fig. 2.1 shows, the unmanned aerial vehicle should be considered as a system. When looking at an unmanned aerial system (UAS) operation, the ground station and the unmanned aerial vehicle (UAV) are the main systems. Considering these systems as subsystems of the unmanned aerial vehicle platform can create confusion.

Subsystems are combinations of components and parts that make up systems and perform various activities for the purposes of the system. To better explain the subsystems, we can make an analogy to the subsystems in the human body. For example, while our digestive subsystem is not a stand-alone operational unit, it enables the operation to be continued within the human body system. It has a specific task definition and continuously cooperates with other subsystems. It has various components and parts such as teeth, stomach and intestines. Let us dig deeper into the analogy between the task of our digestive subsystem and the UAV subsystem. The task of the digestive subsystem is simply to convert the ingested organic

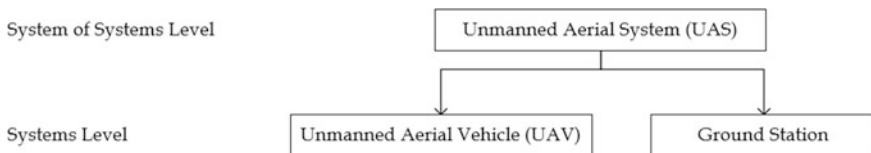


Fig. 2.1 System of systems level and systems level of UAS

nutrients into energy that the system needs. It can be said that the power distribution subsystem does this job for the UAV.

The number of subsystems of unmanned aerial vehicles directly depends on the configuration, class, task and operating conditions of the unmanned aerial vehicle. For example, an unmanned aerial vehicle that will carry out agricultural spraying has a spraying subsystem consisting of components such as a pesticide tank, spray nozzles and pumps. It is not possible to generalize such mission-related subsystems to all drones.

More general subsystems such as structural subsystems, propulsion subsystem and power subsystem are subsystems that we can expect to encounter in all UAVs. In these general subsystems, one can see changes depending on the characteristics of the system. For example, the structural subsystem components differ greatly between a rotary-wing UAV and a fixed-wing UAV. As another example, the propulsion subsystem components and power subsystem components vary widely between an electric UAV and a piston-engine UAV. In this example, one of the main principles of the systems engineering approach, the condition that all of the subsystems show the properties of the system, is reintroduced.

As for the UAV, the ground station should also be considered as a system. Considering the subsystems of the ground station, control unit used, flight operator, sensor/payload operator, communication units and catapult or take-off support units form a single subsystem. Each of these subsystems are subsystems consisting of various features, cooperating to realize the task of the system and meeting the criteria of the system.

Although the cohesion between the system of systems and the system levels is to operate towards a common purpose, all the systems that make up the system of systems have the capacity to operate individually. The cohesion between the subsystems that make up the systems is at a much higher level compared to this. For example, every element in an air traffic management system of systems may not be able to communicate with each other, and air traffic management can be sustainable even in this case. However, it is extremely important that the subsystems that make up a UAV system can function together and communicate with each other. The necessity of designing subsystems such as power subsystem, control subsystem and propulsion subsystem as elements that can cooperate together arises from this co-dependency. Figure 2.2 provides an illustration of subsystems for both a UAV system and a ground station system.

The component level can be defined as the fourth level following the subsystem level. Components lie somewhere between the subsystem level and the component level. These are the units required for the subsystem to perform its task. A component can contain many parts. An engine is a component. One of the components of the electric propulsion subsystem of an electric UAV system will undoubtedly be an electric motor. As in this example, the way the properties of the system spread to lower levels is similar to the relationship between subsystems and systems. Figure 2.3 extends Fig. 2.2 into components level for a UAV electrical propulsion subsystem.

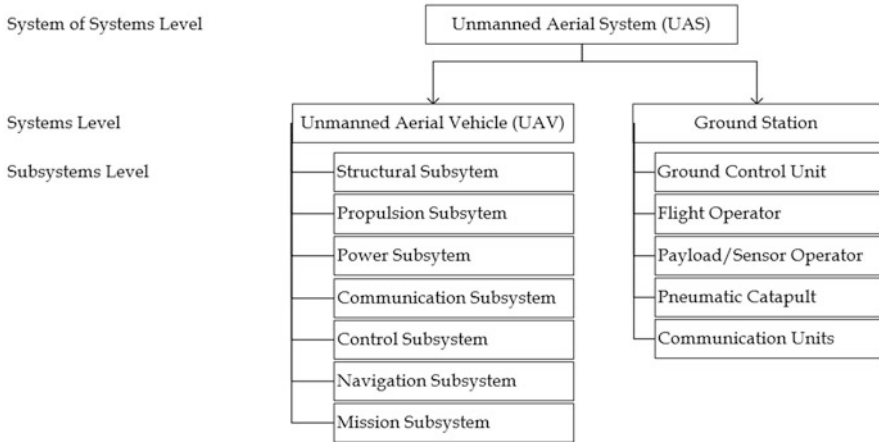


Fig. 2.2 Generalized subsystems of a UAS

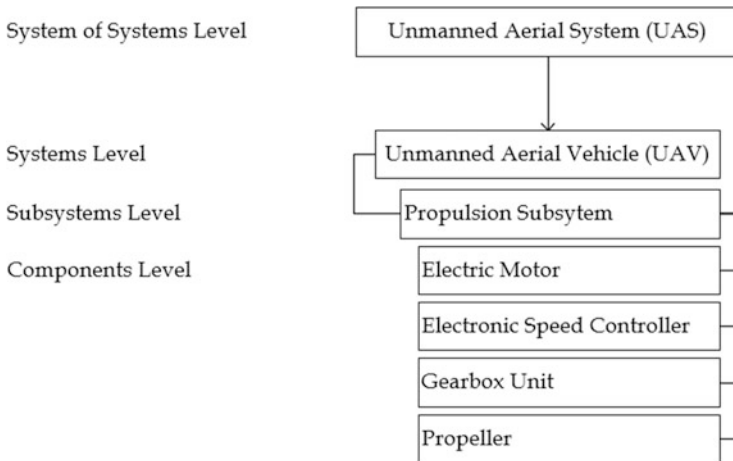


Fig. 2.3 Components of a UAV electrical propulsion subsystem

Part level is the fifth and final level of UAS systems engineering approach hierarchy. Part-level elements assemble the components and contain the fasteners of the parts. Part-level elements are structures that cannot be subdivided. In this context, each bolt, nut and connector can be considered as individual parts.

With the levels revealed by the systems engineering approach, identification tasks such as naming and labelling can be easily performed. Each part can be easily referenced with the five-digit codes such as 01-10-02-04-01, each digit representing the levels of systems engineering. In this way, the design, production and maintenance processes of the aircraft designed with a systems engineering approach become much simpler. The aviation maintenance industry uses the air transport

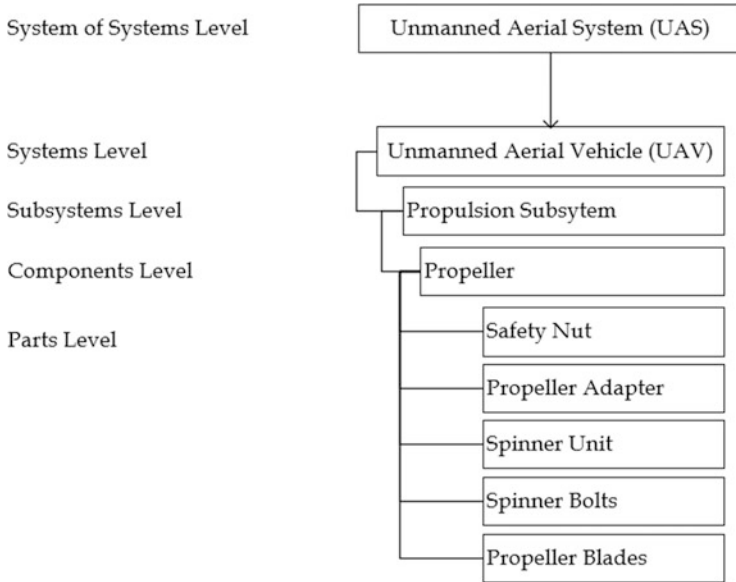


Fig. 2.4 Parts of a UAV propeller component assembly

association (ATA) chapter referencing methodology that was built with this approach for its operations (Jeyaraj 2019).

A full breakdown of the five levels of systems engineering approach applied for a UAS including the parts for a propeller component assembly is illustrated in Fig. 2.4.

2.3 Design Processes of Unmanned Aerial Systems

Although UAS design processes may differ in practice, they can be accomplished with a widely accepted workflow or methodology. This process consists of five successive phases, which can be summarized as the identification of the requirements and needs of the system, concept design phase, preliminary design phase, detailed design phase and testing and development. These five stages can also be expressed as the acquisition process. After this acquisition phase comes the utilization phase, which includes the product use, product support, disposal after its life cycle. Figure 2.5 illustrates the workflow of the described UAS design methodology.

The requirement identification phase is actually an evaluation process. In this phase, the requirements are stated by the firm requesting the UAS or the expectations that are the basis for the start of the design process. At this stage, the designer is faced with both limitations and technical performance criteria. Some specific design limitations for a UAS design process can be identified as follows:

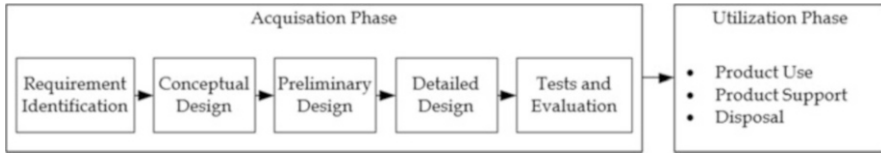


Fig. 2.5 UAS design workflow

- Electric propulsion only.
- UAV must not require a runway for take-off.
- UAV must not exceed 4 kg for legislation limitations.
- UAV must be disassembled to fit a tubular box.

These design requirements are actually example limitations that cannot be negotiated on. Each of these limitations led design decision-making procedures to meet; for instance, if propulsion choices are limited with electric propulsion. Thus, system, subsystem, component and part selections will be affected and must be performed accordingly. There are also requirements that can be negotiated on throughout the design process as listed below:

- Payload weight of the aircraft should be around 700 g.
- The flight operation will be performed at 1000 m altitude.
- The cruise velocity should be above 10 m/s.
- The camera should be directed in the forward direction.
- The flight endurance should be above 50 minutes.
- UAS price should cost lower than 500 \$.
- The UAS acquisition phase should continue for a project time of 12 months.

Although these requirements are negotiable compared to limitation examples, these should also be met by decision-making during the requirement identification phase.

The conceptual design phase starts at the end of design requirement identification and discussions. The conceptual design process could be considered the most systems engineering approach-involved phase of the acquisition phase. In this phase, the overall system configurations, project timetable and feasibility are performed. The conceptual design phase could be summarized in steps:

1. Evaluation of design requirements from the point of view of UAS design and revealing the solutions
2. Evaluation of technical performance measures
3. Evaluation of the features that the designed UAS will need to operate in defined operational and environmental conditions
4. Formulization of defined requirements and setting priorities
5. Production of concepts that will best meet the needs revealed in the light of evaluations by brainstorming
6. Comparison of candidate concepts according to priorities and requirement merits to select the best

7. Putting forward a system proposal
8. System-level assessment of whether the required subsystems can work together
9. Examination of the practical feasibility of the system by carrying out a feasibility study
10. Performance of project planning by creating a Gantt Chart
11. Production planning and assessment of requirements for the maintenance of the system throughout its life cycle
12. Performance of conceptual design assessment to examine if any off-the-course decisions were made in these steps

By the end of these 12 steps of the conceptual design phase, the designer will have the following outputs:

- System-based configuration and general view of the UAS to be produced at the end of the project
- In what ways does the UAS meet the user requests
- Advantages of the selected UAS over other candidate concepts
- Production planning of the UAS
- A Gantt Chart of how the project will proceed
- Technical and financial feasibility study of UAS

In light of these stated features and steps, it can be easily said that the concept design phase is a planning phase. In addition, overall system qualifications are also an output of the conceptual design phase. Recalling the “how successful a UAS is about how well it can do its job” statement, a direct connection could be made between the success of a design and the quality of the decision-making process performed during the conceptual design phase.

The concept design phase is the least cost incurred phase when all other design phases are evaluated. However, concept design is the first and most important step. Since the concept design provides a foundation, its success affects the success of all design processes. Precisely for this reason, necessary time should be devoted to the concept design phase. However, in general, unfortunately, the opposite is done in applications, and systemic changes can be made at later stages by bearing various costs.

Every choice made during the concept design phase should be based on concrete foundations. In these applications, we often come across configuration selection evaluation tables called figures of merit. A formulation is created using the determined design priorities. Then, various candidate concepts are scored, and the most suitable concept is selected. Figure 2.6. shows the general configuration selection matrix for a fixed-wing UAS. The table was originally presented in the technical report of the Harpy UAS for Teknofest International UAV Competition 2018 contest.

As shown in the figure, the selection criteria were evaluated under the name of merit, and the candidate configurations were evaluated by formulating them with the priorities of the design. Evaluating the configurations according to these priorities in this scoring requires serious field literacy. This scoring process should be done in the

Configurations		Conventional	Biplane	Canard
Figure of Merit	Weight	Scoring		
Manufacturability	10	5	3	4
Low Drag	30	5	3	5
Control	10	3	5	3
Max. Velocity	15	4	3	4
Airdrop Safety	20	5	4	4
Stall Characteristic	15	5	3	4
TOTAL	100	465	340	420

Fig. 2.6 An example figure of merit table

light of qualitative information about the advantages and disadvantages of all configurations of unmanned aerial systems. It is important here that subjective knowledge or sympathy for various configurations does not interfere with the selection process.

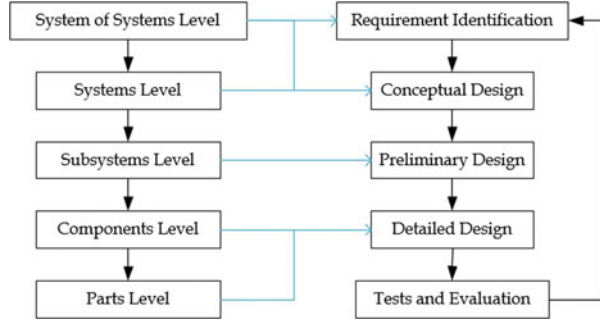
In the preliminary design phase, the selection and sizing of the unmanned aerial system are carried out on the basis of subsystems. The best candidates that meet the compatibility of the subsystems with each other and the expectations from the system are determined. In the detailed design process, components of all subsystems, combinations of components, selections at the part level and their integration with each other are carried out. In these two subsequent design processes, systems engineering is not as big a factor as in the concept design process. In these design processes, other disciplines such as aircraft engineering, mechanical engineering, electrical and electronics engineering and software engineering and analysis methods specific to these disciplines come into play.

When we examine the concepts that emerge during the usage phase such as product use and product support, we encounter sub-tasks such as the assembly of the unmanned aerial system, the supply of spare parts, its maintenance and the creation of training documents. If the systems engineering approach is applied from the beginning of the design in these processes, it will be much easier to create these documents and ensure the sustainability of the product. After summarizing the unmanned aerial system design processes, it is important to underline which levels of systems engineering they relate to.

In the process of designing the unmanned aerial system with the systems engineering approach:

- In which system of systems, the system will be operated, its interaction with other systems and which task it will perform are decided during the conceptual design phase. For example, in the operation to be carried out by an unmanned aerial system, it is decided whether the take-off support unit will be present or not, according to the operational requirements. The features that the ground station

Fig. 2.7 Systems engineering approach involvement in design phases



system should also have been decided at this stage. Therefore, other system interactions and system of systems architecture are designed at this phase.

- The general expectations of the system and the features it will carry are decided during the conceptual design phase. At this stage, which subsystems will be needed and the features that the subsystems should support and provide on a system basis are revealed at this stage.
- The expectations from the subsystems and the quantitative performance characteristics of the subsystems are laid out in the preliminary design phase. At this stage, numeric data starts to get involved. The number of components and the features they will provide are evaluated at the subsystem level.
- The processes of selecting each of the components, sizing, combining them on the basis of parts and determining the parts are carried out during the detailed design process. At this stage, solid models of the system are created. Connections and relationships between components are revealed.

In the guidance of the information provided within the summary, the five levels of systems engineering approach and workflow of unmanned aerial system design process can be matched with blue arrows in Fig. 2.7.

2.4 A UAS Design Practice with Systems Engineering Approach

Throughout the chapter, the basic principles of the systems engineering approach, the design processes of unmanned aerial systems and the interrelationship between the two were covered. A practice can be made on how to use the connections made by giving examples from the processes of a realized project.

2.4.1 Design Requirements

The unmanned aerial system to be designed has been ordered by a building insulation material company. It is desired to measure the heat efficiency of buildings using the unmanned aerial system. This process will be carried out with thermal imaging by performing the hover movement at a certain proximity to the building. The take-off weight of the unmanned aerial vehicle is required to remain below 4 kg for pilot license and flight permits. The unmanned aerial vehicle is expected to be able to vertically take off and land without a runway or clearance dependency and have an endurance of 30–45 minutes.

The client company wants to send a flight crew consisting of one person to the mission. This operator will have pilot training and experience at the beginner level by training an employee from within the company. The UAS has to fit in a bag that can fit in the trunk of a car. A remote control and a tablet computer will be used for piloting. Flights will be operated by manual control. The thermal camera image will be transferred to the tablet and stored on the storage device inside the UAV. It is also desired to keep the total cost of the system as low as possible.

Using the stated requirements above, a list of design requirements for the system can be made:

- Must not exceed 4 kg take-off weight.
- Must be able to perform hover.
- Must have VTOL capability.
- Must be able to have a payload margin for an adequate thermal camera.
- Must be able to stay on air for 30 minutes at least.
- Must be modular in terms of structural parts.
- Must be pilot-friendly in terms of control.
- Must have a manual control-enabled ground control system.
- Must have a real-time image transfer integrated to the mission subsystem.
- Must operate within the altitude and range specifications of <4 kg UAV classification according to the legislation.
- The total monetary cost of the system should be kept as low as possible.

These are the design constraints extracted from the design requirements provided in the form of a needs list. These items define the system of systems and systems-level properties for the design.

2.4.2 Conceptual Design Phase

In the conceptual design phase, decisions should be made about the configuration of the system according to the design requirements. A list of merits could be derived to evaluate candidate configurations. Considering that the priorities may change according to the designer's interpretation, the following formulation can be created for this practice:

Table 2.1 Practice UAS general configuration selection

Merits	Weight (%)	Helicopter	Multirotor
Pilot-friendly	25	2	5
Modularity	20	3	5
Lightweight	20	3	4
Flight endurance	20	5	2
Cost	15	2	5
Total	100	300	420

Table 2.2 Practice UAS sub-configuration selection

Merits	Weight (%)	Quadcopter	Hexacopter	Octocopter
Pilot-friendly	25	3	4	5
Modularity	20	5	4	3
Lightweight	20	5	4	3
Flight endurance	20	3	4	4
Cost	15	5	3	2
Total	100	410	385	355

- 25% – Pilot-friendly
- 20% – Modularity
- 20% – Lightweight
- 20% – Flight endurance
- 15% – Cost (\$)

When deciding about the general configuration of the UAS, this design practice is limited to rotary wing platforms due to VTOL and hover requirements. When an evaluation is made between helicopters and multirotors, the Table 2.1. could be interpreted:

These scores are qualitative scores given based on experience and literature by the designer. The designer must be able to back these decisions made with literature data. Multirotors are user-friendly systems that are easier to control than helicopters (Junaid et al. 2016). Helicopters can provide a longer endurance due to the use of internal combustion engines and fossil fuels (Prudden et al. 2018).

Although the selection of the multirotor determines the general configuration, a choice must still be made about which of the multirotor types will be more suitable for the determined system specifications. In this practice, starting from four rotors, six-rotor and eight-rotor types were evaluated. This is due to the fact that the tri-rotors cause various difficulties in control (Yu et al. 2017). Increasing the number of engines in multirotor UAVs increases the payload per motor and flight safety. However, it also causes great increases in system weight and costs (Suprpto et al. 2017). At this stage, the selection criteria set forth earlier should be applied this time to multirotor sub-configurations. Table 2.2. shows the figure of merit selection for multirotor sub-configurations.

In Table 2.2, the quadcopter configuration scored the highest according to merits derived from design requirements. Thus, one of the aims of the conceptual design phase has been achieved, the best concept that can do this job has now been revealed and its differences from other concepts have been reported quantitatively.

In the concept design phase, it is possible to reveal the number of subsystems and their communication with each other. The subsystems that should be included in this practical UAS design are the structural subsystem, the propulsion subsystem, the power management subsystem, the control subsystem, the communication subsystem and the mission subsystem.

The properties of the subsystems and the features they must have are the subject of the preliminary design phase. Sizing of the structural subsystem will be done here. Dimensional values associated with structural subsystem components, such as the distance between the motors, will affect the diameter of the propellers to be selected in the propulsion subsystem. Such internal connections and interactions need to be managed in this process.

2.4.3 Preliminary Design Phase for Structural Subsystem

The structural subsystem of a quadcopter consists of various components. Frame, motor arms and motor mounts are usually considered the mandatory components for a quadcopter design. There are also optional components that should be evaluated. Landing gear components, for instance, add weight and cost in return for landing safety and protection for payload. Hard landings can be made as it is intended for use by inexperienced pilots. Therefore, it was thought that the use of the landing gear component would be beneficial for this UAS. The aerodynamic case is also another optional component. It increases the aesthetic appearance and provides isolation from external effects. In addition, it adds weight and cost to the platform. This optional component was therefore not used. The prop guard is considered as another optional component. These parts, which are used especially in microquadcopters that will fly indoors and protect the propellers from impact damage. This component was also not used due to weight and costs.

The distance and height between the motors for the dimensions were determined during the preliminary design phase; 450 mm, 650 mm and 800 mm options were evaluated for the distance between the motors. As a result of these evaluations, the distance between the motors of 650 mm was chosen as an optimal point between controllability and weight. The ground clearance is considered to be 170 mm. Thus, the length and weight of the landing gear are optimized.

The features that the structural subsystem should have are as follows: modular, sufficient strength, lightweight, connection with other subsystems without any problems and cheapness of the materials and production methods to be used.

2.4.4 Detailed Design Phase for Structural Subsystem

In the detailed design process, the design of the components and parts should be revealed with all their details and assembly components. The UAS was modelled considering the dimensions and component properties determined during the preliminary design phase. With the addition of the components of other subsystems, a solid model shown in Fig. 2.8 has emerged.

In the detailed design process, the design of the components and parts should be revealed with all their details and assembly components. The revealed UAS was designed to be a platform to meet user requests, combining levels of systems engineering approach and UAS design workflow. Initially, determined priorities were met in every level of systems engineering and the system was prototyped to be folded in a modular fashion as shown in Fig. 2.9.

Fig. 2.8 Practice UAS solid model



Fig. 2.9 Practice UAS prototype modularity demonstration

2.5 Conclusion

In this section, the systems engineering approach is summarized and the benefits of the systems engineering approach are explained. The levels of the systems engineering approach are determined, and examples of unmanned aerial vehicles are given for the levels. How unmanned aerial vehicle design processes and systems engineering approaches can be reconciled and used in coordination are expressed on the basis of levels. Finally, the design methodology has been reinforced by adding a practical application to the design of an unmanned aerial system with a systems engineering approach.

Acknowledgement The research is funded by the Eskisehir Technical University with a project code 20GAP241.

References

- Frank M (2006) Knowledge, abilities, cognitive characteristics and behavioral competences of engineers with high capacity for engineering systems thinking (CEST). *Syst Eng* 9(2):91–103
- Garcia-Aunon P, Roldán JJ, Barrientos A (2019) Monitoring traffic in future cities with aerial swarms: developing and optimizing a behavior-based surveillance algorithm. *Cogn Syst Res* 54: 273–286
- Jeyaraj AK (2019) A model-based systems engineering approach for efficient system architecture representation in conceptual design: a case study for flight control systems (Doctoral dissertation). Concordia University
- Junaid AB, Lee Y, Kim Y (2016) Design and implementation of autonomous wireless charging station for rotary-wing UAVs. *Aerosp Sci Technol* 54:253–266
- Prudden S, Fisher A, Marino M, Mohamed A, Watkins S, Wild G (2018) Measuring wind with small unmanned aircraft systems. *J Wind Eng Ind Aerodyn* 176:197–210
- Quan Q (2017) Introduction to multicopter design and control. Springer, Singapore, pp 150–160
- Ramesh B, Stubbs C, Powers T, Edwards M (1997) Requirements traceability: theory and practice. *Ann Softw Eng* 3(1):397–415
- Suprpto BY, Heryanto MA, Suprijono H, Muliadi J, Kusumoputro B (2017, October) Design and development of heavy-lift hexacopter for heavy payload. In: 2017 international seminar on application for technology of information and communication (iSemantic). IEEE, pp 242–247
- Tran NK, Dao VQ, Nguyen PK, Hoang TKD, Nguyen VK (2019) Numerical investigations of aerodynamics characteristics of main rotors in helicopter UAV used for pesticide spraying in agriculture. *Appl Mech Mater* 889:425–433
- Yu L, Zhang D, Zhang J (2017, July) Transition flight modeling and control of a novel tilt tri-rotor UAV. In: 2017 IEEE international conference on information and automation (ICIA). IEEE, pp 983–988

Chapter 3

Aerodynamic Analysis of Short Landing Solar-Powered UAV for Environmental Monitoring Applications



Chinnapat Thipyopas and Nattapong Warin

Acronyms

AC	Aerodynamic centre
AC	Aircraft
AoA	Angle of attack
AR	Aspect ratio
CD, Cd	Drag coefficient
CFD	Computational fluid dynamics
CG	Centre of gravity
CL, Cl	Lift coefficient
cm	Centimetre
CM, Cm	Moment coefficient
deg	Degree
DES	Detached Eddy simulation
HALE	High-altitude long endurance
kV	Kilovolt
kW	Kilowatt
LALE	Low-altitude long endurance
LES	Large Eddy simulations
m/s	Metre per second
MAC	Mean aerodynamic chord
MPPT	Maximum power point tracking

C. Thipyopas (✉) · N. Warin
Department of Aerospace Engineering, Kasetsart University, Bangkok, Thailand
e-mail: fengcpt@ku.ac.th

NASA	National Aeronautics and Space Administration
PV	Photovoltaic
RANS	Reynolds-averaged Navier–Stokes
UAVs	Unmanned aerial vehicles

3.1 Solar Cell Review and Study

The amount of energy which can be produced by solar panel is very sensitive and affects in the initial conceptual design. It happened many times that solar-powered unmanned aerial vehicles (UAVs) could not fly up in the air for a certain reason, potentially because of the actual energy produced by a limited number of photovoltaic (PV) cells is fairly less than the predicted power requirement. According to the fact that sunlight during the day provides different spectrum and it then results in providing different amount of solar energy to solar cells. The study of variation of net radiation and solar spectrum in Thailand was conducted, and data was obtained during a 1-year period (Limhoon and Bualert 2013). The results showed that the spectrum of sunlight in different seasons are slightly different. The averaged net radiation was, however, taken into account in the preliminary design calculation.

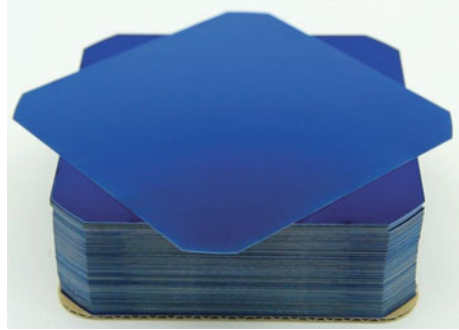
Mono-crystalline silicon PV cells are selected for the study due to their high efficiency and affordability compared to other types of PV cells. Moreover, the current technology of mono-crystalline silicon PV cells provides a good material flexibility which increases manufacturability as each PV cell will be embedded on surface of a curved wing. Table 3.1. reveals comparison of mono-crystalline silicon PV cells produced from a wide range of manufacturers.

According to the information gathered, SunPower C60 model obviously shows the most favourable characteristics among the group of candidates. Apart from its performance, reliability of C60 technology has also been confirmed by its

Table 3.1 Characteristics of the candidate PV cells

Company	PV cell	PV cell efficiency (%)	Flexibility	Weight (g/m ³)	Dimension (mm)
Gochermann Solar Technology	SunPower C60	22.6	Semi-flex	950-1000 (80 g/cell)	125 × 125
Gochermann solar technology	SunPower E60	23.8	Semi-flex	N/A	125 × 125
Bsolar	TG18.5BR	17.5–18.39	N/A	N/A	156 × 156
Delsolar	D6F	18–20	N/A	N/A	156 × 156
Gochermann Solar Technology	SunPower A300	20 min	N/A	N/A	125 × 125
IXYS (IXOLAR)	KXOB22-12X1	22	Semi-flex	2645	27 × 7
Bosch Solar Energy	M3BB	18.43	No-flex	1027	156 × 156
SunOWE	156 MM	18.2	No-flex	1027	156 × 156

Fig. 3.1 Mono-crystalline silicon photovoltaic cells



widespread use in the solar-powered UAVs community. Thus, there is no doubt that SunPower C60 model has been selected to use in this project. Figure 3.1 shows an example of mono-crystalline silicon PV cells.

There is no denying the fact that sunlight also generates thermal energy which induces an elevation of solar cell temperature. The increased cell temperature is potentially considered to be one of the most important parameters in the study as temperature directly reflects an efficiency of solar cells and this is mentioned in many studies. Mostly, solar cell temperature can reach above 25 °C where the number was set by manufacturer for validation of tested temperature. Working above 25 °C fairly reduces the efficiency of PV cells in the sense that the higher the temperature in solar cells, the more the band gap will shrink in a semiconductor material (Silicon), which results in providing less efficiency in converting solar energy to electrical energy. The prediction of PV cell temperature due to variation in ambient temperature was also reviewed from the literature (Jakhrani et al. 2011). An averaged cell temperature was used to predict the possible loss in solar cell efficacy.

As validated by a solar cell's manufacturer, the efficiency of SunPower C60 solar cells can drop up to 0.32% for a degree Celsius change in temperature. When the cell is working far above 25 °C temperature during a hot day, it is predicted that electrical energy produced from solar cells could drop dramatically.

3.2 Design

Required power of UAV is a function of speed and drag force. Due to the limitation of energy obtained from the solar radiation, solar cell UAVs often fly at a very low speed, and this requires a higher lift force coefficient and a great aerodynamic efficiency to maintain level flight. Solar cell UAVs are usually designed with very high aspect ratio wing in order to minimize induced drag. Then, it is followed by the challenge and difficulty in the wing structure design and optimization. High-end technologies such as good-quality lightweight materials and carbon composite material processes and technologies are to be taken into consideration. Therefore, the conventional concept of producing solar cell UAV with a very high aspect ratio is

still ideal. Once the wing has a high aspect ratio, the wing has a reduced chord length which limits the feasibility to configure solar panels on wing. In order to develop a solar cell UAV with available knowledge, on-the-shelf PV panel, technology know-how, facility, and experience in our team, semi low aspect ratio rectangular wing, AR 5-12, is our design concept. The concept is favourable in terms of structural design as well as to gain large surface on the wing.

The second approach for this solar cell UAV project is to cope the challenges in take-off and landing stages. Since the available power of solar cell UAV is very low and it requires long-distance runway to operate. For the take-off phase, the speed of UAV can be increased by a few options: catapult, hand launch, and deploying from a bicycle or car. For the landing phase, recovery by net and sling is commonly applied. However, these methods are possible to create damage to a vehicle which is designed and built by lightweight composite material with low safety factor for structure stiffness. Therefore, a new concept of landing with the high angle of attack so called perching landing or deep-stall landing is introduced in this project.

3.2.1 Airfoil Selection and Wing Design

According to conceptual design, flying wing configuration is the most preferred and challenging option to develop in the current and future phase. A number of airfoils that are popularly used in flying aircraft configuration have been compared and shown in Table 3.2.

HS520 series was selected to be the airfoil profile for our flying solar plane. This airfoil has a good reputation among flying-wing classification and is recommended by the group that it is good for tailless design which have low aspect ratio and zero sweep angle. Figure 3.2 presents the HS520 airfoil geometry.

To obtain aircraft design at the optimal point of operation, the wing chord length was fixed at 45 cm due to the dimensions and attachment pattern of the selected solar cell Sun Power C60 which has a size of 12.5 cm*12.5 cm. The 5 cm area at the

Table 3.2 Characteristics of the candidate airfoils

Airfoils	Thickness (%)	Camber (%)	Cm_0	α_0	Cl/Cd_{max}
B29 tip	9.00	2.23	-0.047	-1.57 deg	74.4
E180	8.58	2.24	-0.034	-1.65 deg	74.1
E186	10.27	1.31	+0.004	-0.52 deg	52
HS520	8.82	2.13	+0.0041	-0.64 deg	68.5
TL55	9.44	1.90	-0.0052	-0.68 deg	68.2

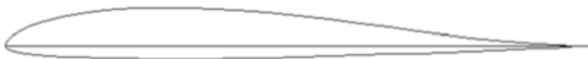
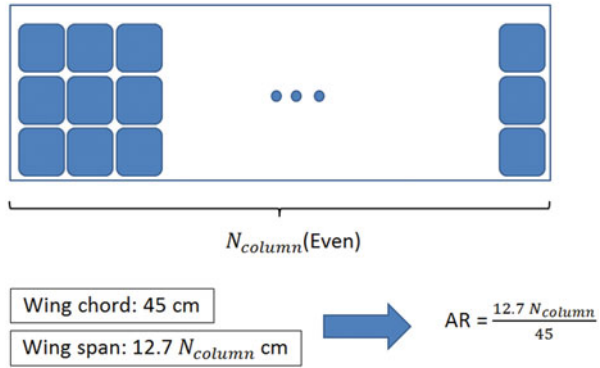


Fig. 3.2 Profile of the flying wing airfoil HS520

Fig. 3.3 Configuration of solar cells attachment on the wing



curved leading edge was not allocated for the attachment of PV cells. As the diagram presented in Fig. 3.3 shows how the length of wing span was continuously extended as a function of the increasing number of solar cell columns attached on the wing surface. In other words, this variation of wing aspect ratio is believed to demonstrate the change influencing aircraft wing structure manufacturability and aerodynamic performance.

3.2.2 Aircraft Performance Evaluation

In wing design process, the final approach is to find an optimal wing configuration which wing can generate sufficient electrical for electric motors. Theoretically, electrical power requirement (for cruising speed at 8 m/s) can be obtained from the equation of aerodynamic performance, while aircraft power available is obtained from the estimation of power generated from solar cells by taking the efficacy loss into account for all cases. Two approaches of calculation were made by fixing the wing at a certain wing setting angle and varying wing setting angle in individual condition.

Approach 1 evaluation represents the relationship of performance predicted when increasing the wing aspect ratio. As can be observed in Fig. 3.4, UAV requires quite a stable amount of energy when it has a longer wing, presumably because of a positive change in aerodynamics. However, the weight condition was concerned due to insufficient amount of lift force generated by the group of wing aspect ratio 5–27 as shown in Fig. 3.5. This calculation approach is general case that can be found in conventional solar cell UAV design resulting in very high aspect ratio wing over AR of 20 which aim to gain most aerodynamic efficiency in design. This is not the case in this project since we are also considering manufacturing and structure issue.

In approach 2 evaluation, the calculation shows the capability of UAV when having wing setting angle adjusted to gain a desirable amount of lift force even though the aircraft does not operate at maximum aerodynamic efficiency but overall

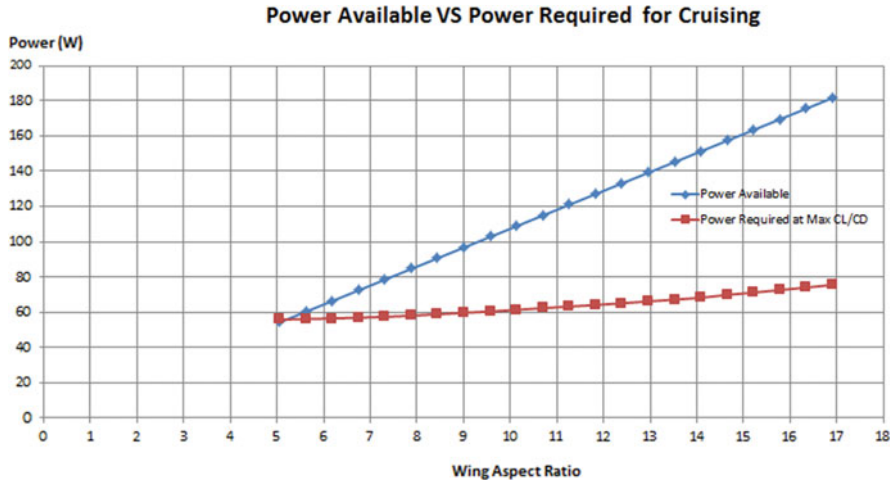


Fig. 3.4 Power available and power required (fixing AOA condition)

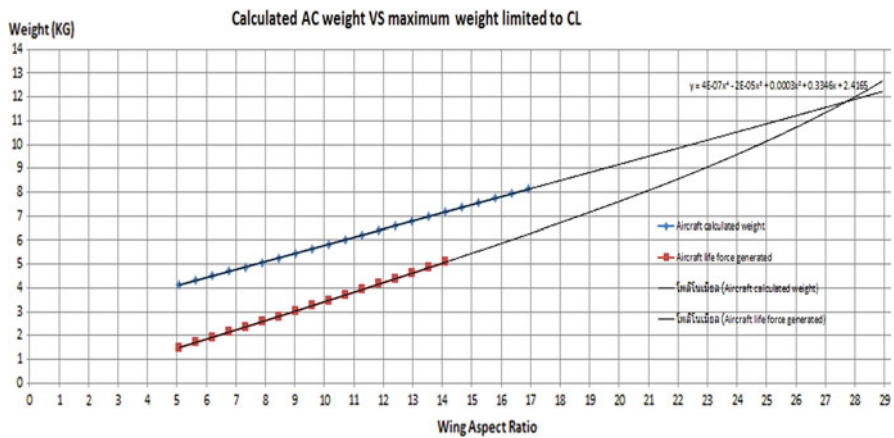


Fig. 3.5 Comparison of aircraft weight predicted and lift force generated by the wing

aircraft can be achieved. The calculation including performance of flying against wind speed up to 5 m/s is presented in Fig. 3.6. Since power available generated from solar cells is higher than power required in all wind speed conditions, the wing aspect ratio of 9.03 was selected to be the optimal point of design.

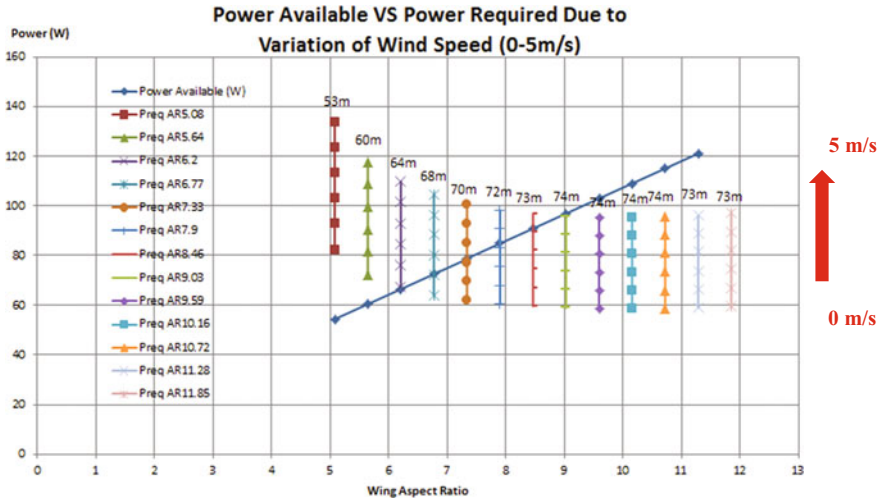


Fig. 3.6 Power available and power required due to variation wing aspect ratio and wind speed

3.2.3 Propulsive and Energy System Design

Prior to the start of the project, two design concepts were discussed between single engine and twin-engine configuration side by side on the wing. While single engine has higher score in the aspect of building and controlling feasibilities, twin engines seem to be more challenging to develop due to new design feature in the category of small solar-powered UAVs. Likewise, the structural point of view is also an advantage for the reason that the twin-engine concept provides better weight distribution along the wing span. So, this will be beneficial in saving a certain amount of structural weight. Sets of single and twin-engine propulsive systems were simulated for performance verification by using eCalc, which is one of the most reliable electric motor calculators. Figures 3.7, 3.8, 3.9, and 3.10 present the propulsive system analysis.

As the results show, there are differences in performance between single-engine and twin-engine configuration under the same flight and battery conditions. Obviously, twin-engine platform reveals noticeable, better performance in the aspects of efficiency and endurance. So, this platform is finalized to be the good choice for this project.

By obtaining the best configuration of propulsive system, each component of hybrid system will be integrated as the schematic shown in Fig. 3.11. As mentioned in the previous topic, lithium-ion type of battery is selected due to its higher power density. SunnySky motors with a size of 700 kV with 11 × 6 inches props are selected due to its availability in Thailand.

After finalizing the best aircraft and engine configuration, a specific number solar cell at optimal design point is planned to be wired in series connection and will then be connected in parallel between left and right wing panel to create a hybrid system as shown in Fig. 3.11.

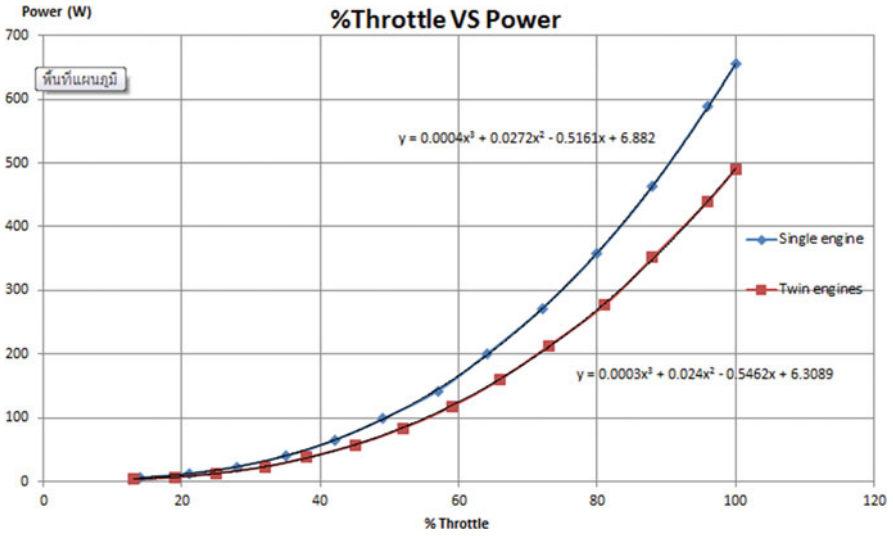


Fig. 3.7 Power due to change in throttle

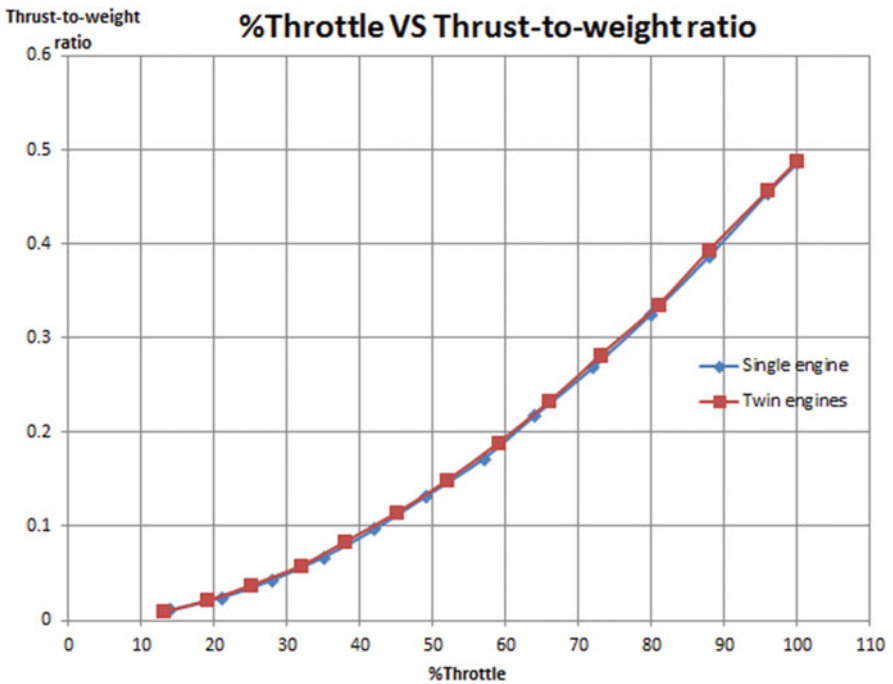


Fig. 3.8 Thrust generated due to change in throttle

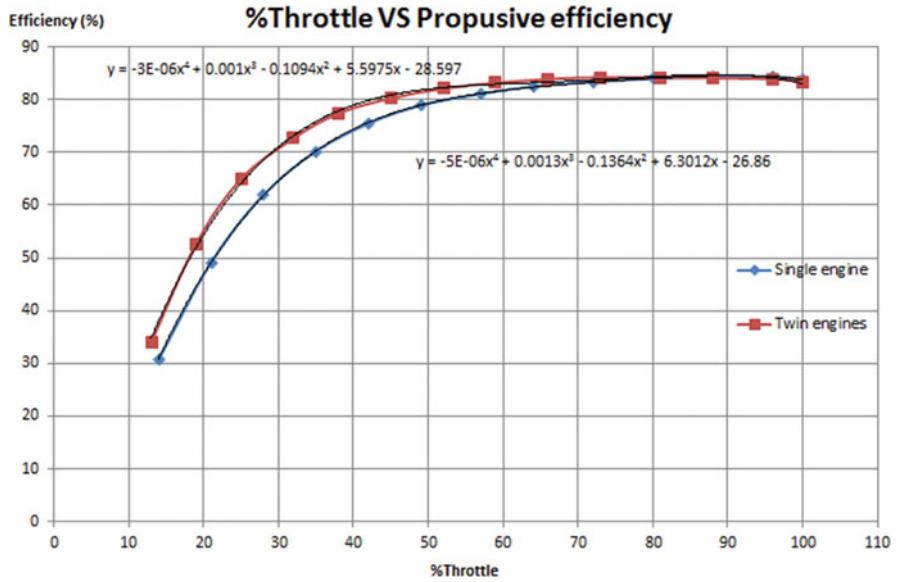


Fig. 3.9 System efficiency at specific level of throttle

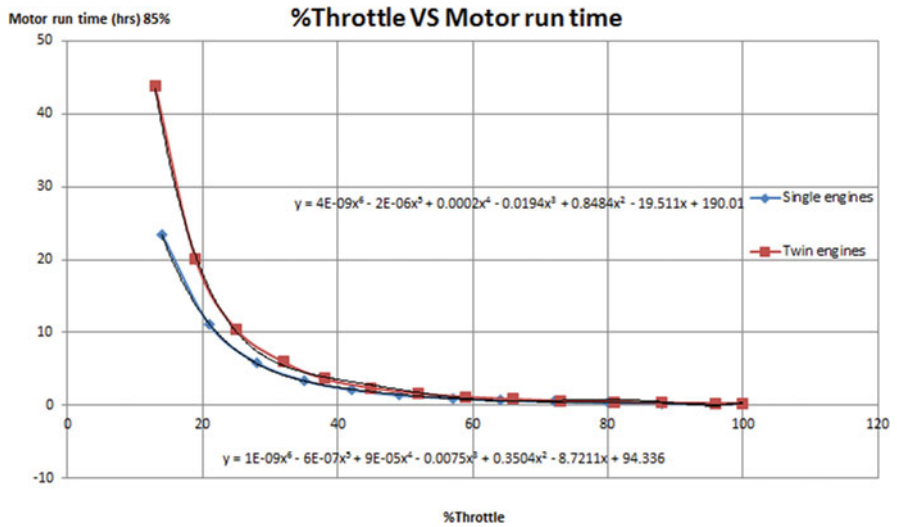


Fig. 3.10 Predicted system endurance at specific level of throttle

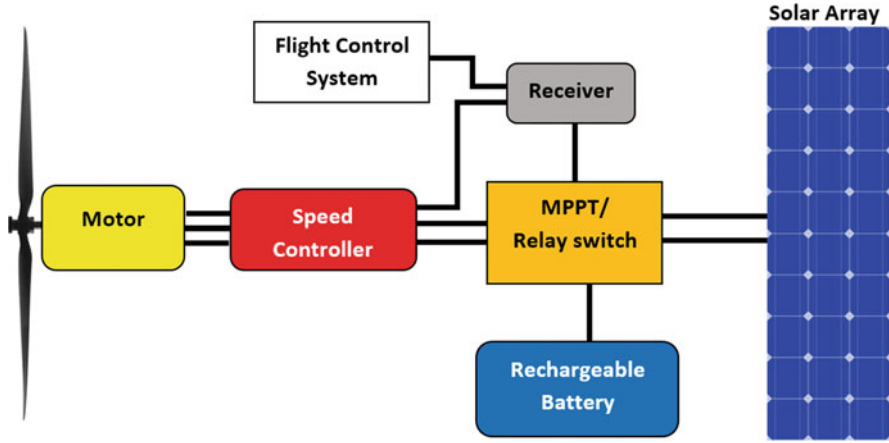


Fig. 3.11 System schematic of solar UAV

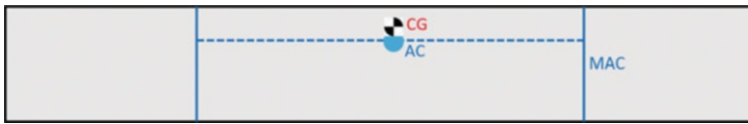


Fig. 3.12 UAV centre of gravity location

3.2.4 Stability Evaluation

The analysis of longitudinal static stability was carried out to validate the configuration of aircraft longitudinal control surfaces. As shown in Fig. 3.12, AC is the aerodynamic centre of the wing (about 25% of chord length), while CG represents the aircraft centre of gravity. A static margin of 5.5% of mean aerodynamic chord (MAC) was taken into the calculation. Thus, the UAV’s centre of gravity will be set at the position 8.8 cm from the leading edge of the wing to have a stable flying condition.

Once the CG location is finalized, the simulation shows that the deflection of control surfaces (flaps) of the wing affects the stability characteristics. Trial of simulation is related to the change of control surface deflection starting from zero degree and continuously increased by a scale of 1 deg until the updated timed configuration is well matched with the optimal aerodynamic condition.

As shown in Figs. 3.13 and 3.14, longitudinal trimmed configuration at a flap deflection of 8 degree is well matched as the trimmed angle of attack is predicted to nearly reach the highest lift coefficient/drag coefficient (CL/CD) value, which is considered to provide the best flight performance.

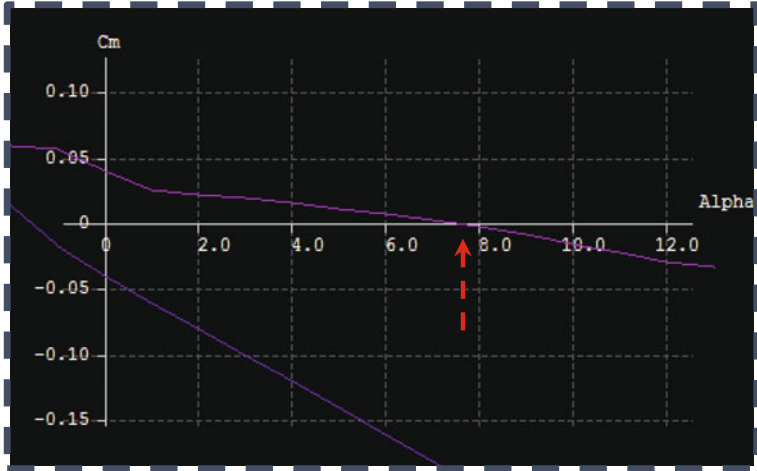


Fig. 3.13 Static stability of trimmed and untrimmed condition

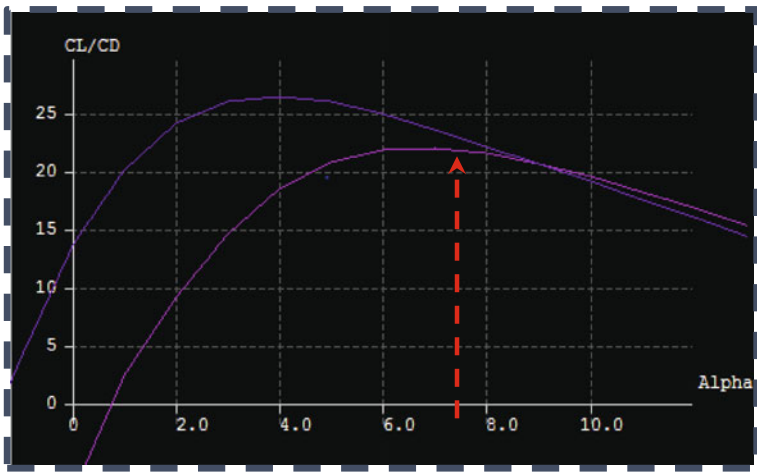
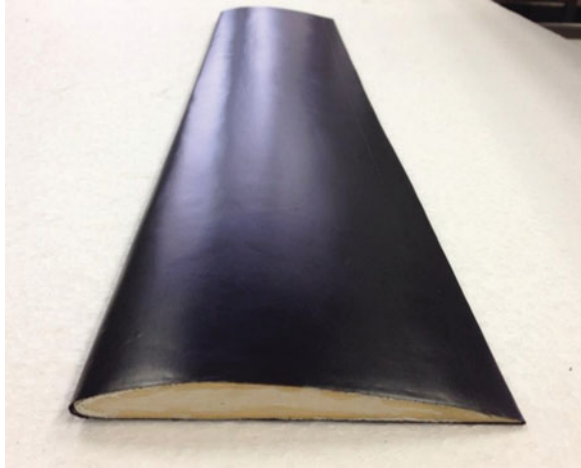


Fig. 3.14 Aircraft aerodynamic performance at trimmed and untrimmed conditions

3.3 Aerodynamics of High Angle of Attack for Landing

As the landing concept of deep stall landing, the test of aerodynamic characteristics at high angle of attack (AoA) is conducted in a wind tunnel and computational fluid dynamics (CFD).

Fig. 3.15 The wing model for wind tunnel test



3.3.1 Wind Tunnel Test

To validate the CFD result and future study on different wing planform, a simple rectangular wing NACA4412 with an aspect ratio of 9 is selected for a wind tunnel test. The wing model was fabricated by hot-wire cut foam core material then covered with the epoxy-resin fibre glass for the rigidity of model and finally covered by sticker for smooth and roughness of wing surface. The model is illustrated in Fig. 3.15. The longitudinal aerodynamic characteristics of the wing is measured by a three-component balance, and the data is collected using the Labview code.

The half-span model is then vertically installed into the turn table so that the model can be adjusted up to 180 deg. The close loop low-speed wind tunnel has a test section of 1 m*1 m*3 m power by 75 kW electric motor which can perform a maximum speed of 45 m/s. Wind speed in the test section is observed by the pitot-static tube installed at the front plan of the test area, and a differential pressure is measured by the KIMO CP300 anemometer. The wind speed in this test is at about 10 m/s.

To determine the reliability of the experiment results, the error of measurement on the load cells that readout force and moment is mandatory. The error is evaluated by using the standard masses for comparison, and the margin of error is calculated by using:

$$\bar{X}_n \pm A \frac{S_n}{\sqrt{n}}$$

where S_n is the standard deviation, A is the critical value derived by the t -distribution table at 95% confidence level. Therefore, the errors of CL, CD, and CM are ± 0.011 , 0.011, and 0.005, respectively, which are considered as acceptable errors.

The margin of error bar is plotted on the 9-aspect-ratio rectangular wing testing data derived from the aforementioned wind tunnel and force balances. The CL, CD, and CM are plotted against the angle of attack (α) in Fig. 3.16.

The CL and CD test results shown in Fig. 3.16 were compared with the referenced data from the previous study of NACA-4412 wing with aspect ratio 9. The comparison analysis presented and confirmed that both CL and CD maintain the same trends as the reference with less than 10% offsets at some regions, which could be negligible. Therefore, this wind tunnel testing is initially acceptable for the experiment result. The data will be validated in the later part that performs the CFD analysis in this study.

3.3.2 Computational Fluid Dynamics

In this study, a Spalart–Allmaras model was adopted for the flow simulation. The Spalart–Allmaras model was proposed to use detached Eddy simulation (DES), which is the combination of large Eddy simulations (LES) and Reynolds-averaged Navier–Stokes (RANS) in order to exploit the advantage of both methods, by using LES in separated flow region and RANS in the attached flow region.

For this model, the transport equation in the non-conservative form is expressed as follows:

$$\begin{aligned} \frac{D\tilde{v}_t}{Dt} = & \frac{1}{\sigma} \left(\frac{\partial}{\partial x_j} \left((v + \tilde{v}_t) \frac{\partial \tilde{v}_t}{\partial x_j} \right) + c_{b2} \frac{\partial \tilde{v}_t}{\partial x_j} \frac{\partial \tilde{v}_t}{\partial x_j} \right) + c_{b1} \tilde{S} (1 - f_{t2}) \tilde{v}_t \\ & - \left(c_{w1} f_w - \frac{c_{b1}}{K^2} f_{t2} \right) \left(\frac{\tilde{v}_t}{d} \right)^2 \end{aligned}$$

The target object of the analysis is the half-span wing with various wing types. The base type of wing is NACA 4412 rectangular wing with an aspect ratio of 9. From the base wing type, various wing variables namely wing thickness, camber, aspect ratio, taper ratio, and swept ratio were adjusted in order to get results for the analysis. For every wing type, the simulation was conducted by changing the angle of attack of the wing ranging from 60 degree to 120 degree.

The operation condition was similar to the standard sea level condition with Reynolds number = 100000. The calculations were carried out in the angle of attack range of 60–120 degree, with 10 degree increment at first. The desired resulting parameters are lift coefficient, drag coefficient, pitching moment coefficient at quarter-chord, location of the centre of pressure, and location of the aerodynamic centre.

In the simulation, the half-cylinder boundary was created as follows. The tested wing was placed in the middle of the flat boundary as shown in the Fig. 3.17. The radius of half cylinder is 17 times the chord length. The test model was placed closer to the inlet with the distance from inlet equal to ten times of chord length, while the

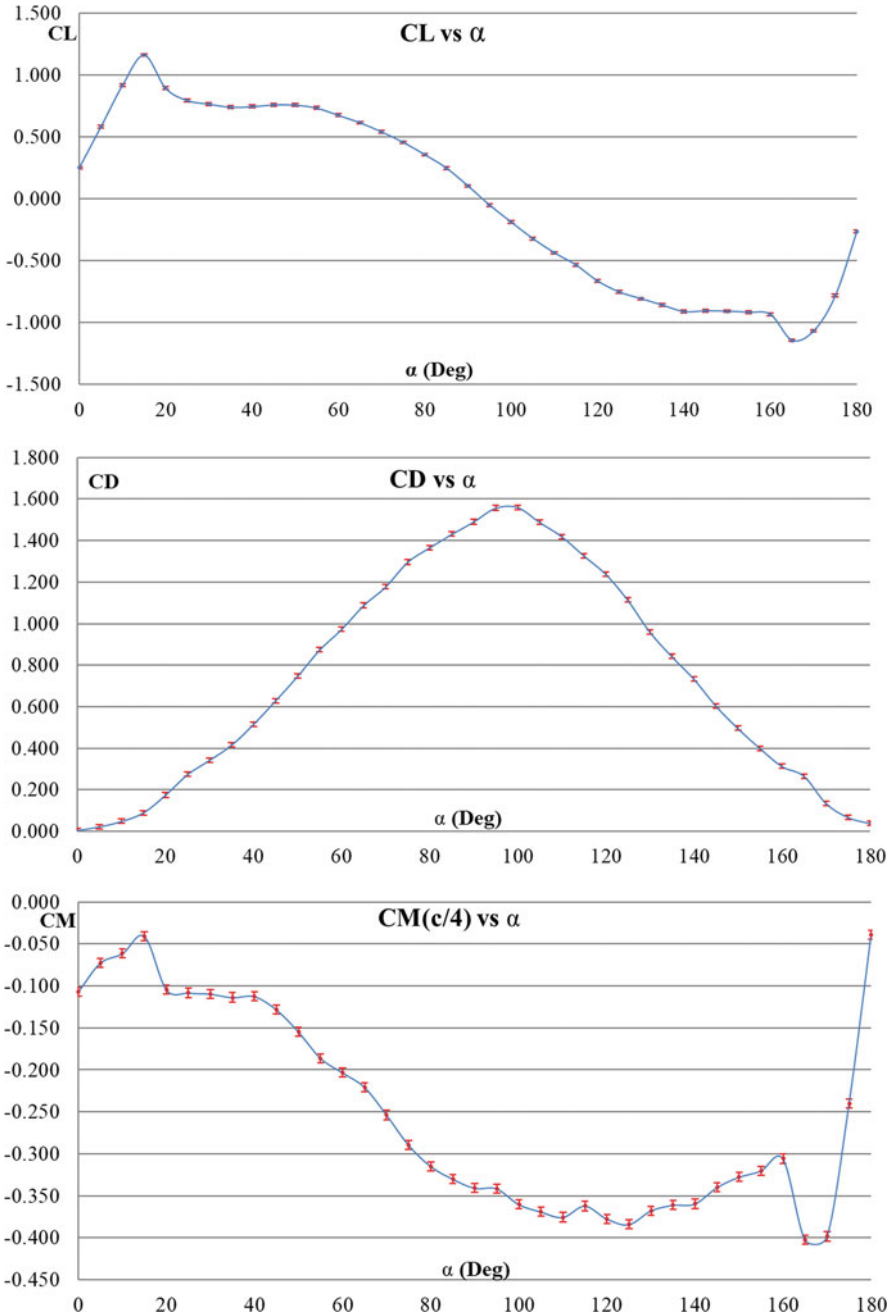


Fig. 3.16 CL, CD, and CM plotted against α of rectangular NACA-4412 wing with an aspect ratio of 9 at the Re of 100,000 fabricated in this study

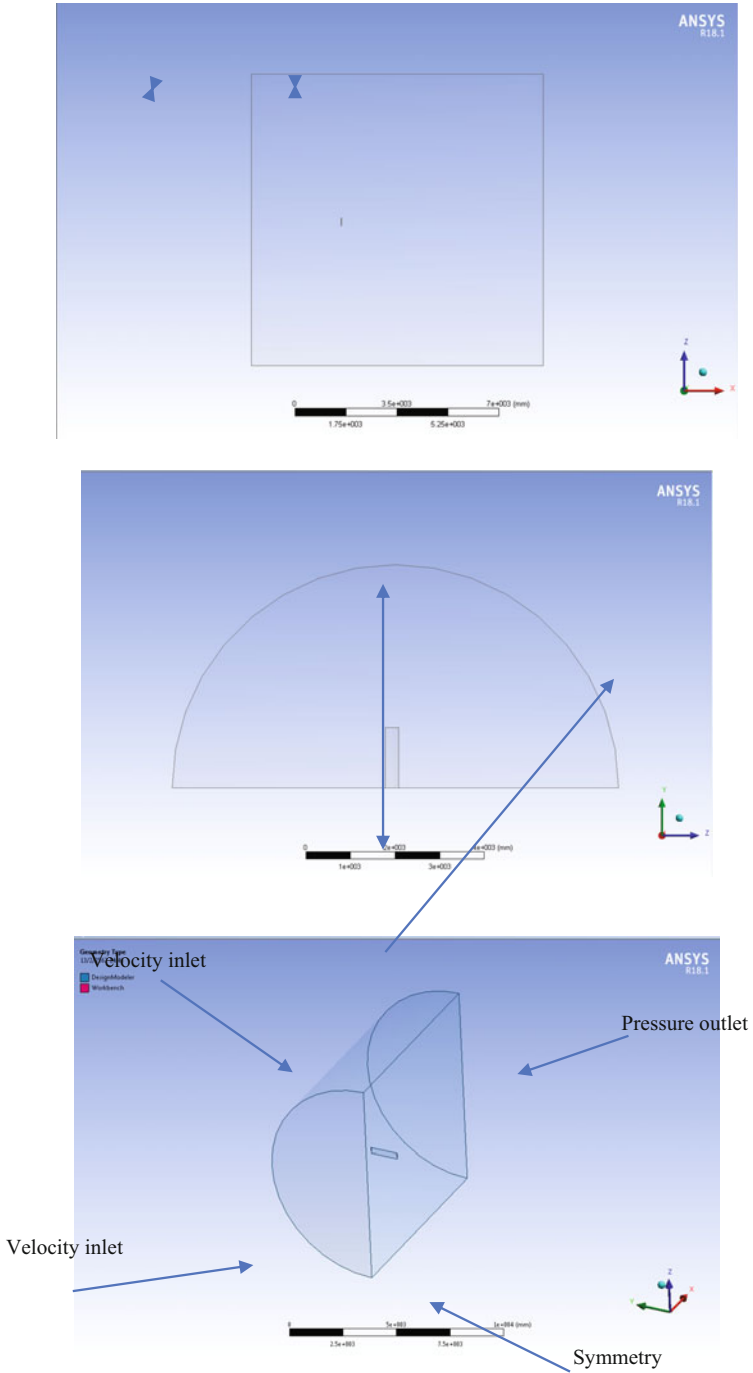


Fig. 3.17 CFD model used for analysis

distance from test model to outlet is 23 times of chord length. The meshing method in this study is the automeshing method with the total mesh elements of 8.5–9 million. Figure 3.17 shows the CFD model used for analysis, and the meshes around the wing are presented in Fig. 3.18.

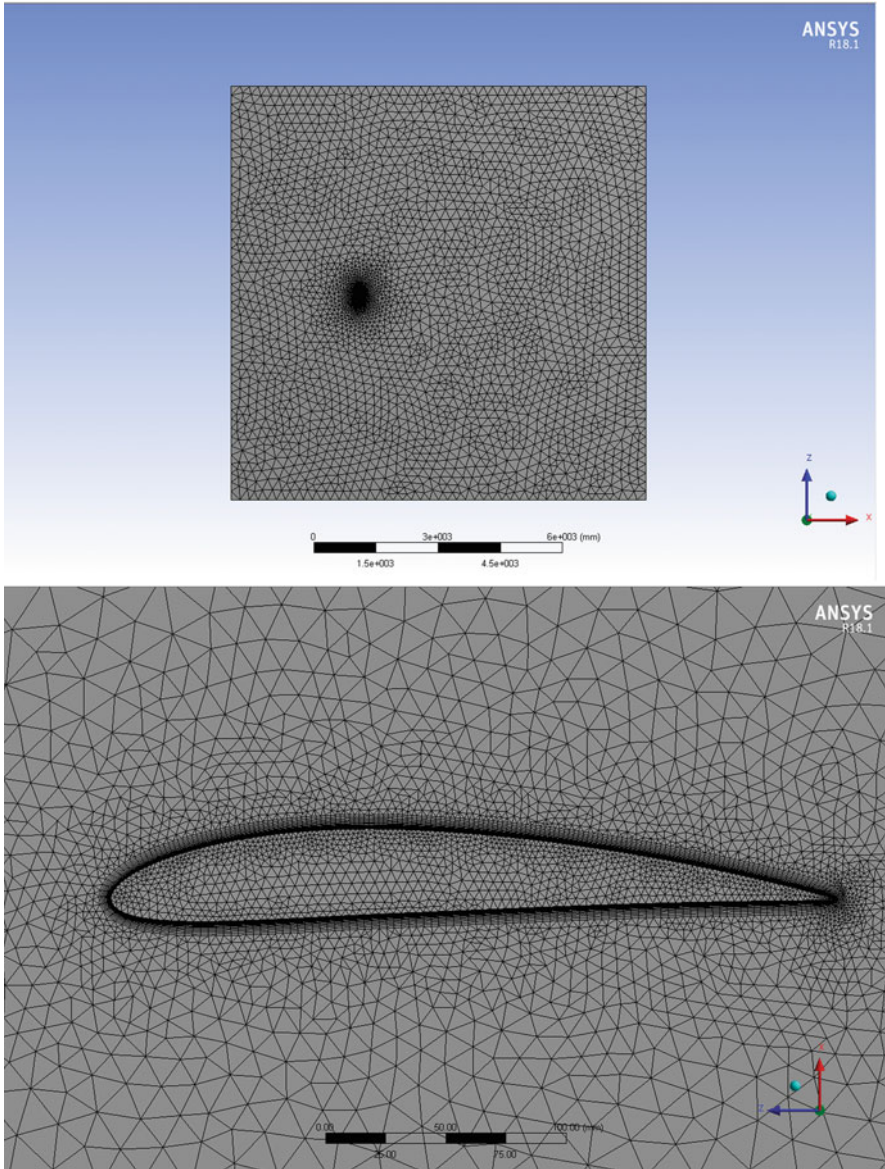


Fig. 3.18 Unstructured tetrahedral mesh with inflation layers around the wing

3.4 Result

The direct results that were obtained from simulation is lift, drag, and moment. The results were put together for comparison at first and then separated into each design parameters. The parameter will be analysed separately to observe the effect of each design parameter compared to the base airfoil, which is NACA 4412 with an aspect ratio of 9. In addition, from these initial direct results, the centre of pressure and aerodynamic centre can be found. The method to find the centre of pressure and aerodynamic centre is shown below.

From the definition, centre of pressure is the point where pitching moment is equal to zero, which can be calculated with the simple moment formula:

$$M = l \times N$$

where M is the moment, N is the normal force, and l is the perpendicular distance.

The definition of centre of pressure is the point where total moment is equal to zero. Therefore, the centre of pressure point can be found by combining the moment obtained from calculation and moment found by multiplying normal force and perpendicular distance. In this case, the perpendicular distance can be defined as the centre of pressure distance.

From Fig. 3.19, the total moment can be defined as:

$$M = M_{c/4} + (N \times x)$$

With the centre of pressure definition, the total moment becomes zero, resulting in following equation:

$$0 = M_{c/4} + (N \times x)$$

In this study, it is preferred to use coefficient value; thus, the equation is converted by multiplying $\frac{2}{\rho V^2 A c}$ on both sides, where ρ is the density, V is the flow velocity, A is the wing area, and c is the chord length:

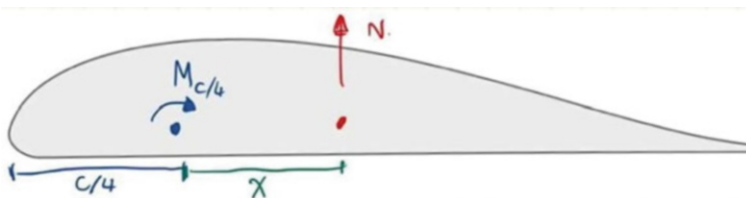


Fig. 3.19 Airfoil and pitching moment analysis

$$\frac{2M_{c/4}}{\rho V^2 A c} + \left(\frac{2N}{\rho V^2 A} \right) \frac{x}{c} = 0$$

which becomes:

$$Cm_{c/4} + \frac{XC_N}{c} = 0$$

Finally, the distance x that was used to define the centre of pressure can be calculated with:

$$x = \frac{-Cm_{c/4}}{C_N} \times c$$

The results of the centre of pressure from the leading edge is the sum of x and $c/4$ values.

Another information obtained is the aerodynamic centre which is the point where pitching moment is constant regarding angle of attack. The value of aerodynamic centre can be found by differentiating the equation of total moment:

$$M = M_{c/4} + (N \times x)$$

which becomes:

$$\frac{dM}{d\alpha} = \frac{dM_{c/4}}{d\alpha} + x \left(\frac{dN}{d\alpha} \right)$$

From the definition of aerodynamic centre, the value of $\frac{dM}{d\alpha}$ is equal to zero. With this condition, the value of aerodynamic centre x can be found. The final equation becomes:

$$\frac{x}{c} = - \frac{dc_{m_{c/4}}/d\alpha}{dc_N/d\alpha}$$

In this study, the aerodynamic centre was validated by calculating the pitching moment at the aerodynamic centre and the point nearby to prove that the moment at the aerodynamic centre does not change or only changes slightly compared to the other point.

3.4.1 Design Parameter Comparison

Figures 3.20, 3.21, 3.22, and 3.23 show the design parameter effects on lift coefficient, drag coefficient, pitching moment coefficient, and location of the centre of pressure.

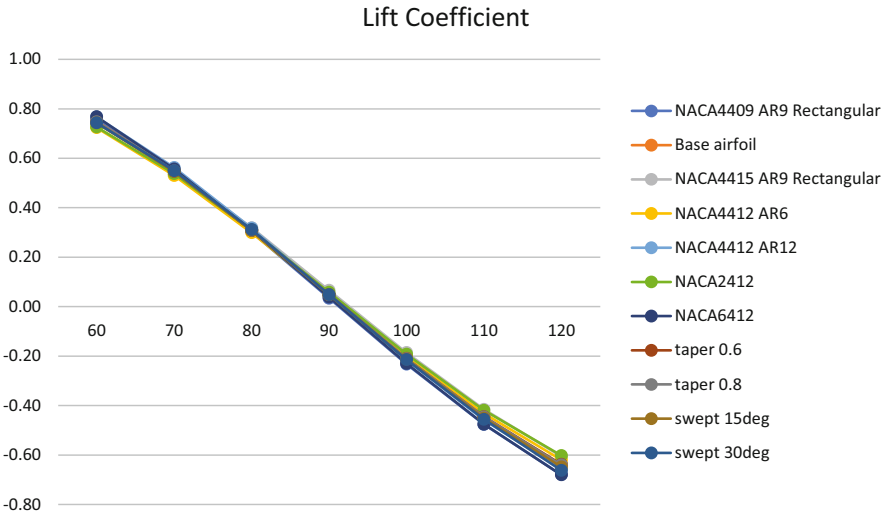


Fig. 3.20 High angle of attack lift coefficient of various wing configurations

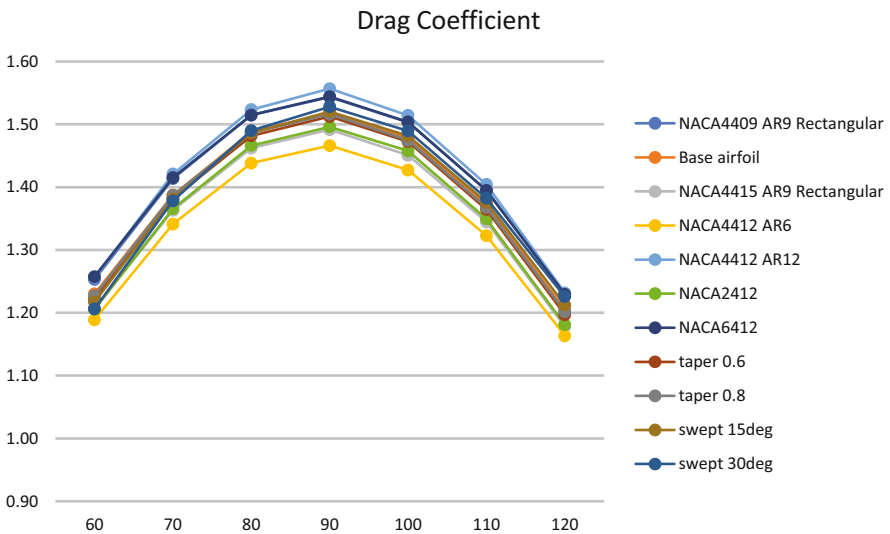


Fig. 3.21 High angle of attack drag coefficient of various wing configurations

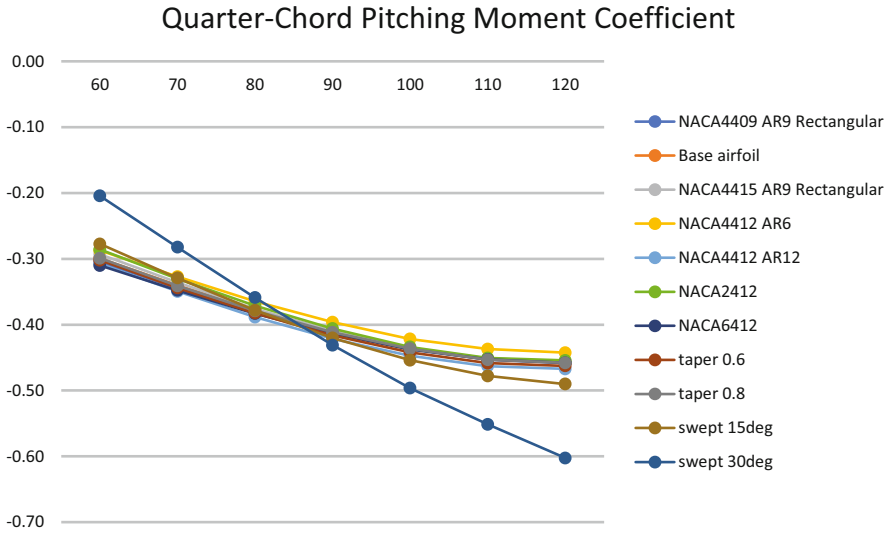


Fig. 3.22 High angle of attack pitching moment of various wing configurations

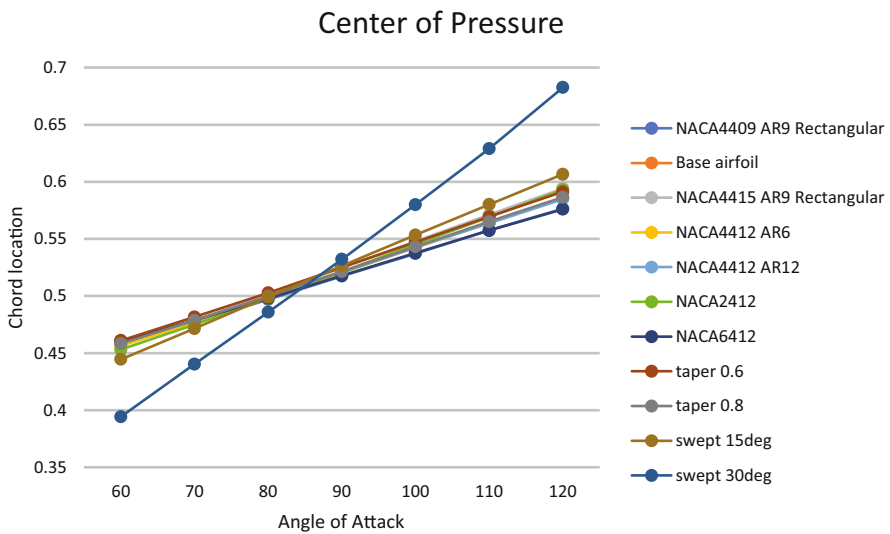


Fig. 3.23 Centre of pressure position versus AoA

The lift coefficient graph appears to be close to linear where the graph becomes negative after a 100-degree angle of attack. The drag coefficient graph appears to be parabolic where the highest point is at 90-degree angle of attack. The pitching moment coefficient graph is curved where the slope is high at low angle of attack and becomes lower at a higher angle of attack. The difference of value between each

design parameter is relatively low, while some parameters affect calculation results more than others. First, the difference in aspect ratio results in more difference between lift and drag coefficient compared to other models. Design with an aspect ratio of 6 resulted in the lowest drag coefficient, and aspect ratio of 12 resulted in the highest drag coefficient. The swept design affect pitching moment more significantly than other models.

The centre of pressure graph appears to be linear. The centre of pressure obtained from simulation is located around the middle of the chord length with the range 40–60% of chord for most models. The graph slope across all models is very similar to each other except for the swept model, which has a higher slope compared to the rest. The trend shares some resemblance to pitching moment coefficient graph because pitching is one of the crucial variables in calculating the centre of pressure.

3.5 Conclusion: Deep Stall Landing Analysis and Flight Test

The aerodynamic characteristics obtain from previous section are then used for the calculation of pitching moment during deep stall phase. As shown in Figs. 3.24 and 3.25, the aircraft is trimmed or has zero pitching moment at an angle of attack of 55 deg when the horizontal tail (elevator) is deflected up to 55 deg if the CG is placed at 10% static margin and then slides to an angle of attack of 108 deg if CG is moved to -10% static margin.

The deep stall flight test is performed by using a conventional type configuration UAV. After level flight at an altitude of 20 m, the deep stall conducts by deflect elevator or horizontal tail to -30 deg. As the result the aircraft can land with the glide slope of 1.33 without damage as shown in Fig. 3.26.

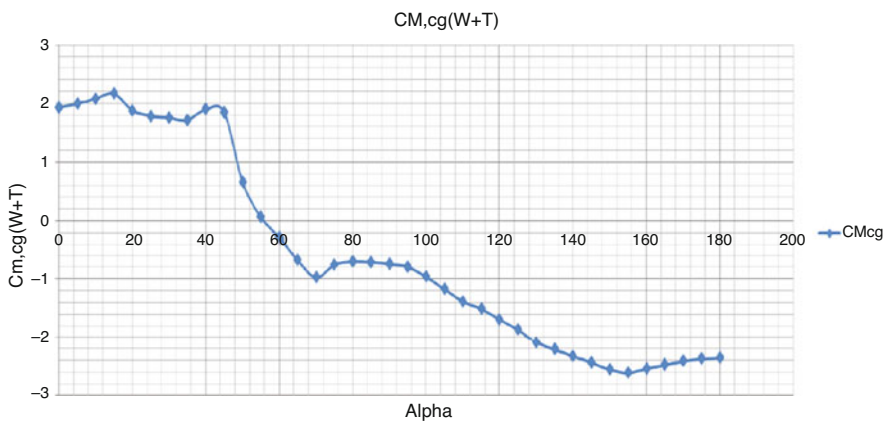


Fig. 3.24 Pitching moment about the CG position (elevator -55 deg, 10% static margin CG)

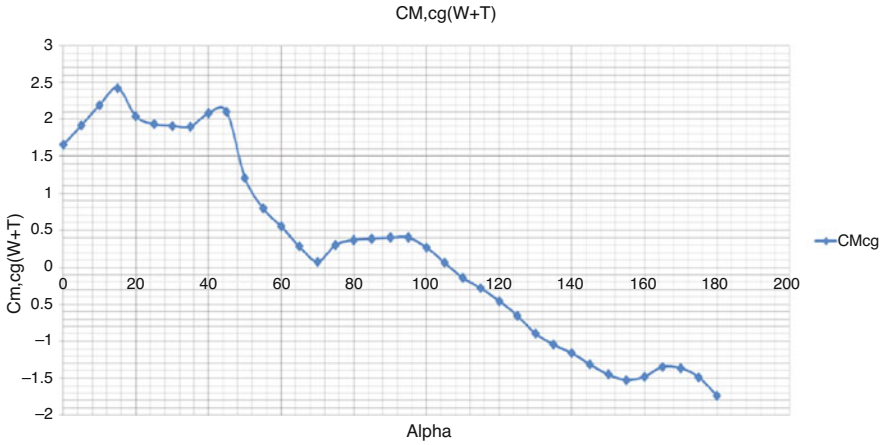


Fig. 3.25 Pitching moment about the CG position (elevator -55 deg, -10% static margin CG)

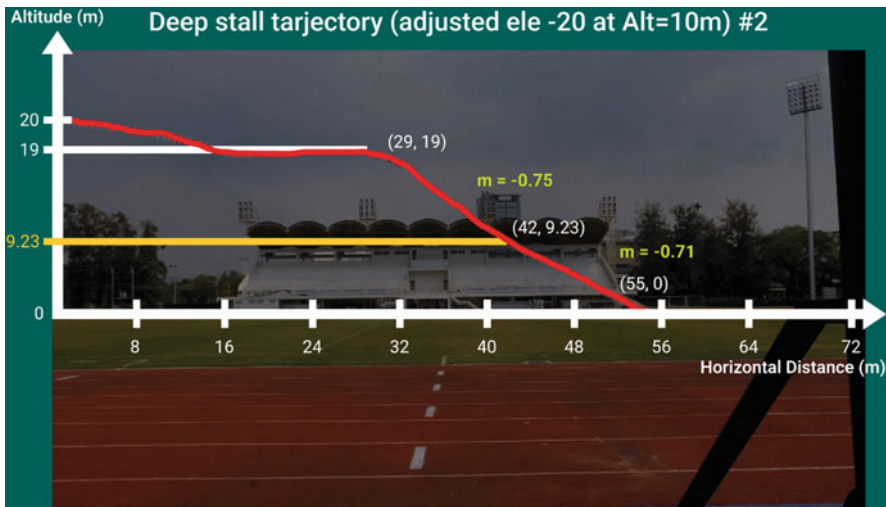


Fig. 3.26 Trajectory of aircraft after deep stall landing

References

Jakhrani AQ, Othman AK, Rigit ARH, Samo SR (2011) Comparison of solar photovoltaic module temperature models. World Appl Sci J 14:1-8

Limhoon P, Bualert S (2013) Variation of net radiation and solar spectrum in Thailand. Int J Environ Sci Dev 4(2):1-4

Chapter 4

Onboard Trajectory Coordination of Multiple Unmanned Air Vehicles



James Sease, Stephen Warwick, and Afzal Suleman

Acronyms

AAV	Autonomous air vehicle
G	Proportional derivative (PD) control gains
i	Respective follower aircraft
P	Virtual or follower position
PX4	Open source autopilot software project
ROS	Robot operating system
RT	Detection range used in flocking
Sal	Alignment term in flocking
Sav	Avoidance term in flocking
Sco	Cohesion term in flocking
UAV	Unmanned aerial vehicle
V	Velocity term in control
Δ	Formation position
θ	Heading of virtual leader

4.1 Introduction

In recent years, the increased use of unmanned air vehicles (UAVs) in aviation has created new challenges and opportunities for improvement in the operation of multi-agent flight systems. A solution for multiple cooperative agent guidance within an urban air mobility environment has been proposed (Yang et al. 2020).

J. Sease · S. Warwick · A. Suleman (✉)
University of Victoria, Centre for Aerospace Research, Victoria, BC, Canada
e-mail: jsease@uvic.ca; swarwick@uvic.ca; suleman@uvic.ca

There are numerous potential benefits for agents if they are able to coordinate their flight trajectories. These benefits include more efficient use of airspace, improved energy efficiency, and more effective mission completion. For example, when aircraft fly in formation, they are able to gain fuel efficiently by taking specific positions in formation. The fuel savings have been measured as high as 18% (Vachon et al. 2003).

Using communication and path coordination, UAVs have the potential to plan their paths more efficiently with respect to each other. It could also allow aircraft to safely fly closer together in a congested airspace. Depending on the mission, proper coordination could significantly improve their mission effectiveness. As an example, in a search and rescue operation, multiple high-altitude aircraft could cover an area quickly and call in low-altitude UAVs to provide confirmation on any findings needing further verification.

4.2 Background

There are many different ways to coordinate a group of agents within a system. Two such methods are virtual leader and flocking.

Virtual leader uses the same coordination scheme as a leader–follower set-up but replaces the leader with a virtual agent. This has previously been simulated in combination with the artificial potential field method (Zhang et al. 2018). Because the virtual leader is simulated, its movement can be predicted. It is also at no risk of a physical collision with other agents if something goes wrong. Because the leader is virtual, all effects that the environment plays on the behaviour of the leader must specifically be programmed into the simulation. For example, if the formation were flying into a strong headwind, the virtual leader may need to be programmed to accommodate a change to its flight speed so as to maintain the optimal airspeed for the UAVs it is leading.

Flocking is a system made up of a number of different decision-making algorithms that can be combined in different ways (Reynolds 1987). The core algorithms are cohesion, which steers agents towards other agents Fig. 4.1a, alignment, which causes the agents to steer in the same direction that all other agents are travelling, as illustrated in Fig 4.1b, and separation, which steers the agents away from other

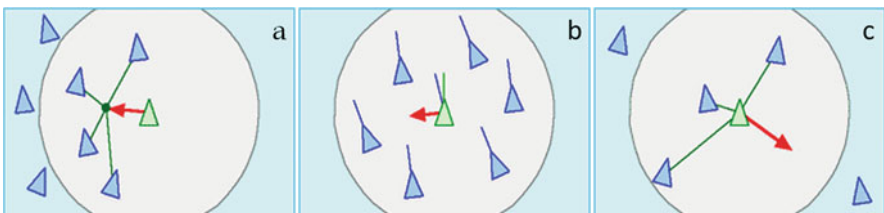


Fig. 4.1 Flocking algorithms: (a) cohesion; (b) alignment; (c) avoidance (Reynolds 2001)

agents that start to get too close, as shown in Fig. 4.1c; proper balancing between these algorithms can lead to agents acting similar to a flock of birds or school of fish.

Many existing multi-AAV systems are actively controlled from a ground station. This allows for the UAV movement to be optimized and verified by a powerful computer, with human oversight. The ground system directs the aircraft through a radio link. It may not always be possible to provide a stable ground link to a group of UAVs operating far from the base station. As an example, UAVs being used for search and rescue in a mountainous environment may not be able to maintain communication links to a ground station at all times.

4.3 Methodology

The multi-UAV coordination system was developed using a combination of virtual leader and flocking to coordinate the aircraft. The primary concerns that must be addressed with the coordination scheme are formation control and collision avoidance. Both will be performed from onboard the aircraft. The combination of virtual leader and flocking allows for a combined centralized/decentralized control structure. The virtual leader uses a centralized system to coordinate the formation. Flocking uses a decentralized system for aircraft interaction and safety.

The coordination software was designed to run on an onboard computer, mounted to each of the UAVs in the system. State and navigation information provided using a Global Positioning System (GPS) augmented inertial navigation system from a PX4 autopilot. The aircraft were able to communicate information between each other using a mesh radio system.

The virtual leader of the formation is simulated onboard one of the aircraft. This aircraft sends the coordination information consisting of the leader's latitude, longitude, altitude, and velocity to all cooperative agents. The virtual leader follows an assigned flight path. The flight path also contains the formation definition.

The virtual leader uses Eq. (4.1) to update its position. The virtual leader uses Eq. (4.2) to update its heading.

$$P_{\text{New}} = P_{\text{Old}} + \vec{V} \times \Delta t_{\text{time step}} \quad (4.1)$$

$$\theta_{\text{New}} = \theta_{\text{Old}} + \dot{\theta} \times \Delta t_{\text{time step}} \quad (4.2)$$

where P is the position, θ is the global heading of the virtual centre, V is the linear velocity of the virtual centre, and Δt is the time interval.

Each follower aircraft calculates its target position relative to the virtual leader using Eq. (4.3). The target velocity is calculated using Eq. (4.4), using the velocity of the virtual leader, modified with the formation's rotational speed and the aircraft's position in formation. The aircraft's target velocity is calculated using the proportional derivative (PD) loop shown in Eq. (4.5), using the aircraft's target velocity

Fig. 4.2 Follower aircraft in delta formation around the virtual leader



(\dot{P}_{Goal}) as a feed forward value, determining the velocity the aircraft must fly to reach and maintain its position in formation.

$$P_{\text{Goal}} = P_{\text{Fleet}} + \theta_{\text{Fleet}} \Delta_{\text{Formation}} \quad (4.3)$$

$$\dot{P}_{\text{Goal}} = \dot{P}_{\text{Fleet}} + \dot{\theta}_{\text{Fleet}} \Delta_{\text{Formation}} \quad (4.4)$$

$$\vec{V}_{\text{Action}} = \dot{P}_{\text{Goal}} + G_P(P_{\text{Goal}} - P_{\text{Actual}}) + G_D(\dot{P}_{\text{Goal}} - \dot{P}_{\text{Actual}}) \quad (4.5)$$

where $\Delta_{\text{Formation}}$ is the local offset of an aircraft's position in formation (this uses the fleet's reference frame) and G_P and G_D are proportional and differential gains of a PD control loop.

The formation was configured so that the aircraft would position themselves 5 m to the left, front, and right of the virtual leader creating a delta formation, as shown in Fig. 4.2. This was increased during flight testing to 10 m to provide a greater safety margin to mitigate the risk of aerial collisions.

In order to reduce risk and prevent collisions, some elements of flocking were added. Each aircraft shares its location with the rest of the fleet. If the distance to another aircraft is too small, an aircraft will take evasive manoeuvres to increase the distance to reduce the risk of collision.

$$\vec{v}_{\text{av}} = \frac{-1}{n} \sum_{i=1}^n \left(\frac{\vec{P}_i \frac{RT}{\|\vec{P}_i\|}}{\|\vec{P}_i\|} \right) \quad (4.6)$$

$$\vec{v}_{\text{al}} = \frac{1}{n} \sum_{i=1}^n (\vec{v}_i) \quad (4.7)$$

$$\vec{V}_{co} = \frac{1}{n} \sum_{i=1}^n \left(\vec{P}_i \frac{\vec{RT}}{\|\vec{P}_i\|} \right) \quad (4.8)$$

$$\vec{V}_{flocking} = S_{av} \vec{V}_{av} + S_{al} \vec{V}_{al} + S_{co} \vec{V}_{co} \quad (4.9)$$

In Eqs. (4.6), (4.7), (4.8), and (4.9), \vec{V}_{av} , \vec{V}_{al} , and \vec{V}_{co} are the velocity targets for avoidance, alignment, and cohesion, respectively; \vec{P}_i is the position of aircraft i with respect to another aircraft; RT is the detection range, default is 20 m; \vec{V}_i is the velocity of follower aircraft i ; and S_{av} , S_{al} , and S_{co} are the scaler values for avoidance, alignment, and cohesion, respectively.

Each follower aircraft combines the velocity targets generated by formation control from Eq. (4.5) and flocking from Eq. (4.9), to generate the velocity command for the aircraft to use, as shown in Eq. (4.10).

$$\vec{V}_{comand} = \vec{V}_{Action} + \vec{V}_{flocking} \quad (4.10)$$

The output from Eq. (4.10) was fed into a previously tuned PX4 multi-rotor controller. For safety purposes, the multi-rotor velocity was limited to a relatively conservative maximum speed.

4.4 Experiments

The proposed system was tested in simulation using Gazebo configured with a representative flight dynamics model of a multi-rotor aircraft. The simulations were followed by a flight test campaign.

4.4.1 Gazebo Simulation

The system was built using robot operating system (ROS). The simulation was performed using Gazebo and the PX4 autopilot firmware software-in-the-loop platform. When simulated in Gazebo, an unexpected communication delay, consistent with hardware tests, was found. This contributed to a transport delay of 0.3 s to all the position and velocity feedback used in each of the aircraft.

The aircraft logged their state information for analysis. The logs are correlated with system timestamps. The time offsets between the aircraft clocks were also recorded. Figure 4.3 shows the position errors of each of the three aircraft simulated as part of the formation. The formation was moving with constant speed to provide a straight and level flight test.

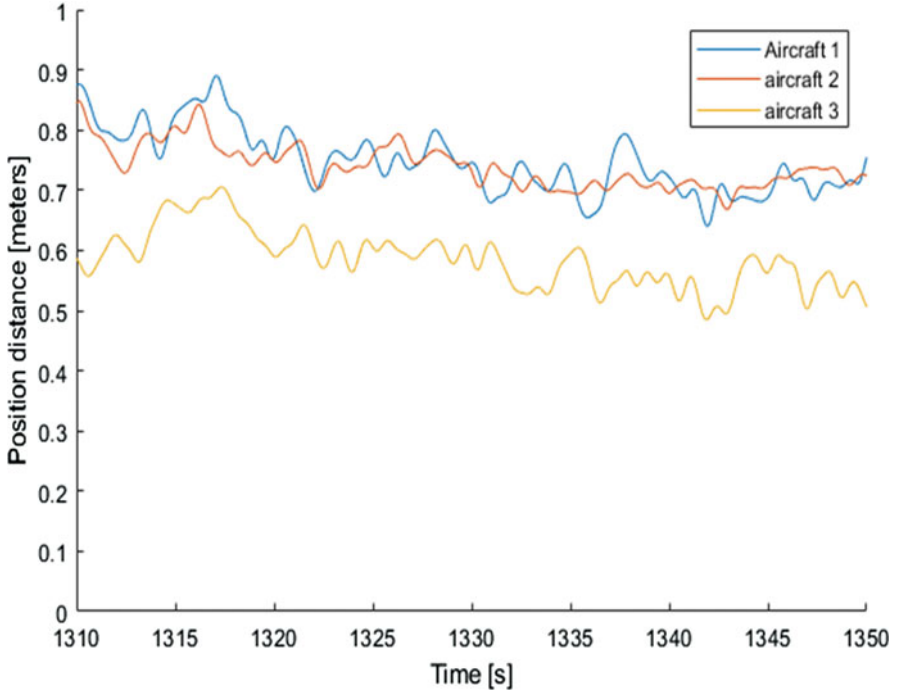


Fig. 4.3 Gazebo simulation, formation position error for straight and level flight

The data in Fig. 4.3 shows that the aircraft are able to maintain a relatively constant position error at approximately 0.75 m from their target location.

A second configuration was tested where the formation was required to track through a coordinated turn providing a heading change for formation position error evaluation. The position errors of this test are shown in Fig. 4.4. The executed turn was a right turn, and aircraft 1 was on the inside of the turn, aircraft 3 was on the outside, and aircraft 2 was in the front.

This indicates that the maximum error for aircraft 1 was just over 3 m, aircraft 2 was just over 5 m, and aircraft 3 was 8 m.

During the coordinated turn test, it was observed that aircraft 1 was required to fly in reverse due to the rotational rate of the formation.

4.4.2 *Experimental Flight Testing*

The system was deployed onto a multi-agent UAV test platform, as shown in Figs. 4.5 and 4.6. The platform consisted of three multi-rotor UAVs, each equipped with an onboard computer that runs the coordination algorithms.

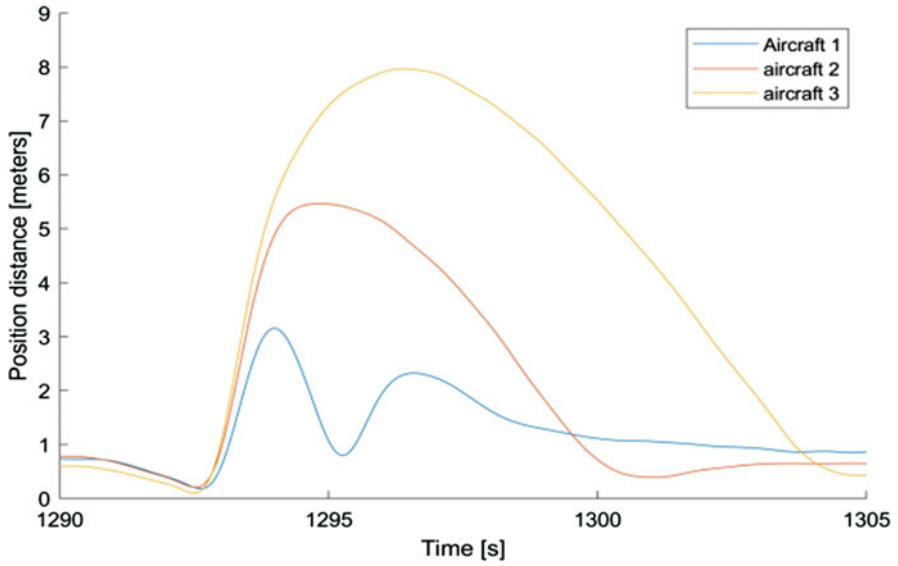


Fig. 4.4 Gazebo simulation, formation position error tracking through coordinated turn



Fig. 4.5 Multi-agent test platform pre-flight



Fig. 4.6 Multi-agent test platform in flight

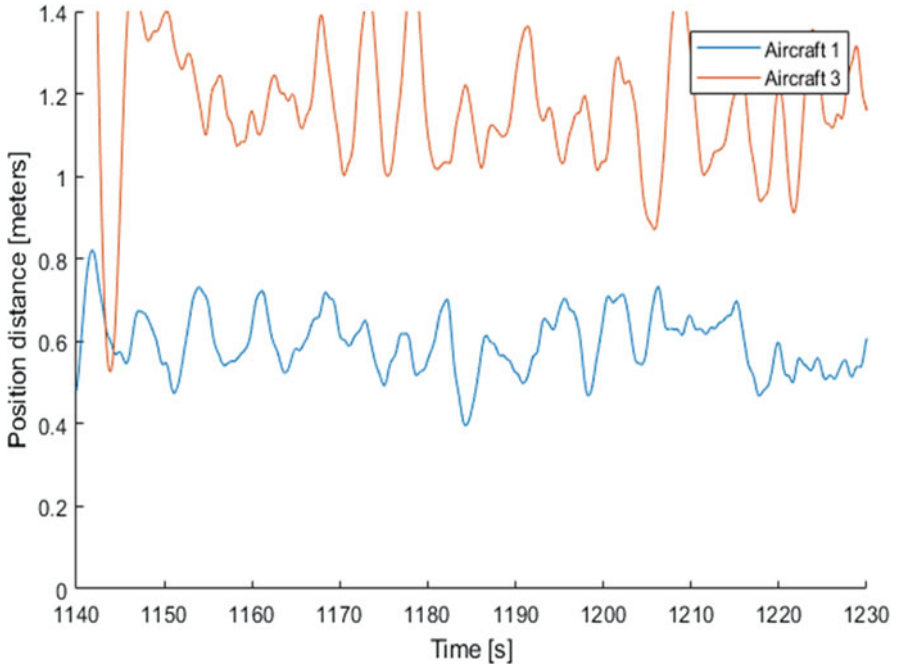


Fig. 4.7 Real-world flight test, formation position error for straight and level flight

The virtual centre was simulated onboard one of the aircraft. Due to a voltage problem with aircraft 2, it could not be operated. Aircraft 1 was set to run the virtual leader while flying and aircraft 3 flew as a follower agent in the system.

Figure 4.7 shows the results of the straight and level flight test. It can be seen that aircraft 1 performed similar to the simulated performance, while aircraft 3 performed noticeably worse with a position error of around 1.2 m.

Figure 4.8 shows the formation position error while the virtual leader performed a coordinated turn. As with the straight flight error, the real world performed quite similarly to the simulated environment. The position errors of both aircraft were slightly larger in the real world than in the simulation, about 1 m and 1.5 m higher maximum errors for aircraft 1 and 3, respectively. These real-world errors are approximately 18–33% larger than in simulation.

The spacing between aircraft 1 and aircraft 3 is expected to be 20 m. Figure 4.9 shows that during the coordinated turn, they maintained this distance with a peak error of 0.6 m.

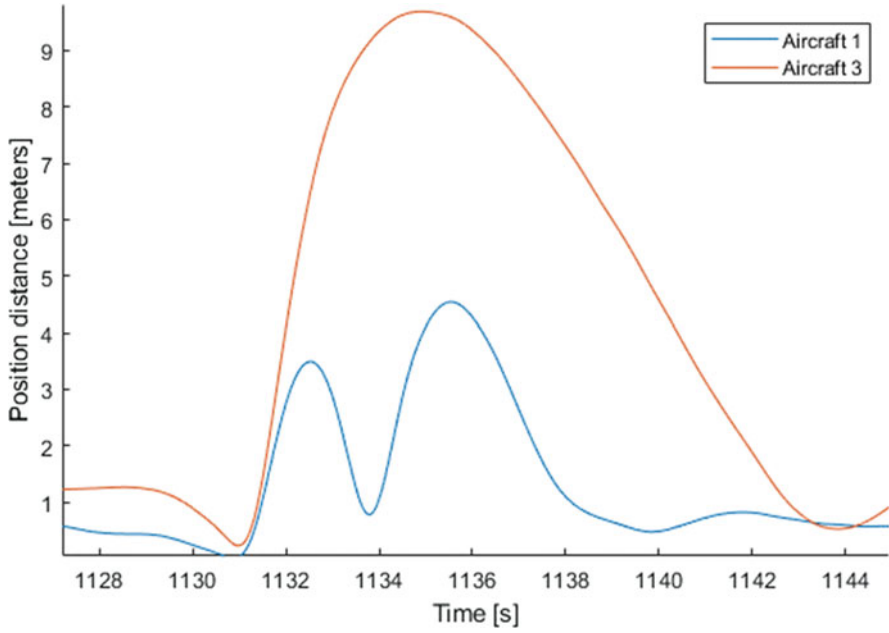


Fig. 4.8 Real flight test, formation position error tracking through coordinated turn

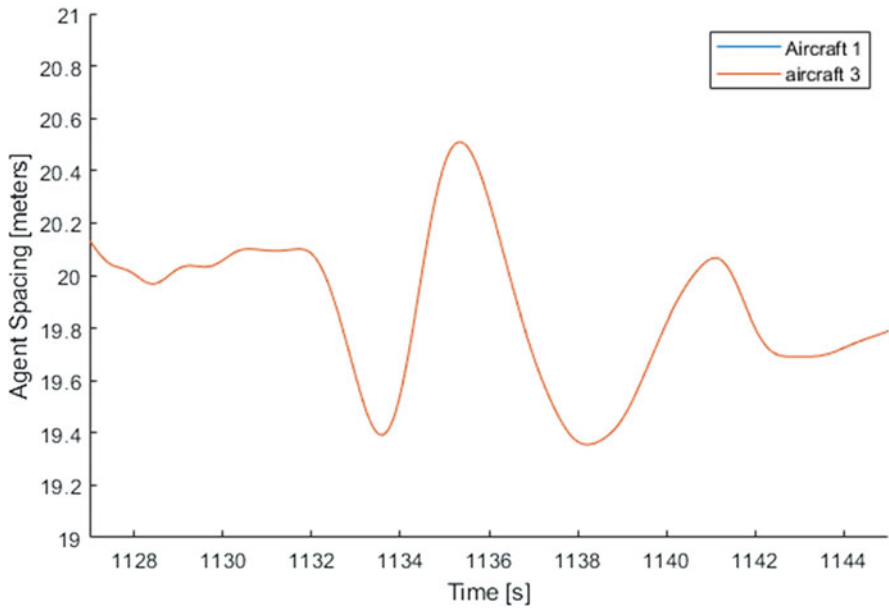


Fig. 4.9 Real-world flight test, agent separation through coordinated turn

4.4.3 Parameter Updates and Re-simulation

Because the aircraft spacing was increased from 5 m to 10 m, the speeds required for each aircraft to maintain position during the turn exceeded the previously set safety limit. In the case of aircraft 3, it was observed that its position in the formation was more than twice its safety limit.

Due to the findings in the simulation and in the flight test, modifications to turning were applied to provide immediate improvement to performance. The maximum turning rate of the formation centre was decreased, which ensured that the maximum required flight speed would be significantly reduced. In addition, the maximum allowed speeds of all aircraft were increased.

The level flight matched with the earlier simulations. Figure 4.10 shows the coordinated turn errors of the system after these changes. These figures show that the straight and level error was not changed, but all three aircraft coordinated turn errors are now comparable.

The maximum error of aircraft 3 was significantly reduced, aircraft 2 was reduced by a small factor, and aircraft 1 drastically increased.

The distance between aircraft 2 and each of the other aircraft should be 14.14 m, which will be the smallest distance for each aircraft. Figure 4.11 shows that the aircraft achieved this with a peak error of 0.2 m during the coordinated turn operation.

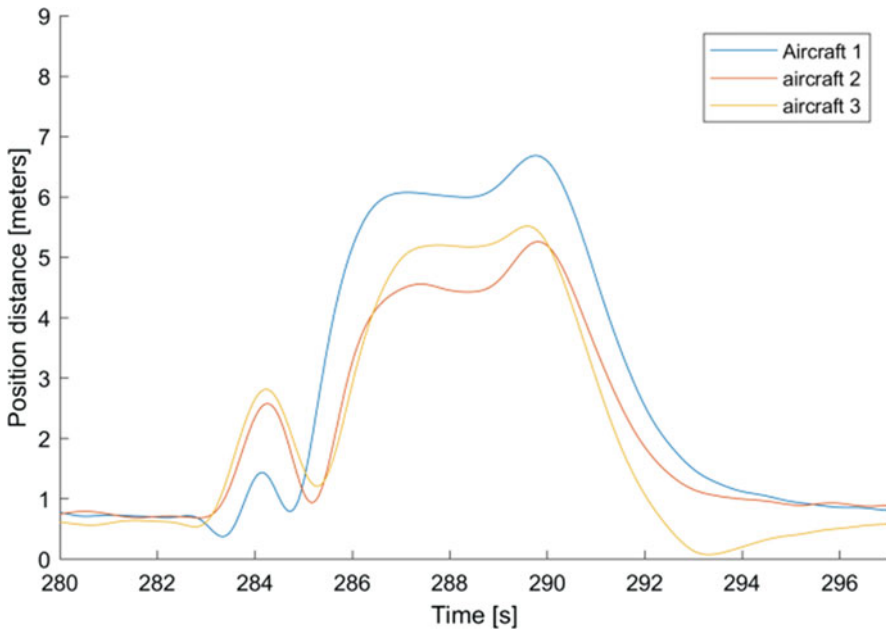


Fig. 4.10 Re-simulation, formation position error tracking through coordinated turn

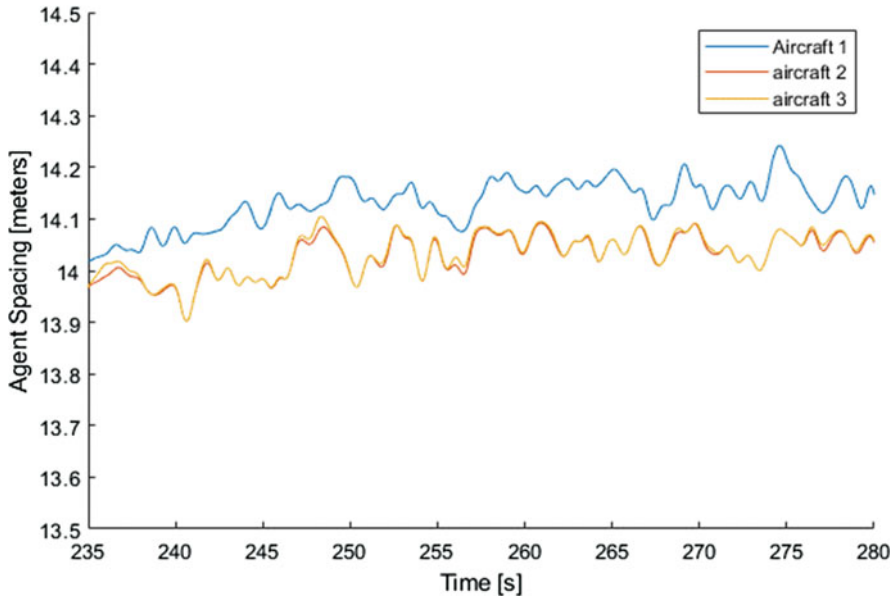


Fig. 4.11 Re-simulation, agent separation through coordinated turn

4.5 Results and Discussion

Two important assumptions were made prior to flight testing. It was assumed that the PX4 and internal delays would not cause any position errors above those found in the simulations. It also was assumed that the radios would not be a significant source of delays above the internal delays. This assumption was based on the radio delay of 0.09 s. A minimum safe spacing was calculated for the aircraft, using worst-case errors. Worst cases included long internal delays, several dropped radio messages in a row, and compounding position drift in the PX4s, bringing the aircraft closer together. Additional distance was added between aircraft so that they would correct spacing before human safety pilots were required to intervene in control.

The flight test set-up consisted of a ground station and a crew of trained UAV operators. Three batteries were on hand for each aircraft, allowing the full system to be flown three times without needing to recharge batteries. The flight crew included a manual UAV safety pilot for each of the three aircraft, who for safety could override aircraft control. One UAV ground station operator monitored all the telemetry of all aircraft. Other ground crew included the flight test director, one range safety officer, and photographers and videographers.

4.5.1 *Experimental Results*

Aircraft 1 hosted the virtual leader. The virtual leader flight test is comparable to the virtual leader simulation, because the simulations were redone using the same formation spacing of 10 m. The behavior of the virtual leader was identical in both tests.

The internal delay of the system was calculated using aircraft 1 position error. The observed error of aircraft 1 was 0.2 m, and timestamp error was 0.6 m. The difference between the observed and timestamp errors, 0.4 m, was used with the flight speed of 2.7 m/s to calculate that the internal delay was approximately 0.15 s.

The radio delay in the system was calculated using the position errors of aircraft 3 and the internal time delay. Aircraft 3 observed its position error as 0.3 m, while its timestamp error was 0.9 m. This increase in observed error shows that the control systems performance is degraded when the virtual leader information is passed through a radio. The position error difference of aircraft 3 is 0.6 m, corresponding to a delay of 0.33 s. This delay includes the internal time delay of the onboard computer, which when removed reveals a radio induced time delay of 0.18 s.

The coordinated turn position errors of aircraft 3 agree with the time delay calculated above. The position error difference of aircraft 3 was 1.2 m. Because aircraft 3 was on the outside of the turn, its formation position moved faster than the 4.0 m/s maximum speed allowed. The time delay was 0.3 s, similar to the 0.33 s time delay found during straight and level flight.

During the flight test, neither aircraft deviated markedly from the intended spacing. The timestamp-evaluated spacing between the aircraft is shown in Fig. 4.12, showing the spacing during a large portion of the flight. Most of the flight was straight and level, with two coordinated turns at times 1415 s and 1480 s. The aircraft maintained the correct spacing of 20 m during most of the operation, while spacing discrepancies during the turns were less than 1 m.

4.5.2 *Discussion of Flight Test Data*

Flight testing results exhibited delays in the system. Sources of these delays were internal to the aircraft, as well as from inter-agent communication. Delays internal to each aircraft systems were 0.15 s, resulting in consistent position errors. This delay was created by the messaging time between the ROS nodes and the time for MAVROS and PX4 to communicate. The total delay limited the performance of each aircraft.

The radio-induced delay during the transmission of messages from the aircraft running the Big Sister to follower aircraft affected the follower's performance. This radio delay of 0.18 s contributed to the followers' overall position errors. This delay also affected each aircraft's knowledge of other aircrafts' positions. The radio delay between aircraft increased the minimum safety distance required.

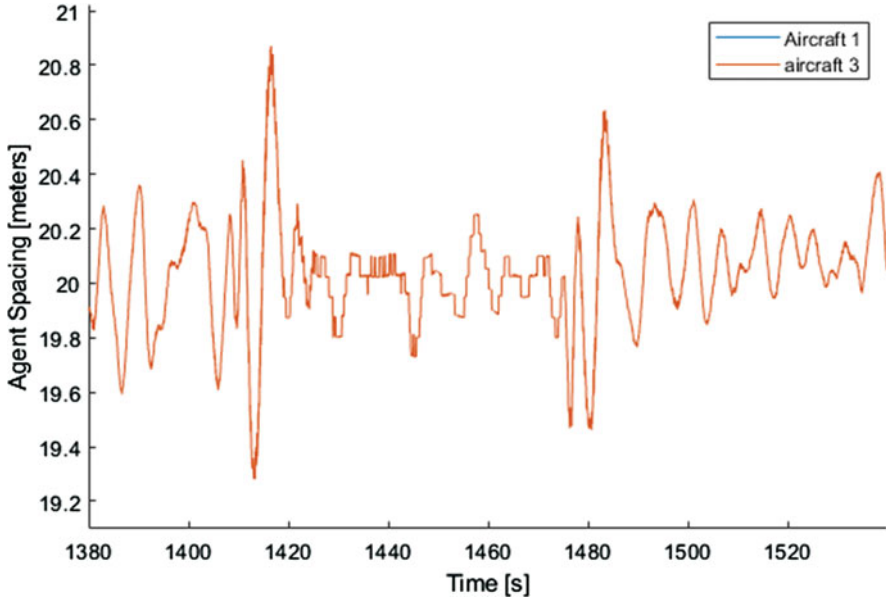


Fig. 4.12 Aircraft spacing, calculated with timestamp data, during virtual leader flight test. The two lines are identical and superposed

The observed position errors of each aircraft provided the information needed to evaluate the performance of the PD control loop. During straight and level flight, the observed errors were less than 0.3 m. This showed that the PD control loop was able to effectively guide aircraft during steady-state flight. During the coordinated turn, however, the observed errors were 4.5 m or greater. This showed that the PD control loop was not well suited to guide the aircraft in non-steady-state conditions.

While the above position errors were with respect to the virtual leader, relative to each other, the two aircraft were able to maintain the correct spacing, with an error of less than 0.9 m.

4.5.3 Comparison of Simulation vs Flight

The results of the flight test were compared to the simulation to evaluate the performance of the multi-agent coordination system and to evaluate how well the simulator models the flight test platform. Internal delays onboard each aircraft (e.g., ROS, PX4) were shorter on the flight test aircraft than in the simulation. The delay onboard the flight test aircraft was 0.15 s, compared to 0.23 s in the simulation. The radio communication added a 0.18 s delay to all aircraft communications, which was not modelled in the simulation.

In straight and level flight, the simulator accurately modelled flight test aircraft performance. In coordinated turns, position errors were smaller in the simulator than with the flight test aircraft. The higher performance level of the simulator was explained by the lack of radio delays.

In both the simulator and the flight test, the PD controller was shown to have reasonable performance during straight and level flight, whereas it was ineffective during coordinated turns. These problems were compounded on the flight test aircraft by the addition of radio delays.

In both the simulator and the flight test, even when the aircraft had significant position errors with respect to the virtual leader, they were able to maintain the correct spacing among themselves, showing that both systems were able to maintain system safety, even during coordinated turns.

Thus, the flight testing data shows that the aircraft are able to maintain a position within a formation with an error of approximately 1.2 m in straight and level flight. The coordinated turn error peaks at 9 m. Improvements made and verified in the simulation are expected to transfer to the real world, reducing the peak error in coordinated turns to less than 7 m. Given the spacing between the aircraft, the position errors represented a 6% straight and level flight position error. The coordinated turn error was recorded as up to a 95%, but it should be easily improvable to 75%. The aircraft spacing was normally close to the expected distances, and any significant variations were larger distances between aircraft not smaller distances.

4.6 Conclusion

This work has demonstrated an onboard, multi-agent, formation control system based on a virtual leader. The coordination system was able to run onboard the aircraft, without any ground station support. The aircraft coordination system was able to maintain aircraft positions with respect to the virtual leader with an error of less than 0.7 m when travelling in straight and level flight. The position error with respect to the virtual leader was larger (≤ 9.2 m) during a coordinated turn. However, the error between the follower aircraft was less than 1 m.

The PD control system of the follower aircraft was shown to have poor performance in both simulation and flight testing. Although it performed well during straight and level flight, the PD loop did not accurately guide the aircraft during the coordinated turns. It was also shown that other aspects of the control, such as the safety speed limit, were detrimental to the system performance, preventing the aircraft from flying at the speeds that were required by the formation. Additionally, delays both internal to the aircraft system and from radio communication added to the position error.

The emergency evasion system created for this project was effective. The time delay between the aircraft affected the minimum safe spacing of the aircraft. Longer communication delays required larger minimum spacing.

The virtual leader coordination system developed here is a centralized system, which can be run onboard any aircraft in the system. Presently, the virtual leader is not fully agent-independent and is only run on one aircraft. If the virtual leader stops functioning on one of the host aircraft, it does not automatically resume on another aircraft. The emergency evasion system created for this work was decentralized and, therefore, fully agent-independent.

This system provides a foundation that can be used for further multi-agent development or can be used to allow multiple aircraft to be operated in formation flight.

References

- Reynolds CW (1987) Flocks, herds, and schools: a distributed behavioral model, in computer graphics. SIGGRAPH '87 conference proceedings
- Reynolds C (2001) Boids: background and update. September 6. Accessed 14 Aug 2020. <http://www.red3d.com/cwr/boids/>
- Vachon M, Ray R, Walsh K, Ennix K (2003) F/A-18 performance benefits measured during the autonomous formation flight project. <https://doi.org/10.2514/6.2002-4491>
- Yang X, Deng L, Wei P, Li H, Liu J (2020) Multi-agent autonomous operations in urban air mobility with communication constraints. <https://doi.org/10.2514/6.2020-1839>
- Zhang J, Yan J, Zhang P (2018) Fixed-wing UAV formation control design with collision avoidance based on an improved artificial potential field. IEEE Access 6:78342–78351. <https://doi.org/10.1109/ACCESS.2018.2885003>

Chapter 5

Applications of Drones in the Health Industry



Kursat Alp Yigit, Alper Dalkiran, and T. Hikmet Karakoc 

Acronyms

AED	Automated external defibrillator
CPR	Cardio-pulmonary resuscitation
EMS	Emergency medical services
GNSS	Global navigation satellite system
OHCA	Out-of-hospital cardiac arrest
UAS	Unmanned aerial system
UAV	Unmanned aerial vehicle

5.1 Introduction

The definition of Unmanned aerial systems (UASs), Unmanned aerial vehicles (UAVs), or drones can be made as no passenger carries pilotless devices in the air (Gupta et al. 2013). Those airplanes have some types of equipment as a payload; those can be cameras such as high-resolution cameras, thermal cameras, laser

K. A. Yigit (✉)

Eskisehir Technical University, Institute of Higher Education, Eskisehir, Türkiye

A. Dalkiran

School of Aviation, Suleyman Demirel University, Kecioburlu, Isparta, Türkiye

e-mail: alperdalkiran@sdu.edu.tr

T. H. Karakoc

Faculty of Aeronautics and Astronautics, Eskisehir Technical University, Eskisehir, Türkiye

Information Technology Research and Application Center, Istanbul Ticaret University, Istanbul, Türkiye

e-mail: hkarakoc@eskisehir.edu.tr; thkarakoc@ticaret.edu.tr

scanners, location sensors for navigation, or other valuable payloads. In recent years, users have preferred to command UAVs with their autonomous functions instead of remote control. Furthermore, the use of UAVs is increasing worldwide for hobby and commercial purposes such as photography; military and scientific benefits are also preferred (ICAO 2011). This demand has created an industry that is altering the plans worldwide. The primary reason for choosing UAVs can be summarized as easily reachable worldwide.

There are many names for UAVs. “Drones” or “UAV/UAS” can be found in the international literature, and they mean the same thing. There is no distinct separation between those names, except for a particular technical feature. UAVs should not be understood only as an airplane flying in the air. In this context, UAVs consist of three components (Narayanan and Ibe 2015)

- The aircraft itself
- The payload on the plane
- The ground control station

Recently, significant innovations have been observed in hardware, software, and networks related to drones. The use of lighter composite materials in the structure of the drones and the integration of the Global Positioning System (GPS) enable the drones to perform more efficient flights. Depending on the technological developments in lithium batteries, drones can fly longer distances (Raffaello 2014). Moreover, with a webcam integrated into the drones, communication is provided by a control center (Prigg 2014).

The applications of drones in the healthcare field is a new but rapidly developing technology. With their valuable functions, drones successfully deliver drugs, blood (Amukele et al. 2015), vaccines (Haidari et al. 2016), and similar medical samples that are urgently needed to places where access is difficult. As far as we know, there is no comprehensive review presenting research on the health applications of drones. This review summarizes the current knowledge on the use of drones in healthcare and sheds light on future research.

5.1.1 Health Industry Needs for Transportation

AED Access to Cases

The defibrillator device is essential for recovering the heart rhythm in the prehospital event. The UAVs can provide 32% faster access rates to deliver defibrillator devices to patients in urban areas (Claesson et al. 2016). This figure becomes 93% in rural areas where helicopters and ambulances cannot reach most cases.

Drug/Tissue, Blood Product Transportation

Studies have shown that drone use can be strikingly detailed on organ transfers. The transferred tissue can be affected by vibration during flight. Also, other physical effects such as pressure and temperature may affect the transported tissue. Transportation must be planned in detail to overcome the abovementioned problems. Tissue transfers to complex regions can be effective compared to traditional logistic methods.

Telemedicine/Telesurgery

The resuscitation task could be harmful and complex for those who haven't learned this in medical school. It has become a simple task with the aid of peripherals equipped like a camera, microphone, speaker, and Automated External Defibrillators (AEDs) used over a patient who needs CPR.

5.1.2 Commercial Applications of Drones

Severe developments in information technologies, which started in the 1980s, made it necessary for companies to reorganize their activities and brought radical changes in the modern economy. Today, drone technology affects all sectors from infrastructure to agriculture on a large scale, creating effects similar to severe developments in information technologies (Mazur et al. 2016). In a short time, all customers will begin to see the impact of drones in all areas of the economy.

The fact that drones can travel their flight distances quickly and concisely has made their use very attractive in sectors requiring mobile and higher image quality. Using drones in daily activities in large-capital projects such as infrastructure and agriculture provides excellent benefits. The potential for drones to advance in the insurance and mining industries will drastically change the delivery process in the transportation industry. The increase in technological opportunities, legal regulations, and developments in investment support has enabled drones to be used in many new areas. Drone technology in these areas has led to new business and operation models. The Drones can be a helpful solution in some industries that require delivery constraints like time and capacity. Also, those industries may have gained some competitive advantage by using a low-cost solution.

Infrastructure

Drones have been used in various infrastructure management recently. Over time, this usage will become permanent and will develop further. While drones perform

dangerous jobs successfully, they also serve different data efficiently, precisely, and at low cost. The contribution of drones in many infrastructure sectors is faster than in the energy, road, oil, and gas sectors. Small-sized drones are often used in civil infrastructure works. These drones are easy to use and have flexibility in infrastructure-related activities. The flight altitude is up to 10,000 feet (Nex and Remondino 2013). Current Federal Aviation Administration (FAA) regulations limit flight altitudes for civilian drones to 400 feet (FAA 2013). We can list drones in the infrastructure sector as investment monitoring, maintenance, and asset inventory.

Providing real-time awareness and accuracy during the construction process is complicated. It is accepted that drones will successfully deliver actual data to this challenging process. Drones can significantly increase the speed and quality of the design process by providing precise field data during the preconstruction process. It can also quickly observe construction sites during construction, collecting detailed data for progress reports. It supports investors in monitoring the construction sites, controlling the determination of the site boundaries, and storing the materials to be used. The information provided by the drones is automatically recorded, which allows the investor to access complex data more quickly. This rapid process shortens the response to problems and enables a more accurate analysis of results.

Maintenance is one of the essential parts of the infrastructure sector. Today, most maintenance work is done manually and is provided by personal inspections. On the other hand, this process leads to slow, costly, and low-quality results. With the use of drones in maintenance, acceleration of the process, reduction of costs, and significant quality improvement have been achieved.

Per developing technology, drones have also started to be used in inventory counting and inventory management in infrastructure companies. The use of drones allows the company to reduce costs, speed up the process, and, at the same time, provide detailed information about the assets. Since rotary-wing drones can easily reach hard-to-reach and dangerous areas, workplace safety is increased by preventing human life from being put at risk.

Insurance

Two negative trends affecting the insurance industry today are the increase in natural disaster damage and fraud. An insurance company can improve its procedures using drones, including risk monitoring, risk assessment, and claims method.

Insurance claims arising from natural disasters in the insurance sector have been on the rise recently. For this reason, it is of vital importance to respond quickly to the monitoring centers of the areas exposed to natural disasters by monitoring them with drones. To reduce this increase, monitoring activities to be carried out by drones and analysis of the collected data are required.

Using drones while making risk assessments in insurance transactions will be useful in solving many problems that may arise. Accurate risk management can be done, and insurance processes can be supported thanks to the data provided by drones.

Media and Entertainment

In parallel with the developing technology, one sector that uses drone-assisted solutions is the media and entertainment sector. Aerial photography is the area where drones are commonly used. Another application is to use drones as broadcast relays. In massive sporting events, such as bicycle races and motorcycles record competitions. The streams are sent to TV studios or stage management using helicopters. Because using drones to transmit video streams is cheaper than using a helicopter or setting up a road-wide infrastructure (Freitas et al. 2010). Shooting commercials and movies using drones is a frequently used method today. Drones are commonly used in wildlife documentaries. Using drones creates a lower cost for image capture than airplanes and helicopters. Drones were used in shooting movies, and outstanding results were obtained.

Telecommunication

Drones can take an active part in some of the most challenging tasks facing companies in the telecommunications industry. It can help this industry get rid of maintenance, system optimization, and cost problems. It also contributes to infrastructure services by using it in the broadcasting of telecommunication signals. Drones help with antenna control by taking video, measurement, pictures, and reading information. They help companies by using the advantages of security, low cost, and high speed.

Agriculture

Drones have a wide range of uses in the agricultural sector in the fields of irrigation, spraying, soil analysis, planting, and crop monitoring (Ahirwar et al. 2019) Drone technology attracts producers in the agricultural sector for low cost and takes necessary precautions by monitoring the crop. Drones are used at every stage of a crop's life cycle, from choosing the right time to harvest to analyzing the soil to planting the seed. Drones help to drastically reduce planting costs by creating excellent three-dimensional (3D) maps that allow soil analysis while planting seeds. Drones also successfully carry out crop spraying activities. As a result, drones will continue to provide important services to the agricultural sector in terms of crop growth and productivity with their ease of use and low cost.

Security

With their speed, size, and maneuverability, drones help to perform imaging tasks faster and more effectively in current technology. Drones can quickly reach hard-to-

reach and large-scale areas, allowing operators to perform their traditional monitoring tasks more effectively. Drones can scan to a large extent by tracking objects safely by providing live streaming. Drones can remotely explore whether the area is safe for the response team to enter a location and perform an accident assessment.

Mining

Drones can do the activities of humans in the mining industry, where dangerous work is done intensively with the workforce. Its less costly and versatile use has accelerated the implementation of this preference. Drones cause less pollution than mining vehicles due to their ease of use.

Appropriately, drones can be beneficial in monitoring, surveying, and mapping of mines (Xiang et al. 2018). Drones can quickly map the open pit site, optimize mine transport routes, and securely provide control information. It can also reduce the cost of mining by supporting and automating the entire extraction process.

Transport

Depending on technological developments, it is seen that drones have outstanding potential in the transportation sector. Drones continue to be used in a wide area in this sector, especially in e-commerce package delivery, drug transportation, spare parts delivery, and intraday food delivery. It is indisputable that drones will be used more in the transportation sector than other methods based on human power, speed, accessibility, and low-cost advantages. We can classify the usage areas of drones in transportation as package delivery, spare parts delivery, medical logistics transportation, and food delivery.

Drones can make fast delivery to a predetermined point without much human activity. Other areas where drones are gaining popularity for delivery are spare parts and food delivery. Due to the fast delivery time and low cost of drones, many corporate companies are looking for the most economical way to make their deliveries. However, drones' most significant obstacles in their delivery business are limited flight endurance and payload capacities, which directly affect the costs. Improving the energy capacity using batteries does not mean improving the distance of the flight. The optimum number of batteries and energy capacity should be determined and engineered to achieve maximum flight endurance for electrically powered drones (Dorling et al. 2016).

Medical Logistics

The two most important areas where drones are used in medical logistics are drug and defibrillator transport. In delivering medical supplies to remote rural areas with drones, the high need in these regions and the low risk come to the fore. Since drones

are not affected by traffic delays, they can deliver medical samples to healthcare workers faster under ideal storage conditions. Drones can provide defibrillators very quickly to patients who have had a heart attack, significantly increasing the survival rate.

5.1.3 Most Chosen Drone Types in Health Use

Multi-rotors Drones

Multi-rotor drones consist of two or more rotors and propellers, while the flight mechanism relies on the lift produced by the propeller. These drones are piloted by varying the speed of the rotor. The quad-rotor is the most used one among these types of drones. These drones can fly at high speeds and hover at any altitude or fly at low speeds. Also, these drones can take off and land vertically. Multi-rotor drones are used for short-range and short-term missions because of their low durability (Petricca et al. 2011).

Multi-rotors are suitable for specific missions, and their configuration depends on the requirements of those missions. However, rotary-wing drones have a simple system and high maneuverability. However, they have a very high power consumption due to their aerodynamic disabilities. Weight and energy are also serious barriers for multi-rotors.

Multi-rotor drones are more reliable in motor failures than quad-rotor or tri-rotor drones and are suitable if high efficiency is desired. However, bi-rotor drones are inefficient systems and always require other mechanisms such as tilt rotors or moving masses to control (Siddhardha 2018). If the torques of the opposing motors of the quad-rotor are unequal, the drone can rotate about the longitudinal and lateral axes.

Quad-rotors

Quad-rotors have been one of the most popular drones among drone designers due to their simplicity of construction and control. A lot of research is being done on these types of drones. The general structure of quad-rotors consists of four motor-propeller pairs mounted at all four corners of the frame. The quad-rotor drone movement has been designed to turn the same direction on the same handle and the opposite direction in the neighbor motor. The engine speed or the rotor speed must be increased or decreased while climbing and descending with these drones accordingly. Also, the rotor speed change allows the quad-rotor drone turn around the yaw axis and vice versa (Ghazbi et al. 2014).

This drone has many advantages: low cost, high maneuverability, simple dynamics, and a fixed-pitch propeller. Like multi-drones, energy management is an issue in those drones—the dangers of use in an urban environment are another issue

(Sabatino 2015). As a result, their simple structure, ease of use, and hovering capability in the air increase the interest in this type of drone. Compared to fixed-wing drones, their efficiency and cruising speed are lower, and their maximum altitude is limited.

Fixed-Wing Drones

Fixed-wing is a classified version of a classic drone application that uses its wings for takeoff. These drones have different wing designs. Depending on the task they perform (Hassanalian and Abdelkefi 2017), there can sometimes be more than a pair of wings (Stempeck et al. 2018). Configurations of fixed-wing drones may vary by the shape of their tail, the number of wings placed, and the shape of the wing. However, the flight phenomenon is realized by the created lift using the wing surfaces dynamically. The differences in fixed-wing drones increase the maneuverability, payload capacity, and performance characteristics.

Fixed-wing drones consist of a wing, tail configuration, and fuselage. The engine produces the necessary forward movement to create lift. These drones have a simple structure and generate propulsion using fuel motors (Guido et al. 2019), solar energy, and battery-powered electric motors (Hassanalian et al. 2014a, b). Compared with the other types of drones, fixed-wing drones' endurance or operational ceiling is more remarkable. They need a runway for takeoff and landing, and they cannot hover. Despite these current shortcomings, the most widely used drones are fixed-wing drones.

Compared to other drones, fixed-wing drones have the most advanced design and are easiest to manufacture. Search, rescue, surveillance, delivery, imaging, defense, and fire extinguishing activities are the most used application areas. Because of this wide usage area, many companies and researchers worldwide are developing fixed-wing drones. At the same time, it has many advantages such as low cost of use, flight durability, and use in dangerous missions (Panagiotou and Yakinthos 2020). The available fuel limits the longer endurance of fixed-wing drones. More potential is available as long as performance characteristics can be improved.

Large fixed-wing drones perform very well at high altitudes and speeds, while small-wing drones may face difficulties due to their low speed and size. These drones are susceptible to wind speed and direction and can fly at low altitudes with a high level of turbulence.

VTOL Operations

Vertical Take-off and Landing (VTOL) drones can land and take off vertically using helicopter mode and perform high-speed forward flight in airplane mode. These drones are excellent aircraft that combine fixed-wing aircraft's speed and fuel efficiency with the hovering and flexibility of rotary aircraft. It can fly at varying altitudes depending on the body profile, but this flight is usually at low altitudes.

Thanks to its high maneuverability, it has a significant potential for building damage analysis and rescue operations in a complex urban building environment and the detection and image transfer of an incident area with its hovering ability. Their small size dramatically increases the potential for these drones to be used in scientific research applications (Watts et al. 2012).

The fact that VTOL drones do not need a runway for landing and takeoff and can fly for a long time by floating in the air causes them to attract close attention from researchers and commercial companies (Jo and Kwon 2017). The fact that they can land and take off vertically and have the advantages of both multi-rotor and fixed-wing drones increases the demand for these drones (Yu et al. 2016). Countries are investing to do more research on these drones to improve the advantages of VTOL drones (Zhao and Zhou 2018).

5.2 Operational Usage of Drones in Health Industry

A drone is a flying device remotely controlled by a person or computer. It is used as an actual study. It has a wide range of audio-visuals (Amukele 2019), security, surveillance, energy (Sreenath et al. 2020), and health (Mallek et al. 2020). The possibilities offered by drones allow researchers, manufacturers, and other organizations to conduct research that increases the efficiency of these devices and improves their medical results (Tucker 2017).

Drones are used in health industry due to their technical possibilities and ease of use. In the healthcare industry, drones can be used to ensure disaster assessment when the disaster area is severely restricted to human access. Also, drones can be useful for delivering medicine, vaccines, blood, and other medical supplies to remote locations in disaster areas. Furthermore, medical staff can benefit from drones by transporting test samples, and medical kits, if it is not a disaster case.

As a result of the extensive literature research, it has been observed that the resources related to medical applications are gathered under three main headings. These main topics are public health/disaster relief, telemedicine, and medical transport. We can examine public health/disaster relief under the headings of mass casualty care, data collection, infectious diseases, disaster relief, and emergency medicine. Diagnosis–treatment and telesurgery categorize telemedicine applications into two subjects. We can divide the medical transportation application into tissue, medication, medical device, and patient subheadings.

5.2.1 *Public Health and Medical Surveillance*

There is an advantageous use of drones in disaster areas, primarily used for surveillance of disaster areas, in monitoring activities of the regions where epidemic disease is present, and in places where biological and chemical hazards occur. They



Fig. 5.1 Five people in search with the classic line (Karaca et al. 2017) technique

effectively collect real-time information that makes up the current data of victims and patients in high-risk areas where urgent intervention is needed (Hlad 2015).

After Typhoon Haiyan hit the Philippines in 2013, drones evaluated the initial damage and prioritized required tasks before the rescue operations (Hlad 2015). The use of drones is being investigated to estimate injuries caused by chemical, biological, and nuclear materials to increase the effectiveness and improve the response field teams in England (Aron 2016).

Drone technology is used to combat severe chemical hazards that threaten health, such as heavy metals, aerosols, and radiation. A high-resolution-equipped drone was used to accurately detect and predict cancer risk from high concentration of copper present in the agricultural region in Southern Italy (Capolupo et al. 2015). Brady et al. (2016) used a quad-rotor drone to measure aerosol and gas levels in complex terrain. In addition, drones are used to map radiation from uranium in nuclear accidents (Tang et al. 2016) and to detect radionuclides (Martin et al. 2016). Fornace et al. (2016) used drones to identify the distinctive features of the terrain and the shape of deforestation patterns of malaria parasites in Malaysia. Also, researchers mentioned using drones to detect *Staphylococcus aureus* and Ebola virus in recent studies (Priye et al. 2016).

Disinfecting large areas and hard-to-reach areas in the fight against the coronavirus is critical in changing the course of the epidemic. The use of drones in such regions will minimize the struggle with humans and ensure the protection of human resources. In many public areas, spraying disinfectant is carried out by drones. This process increases work efficiency and safety compared to manual disinfection (Poljak and Šterbenc 2020). Figures 5.1 and 5.2 show the application of the classic line technique.

Drones integrated with a thermal camera can detect each person in crowded areas with high-sensitivity infrared rays. Thanks to these possibilities of drones, it is possible to detect people with high fever and take precautions by detecting the



Fig. 5.2 When any image that was judged to be representative of the mannequin was detected, the drone began descending to sharpen the image (Karaca et al. 2017)

human body temperature in the group. The use of drones, which can be integrated with all kinds of cameras and sensors, as a public health surveillance tool is applied in many life-saving events. Recently, police units have been using drones for surveillance to identify criminals (Bennett 2011).

In reaching victims stranded in mountainous areas, drones have proven to be an essential tool by detecting victims in 10 minutes, which search and rescue teams can do in 60 minutes (Karaca et al. 2017).

Drones are also useful in finding and identifying water areas, which are the habitats of mosquitoes, with their surveillance activities such as video and photography. In a study conducted in the Zanzibar archipelago, drones' detection of mosquito habitats has been done effectively (Hardy et al. 2017). Drones have a wide range of use in the surveillance/epidemiology of infectious diseases, especially vector-borne diseases. Drones equipped with sensors and artificial intelligence can access geographically referenced information about water, salinity, vegetation, and temperature (Peckham and Sinha 2019).

5.2.2 *Telemedicine*

The health industry encourages using drones for telemedicine applications—the application of diagnosis and treatment of patients remotely via telecommunication is a well-known approach (Breen and Matusitz 2010). The most crucial element in the field of telemedicine is telecommunications. On the other hand, telesurgery enables surgical procedures to be performed using robotic technology at a distance from the surgeon and patients (Harnett et al. 2008).

Medical and aviation experts in the United States have also developed a drone with special sensors, infrared devices, and telemedicine capabilities as part of the Health Integrated Rescue Operations (HIRO) Project. With this technology, which combines medical and aviation technologies, it has been ensured that healthcare professionals provide guidance services by using telemedicine, which is the need during the first response. Drones perform vital tasks as a point of contact for telesurgery use in military battlefields to reduce delays in surgical intervention (Harnett et al. 2008).

5.2.3 Drones as Medical Transport Systems

In recent years, rapid developments and growth in robotization and process automation have enabled companies to turn to drone technology. When drones' speed and low costs are added to these rapid developments in technology, the use of technology-integrated drones in solving transportation problems becomes attractive (Kim, 2020; Euch, 2020). The effectiveness of drones is felt most in the distribution of medical drugs and materials to critical areas and the transport of test samples from these areas to the relevant laboratories (Spring 2017).

In healthcare, the use of drones in medical transportation is presented in a wide range of areas, including the delivery of drugs (Hackman and Nicas 2015), defibrillators, blood samples (Preimesberger 2016), and vaccines to the areas where they are needed (Prigg 2014). For example, autonomous drones used by Matternet use GPS and other sensors to deliver medicines to hard-to-reach areas (Raptopoulos 2013). After the earthquake in 2010, the Matternet drone took part in the distribution of drugs in Haiti and the Dominican Republic (Choi-Fitzpatrick et al. 2016) and New Guinea and Switzerland (French 2015). Matternet also works with United Nations International Children's Emergency Fund (UNICEF) and the Doctors Without Borders group. Figure 5.3 shows an example of inaccessible locations.

Matternet drones can carry payloads between 1 and 2 kg (French 2015). It has the opportunity and ability to cover a distance of approximately 10 km at a speed of 40 km per hour (Raffaello 2014), including takeoffs and landings, in 18 minutes (Prigg 2014). With a smartphone application, senders can choose from the list of possible destinations. The drones automatically create a route in the next stage depending on the terrain, weather, airspace, and population density. Airports, schools, squares, hills, and buildings should be avoided while creating the route.

The German logistics company DHL Parcel has explored four generations of medical delivery with drones called Parcelcopter (DHL 2016). The first generation drone shown in Fig. 5.4. has completed its mission of delivering blood samples, covering the 1 km route along the Rhine in Bonn. The second generation was tested in 3 months' delivery of medicines and other urgently needed supplies to Juist, Germany's most remote settlement in the North Sea Islands (Agatz et al. 2015). During this delivery, the drone covered 12 km in open seas (Varnholt 2016). The third-generation drone was tested between January and March 2016 as part of the



Fig. 5.3 Difficulties due to inaccessible roads, use of Matternet drone (What to Know When Using Humanitarian UAVs for Transportation 2015)

Fig. 5.4 Parcelcopter:
DP/DHL's future air courier
(DHL 2016)



aging activity between two Bavarian Alpine Villages and Skyparts of more than 130 parcels of urgently needed medicines and sporting goods. This drone achieved serious success by making deliveries in 30 minutes under winter conditions in as little as 8 minutes (DHL 2016). The fourth-generation drone was tested over 6 months for drug delivery to an island in Lake Victoria, Tanzania.

This drone is a fixed-wing trimotor that can carry medical supplies up to 4 kg, has a flight range of 65 km, and can reach speeds of up to 140 km per hour (Deutsche post DHL group 2018).

It is indisputable how vital the concept of time is in emergency medical situations. The logistics company UPS and Zepline companies continue to work on a network of drones to transport vaccines and blood samples to 20 long-distance clinics in Rwanda (Preimesberger 2016; Tilley 2016). Rwanda has one of the highest rates of maternal death and infant mortality in the world due to malaria. Because the roads become unusable during the rainy seasons in this region, the urgently needed rabies vaccines can be transported to the relevant regions using drones. Only one third of

the people in Africa live 2 km from the highways that can be used all year (Khazan 2016).

Zepline drones deliver medical supplies by launching them from a slot and dropping them into needed areas with paper parachutes. After the drone completes its mission and returns to its home, blood or vaccines are loaded for the next delivery, and the activity is continued by inserting a sim card and a new battery. Zeppelin drones can fly 45 miles in 30 minutes, and delivery routes are tracked with a tablet application, and this route can be changed if desired (Khazan 2016).

The first medical supplies delivery using an FAA-approved drone has been successfully made to a healthcare clinic in southwestern Virginia (Pepitone 2015). This clinic can serve 3000 patients at the end of each week of the year (Hackman and Nicas 2015). Flirtey drones took the prescription products from the Wise County regional airport and delivered them to the clinic at the fairground, about 3 minutes away.

In 2007, a study with drones was conducted by the National Health Laboratory Service (NHLS) and Denel Dynamics researchers to more efficiently transport microbiological samples from rural clinics to NHLS centers for HIV testing. As a result of this research, the capabilities of drones that facilitate rapid diagnosis and medical decision-making have been determined (Mendelow et al. 2007).

In 2014, Me'decins Sans Frontie'res (MSF) used a drone-based system to send tuberculosis test samples to hospital laboratories. It was observed that the samples sent using drones took only 25% of the time taken for delivery by road (Médecins Sans Frontières 2014). Other studies determined that the integrity samples in fixed blood samples were similar to the blood samples carried by drones (Thiels et al. 2015). With the government's approval, the first medical delivery by drone in the United States was carried out at a clinic in Virginia. Thanks to this process performed by drones, the drug delivery process has been accelerated, and patient care has been improved (Hackman and Nicas 2015).

A similar practice was carried out between the UN Population Fund and the Dutch government, delivering birth control pills and gynecological materials to the relevant women's health clinics by drones to Ghanaian women (Cousins 2016). The US Postal Service has cooperated with Zepline company to deliver medicine, blood, vaccine, and medical supplies needed in Rwanda (Rosen 2017). Similar projects have started to be implemented in other developing countries such as Ghana (Mogombo 2016) and Rwanda (Mis 2016).

Although half of the world's population lives in rural areas, only a tiny part of them is located near the areas where professional health studies are carried out (World Health Organization 2010). Even in the United States, which is considered the most developed country globally, only 11% of doctors can serve people living in rural areas (University of Washington School of Medicine 2010). When the lack of health personnel, especially doctors, in these regions is added to the lack of appropriate diagnosis, testing equipment, and infrastructure problems, health services are faced with serious limitations. In addition, the lack of communication, Internet, and telephone can prevent healthcare professionals from reaching remote specialists and

laboratories, which negatively affects patient treatment (Anticona Huaynate et al. 2015).

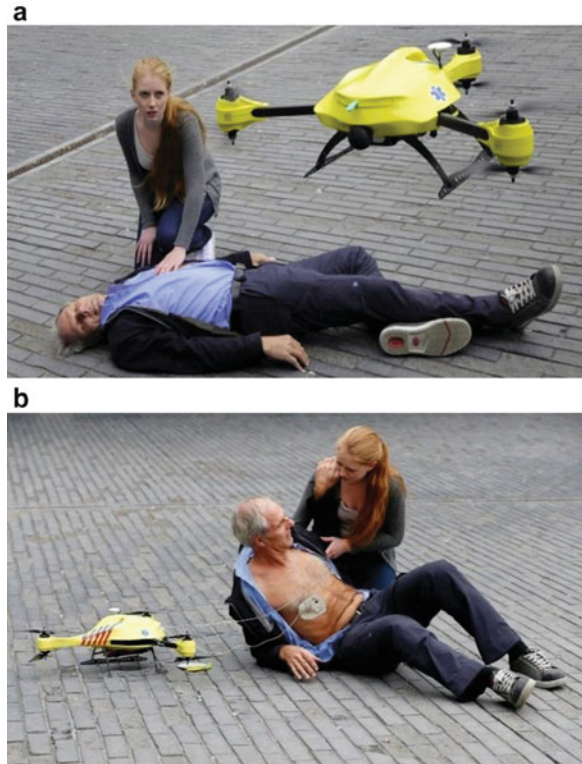
Amukele et al. conducted a study comparing the results obtained by transporting chemistry, hematology, and coagulation samples from healthy individuals using drones with the same type of samples in the laboratory environment. The test results determined that there was no significant difference between the two applications (Amukele et al. 2015). Preliminary reports of biological samples' routine chemistry, hematology, and coagulation analysis are appropriate for short-haul flights with drones at room temperature or colder (Amukele et al. 2017).

Drone activity is carried out successfully in Tanzania, one of the countries with the highest maternal mortality (556/100,000) globally. Drones could deliver the needed blood, vaccine, antiretroviral, and malaria drugs to more than 1000 health facilities with biodegradable parachutes faster than land transportation (Makoye 2019). Currently, organ/tissue transport uses a complex network of couriers, transport personnel, and commercial and private charter aircraft. Recently, a six-rotor drone has been used to model parameters related to organ transport (Scalea et al. 2019). In the kidney biopsy activities performed by keeping the temperatures constant and below 2.5 °C in 14 drone transport missions, no damage caused by drones was detected before and after the flight (Scalea et al. 2018). The first successful transport of a donated kidney to the University of Maryland Medical Center with a custom-built drone was carried out in April 2019 (Freeman 2019).

The ability of drones to move at high speed has made them vital in the transportation of AED devices that out-of-hospital cardiac arrests (OHCAs) need. This allows for reducing the defibrillation time in OHCA. In OCHA cases, the use of external defibrillators before the arrival of EMS makes a significant contribution by increasing the survival time by up to 30 days. Drones integrated with AED can reduce the defibrillation time in OHCA. Drones are used to deliver defibrillators to people to assist patients suffering from cardiac arrest. Researchers at Delft University in the Netherlands found how drones make things easier by providing AEDs within 2 minutes to any location within a 1.2 square mile radius (Hornyak 2014). In a computer-aided simulation study conducted in Salt Lake County, Utah, it was observed that drones could reach 96% of the county's population in less than a minute. In the traditional intervention by ambulance, only 4.3% of the cases could be born during this time (Pulver et al. 2016). In addition to these advantages, studies should increasingly continue to further improve the efficiency and performance of drones (Lippi and Mattiuzzi 2016).

Approximately 300,000 people in Europe are affected by out-of-hospital cardiac arrest (OHCA), which indicates that OCHA ranks among the top causes of death (Perkins 2015). The emergency medical services unit (EMS) in Sweden records about 5000 OHCA cases each year in the Swedish cardio-pulmonary resuscitation (SRCR) records (Herlitz 2015). Early defibrillation interventions have been shown to increase survival in OHCA cases. Delivery of the AED to the area of the OHCA event within the first minutes of the event results in significant increases in survival rate (Nordberg 2015). Studies show that in serious accident situations and for video

Fig. 5.5 The usage of drone in heart attack of a patient (Momont 2019). (a) Landing of AED-equipped drone. (b) Intervene with the patient



surveillance, drones will continue to be used by EMS to replace medical equipment (Floreano 2015, 85).

The ambulance drone used to resuscitate people who had a heart attack includes one AED. The ambulance drone moves at a speed of 100 km, has a 10-minute battery life, six propellers, and is painted yellow for easy identification. The drone in the ambulance has AED 50 shock delivery feature. A drone ambulance is integrated with GPS to locate the incoming emergency call. Figure 5.5 shows how a drone can intervene during a heart attack situation.

When the emergency call comes to the command center, the drone ambulance is directed to where the call was made. The webcam on the ambulance drone is the most important assistant of the health personnel in the call center. Thanks to this camera, instructions can be given to the personnel who will intervene with the person who has a heart attack. The AED is removed from the hatch with the instructions given from the emergency center using the webcam. The responder applies the AED according to the instructions from the webcam.

5.3 Assessment of Advantages and Disadvantages of Drone Types

Four primary types of drones can be addressed in the health industry. Those have been compared in Table 5.1 as fixed-wing, quad-rotor, multi-rotor, and VTOL drones. Multi-rotor and quad-rotor drones have been differentiated because of their fast maneuver and carry capacity. On the other hand, VTOL can describe both multi-rotor and quad-rotor drones; however, a particular function of operational endurance of fixed-wing and vertical movement capacity must have been highlighted. This capacity can be the powerful active function to be flexible through the long-range and limited takeoff and landing possibilities. Table 5.1 presents performance data of drone types used in health applications.

Operational usage of drones can be divided into two main branches: rigid-wing-type drones and rotational-wing-based drones. We may assume the first one as rotational-wing drones that we named them quad-rotor and multi-rotor ones. Also, the rigid-wing, also known as fixed-wing drones, can be divided into fixed-wing and VTOL drones. All the four categorized types of drones can be seen in Table 5.2.

The rotary-wing drones offer greater reachability and cost-effective solutions as described in the left two options. However, the need for energy and stability problems in windy meteorological conditions fails to conserve stability and control. Conversely, fixed-wing-style drones can be more stable and hard to reach because of non-cost-effective production properties. However, those drones have great endurance of the same amount of energy. Compared to the VTOL-capable fixed-wing drones, they have higher endurance than the rotary-wing drones, and they do not need a specialized long runway investment in crowded city areas. But both need long hours of training and experience to operate in congested areas.

Table 5.1 Drone types and health applications (Braun et al. 2019)

	Cargo capacity	Range	Maximal speed	Takeoff	Application in healthcare
Fixed wing	1.75 kg	160 km	128 km/h	Runway	Blood sample, vaccines
Quad-rotor	2.2 kg	20 km	40 km/h	VTOL	Blood sample, medications, equipment
Multi-rotor	2 kg	32 km	–	VTOL	Blood sample, medications,
VTOL	4 kg	65 km	140 km/h	VTOL	Blood sample, organs

Table 5.2 Operational usage reasons and drone types (Heutger and Kückelhaus 2014; Kelek 2015)

	Quad-rotor	Multi-rotor	Fixed-wing	VTOL
Advantages	Low cost High maneuverability Low energy consumption	Low cost High accessibility Great maneuverability Ease of use Vertical takeoff and landing (VTOL) Good camera control	Long endurance Large area coverage Fast flight speed Great stability Gliding capability	Long endurance Large area coverage Vertical takeoff and landing capabilities Easier to navigate in dense, urban environments, and even inside buildings Great stability Gliding capability
Disadvantages	Low endurance Limitation of battery capacity Small payload capacity Shallow stability in the wind	Higher energy consumption Short flight times Small payload capacity Low stability in the wind	High price Large take-off/landing zone required No VTOL/hover Challenging to fly; training is needed Low efficiency for area mapping	Shorter flying range Lower speed Smaller payload capacity High price Challenging to fly Challenging for landing

5.4 Future of Drones in Health Industry

Considering the growth in the drone industry, with the help of technology, the hearth of the operation will be the automation and the regulating legislation. The main question is to oversee and answer the future of artificial intelligence (AI) in the three-dimensional world (Li et al. 2016). Moving forward to the health industry's use of drones to help the patient recover, what if the drone injured somebody? Furthermore, what if the drone kills someone? Will there be a person responsible for this autonomous delivery?

Most of the problems of autonomous drones have not been discussed; however, the authorities listed below minimize the impact of the legal difficulties globally:

- International Civil Aviation Organization (ICAO)
- Joint Authorities for Rulemaking of Unmanned Systems (JARUS)
- European Aviation Safety Agency (EASA)
- Federal Aviation Authority (FAA)

The primary use of drones is to gain from time and the cost from the process of human interference and to ensure the operational processes are successful. It does

not matter whether the operation is a cargo or paper delivery. Monitoring a process by drones remotely with a high-definition video camera is another way of drone use in our world. Shortly, the health industry will find ways to integrate drones. Technology will answer the request from fast deliveries of blood samples, vaccines, medications, organs, and types of equipment.

The lack of infrastructure limits drone use in any industry as the persisting technical issue is another problem. As discussed earlier, the current quad-copter and multi-copter operational times are limited because of energy storage problems. Those drones cannot change the batteries automated or the next step interchangeable with other carrier companies. There may be ideas to use current gas station rooftops for automated interchangeable battery stations. But who will standardize the global battery standards for those devices? How could the stations account for the use of battery life cycle out of a thousand?

Using VTOL and fixed-wing drones for longer distances needs runway and heliport-like infrastructure investments, which seems it would not be possible in the current cost profiles. On the other hand, those drones need experienced pilots to be managed under control, especially on takeoff and landing phases. Certainly, there will be considerable time and cost-saving for those operations if the drones are integrated into the health industry.

Nonetheless, air traffic rules cannot be evaluated under only the traffic congestion in the urban areas; there are undoubtedly many risks carried with its operations by the health industry (Merkert and Bushell 2020). There can be a chaotic, uncontrolled environment with many drones in urban areas. So collision scenarios and collision avoidance must be in place as hardware-embedded rules if the autonomous flight and air rules are primary focus area. There is a ruling system that has been offered by Foina et al. (2015) UAS Traffic Management (UTM) system. This system provides three-dimensional parcel maps for landlords to approve or disallow the drone flights above their real estate boundaries. Another literature entry has been found to discuss the separation distances between the drones by Tan et al. (2017) in urban areas in two scenarios: (i) direct flight path and (ii) direct flight path with limited speed. The authorities mentioned namely ICAO, JARUS, EASA, and FAA will undoubtedly continue to discuss air traffic studies for the drones.

The size of the drone will be another issue in the future. Open skies will have significant and small players like ships in the open seas. There are sailing boats, giant cargo ships, and small boats in the open seas. The impact of a small drone and a heavy drone would not be equalized if an incident happens. The size of drones will change in the future to adapt to the needs of the health industry.

5.5 Conclusions

Drones have become a rapidly developing technology worldwide due to their technical features. Due to these features, UAVs have become significantly used in both military and civilian fields today. Since the health sector has sensitivities and

the need to react quickly, it has started to use drones effectively. It has become a valuable tool in the field of medicine, thanks to its ability to quickly solve the problems faced by both health personnel and patients. In this study, it is seen how drones increase the quality and effectiveness of helping healthcare professionals and patients in certain applications. UAVs play an important role in delivering medicines, vaccines, blood, and other medical supplies to rural communities. The essential healthcare area where drones are used is prehospital medical systems. The medical use of drones can be summarized as follows:

- AED transportation to the scene, medicine, tissue, blood products transportation, trauma kit
- Transportation of other materials
- Guiding for applications such as telemedicine

The use of drones in the intervention of a heart attack, which is one of the most common conditions in health, significantly increases the patient's survival rate. AED transport with drones and the use of ambulance drones in the healthcare field have been a beacon of hope for patients who have had a heart attack. In the future, improvements in the technical features of drones (speed, battery life, enlargement of size) will make it inevitable to use them in many different applications in the healthcare field.

Drones play an essential role in nonhospital interventions in the health sector due to their technical features. It is known how vital even seconds are for the survival of a person who has had a heart attack. Drones can provide rapid intervention to patients who have had a heart attack with the AED they carry. As can be observed from this study, it has been determined how quickly drones can intervene in the transport of AEDs to patients who have had a heart attack. This study will make it possible for us to see drones taking blood tubes in the emergency departments of hospitals in a short time. Depending on the developments in drone technology, it will be possible to transport patients who met with an accident to the emergency services or hospitals after the first intervention. As a result, the use of UAVs in the health sector will be an area that offers many opportunities for effective future studies.

References

- Agatz N, Bouman P, Schmidt M (2015) Optimization approaches for the traveling salesman problem with drone. ERIM report series research in management, Erasmus Research Institute of Management, Erasmus University Rotterdam. <https://doi.org/10.2139/ssrn.2639672>
- Ahirwar S, Swarnkar R, Bhukya S et al (2019) Application of drone in agriculture. *Int J Curr Microbiol App Sci* 8(01):2500–2505. <https://doi.org/10.20546/ijemas.2019.801.264>
- Amukele T (2019) Current state of drones in healthcare: challenges and opportunities. *J Appl Lab Med* 4(2):296–298. <https://doi.org/10.1373/jalm.2019.030106>
- Amukele TK, Sokoll LJ, Pepper D et al (2015) Can unmanned aerial systems (drones) be used for the routine transport of chemistry, hematology, and coagulation laboratory specimens? *PLoS One* 10:0134020. <https://doi.org/10.1371/journal.pone.0134020>
- Amukele T, Ness PM, Tobian A et al (2017) Drone transportation of blood products. *Transfusion* 57:582e8. <https://doi.org/10.1111/trf.13900>

- Anticona Huaynate CF, Pajuelo Travezaño MJ, Correa M et al (2015) Diagnostics barriers and innovations in rural areas: insights from junior medical doctors on the frontlines of rural care in Peru. *BMC Health Serv Res* 15:454. <https://doi.org/10.1186/s12913-015-1114-7>
- Aron J (2016) NHS to use drones to help chemical, bio and nuke response teams. *New Scientist*. Available via DIALOG. <https://www.newscientist.com/article/2075625-nhs-to-use-drones-to-help-chemical-bio-and-nuke-response-teams/>. Assessed 12 Nov 2017
- Bennett B (2011) Los Angeles Times. Police employ predator drone spy planes on home front. Available via DIALOG. <http://articles.latimes.com/2011/dec/10/nation/la-nadron-arrest-20111211>. Accessed 22 July 2017
- Brady JM, Stokes MD, Bonnardel J et al (2016) Characterization of a quad-rotor unmanned aircraft system for aerosol–particle-concentration measurements. *Environ Sci Technol* 50:1376–1383. <https://doi.org/10.1021/acs.est.5b05320>
- Braun J, Gertz SD, Furer A et al (2019) The promising future of drones in prehospital medical care and its application to battlefield medicine. *J Trauma Acute Care Surg* 87(1S):S28–S34
- Breen GM, Matusitz J (2010) An evolutionary examination of telemedicine: a health and computer-mediated communication perspective. *Soc Work Public Health* 25:5. <https://doi.org/10.1080/19371910902911206>
- Capolupo A, Pindozi S, Okello C et al (2015) Photogrammetry for environmental monitoring: the use of drones and hydrological models for detection of soil contaminated by copper. *Sci Total Environ* 514:298–330. <https://doi.org/10.1016/j.scitotenv.2015.01.109>
- Choi-Fitzpatrick A, Chavarria D, Cychosz E et al (2016) Up in the air: a global estimate of non-violent drone use 2009–2015. In: Joan B (ed) *Kroc School of Peace Studies at Digital University of San Diego*. <https://doi.org/10.22371/08.2016.001>
- Claesson A, Fredman D, Svensson L et al (2016) Unmanned aerial vehicles (drones) in out-of-hospital-cardiac-arrest. *Scand J Trauma Resusc Emerg Med* 24(1):1–9. <https://doi.org/10.1186/s13049-016-0313-5>
- Cousins S (2016) Condoms by drone: a new way to get birth control to remote areas. National Public Radio, Washington, DC. Available via DIALOG. <https://www.npr.org/sections/goatsandsoda/2016/05/19/478411186/condoms-by-drone-a-new-way-to-get-birth-control-to-remote-areas/>. Accessed 12 Nov 2017
- Deutsche Post DHL Group (2018) Rapid response from the air: medicines successfully delivered using a parcel drone in East Africa. <https://www.dpdhl.com/en/media-relations/press-releases/2018/rapid-response-from-the-air-medicines-successfully-delivered-using-a-parcel-drone-in-east-africa.html>. Accessed 17 Dec 2018
- DHL (2016) Successful trial integration of DHL parcelcopter into logistics chain
- Dorling K, Heinrichs J, Messier GG et al (2016) Vehicle routing problems for drone delivery. *IEEE Trans Syst Man Cybern* 70–85. <https://doi.org/10.1109/TSMC.2016.2582745>
- Euchi J (2020) Transportation, logistics, and supply chain management in home healthcare: emerging research and opportunities. IGI Global, Hershey. <https://doi.org/10.4018/978-1-7998-0268-6>
- FAA (2013) Integration of civil unmanned aircraft systems (UAS) in the national airspace system (NAS) roadmap. Washington, DC, USA. Available via DIALOG. https://www.faa.gov/uas/resources/policy_library/media/2019_UAS_Civil_Integration_Roadmap_third_edition.pdf. Accessed 16 Feb 2022
- Floreano D (2015) Science, technology and the future of small autonomous drones. *Nature* 521: 460–466. <https://doi.org/10.1038/nature14542>
- Foina AG, Krainer C, Sengupta R (2015) An unmanned aerial traffic management solution for cities using an air parcel model. In: 2015 International Conference on Unmanned Aircraft Systems (ICUAS), p 1295–1300. <https://doi.org/10.1109/ICUAS.2015.7152423>
- Fornace KM, Drakeley CJ, William T et al (2016) Mapping infectious disease landscapes: unmanned aerial vehicles and epidemiology. *Trends Parasitol* 30(11):514–519. <https://doi.org/10.1016/j.pt.2014.09.001>

- Freeman D (2019) A drone just flew a kidney to a transplant patient for the first time ever. It won't be the last. Available via DIALOG: <https://www.nbcnews.com/mach/science/drone-just-flew-kidney-transplant-patient-firsttime-ever-it-nca1001396>. Accessed 16 July 19
- Freitas EP, Heimfarth T, Netto IF et al (2010) UAV relay network to support WSN connectivity. International congress on ultra modern telecommunications and control systems, pp 309–314. <https://doi.org/10.1109/ICUMT.2010.5676621>
- French S (2015) Drone delivery is already here-and it works. Marketwatch
- Ghazbi SN, Akbari AA, Gharib MR (2014) Quad-rotor: full dynamic modeling, nonlinear simulation and control of attitudes. *Indian J Sci Res* 1(2):759–772
- Guido N, Mohammadi S, Hassanalian M et al (2019) Surface temperature effects of solar panels of fixed wing unmanned aerial vehicles on flight performance. AIAA Aviation Forum 17–21. Dallas, TX. <https://doi.org/10.2514/6.2019-3689>
- Gupta SG, Ghonge MM, Jawandhiya PM (2013) Review of unmanned aircraft system (UAS). *Technology* 2(4)
- Hackman M, Nicas J (2015) Drone delivers medicine to rural Virginia clinic. *Wall Street Journal*. Available via DIALOG. <https://www.wsj.com/articles/drone-delivers-medicine-to-rural-virginia-clinic-1437155114/>. Accessed 12 Nov 20
- Haidari LA, Brown ST, Ferguson M et al (2016) The economic and operational value of using drones to transport vaccines. *Vaccine* 34:4062–4067
- Hardy A, Makame M, Cross D et al (2017) Using low-cost drones to map malaria vector habitats. *Parasit Vectors* 10(29):1–13. <https://doi.org/10.1186/s13071-017-1973-3>
- Harnett BM, Doarn CR, Rosen J et al (2008) Evaluation of unmanned airborne vehicles and mobile robotic telesurgery in an extreme environment. *Telemed J Environ Health* 14:539–544. <https://doi.org/10.1089/tmj.2007.0087>
- Hassanalian M, Abdelkefi A (2017) Design, manufacturing, and flight testing of a fixed wing micro air vehicle with Zimmerman planform. *Meccanica* 1265–1282. <https://doi.org/10.1007/s11012-016-0475-2>
- Hassanalian M, Khaki H, Khosrawi M (2014a) A new method for design of fixed wing micro air vehicle. In: *Proceedings of the Institution of Mechanical Engineers*, pp 837–850. <https://doi.org/10.1177/0954410014540621>
- Hassanalian M, Radmanesh M, Sedaghat A (2014b) Increasing flight endurance of MAVs using multiple quantum well solar cells. *Int J Aeronaut Space Sci* 15(2):212–217. <https://doi.org/10.5139/IJASS.2014.15.2.23>
- Herlitz J (2015) Swedish register for cardiopulmonary resuscitation, annual report 2015. <http://www.hlr.nu/hjart-lungraddningsregistret/>. Accessed 20 July 2016
- Heutger M, Kückelhaus M (2014) Unmanned aerial vehicle in logistics: a DHL perspective on implications and use cases for the logistics industry. DHL Customer Solutions & Innovation, Troisdorf, Germany
- Hlad J (2015) Drones: a force for good when flying in the face of disaster. *The Guardian*. <https://www.theguardian.com/global-development/2015/jul/28/drones-flying-in-the-face-of-disaster-humanitarian-response/>
- Hornyak T (2014) Ambulance drones could bring defibrillators in minutes. *PC World*. Available via DIALOG. <https://www.pcworld.idg.com.au/article/558453/ambulance-drones-could-bring-defibrillators-in-minutes/>. Accessed 12 Nov 2017
- ICAO (International Civil Aviation Organization) (2011) Unmanned aircraft systems (UAS), Cir. 328, An/190
- Jo D, Kwon Y (2017) Analysis of VTOL UAV propellant technology. *J Comput Commun* 5(7): 76–82. <https://doi.org/10.4236/jcc.2017.57008>
- Karaca Y, Cicek M, Tatli O et al (2017) The potential use of unmanned aircraft systems (drones) in mountain search and rescue operations. *Am J Emerg Med* S0735-6757(17):30750–30757. <https://doi.org/10.1016/j.ajem.2017.09.025>
- Kelek BS (2015) Blue sky birds come to the world. *J Int Trade Logist Law* 1(1):41–49
- Khazan O (2016) A drone to save the world. *The Atlantic*

- Kim SH (2020) Choice model based analysis of consumer preference for drone delivery service. *J Air Transp Manage* 84:1017–1085. <https://doi.org/10.1016/j.jairtraman.2020.101785>
- Li J, Zhao X, Cho M et al (2016) From trolley to autonomous vehicle: perceptions of responsibility and moral norms in traffic accidents with self-driving cars. SAE technical paper 01. <https://doi.org/10.4271/2016-01-0164>
- Lippi G, Mattiuzzi C (2016) Biological samples transportation by drones: ready for prime time? *Ann Translat Med* 4:92. <https://doi.org/10.3978/j.issn.2305-5839.2016.02.03>
- Makoye K (2019) Buzz as world's biggest drone drug deliveries take off in Tanzania. Available via DIALOG. <https://www.reuters.com/article/ustanzania-health-drones/buzz-as-worlds-biggest-drone-drug-deliveries-take-off-in-tanzania-idUSKCN1B91F7>. Accessed 17 July 2019
- Mallek M, Euchti J, Jerbi Y (2020) A review on optimization modeling of hybrid energy systems. In: Euchti J (ed) *Transportation, logistics, and supply chain management in home healthcare: emerging research and opportunities*. IGI Global, Hershey. <https://doi.org/10.4018/978-1-7998-0268-6.ch003>
- Martin PG, Payton OD, Fardoulis JS et al (2016) The use of unmanned aerial systems for the mapping of legacy uranium mines. *J Environ Radioact* 143:135–140. <https://doi.org/10.1016/j.jenvrad.2015.02.004>
- Mazur M, Wisniewski A, McMillan J (2016) PwC global report on the commercial applications of drone technology. PricewaterhouseCoopers, tech. Rep
- Médecins Sans Frontières (2014) Papua New Guinea: innovating to reach remote TB patients and improve access to treatment Geneva: Médecins Sans Frontières (MSF) International. Available via DIALOG. <http://www.msf.org/article/papuanew-guinea-innovating-reach-remote-tb-patients-and-improveaccess-treatment/>. Accessed 9 June 2017
- Mendelow B, Muir P, Boshielo T (2007) Development of e-Juba, a preliminary proof of concept UAV (Unmanned Aerial Vehicle) designed to facilitate the transportation of microbiological test samples from remote rural clinics to NHLS laboratories. *South African Med J* 97:1215–1218
- Merkert R, Bushell J (2020) Managing the drone revolution: a systematic literature review into the current use of airborne drones and future strategic directions for their effective control. *J Air Transp Manag* 89:101929. <https://doi.org/10.1016/j.jairtraman.2020.101929>
- Mis M (2016) UK-funded drone deliveries aim to save mothers, babies in Tanzania. Available via DIALOG. <https://www.reuters.com/article/us-britain-aid-drones-idUSKBN14118C/>. Accessed 12 Nov 2017
- Mogombo KG (2016) UNICEF test first drone for infant HIV diagnosis. Africa News Service. Malawi News Agency. Available via DIALOG. <http://allafrica.com/stories/201603151652.html>. Accessed 12 Nov 2017
- Momont A Ambulance drone. [Online]. Available: <https://www.tudelft.nl/en/ide/research/researchlabs/applied-labs/ambulance-drone/>. Accessed: 06 Aug 2019
- Narayanan RGL, Ibe OC (2015) Joint network for disaster relief and search and rescue network operations. 10.1016/B978-1-78548-022-5.50006-6
- Nex F, Remondino F (2013) UAV for 3D mapping applications: a review. *Appl Geomat* 1–15. <https://doi.org/10.1007/s12518-013-0120-x>
- Nordberg P (2015) The survival benefit of dual dispatch of EMS and fire-fighters in out-of-hospital cardiac arrest may differ depending on population density a prospective cohort study. *Resuscitation* 90:143–149. <https://doi.org/10.1016/j.resuscitation.2015.02.036>
- Panagiotou P, Yakinthos K (2020) Aerodynamic efficiency and performance enhancement of fixed-wing UAVs. *Aerosp Sci Technol* 99:105575. <https://doi.org/10.1016/j.ast.2019.105575>
- Peckham R, Sinha R (2019) Anarchitectures of health: futures for the biomedical drone. *Glob Public Health* 14:1204e19. <https://doi.org/10.1080/17441692.2018.1546335>
- Pepitum J (2015) First FAA-approved drone delivery drops medicine in Virginia. NBC News
- Perkins GD (2015) European resuscitation council guidelines for resuscitation 2015: section 2. Adult basic life support and automated external defibrillation. *Resuscitation* 95:81–99. <https://doi.org/10.1016/j.resuscitation.2015.07.015>



- Petricca L, Ohlckers P, Grinde C (2011) Micro-and nano-air vehicles: state of the art. *Int J Aerosp Eng.* <https://doi.org/10.1155/2011/214549>
- Poljak M, Šterbenc A (2020) Use of drones in clinical microbiology and infectious diseases: current status, challenges and barriers. *Clin Microbiol Infect* 26(4):425–430. <https://doi.org/10.1016/j.cmi.2019.09.014>
- Preimesberger C (2016) Drones will soon be dropping medicines to save lives in Rwanda. *eWeek*
- Prigg M (2014) The ambulance drone that could save your life. *Daily Mail* 2014
- Priye A, Wong S, Bi Y et al (2016) Lab-on-a-drone: toward pinpoint deployment of smartphone-enabled nucleic acid-based diagnostics for mobile health care. *Anal Chem* 88:4651–4660. <https://doi.org/10.1021/acs.analchem.5b04153>
- Pulver A, Wei R, Mann C (2016) Locating AED enabled medical drones to enhance cardiac arrest response times. *Prehosp Emerg Care* 20:378–389. <https://doi.org/10.3109/10903127.2015.1115932>
- Raffaello DA (2014) Guest editorial can drones deliver? *IEEE Trans Autom Sci Eng* 11(3): 647–648. <https://doi.org/10.1109/TASE.2014.2326952>
- Raptopoulos A (2013) No roads? There's a drone for that. *TED Global*, p 2013
- Rosen JW (2017) Zipline: help from above. *MIT Technol Rev* 120:36–45
- Sabatino F (2015) Quad-rotor control: modeling, nonlinear control design, and simulation (Master thesis). School of Electrical Engineering, Automatic Control, KTH Royal Institute of Technology
- Scalea JR, Restaino S, Scassero M et al (2018) An initial investigation of unmanned aircraft systems (UAS) and real-time organ status measurement for transporting human organs. *IEEE J Transl Eng Health Med* 6:4000107. <https://doi.org/10.1109/JTEHM.2018.2875704>
- Scalea JR, Restaino S, Scassero M et al (2019) The final frontier? Exploring organ transportation by drone. *Am J Transplant* 19:962–964. <https://doi.org/10.1111/ajt.15113>
- Siddhardha K (2018) A novel bi-rotor configuration and its control. *IFAC* 456–461. <https://doi.org/10.1016/j.ifacol.2018.05.076>
- Spring T (2017) In pictures: 15 current and future uses of drones. *Computerworld* Available via DIALOG. <http://www.computerworld.com.au/slideshow/.../pictures-15-current-future-uses-drones/>
- Sreenath S, Malik H, Husnu N et al (2020) Assessment and use of unmanned aerial vehicle for civil structural health monitoring. *Procedia Comput Sci* 170:656–663. <https://doi.org/10.1016/j.procs.2020.03.174>
- Stempeck A, Hassanalian M, Abdelkefi A (2018) Aerodynamic performance of albatross-inspired wing shape for marine unmanned air vehicles. In: 36th AIAA applied aerodynamics conference, Atlanta, Georgia, pp 25–29. <https://doi.org/10.2514/6.2018-3899>
- Tan DY, Chi W, Bin Mohamed Salleh MF et al (2017) Study on impact of separation distance to traffic management for small UAS operations in urban environment. In: *Transdisciplinary engineering: a paradigm shift: proceedings of the 24th ISPE Inc. international conference on transdisciplinary engineering*, vol 5. IOS Press, p 39. July 10–14
- Tang X-B, Meng J, Wang P et al (2016) Efficiency calibration and minimum detectable activity concentration of a real-time UAV airborne sensor system with two gamma spectrometers. *Appl Radiat Isot* 110:100–108. <https://doi.org/10.1016/j.apradiso.2016.01.008>
- Thiels CA, Aho JM, Zietlow SP et al (2015) Use of unmanned aerial vehicles for medical product transport. *Air Med J Assoc* 34:104–108. <https://doi.org/10.1016/j.amj.2014.10.011>
- Tilley A (2016) UPS experiments with drone delivery in partnership with Zipline. *Forbes* 2016
- Tucker J (2017) Drones in healthcare. Retrieved on 13 Feb 2021 from: <https://www.dronesinhealthcare.com>
- University of Washington School of Medicine; Department of Family Medicine (2010) The future of family medicine and implications for rural primary care physician supply. Available at https://depts.washington.edu/uwrhrc/uploads/RHRC_FR125_Rosenblatt.pdf. Accessed 22 July 2017
- Varnholt H (2016) DHL's drone demonstration fails to deliver. *Wall Street Journal*

- Watts AC, Ambrosia VG, Hinkley EA (2012) Unmanned aircraft systems in remote sensing and scientific research: classification and considerations of use. *Rem Sens* 4(6):1671–1692. <https://doi.org/10.3390/rs4061671>
- What to Know When Using Humanitarian UAVs for Transportation (2015). Available at: <https://irevolutions.org/2015/03/03/using-humanitarian-uavs-transportation>
- World Health Organization (2010) Increasing access to health workers in remote and rural areas through improved retention: Global policy recommendations. Available at www.searo.who.int/nepal/mediacentre/2010_increasing_access_to_health_workers_in_remote_and_rural_areas.pdf. Accessed 22 July 2017
- Xiang T-Z, Xia G-S, Zhang L (2018) Mini-UAV-based remote sensing: techniques, applications and prospectives. *arXiv* 2018, arXiv:1812.07770v1. *IEEE Geosci Remote Sens Mag* (Vol 7, Issue: 3, Sept. 2019) <https://doi.org/10.1109/MGRS.2019.2918840>
- Yu S, Heo J, Jeong S, Kwon Y (2016) Technical analysis of VTOL UAV. *J Comput Commun* 04(15):92–97. <https://doi.org/10.4236/jcc.415008>
- Zhao X, Zhou XZ (2018) Design of a lift-propulsion VTOL UAV system. *IEEE international conference on mechatronics and automation (ICMA)*. <https://doi.org/10.1109/ICMA.2018.8484448>

Chapter 6

An Evaluation of the Current Status and Trends in All Electric Urban Air Mobility UAVs



Emre Özbek , Alper Dalkiran, Evren Yilmaz Yakin, Selcuk Ekici, and T. Hikmet Karakoc 

Acronyms

CO	Carbon monoxide
CO ₂	Carbon dioxide
CORSIA	Carbon Offsetting and Reduction Scheme for International Aviation
DOC	Direct operational cost
EASA	European Union Aviation Safety Agency
eVTOL	Electric vertical takeoff and landing
FAA	Federal Aviation Administration
GHGs	Green house gases
ICAO	International Civil Aviation Organization
MTOW	Maximum take-off weight
NMVO	Non-methane volatile organic compound

E. Özbek (✉) · E. Y. Yakin
UAV Technology and Operatorship Program, Eskisehir Technical University, Eskisehir, Türkiye
e-mail: emreozbek@eskisehir.edu.tr

A. Dalkiran
School of Aviation, Suleyman Demirel University, Kecioburlu, Isparta, Türkiye
e-mail: alperdalkiran@sdu.edu.tr

S. Ekici
Iğdir University, Iğdir, Türkiye

T. H. Karakoc
Faculty of Aeronautics and Astronautics, Eskisehir Technical University, Eskisehir, Türkiye
Information Technology Research and Application Center, Istanbul Ticaret University, Istanbul, Türkiye
e-mail: hkarakoc@eskisehir.edu.tr; thkarakoc@ticaret.edu.tr

NO _x	Nitrous oxide
PV	Photovoltaic
SO ₂	Sulfur dioxide
TRL	Technological readiness level
UAM	Urban air mobility
UAV	Unmanned aerial vehicle

6.1 Motivations and Background of Electrification in Aviation

Many sources have addressed emissions caused by air transportation, and well-round reviews have been made about the topic (Van et al. 2018; Pénard-Morand and Annesi-Maesano 2004). Although it declined during the Covid-19 pandemic, the recovery phase started (Arena and Aprea 2021). The anticipated annual growth of the aviation industry was 5–6% per year before the pandemic (Schäfer and Waitz 2014). With the continuation of this growth, environmental issues caused by aviation must be addressed. Also, dependency on crude oil has damaged the growth of the aviation industry before and during the Gulf War period (Lieber 1992). Nowadays, the invasion of Russia on Ukraine also unearthed the same chronic problem as crude oil prices increased gradually (Liadze et al. 2022). Being aware of the aforementioned problems, electrification of the aircraft industry has motivations to gradually decline the sustainability issues and remove them in the future if possible. These problem sources can be listed as:

- Air pollutant emissions
- Noise emissions
- Climate change effects
- Crude oil dependency

Air pollutant emissions caused by the aviation sector are primarily a result of fossil fuel usage on internal combustion engines. Sulfur dioxide (SO₂), nitrous oxide (NO_x), carbon monoxide (CO), carbon dioxide (CO₂), and non-methane volatile organic compounds (NMVOCs) can be the primary air pollutant particles. These particles adversely affect human health and the ozone layer (Harrison et al. 2015).

Noise emissions caused by the aviation sector arise from aircraft engines, aircraft fuselage, and high-lift devices employed in takeoffs and landings (Li et al. 2013). Noise emissions are considered a significant problem that decreases life quality, especially for those in the vicinity of airports (Pillay et al. 2011). Even the property values decrease with the increasing proximity to airports (Pennington et al. 1990).

Climate change effects mainly arise from green house gas (GHG) emissions. As a combustion product from the internal combustion engine, CO₂ could be addressed as the main GHG that should be dealt with in aviation sustainability. Air transportation emission estimations suggest that values could rise to more than 15% of total carbon dioxide emissions from all sources by 2050 (Dubois and Ceron 2006). Also, the

International Civil Aviation Organization (ICAO) has agreed to implement a mechanism to reduce and control CO₂ emissions under the Carbon Offsetting and Reduction Scheme for International Aviation (CORSIA), which measures 2.5% of the total carbon emissions in 2019.

Crude oil dependency is another motivational factor that has been addressed by sustainable aviation researchers (Nygren et al. 2009). As mentioned before, oil supply crises have affected the aviation industry badly. Nowadays, another regional conflict is also affecting the oil supply and resulting in a price surge that may cause problems with the stability of the sector.

These four issues addressed and detailed above could be considered the driving motivational source of sustainable aviation topics related to alternative propulsion energy sources. Different technologies and approaches could offer to reduce or solve these problems arising from fossil fuel usage for thrust generation. These approaches are topics of sustainable aviation research and are being studied in academia and aviation industry.

Biofuel usage is one of these technologies implemented as a percentage mixture of jet fuel. Biofuels can be produced using sustainable sources such as algae and crops. Although biofuel usage can reduce dependency on fossil fuels using the existing fleets and engines, these fuels cannot entirely replace the fossil fuels with the currently allowed blending ratios (Marsh 2008).

Apart from the usage of biofuels, two different electrification concepts are being developed for aircraft: the more-electric and all-electric aircraft. The more-electric aircraft concept focuses on increasing electrical energy usage in aircraft subsystems by excluding the propulsion subsystem (Sarlioglu and Morris 2015). Thus, the goal is to reduce fuel consumption and emissions. In the new generation commercial airliner, Boeing 787 Dreamliner, electric energy usage dramatically increased, and bleed air usage was removed (Naayagi 2013).

Onboard energy generation systems have also been a trending direction for the electrification of aviation research. Hydrogen fuel cells are a promising technology used in unmanned aerial vehicles (UAVs) as testbeds (Özbek et al. 2020). Also, general aviation manned aircraft are being developed using fuel cells both as concepts and prototypes (Nicolay et al. 2021). Although hydrogen fuel cells can significantly increase the aircraft's endurance, there are problems with the power requirement for taking off and climbing phases. Thus, hybridization models and hybrid powertrains are attracting more attention (Chandran et al. 2022). Usually, these hybrid powertrains include lithium-based batteries, but ultracapacitor- and supercapacitor-integrated powertrain studies should also be mentioned (Soltani and Benchouia 2022). As another feasible onboard energy generation unit, photovoltaic (PV) arrays are also being implemented into unmanned aerial systems power subsystems. Just like the fuel cells, unmanned aerial vehicle projects are ongoing, which use PV arrays located over the wing sections (El-Atab et al. 2021). Some limitations should be mentioned, such as technological readiness, availability, hydrogen storage problems for fuel cells, PV array cloudy day problems, manufacturing costs, and lack of available power that can be used for propulsion during takeoff and climb. Although there are issues listed, hybrid powertrain studies

are currently the most promising systems for all-electric aircraft. Current directions revolve around combining batteries and capacitors as energy storage buses and implementing fuel cells and PV arrays as onboard energy generation units (Barzkar and Ghassemi 2020).

6.2 All Electric Unmanned Urban Air Mobility Electric UAV Concept

Urban air mobility (UAM) concept is based on the development of unmanned aerial taxi platforms that can navigate around platforms located around the metropolitan area (Vascik et al. 2018). Urbanization in cities and congestion in road traffic are the primary motivations for the UAM-electric vertical take off and landing unmanned aerial vehicle (e-VTOL) concept. Essentially, it (is) a familiar concept for manned helicopters to travel between helipads above company buildings, driven by those who could bear the costs (Dodge 2016). Along with the developments in unmanned aircraft navigation, electrification, and aircraft design developments, urban air mobility costs could be significantly reduced in terms of pilot man-hours, aviation fuel, aircraft maintenance, and aircraft unit costs. Also, vertical takeoff and landing (VTOL) capability is considered a necessity for UAM eUAV designs to minimize runway availability problems. Due to the urban area land availability problems, conventional runway usage cannot be considered a feasible takeoff and landing option. Thus, another acronym should be defined here: electric vertical takeoff and landing (eVTOL) UAV. The implementation of eVTOL UAVs in UAM scenarios is being developed (Straubinger and Rothfeld 2020). An airspace development procedure currently includes infrastructure planning, zone planning, and air traffic control topics for UAM with eVTOL UAVs (Bauranov and Rakas 2021). To better understand the promised concept and the driving factors, the expected advantages of the concept should be defined. The key advantages can be listed as follows:

- Being the fastest travel option compared to taxis or subways
- Having reasonable fares compared to manned helicopter taxis
- Providing a safe and reasonable flight experience that passengers can enjoy the view
- Seamless connections to other transportation methods and promising integrated mobility solutions around hubs such as airports (Berger 2018)

The future predictions about UAM with the eVTOL UAV concept are shining bright. In 2019, there were over 1000 test flights of full-size eVTOL aircraft prototypes. Also, as of March 2020, at least 12 eVTOL aircraft were in the process of certification from the US [Federal Aviation Administration](#) (FAA) (Dietrich and Wulff 2020). Many projects are also in the pipeline and being tested and developed worldwide. According to Roland Berger, market predicts that the first commercially used urban air mobility routes will start in 2025 (Berger 2018).

Although the advantages and predictions of this technology promise a lot, there are still challenges that have to be addressed by researchers. The bottlenecks of the UAM with the eVTOL concept could be defined as follows:

- Infrastructural requirements (Takacs and Haidegger 2022)
- Regulatory issues and legal framework (Takacs and Haidegger 2022)
- Identification of testing and certification processes (Mitchell et al. 2022)
- Noise emissions (Fuerkaiti et al. 2020)
- Social acceptance (Koumoutsidi et al. 2022)
- Fleet scheduling (Paul and Chowdhury 2022)
- Battery limitations and thermal control (Mudumba 2022)
- Air traffic density and control (Deniz and Wang 2022)
- Navigation issues, collision avoidance, and interference (Desai et al. 2021)

By checking the list provided above with references, the reader could easily navigate through one of these topics to study. These topics will affect the integration of UAM with the eVTOL concept in our lives directly. Modeling and simulation methods have been widely used in these topics to suggest and establish a sustainable model for UAM using eVTOL aircraft.

As previously mentioned, the UAM is not a new concept. It has been held with manned helicopters for premium individuals who can afford it for over 50 years. Developments in technologies such as electrical propulsion, batteries, composites, and sensors enabled this concept to become a low-cost and widely used emerging option. Thus, promising technologies should also be mentioned here to develop this concept further. Fifth generation (5G) cellular networks and their integration studies are expected to enable more robust real-time informatics and navigation for eVTOLs (Athavale et al. 2020). Also, as a trend, electrification of all transportation models is paving the way for more mass-produced batteries and electric propulsion systems, resulting in cheapening these components. The increase in the robustness of autonomous flight technologies and flight sensors should also be mentioned. Removing pilots from aircraft and adding one more passenger seat is a crucial factor that increases profitability. Thus, improved autonomous flight systems in terms of navigation, control, and fault tolerance will significantly impact the social acceptance and profitability of the UAM with the eVTOL concept.

6.3 Evaluation Criteria for Urban Air Mobility UAVs

A definition of the evaluation criteria framework should be established to understand the trends of these UAM UAVs. Although different factors affect the success of a designed product, such as performance parameters, navigation model details, autonomous flight details, and business model, in this evaluation, the authors relayed on evaluating the aircraft performance-based criteria. UAVs that employ hybrid propulsion solutions (are) neglected, focusing on all-electric propulsion. Piloted UAM eVTOL models, such as Archer Maker, Blackfly v3, AIR ONE, and Joby S4, are

also neglected because these models cannot be considered autonomous UAVs (Swaminathan and Reddy 2022). Projects that are initially presented as piloted and going to be converted into autonomous were also included as UAV candidates. The below-listed and explained criteria are used to perform an assessment of available data of seven all-electric UAM UAVs.

6.4 Maximum Takeoff Weight (MTOW)

The maximum takeoff weight (MTOW) indicates the maximum kilos or pounds an airplane can carry. MTOW is the maximum takeoff weight at which an aircraft is certified for flight due to structural or other limitations. These limitations are not fixed. This value is a function of airspeed, temperature, and air density, which is also a function of temperature. The air's density drops when the temperature increases while its pressure remains constant. The effects of rising temperature on aircraft takeoff performance have been studied (Coffel et al. 2017). This density drop causes a wing to create less lift at a given airspeed, which could result in a weight restriction for departing aircraft. Their research offers a general model that may predict future weight limits for a fleet of aircraft with varied takeoff weights operating from various airports.

MTOW calculations are essential to finding an economic model for aircraft operations. Structurally well-designed and optimized aircraft can carry more payload, and their MTOW can be lower than expected. Thus, there is a relationship between payload range and MTOW. Analyzing the payload range includes examining the aircraft and its components to identify not only the payload capabilities of the aircraft at various ranges but also the range capability with a variety of payloads, which are contained within the MTOW value.

All-electric aircraft have a few disadvantages. The prominent disadvantage is the energy density problem for a unit of weight. Although much effort is ongoing for battery and fuel cell technologies, battery cells' feasibility and energy performance need to be doubled for all-electric commercial aircraft (Karadotcheva et al. 2021). However, small aircraft for general and regional aviation can be achievable. According to the studies, most direct operating costs comprise maintenance and depreciation expenses for most daily flight frequencies (Monjon and Freire 2020). In addition, when the number of daily trips increases, the expense associated with battery replacement climbs dramatically. A sensitivity analysis also revealed that changes in the battery life cycle and aircraft purchase price impact the direct operating costs (DOCs) more than any other factors considered and might carry uncertainty.

6.5 Piloting Type

Piloting type is also considered one of the critical metrics for this evaluation. As this chapter deals with unmanned aerial vehicles, autonomous flight capability was (is) taken as a necessity. Some current designs employ a pilot only to modify it to be fully autonomous after development procedures. These designs were (are) included in the evaluated UAM UAV list. But some eVTOL designs focus on the “flying car” concept, which had to be excluded from the evaluation.

6.6 Configuration

The configuration of an aircraft refers to the layout of its systems and components. The three main configurations could be summarized as fixed wings, rotary wings, and hybrids. Fixed-wing aircraft offer great endurance but require a runway to take off and land conventionally. Rotary aircraft such as helicopters and multirotors can take off and land vertically without needing a runway and can also perform hovering. However, their endurance is minimal due to the inefficiency of propellers and batteries. Hybrid aircraft in the form of fixed VTOLs, tiltrotor/tilt-wing, and tail sitters combine fixed and rotary-wing aircraft advantages. Understanding the trending configurations in UAM UAVs is essential. Thus, the configuration type was (is) selected as the third evaluation measure.

6.7 Range

Urban air mobility is a task that requires the transport of payload from point A to B. In every model of transport, the availability of a higher range is preferred. The range could be defined as a function of both flight endurance and cruising speed. A higher range with the same payload could directly relate to the UAV platform’s efficiency. Thus, the range was (is) selected as the fourth evaluation basis.

6.8 Passenger Capacity

Passenger capacity is also an important consideration in terms of transportation modes. As the passenger capacity increases, the size and weight of the vehicle tend to increase. Thus, the aircraft with the same passenger capacity should be compared. Comparing a two-seated vehicle with a four-seated one would not accurately determine the performance. Also, the seating capacity affects passenger reach since a two-seated aircraft for urban mobility cannot perform transportation of

a four-person family with one sortie. Thus, the seating capacity was (is) selected as the fifth evaluation data.

6.9 Payload

Payload is a term that defines paid weight on the aircraft. In aviation, the aircraft's mission usually determines the payload. For instance, for a reconnaissance UAV, the payload is generally cameras and video transmitters. In UAM UAVs, the payload definition is similar to that of airliners. Passengers and passenger luggage should be considered as payloads in these operations. One of the planned primary usage areas for the UAM projects is distributing people from airports to urban areas. Apart from passenger capacity, the luggage capacity should also be considered essential to perform these missions efficiently since, generally, people fly with their items and pieces of baggage. Due to these reasons, the payload capacity was (is) selected as the sixth evaluation criterion.

6.10 Cruise Speed

Cruise is a phase of flight that defines a situation where forces and moments on the aircraft are zero. After the aircraft's takeoff and climb, the aircraft cruises until it gets closer to its final destination and starts its descent for landing. In almost every flight, the cruise phase dominates the flight time compared to other flight phases. Nominally, aircraft designers design an aircraft based on its cruise efficiency goal. The cruise speed of an aircraft is essential in terms of endurance, range, and efficiency. Also, the cruising speed is essential for passenger behaviors. Usually, premium passengers with luxury consumption habits value time extremely. Thus, the cruise speed has been selected as the seventh evaluation component.

6.11 Power Source

In terms of the development efforts of all-electric aircraft, the selection of the power source is essential to sustain good aircraft performance. There are problems with lithium-based batteries since they are heavier and can provide only a fraction of the energy density compared to conventional combustion engine fuels. The addition of onboard energy generation systems to the powertrain, such as solar panels and hydrogen fuel cells, could improve the energy efficiency of an eVTOL. However, this increment came with a cost in terms of weight, complexity, unit cost, and maintenance costs. There is another issue that should be mentioned with the hybrid

powertrains. Taking off and climbing phases of a flight mission usually require higher power than the cruise phase.

For this reason, studies focus on integrating ultracapacitors and supercapacitors into hybrid powertrains due to their high discharge capacity (Kim et al. 2020; Tao et al. 2019). The selection of power sources will be important in terms of infrastructure in the near future for UAM UAVs. For instance, if Proton Exchange Membrane (PEM) hydrogen fuel cells will be employed in most systems, there should be hydrogen storage that can store hydrogen safely and securely. Thus, the power source selection trends in developing projects are vital for catching foresight, and this criterion has also been covered during the evaluation.

6.12 Number of Motors

The number of motors used is also an essential parameter regarding aircraft performance and efficiency. In some aircraft configurations, such as fixed VTOLs, vertically placed motors are only used in taking off and landing. The weight and drag force addition of these non-used motors during the cruise phase drastically reduces the aircraft's cruise performance. On the other hand, aircraft configurations designed with tilting wings or tilting motors have greater efficiency since motors provide vectored thrust and are used in all phases of flight. Also, the increasing number of motors in UAVs has pros and cons that should be mentioned. The increasing number of motors increases the reliability of a UAV in terms of single or multiple motor failures, the weight of the system, payload capacity, maximum speed, complexity of the system, cost of the system, and energy requirement of the system. For these reasons, the number of motors on the UAM UAVs was (is) also considered an evaluation basis.

6.13 Current Status of Development

The statuses of development for projects are usually categorized with technological readiness levels (TRLs) (Mankins 1995). Technological readiness levels of a project define the maturity of a project. This evaluation included projects over TRL 4 "Technology Validated in LAB Environment." Many projects have recently been announced with TRLs lower than 4. However, these projects should be considered aircraft designs at their conceptual or preliminary design phases. There are performance data released regarding projects lower than TRL 4. However, as common in aircraft design, design requirements and design values on paper rarely entirely meet the flight performance of flight test prototypes. In order to provide the reader with an accurate evaluation, data from the aircraft with appropriate technological maturity was (is) provided in particular.

6.14 Results of Urban Air Mobility UAV Evaluation

6.14.1 Model Reviews

1. *Volocopter* is one of the pioneers in the UAM UAV concept (Volocopter 2022). The company is located in Germany and Singapore. Along with the UAV development, the company has also been working on infrastructure, and they have built the first VoloPort in Lion City. The covered model in the evaluation is named VoloCity. The VoloCity model is a zero-emission air taxi project. It is the first aircraft of its kind that meets the exacting safety standards regulated by the European Union Aviation Safety Agency. The first flight test consisting of a hover flight of a full-scale prototype was performed in April 2022 (eVTOL.com 2022).
2. *Ehang 216* is the UAM UAV developed by Ehang company from China. The company embraces full redundancy to ensure security, autonomous pilot, and centralized control of the intelligent command-and-control center (EHang 2022).
3. *Baykar Cezeri* is an UAM UAV model being developed by Baykar Makine Company located in Turkey (Baykar 2022). The Cezeri is being developed to bring a reliable solution to aerial delivery of time-critical packages and medicines in congested urban cities. The company defines the Cezeri as a flying car model but provides a vision to switch to a fully autonomous system.
4. *Y6S Plus* is a model being developed by Autonomous Flight. British entrepreneur Martin Warner founded the company. Autonomous Flight designs and manufactures electric VTOL aircraft like the Y6S Plus project. Y6S Plus is a six-seater electric vertical takeoff and landing (eVTOL) aircraft with a carbon fiber structure, fully electric powertrain, and zero-emission goal (Autonomous Flight 2022).
5. *Lilium Jet 5 Seater* is a UAM UAV model developed by Lilium company from Germany (Lilium 2022). Lilium Jet employs ducted electric vectored thrust technology for vertical takeoff and landings. The Lilium Jet is built on aerodynamic efficiency, market-leading payload, zero emissions, and low noise profile.
6. *e-Starling* is a piloted eVTOL model that Arc Aero Systems has developed in the United Kingdom. The company has successfully flown the half-scaled version of their e-Starling model and now has a proof of concept. The company has remarked that the project will lead to the commercialization of e-Starling in 2026 (ARC Aerosystems 2022).
7. *Cora* is a model developed by Wisk Aero, a joint venture between the Boeing Company and the Kitty Hawk Corporation. Headquartered in Mountain View, California, with locations in Atlanta, Georgia, and New Zealand, Wisk Aero's vision is delivering safe, daily flight to the masses. The company claims to be the first in the United States to successfully fly an autonomous, eVTOL aircraft designed for passenger use (Wisk Aero 2022).

Tables 6.1 and 6.2 present and summarize the data collected from various sources about the aircraft listed above.

Table 6.1 Model data according to the evaluation criteria –1 (Volocopter 2022; eVTOL.com 2022; EHang 2022; Baykar 2022; Autonomous Flight 2022; Lilium 2022; ARC Aerosystems 2022; Wisk Aero 2022; EVTOL News 2022)

No	Model	Country	Piloting	Configuration	MTOW (kg)	Payload (kg)
1	VoloCity	Germany	M/A	Multicopter	900	200
2	Ehang 216	China	A	Multicopter	600	220
3	Cezeri	Turkey	M/A	Multicopter	241	100
4	Y6S Plus	UK	M/A	Hybrid	N/A	N/A
5	Lilium Jet 5 Seater	Germany	M/A	Hybrid	N/A	N/A
6	e-Starling	UK	M/A	Hybrid	600	60
7	Cora	USA	A	Hybrid	1270	181

Table 6.2 Model data according to the evaluation criteria –2 (Volocopter 2022; eVTOL.com 2022; EHang 2022; Baykar 2022; Autonomous Flight 2022; Lilium 2022; ARC Aerosystems 2022; Wisk Aero 2022; EVTOL News 2022)

No	Model	Pax	Range (km)	Cruise speed (km/h)	Power source	Number of motors	Current status
1	VoloCity	2	35	110	Battery – Lithium-Ion	18	Prototype
2	Ehang 216	2	30	100	Battery	16	Prototype
3	Cezeri	1	80	100	Battery – Lithium-Ion	8	Prototype
4	Y6S Plus	6	130	113	Battery	6	Scaled Prototype
5	Lilium Jet 5 Seater	5	300	300	Battery	30	Prototype
6	e-Starling	1	217	342	Battery	6	Scaled Prototype
7	Cora	2	40	160	Battery	13	Prototype

6.15 Conclusions

In this chapter, an evaluation of UAM UAVs was (is) performed on the basis of a well-defined and performance-focused evaluation framework. Some eVTOL ongoing projects with TRL levels above four have been excluded due to being flying car models instead of UAVs. Although some manned/piloted aircraft are listed above, the companies' will and vision to switch autonomously piloted versions in the future were (are) decisive in which model to index. From the evaluation results, it can be pointed out that:

- Models with different seating capacities are in development in terms of passenger count.
- Lithium-based battery packs are dominating the sector now. Although hybrid powertrains are promising in flight endurance, these pioneers have not included fuel cells or solar panels in their power systems.

- Currently, the multicopter models with the current experience on these platforms are the most developed ones. Although hybrid models provide more efficiency, their design and development procedures take more time.
- Regulation requirements are being taken seriously by the sector. The companies are listing reliability, safety, and passenger safety as their primary objectives as the aviation sector demands.

The following topics, such as flight control, data transmission, navigation, structural design, battery management, hybrid powertrain design, and airspace integration, should be mentioned as possible research topics on UAV UAM technology. Also, passenger and consumer behavior should be discussed and evaluated. Consumers' perspective of these UAV UAMs will be a primary driving factor for this sector's growth. The effect of an increased level of autonomy and the effect of the availability of backup systems such as parachutes on passenger behavior could be investigated.

Apart from the vehicle, the UAV UAM operations infrastructure and eVTOL flying cars must be a point of focus to sustain growth in this sector. Fast charging points for these all-electric vehicles should be established along with the vertical airports or vertiports as short. Feasibility studies should be conducted between transforming the existing infrastructure and establishing new infrastructure.

All-electric UAV UAMs are developed with a zero-emission goal. However, multiple rotors and propellers emit noise, especially in multicopter configurations. GHG emissions could be zero, but noise emissions should also be covered in terms of passenger ergonomics and residents around the vertiports. It should be noted that these aircraft fly at very low altitudes and can affect the psychology of people and pets. Researchers and technology pioneers should also cover these areas to pave the way for zero-emission all-electric unmanned urban aerial transportation.

References

- ARC AeroSystems (2022) About us. <https://arcaerosystems.com/about-us/>. Accessed July 2022
- Arena M, Aprea C (2021) Impact of Covid-19 pandemic on air transport: overview and implications. *Advances in Environmental and Engineering Research* 2(1):1. <https://doi.org/10.25082/AEER.2021.01.001>
- Athavale J, Baldovin A, Mo S et al (2020) Chip-level considerations to enable dependability for EVTOL and urban air mobility systems. In 2020 AIAA/IEEE 39th digital avionics systems conference (DASC) IEEE. <https://doi.org/10.1109/DASC43569.2020.9241527>
- Autonomous Flight (2022) Autonomous flight – unmanned aerial vehicles (UAVs) for every industry. <https://autonomousflight.com/>. Accessed July 2022
- Barzkar A, Ghassemi M (2020) Electric power systems in more and all electric aircraft: a review. *IEEE Access* 8:169314–169332. <https://doi.org/10.1109/ACCESS.2020.3035316>
- Bauranov A, Rakas J (2021) Designing airspace for urban air mobility: a review of concepts and approaches. *Prog Aersp Sci* 125:100726. <https://doi.org/10.1016/j.paerosci.2021.100726>
- Baykar (2022) Baykar fighting car. <https://www.baykartech.com/en/fighting-car/>. Accessed July 2022

- Berger R (2018) Urban air mobility: the rise of a new mode of transportation. Springer. <https://doi.org/10.1007/978-3-319-69183-9>
- Chandran M, Palanisamy K, Benson D et al (2022) A review on electric and fuel cell vehicle anatomy, technology evolution and policy drivers towards EVs and FCEVs market propagation. *Chem Rec* 22(2). <https://doi.org/10.1002/tcr.202100235>
- Coffel ED, Thompson TR, Horton RM (2017) The impacts of rising temperatures on aircraft takeoff performance. *Clim Chang* 144(2):381–388. <https://doi.org/10.1007/s10584-015-1468-4>
- Deniz S, Wang Z (2022) A multi-agent reinforcement learning approach to traffic control at future urban air mobility intersections. In: AIAA SCITECH 2022 Forum. <https://doi.org/10.2514/6.2022-1509>
- Desai K, Al Haddad C, Antoniou C (2021) Roadmap to early implementation of passenger air mobility: findings from a delphi study. *Sustainability* 13(19):10612. <https://doi.org/10.3390/su131910612>
- Dietrich A, Wulff Y (2020) Urban air mobility: adding the third dimension to urban and regional transportation. In: Presentation for: an introduction to urban air mobility for state and local decision makers: a virtual workshop, sponsored by the Community Air Mobility Initiative (CAMI). <https://www.communityairmobility.org/uam101>
- Dodge M (2016) Verticality and urban mobility: learning lessons from past visions of elevated transport systems in the post-war city. In: Above, degrees of elevation. <https://doi.org/10.4324/9781315639683>
- Dubois G, Ceron JP (2006) Tourism/leisure greenhouse gas emissions forecasts for 2050: factors for change in France. *J Sustain Tour* 14(2):172–191. <https://doi.org/10.1080/09669580608668622>
- EHang (2022) Autonomous Aerial Vehicle (AAV). <https://www.ehang.com/ehangaav>. Accessed July 2022
- El-Atab N, Mishra RB, Alshambari R et al (2021) Solar powered small unmanned aerial vehicles: a review. *Energ Technol*. <https://doi.org/10.1002/ente.202100587>
- EVTOL News (2022) eVTOL Aircraft. <https://evtol.news/aircraft>. Accessed July 2022
- EVTOL.com (2022) Volocopter's first hover flight test of Volocity eVTOL aircraft. <https://evtol.com/video/volocopters-first-hover-flight-test-velocity-evtol-aircraft/>. Accessed July 2022
- Fuerkai Y, Casalino D, Avallone F et al (2020) Urban air mobility noise prediction in a 3D environment using Gaussian beam tracing. *Aerospace* 7(9):122. <https://doi.org/10.3390/aerospace7090122>
- Harrison RM, Masiol M, Vardoulakis S (2015) Civil aviation, air pollution and human health. *Environ Res Lett*. <https://doi.org/10.1088/1748-9326/10/4/041001>
- Karadotcheva E, Nguyen SN, Greenhalgh ES et al (2021) Structural power performance targets for future electric aircraft. *Energies*. <https://doi.org/10.3390/en14196006>
- Kim J, Baek S, Choi Y et al (2020) Hydrone: reconfigurable energy storage for UAV applications. *IEEE Trans Comput-Aided Design Integr Circuits Syst* 39(11):3686–3697. <https://doi.org/10.1109/TCAD.2020.3015655>
- Koumoutsidi A, Pagoni I, Polydoropoulou A (2022) A new mobility era: stakeholders' insights regarding urban air mobility. *Sustainability*. <https://doi.org/10.3390/su14053128>
- Li Y, Wang X, Zhang D (2013) Control strategies for aircraft airframe noise reduction. *Chin J Aeronaut* 26(2):249–260. <https://doi.org/10.1016/j.cja.2013.01.018>
- Liadze I, Macchiarelli C, Mortimer-Lee et al (2022) The economic costs of the Russia-Ukraine conflict. NIESR Policy Paper. <https://doi.org/10.1920/re.ifs.2022.0012>
- Lieber RJ (1992) Oil and power after the Gulf War. *Int Secur* 17(1):155–176. <https://doi.org/10.2307/2539006>
- Lilium (2022) Lilium – the electric vertical take-off and landing jet. <https://lilium.com/>. Accessed July 2022
- Mankins JC (1995) Technology readiness levels. White paper
- Marsh G (2008) Biofuels: aviation alternative? *Renew Energy Focus* 9(4):48–51. [https://doi.org/10.1016/S1471-0846\(08\)70087-3](https://doi.org/10.1016/S1471-0846(08)70087-3)

- Mitchell DG, Klyde DH, Shubert et al (2022) Testing for certification of urban air mobility vehicles. In: AIAA SCITECH 2022 Forum. American Institute of Aeronautics and Astronautics. <https://doi.org/10.2514/6.2022-0891>
- Monjon MMM, Freire CM (2020) Conceptual design and operating costs evaluation of a 19-seat all-electric aircraft for regional aviation. In 2020 AIAA/IEEE electric aircraft technologies symposium (EATS) IEEE. <https://doi.org/10.1109/EATS47652.2020.9174126>
- Mudumba SV (2022) Automated contingency management for passenger-carrying urban air mobility operations (Doctoral dissertation). Purdue University Graduate School. <https://doi.org/10.25394/pgs.16772836>
- Naayagi RT (2013) A review of more electric aircraft technology. In: 2013 international conference on energy efficient technologies for sustainability IEEE. <https://doi.org/10.1109/ICEETS.2013.6533586>
- Nicolay S, Karpuk S, Liu Y et al (2021) Conceptual design and optimization of a general aviation aircraft with fuel cells and hydrogen. *Int J Hydrog Energy* 46(64):32676–32694. <https://doi.org/10.1016/j.ijhydene.2021.09.140>
- Nygren E, Aleklett K, Höök M (2009) Aviation fuel and future oil production scenarios. *Energy Policy* 37(10):4003–4010. <https://doi.org/10.1016/j.enpol.2009.06.062>
- Özbek E, Yalin G, Ekici S et al (2020) Evaluation of design methodology, limitations, and iterations of a hydrogen fuelled hybrid fuel cell mini UAV. *Energy*. <https://doi.org/10.1016/j.energy.2020.118757>
- Paul S, Chowdhury S (2022) A graph-based reinforcement learning framework for urban air mobility fleet scheduling. In: AIAA AVIATION 2022 Forum. <https://doi.org/10.2514/6.2022-3911>
- Pénard-Morand C, Annesi-Maesano I (2004) Air pollution: from sources of emissions to health effects. *Breathe* 1(2):108–119. <https://doi.org/10.1183/20734735.0102.108>
- Pennington G, Topham N, Ward R (1990) Aircraft noise and residential property values adjacent to Manchester International Airport. *JTEP* 24(1):49–59. <https://www.jstor.org/stable/20052966>
- Pillay D, Archary K, Panday S (2011) A preliminary study of the effects of aircraft noise on families who reside in close proximity to an airport. *S Afr Fam Pract* 53(4):361–365. <https://doi.org/10.1080/20786204.2011.10874125>
- Sarlioglu B, Morris CT (2015) More electric aircraft: review, challenges, and opportunities for commercial transport aircraft. *IEEE Trans Transport Electr* 1(1):54–64. <https://doi.org/10.1109/TTE.2015.2404142>
- Schäfer AW, Waitz IA (2014) Air transportation and the environment. *Transp Policy* 34:1–4. <https://doi.org/10.1016/j.tranpol.2014.04.009>
- Soltani B, Benchouia NE (2022) Combining batteries with super-capacitors to store energy in fuel cell vehicles: a review with suggestions. *Ann Romanian Soc Cell Biol* 26(4):1985–1992. <https://doi.org/10.2478/arscb-2021-0013>
- Straubinger A, Rothfeld R, Shamiyeh et al (2020) An overview of current research and developments in urban air mobility—setting the scene for UAM introduction. *J Air Transp Manag* doi: <https://doi.org/10.1016/j.jairtraman.2020.101852>
- Swaminathan N, Reddy SRP, Rajashekara et al (2022) Flying cars and eVTOLs-technology advancements, powertrain architectures and design, *IEEE Trans Transport Electr* doi:<https://doi.org/10.1109/TTE.2022.3151399>
- Takacs A, Haidegger T (2022) Infrastructural requirements and regulatory challenges of a sustainable urban air mobility ecosystem. *Buildings*. <https://doi.org/10.3390/buildings12060747>
- Tao LEI, Zhou YANG, Zicun LIN et al (2019) State of art on energy management strategy for hybrid-powered unmanned aerial vehicle. *Chin J Aeronaut* 32(6):1488–1503. <https://doi.org/10.1016/j.cja.2019.03.017>
- Van FY, Perry S, Klemeš JJ et al (2018) A review on air emissions assessment: transportation. *J Clean Prod* 194:673–684. <https://doi.org/10.1016/j.jclepro.2018.05.056>

Vascik PD, Hansman RJ, Dunn NS (2018) Analysis of urban air mobility operational constraints. *J Air Transport* 26(4):133–146. <https://doi.org/10.2514/1.D0089>

Volocopter (2022) Urban air mobility. <https://www.volocopter.com/urban-air-mobility/>. Accessed July 2022

Wisk Aero (2022) Aircraft. <https://wisk.aero/aircraft/>. Accessed July 2022

Chapter 7

Aerodynamic Shape Optimization and the Effect of Morphing Winglet-Induced Tip Vortex Structure on the UAS-S45



Musavir Bashir, Simon Longtin-Martel, Ruxandra Mihaela Botez,
and Tony Wong

Acronyms

c_l	Lift force per unit span
$C_{N_1}^{N_2}$	CST class function
c_d	Drag force per unit span
C_L	Lift coefficient
C_D	Drag coefficient
c	Chord
c_p	Specific fuel consumption
C_f	Skin friction coefficient
D	Drag force
E	Endurance
E_a	Aerodynamic endurance efficiency
K_i^n	Binomial coefficient K
L	Lift force
M	Mach number
S	Wing surface
v	Aircraft speed
X_{tu}	Translation variable in x for the upper surface
X_{tl}	Translation variable in x for the lower surface
ρ	Air density
Θ	Morphing deflection angle

M. Bashir · S. Longtin-Martel · R. M. Botez (✉) · T. Wong
Research Laboratory in Active Controls, Avionics and Aeroservoelasticity (LARCASE),
Université du Québec, École de Technologie Supérieure, QC, Canada
e-mail: ruxandra.botez@etsmtl.ca

CST	Class shape transformation
PSO	Particle swarm optimization
UAV	Unmanned Aerial Vehicle

7.1 Introduction

Increasing fuel costs have necessitated the need for highly fuel-efficient aircraft. Industry and academic researchers are continually looking for ways to increase aircraft performance (ICAO 2019). One way is to reduce total aircraft drag, thereby improving aerodynamic efficiency without compromising structural integrity. The increase in efficiency directly benefits airlines by allowing for more frequent flights with less fuel consumption, resulting in economic benefits. Wingtip devices are already available in various shapes and sizes, and they all serve to minimize drag by recovering tip vortex energy, thereby improving fuel efficiency (Oliviu et al. 2016). Several methods have been proposed for achieving the required morphing wing adaptability, resulting in considerable performance improvements over conventional wing design, such as a camber morphing wing flap for large civil aircraft in the Clean Sky program (Pecora 2021). The morphing camber system consists of the trailing and leading edges for an unmanned aerial vehicle (UAV) (Communier et al. 2020), morphing wing with a portion of the wing's upper and lower surfaces with a flexible skin (Gabor 2015). Similarly, other studies reviewing the morphing aircraft and outlining the structural, shape-adaptive morphing concepts for fixed and rotary wings (Barbarino et al. 2011); the multidisciplinary design optimization tool using an aerodynamic shape optimization code and a structural morphing wing for minimizing drag (Gamboa et al. 2009); and the effect of morphing winglets were carried out (Eguea et al. 2018, Dimino et al. 2021). Our Research Laboratory in Active Controls, Avionics, and AeroServoElasticity (LARCASE) has a team of dedicated researchers focusing on various approaches to reduce aircraft fuel consumption (Botez 2018, 2022; Hamy et al. 2016; Félix Patrón et al. 2014); several projects were carried out in numerical studies (Bashir et al. 2021; Botez et al. 2007, 2018; Elelwi et al. 2020) and control studies (Khan et al. 2020; Dancila et al. 2013; Kammegne et al. 2019; Grigorie et al. 2015).

Wingtip devices have become one of the most popular methods for increasing aerodynamic efficiency (Rivero 2020; Gavrilović et al. 2015; Dimino et al. 2021). Designers, researchers, and aircraft operators have obtained various benefits by incorporating morphing winglets, including increased takeoff and climb performance, decreased fuel consumption, and a higher payload range (Haddad 2015). Reduced fuel usage also translates into reduced pollutant emissions, contributing to the aviation industry's sustainability. One of the most critical factors to consider when designing a wingtip device is its flexibility and ease of refit into already-in-service wings. For example, a blended winglet requires fewer structural changes to the wing. In addition, a well-designed blended winglet allows the chord distribution

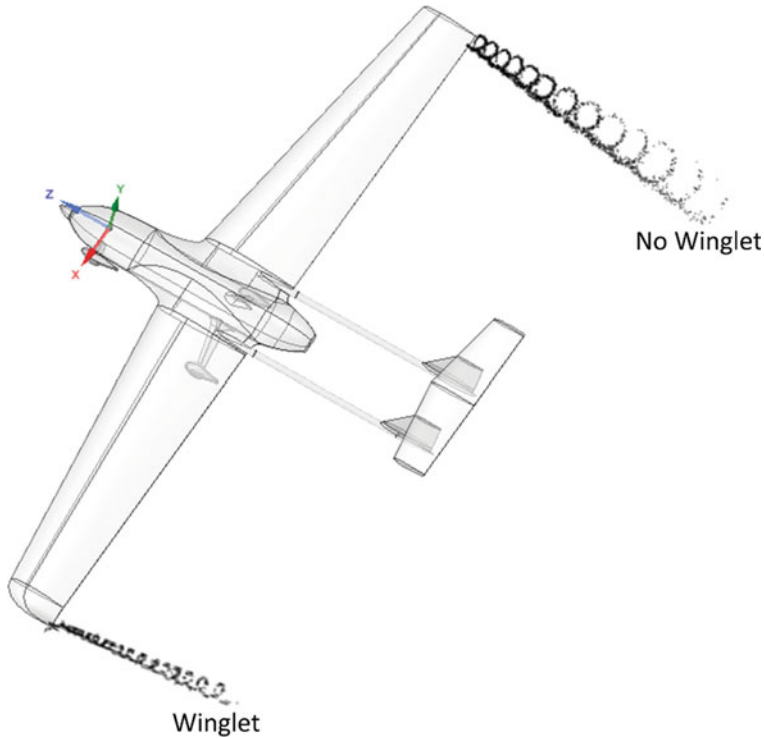


Fig. 7.1 Wingtip vortex structure with and without winglet

to transition smoothly from wingtip to winglet by optimizing span load lift distribution and minimizing aerodynamic interference or airflow separation. The difference in the strength of the wingtip vortices between the winglet and the reference wingtip is illustrated in Fig. 7.1.

Morphing structures allow an aircraft's shape to be optimized for its performance under all flight conditions (Ameduri and Concilio 2020; Arena et al. 2019; Concilio et al. 2021). The aircraft's geometry is (generally) restricted to a single fixed shape that has been tuned for optimal performance during a typical mission (Bashir et al. 2021, 2022a, b). This does not imply that it performs optimally during each flight phase, as it may operate at a suboptimal level for other flight conditions. Morphing structures allow for optimal performance over the flight envelope by lowering wing loads, fuel consumption, and greenhouse gas emissions. The notion of a morphing winglet can significantly improve aircraft performance by reducing drag and emissions (Eguea et al. 2020, Dimino et al. 2021, Meyran et al. 2021, Noviello et al. 2019, Liauzun et al. 2018).

To the best of the authors' knowledge, the approach for optimizing the winglets with leading-edge morphing presented here has not yet been studied. This study investigates the effect of leading-edge morphing on winglet performance. The aerodynamic properties of a leading-edge morphing winglet for the UAS-S45

wing are calculated using the modified class shape transformation (CST) parameterization technique and a particle swarm optimization (PSO) algorithm combined with pattern search as an optimization algorithm, as well as the VSPAERO solver.

7.1.1 Bibliographical Review

Winglets are wingtip devices that generate thrust by reducing the size and strength of the vortex in the wingtip flow (Kroo 2001), thereby reducing the wing-induced drag component. Whitcomb (1976) evaluated the performance of winglets mounted on the wingtip of a first-generation, narrow-body jet transport wing in a wind tunnel at high subsonic speeds. Whitcomb's investigation found that the lift-dependent drag, which accounts for roughly 30% of the overall drag in cruise flight conditions and at lower speeds, was highly affected by the addition of winglets. The impact of winglets on the lift coefficient was more than double than that obtained with span extension. Another investigation was conducted to confirm the impact of the Whitcomb winglet (Heyson et al. 1977) and found that the winglet gives higher induced efficiency than a wingtip extension for the same bending moment. A winglet offers a trade-off between efficiency and root bending moment. The new winglet configurations offer designers the freedom to trade small percentage reductions in the induced efficiency increase for larger percentage reductions in the root bending moment increase.

Another study on the winglet-span extension trade-off was performed by (Jones 1980). The authors compared the winglet configurations using the integrated bending moment along the wingspan. The computational analysis demonstrated that both winglets and span extensions gave the same level of induced drag reduction, while the optimal wing weight was kept constant. In a circulatory vortex flow, the increasing pressure field below the wing had the tendency to vanish around the wingtip (Jupp 2001). The study demonstrated that the endplate concept has never worked in practice due to its large surface area and its (often) split flow. The associated skin friction and form drag frequently countered the benefit of minimizing induced drag (Jupp 2001). Whitcomb (1976) replaced the endplate with an aerodynamic lifting surface that used the circulation around the winglet to counter the flow near the wingtip.

Numerical approaches were used to study the anhedral winglets that may reduce the wing root bending moment more than dihedral winglets (Büscher et al. 2006). Various wing planforms have been optimized for fast speeds and high lift. The load distributions vary greatly depending on the design goal. Using computational fluid dynamics methods, the influence of root bending moment on the drag was analyzed. A multidisciplinary design exploration technique was developed for a commercial jet winglet (Takenaka et al. 2008). This technique was integrated with an automatic numerical mesh design method, a kriging surrogate model, and a multi-objective genetic algorithm. An optimal geometry found using these techniques increased the maximum takeoff weight by around 0.6% while reducing fuel by more than 5%

(41) A study on the cant angle effect on winglets demonstrated an increase in C_L/C_D of 11% for the best cant angle winglet compared to a wing with no tip device (Khalil et al. n.d.).

The effect of the wingtip blowing technique on fixed and adaptive multi-winglets was evaluated in a wind tunnel with Coanda jets (Céron-Muñoz et al. 2013), and the impact of each wingtip configuration on aircraft performance (the induced drag reduction) was determined. Due to the enormous amount of energy required by wingtip blowing, multi-winglets appear to be a more promising alternative for practical use in commercial aircraft, with an increase of 55% in the effective aspect ratio of the wings, while increasing the maximum range and rate of climb by 7% and 12%, respectively. Winglets affect the aerodynamic efficiency, fuel consumption, and aircraft weight. Thus, the addition of winglets on an existing aircraft has an effect on its immediate operational expenses. For a long-range passenger aircraft, winglet installation resulted in a 2% reduction in operating costs (Elham and Van Tooren 2014).

In 2020, winglet spanwise camber morphing was optimized using a genetic algorithm (Eguea et al. 2020). These camber adjustments were to the leading and trailing edge parts, with a fixed center section for structural reasons. The camber morphing winglet concept was tested in a midsize business jet and showed fuel consumption reduction over a fixed geometry winglet. Using morphing technology, an integrated design of a full-scale morphing winglet can improve aircraft aerodynamic efficiency in off-design flight conditions, reduce the wing-bending moments due to maneuvers, and increase flight stability (Dimino et al. 2021). This design used two independent and synchronous control surfaces with variable camber and differential settings. The system was designed to work for various flight cases by moving the control tabs. The aerodynamic performance and the actuation systems' integration in the winglet surface geometry were analyzed quantitatively.

A control surface with Fluid-Actuated Morphing Unit Structures (FAMoUS) was investigated in (Vasista et al. 2020). The narrow profile of this control surface made it difficult to install as a morphing winglet trailing edge for load reduction. The FAMoUS concept uses reinforced elastomeric unit structures (cells) that extended under hydraulic pressure. The camber morphing winglet of a business jet was studied using full-potential code and ANSYS CFX (Eguea et al. 2021). The full-potential model was based on the Boundary Layer Wing Flow (BLWF) code due to its capability of performing rapid preliminary aerodynamic analysis, and it provided results with adequate accuracy. Its performance was evaluated using an aircraft drag and wingtip vortex analysis. The camber morphing winglet minimized the drag by reducing the vortex size. The redesigned winglet reduced the aircraft drag, despite encountering flow separation during climb and weak shock waves during cruise.

An adaptive winglet to improve the CRJ700's aerodynamics was investigated in (Segui et al. 2021b). A single-rotation axis adaptive winglet was added to the aircraft's geometry. The adaptive winglet design was analyzed for 16 flight conditions including climb and cruise. This evaluation showed that the adaptive winglet can reduce the drag by up to 2.65% while increasing the lift. The study investigated the aerodynamic polar and pitching moment coefficient fluctuations of adaptive and

fixed winglets on the Bombardier CRJ700. A structural model with hinges inside mechanically powered adaptive winglet topologies was investigated (Dimino et al. 2019). The distorted shape was evaluated to find the strain map and internal force distribution changes required for stress analysis and design, and then the mode variations that could affect aeroelastic stability margins were assessed. These static and dynamic investigations considered the lag impact.

Our work is presented in the following sections. An optimization framework outlines the overall optimization approach in Sect. 7.2, where the parameterization technique is utilized to obtain the optimal aerodynamic shapes and the best computational solvers as presented in 7.2.1 and 7.2.2 respectively. The optimization framework includes the two objective function formulations, “drag minimization” and “endurance maximization” as presented in Sect. 7.2.3. The results obtained using these algorithms for the UAS-S45’s optimized designs are compared with the reference UAS-S45 model results in Sect. 7.3. Our conclusions and recommendations for future work are presented in Sect. 7.4.

7.2 Methodology

A full-scale morphing wing model of an UAS-S45 with a 2.2-m span and a 0.6-m root chord was used in this optimization study. To use morphing winglets on the UAS-S45, the winglet sections must morph the shape and be structurally feasible. All numerical optimizations must account for the fabrication restrictions and technological capabilities. The leading-edge morphing starts at $x/c = 20\%$ of the chord length.

The optimization case was considered at the Reynolds number $= 2.4 \times 10^6$ and Mach number $= 0.1$. The Mach number used is the design Mach number of the UAS-S45, whereas the Reynolds number was calculated based on this Mach number, mean aerodynamic chord of the UAS-S45, and standard atmospheric conditions. Some restrictions in morphing geometry variations were necessary due to the flexible nature of the airfoil’s arc length and to maintain control over shape variation while ensuring that the other constraints given in Table 7.1 were respected. The area morphed on the flexible airfoil and its fixed (wing) spar at $0.20c$ should not be higher than 10% of the reference geometry. Constraints on the design variables were introduced to avoid the development of extremely deformed shapes that would not

Table 7.1 Optimization criteria and constraints

Function/Variable	Description
Airfoil	UAS-S45 root airfoil
Objective function	Maximize $\frac{C_L}{C_D}$
Subjected to	$C_{L_{\text{morph}}} \geq C_{L_{\text{min, baseline}}}(x, \alpha, M)$ $x \in \text{airfoil set}$
Geometric constraints	Morphing begins at $x/c = 20\%$
Termination criteria	When the constraints are respected

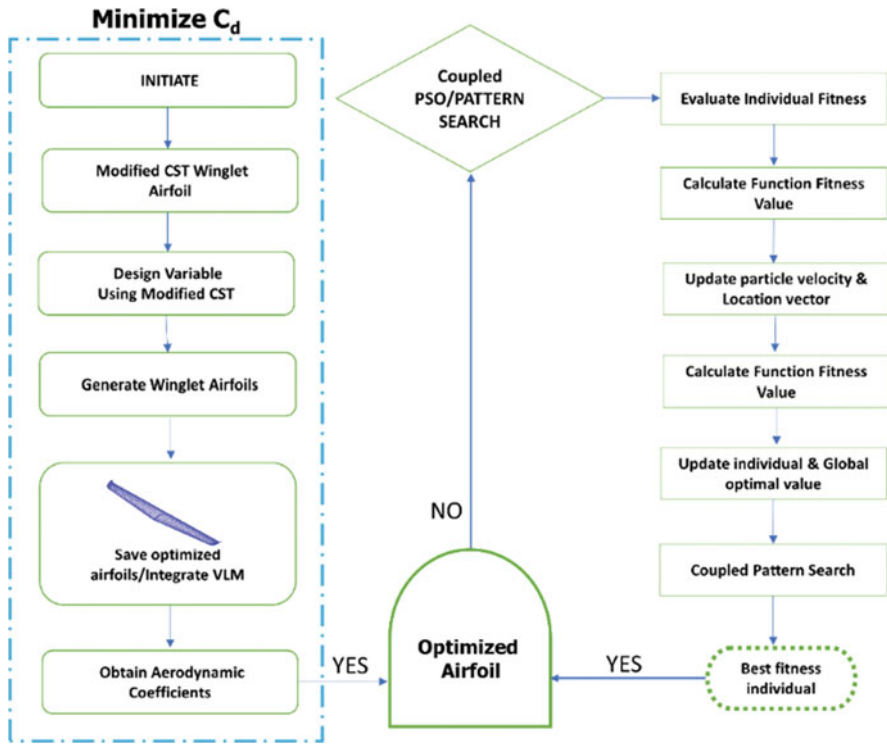


Fig. 7.2 Schematic of the optimization procedure

be aerodynamically efficient, while still meeting other constraints and requirements. In terms of aerodynamics, the lift coefficient does not decrease in relation to its reference value.

The optimization tool consists of a standard optimization loop written and executed in MATLAB. The class shape transformation (CST) method was used for aerodynamic shape parameterization, and the particle swarm optimization (PSO)-pattern search was used as an optimization algorithm. The aerodynamic solver used in this study is VSPAERO. The sections will be explained later. The flowchart of the overall methodology is depicted in Fig. 7.2.

7.2.1 Modified CST Parameterization

Aerodynamic optimization occurs in both preliminary and detailed aircraft design phases. Aerodynamic optimization relies on airfoil parameterization or on its design parameters. This parameterization is required to represent the reference airfoil, which

can then be optimized to obtain new airfoils with improved aerodynamic coefficients.

For optimum aerodynamic designs, Kulfan (2010) suggested a geometric representation of an airfoil that performs well, produces smooth and realistic shapes, and uses a minimum number of design variables to describe the complete airfoil. Kulfan formed the CST parameterization method to represent an airfoil. The CST's control parameters are the leading-edge radius, the boat-tail angle, and the trailing-edge thickness. However, for most airfoils, their upper and lower leading-edge radii are different. Since CST uses a Bernstein polynomial for modeling both two-dimensional and three-dimensional (3D) aerodynamic shapes, the leading edge is not modeled well using Bernstein polynomial. A new basis function that will improve the airfoil's precision and reduce the number of its control parameters is considered in this study.

The airfoil parameterization used in this study is also based on a modified class shape transformation (CST) method. First, the generalized CST equations are described as they are applied to the airfoil. Then, the upper and lower surfaces are defined individually, using a class function $C(\frac{x}{c})$ and a shape function $S(\frac{x}{c})$ as shown in Eqs. (7.1) and (7.2):

$$y_{\text{upper}} = C_{N_2}^{N_1} \left(\frac{x}{c} \right) S_{\text{upper}} \left(\frac{x}{c} \right) + y_{\text{upperLE}} \left(\frac{x}{c} \right) \quad (7.1)$$

$$y_{\text{lower}} = C_{N_2}^{N_1} \left(\frac{x}{c} \right) S_{\text{lower}} \left(\frac{x}{c} \right) + y_{\text{lowerLE}} \left(\frac{x}{c} \right) \quad (7.2)$$

where $\frac{x}{c}$ is defined as a percentage of the airfoil chord (therefore, $\frac{x}{c}$ has a value between 0 and 1), and N_1 and N_2 are 0.5 and 1, respectively. Here, x_{upperLE} and x_{lowerLE} translation is also applied to the $\frac{x}{c}$ values.

For the skin length to remain at a constant while being morphed, a deformation factor was introduced. This deformation factor is not controlled by the user but is instead limited by the possible geometry of the final airfoil. The initial length of the skin is determined by using the following equations based on the reference airfoil's surfaces, where y_{upper_r} and y_{lower_r} are the lengths of the reference upper and lower surfaces, respectively:

$$\text{Length}_{\text{ru}} \left(\frac{x}{c} \right) = \int_0^{\frac{x}{c}} \sqrt{1 + \left(\frac{d}{d(\frac{x}{c})} \left(y_{\text{upper}_r} \left(\frac{x}{c} \right) \right) \right)^2} d \left(\frac{x}{c} \right) \mid \frac{x}{c} < \text{Morph}_{\text{length}} \quad (7.3)$$

$$\text{Length}_{\text{rl}} \left(\frac{x}{c} \right) = \int_0^{\frac{x}{c}} \sqrt{1 + \left(\frac{d}{d(\frac{x}{c})} \left(y_{\text{lower}_r} \left(\frac{x}{c} \right) \right) \right)^2} d \left(\frac{x}{c} \right) \mid \frac{x}{c} < \text{Morph}_{\text{length}} \quad (7.4)$$

$$\text{Reflength}_r\left(\frac{x}{c}\right) = \text{Length}_{ru}\left(\frac{x}{c}\right) + \text{Length}_{rl}\left(\frac{x}{c}\right) \quad (7.5)$$

It is assumed that a $\text{Morph}_{\text{length}}$ provides the length of the morphing section.

The deformation factor relative to $\frac{x}{c}$ is determined from the unmorphed airfoil's skin length. Assuming that z is the correction value, a sinusoidal function is applied to the section between $\frac{x}{c} = 0$ and $\frac{x}{c} = \text{Morph}_{\text{length}}$, providing the following equations:

$$\text{Factor}_u\left(\frac{x}{c}\right) = 1 - \sqrt{\sin\left(\frac{\text{Length}_{ru}\left(\frac{x}{c}\right)}{\text{Length}_{ru}\left(\text{morph}_{\text{length}}\right)} \times \pi\right) \times z} \quad (7.6)$$

$$\text{Factor}_l\left(\frac{x}{c}\right) = 1 - \sqrt{\sin\left(\frac{\text{Length}_{rl}\left(\frac{x}{c}\right)}{\text{Length}_{rl}\left(\text{morph}_{\text{length}}\right)} \times \pi\right) \times z} \quad (7.7)$$

Since the difference between the reference airfoil and the morphed airfoil is based on an arc, the distance between the skin and the arc is affected by the deformation factor.

$$x_{\text{upper}_{\text{constlength}}} = x_{\text{upper}}\left(\frac{x}{c}\right) + \left(x_{\text{upper}}\left(\frac{x}{c}\right) - x_{\text{arc}}\left(\frac{x}{c}\right)\right) \times \text{factor}_u\left(\frac{x}{c}\right) \quad (7.8)$$

$$y_{\text{upper}_{\text{constlength}}} = y_{\text{upper}}\left(\frac{x}{c}\right) + \left(y_{\text{upper}}\left(\frac{x}{c}\right) - y_{\text{arc}}\left(\frac{x}{c}\right)\right) \times \text{factor}_u\left(\frac{x}{c}\right) \quad (7.9)$$

where $\left(\frac{x}{c}\right)_{\text{arc}}$ and $\left(\frac{y}{c}\right)_{\text{arc}}$ are the x and y arc positions. The same would apply to the lower surface. Using Eqs. (7.3), (7.4), and (7.5) to determine the length of the morphed airfoil, it is possible to determine the z value using:

$$\text{Reflength}_r(\text{morph}_{\text{length}}) = \text{Reflength}_m(\text{morph}_{\text{length}}) \quad (7.10)$$

By using the morphed airfoil deflection y_{upper_m} and y_{lower_m} values, we resolve the functions as shown in Eq. (7.7) so that the lengths of both the reference and morphed skin are the same.

The morphing airfoil shapes were obtained from the CST parameters by perturbing the original curvature coefficients for both the upper and lower surfaces of the airfoil, as well as by varying the airfoil's leading edge, as shown in Fig. 7.3.

7.2.2 Aerodynamic Solver

OpenVSP's aerodynamic tool (Open Vehicle Sketch Pad), VSPAERO solver, was used to estimate the wing drag as well as to analyze the morphing airfoil. VSPAERO provides rapid aerodynamic analysis using the vortex lattice method (VLM) or panel

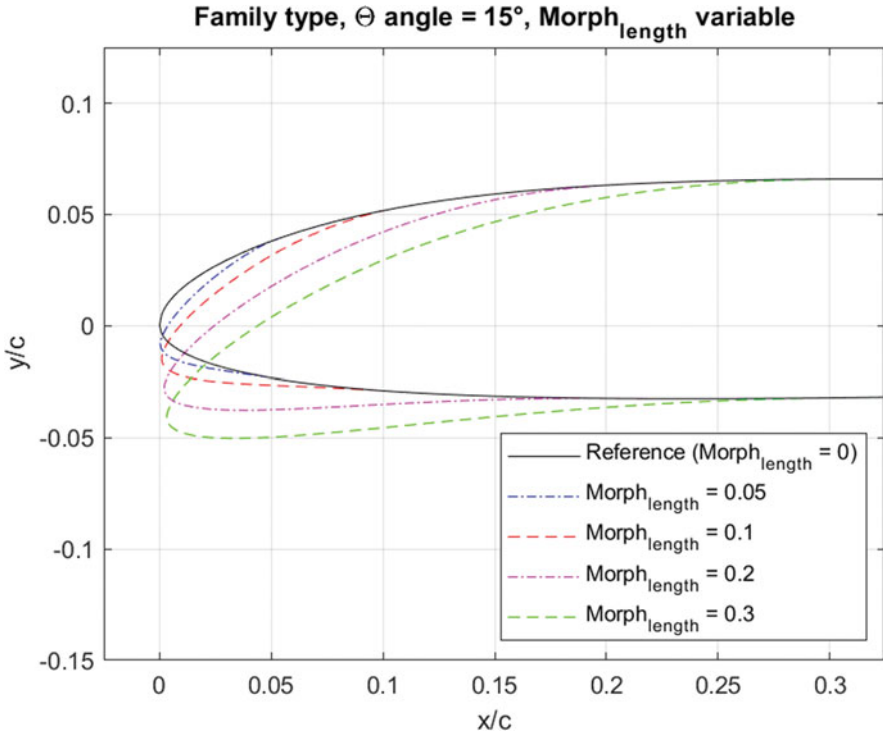


Fig. 7.3 Class function shape with $N_1 = 0.5$ and $N_2 = 1$

method. It is a well-recognized computational mean-adopting vortex lattice solver that uses a simple actuator disk model to represent the flow over a section of panels for aero-propulsive investigation and offers a visualization for wake and pressure coefficient changes. VSPAERO uses a mesh agglomeration scheme to improve the scaling of meshes with large-scale meshes and that can be used for subsonic and supersonic aerodynamics. The generalized minimal residual method (GMRES) technique is used in the solver. Both the VLM and the panel technique using generalized vortex loops are included in VSPAERO (McDonald 2016). In addition, it supports the integration of a coupled BEAM3D, which is finite element code, for steady-state aeroelastic analyses. VSPAERO is part of the OpenVSP design package and is an open-source code. The wing geometry for the UAS-S45 modeled in VSPAERO is shown in Fig. 7.4.

7.2.3 Optimization Algorithm

An intelligent search algorithm was chosen to evaluate the objective function in the numerical optimization of the airfoil design. First, a shape parameterization approach

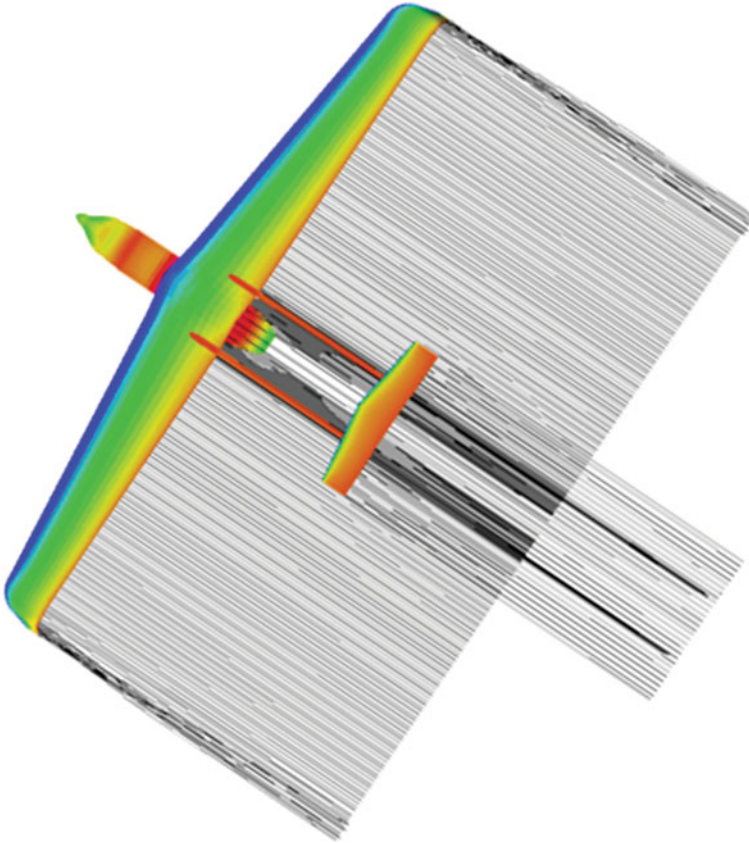


Fig. 7.4 UAS-S45 model with winglet design as modeled in VSPAERO solver

defined the airfoil shape, and then a flow solver was used to obtain the aerodynamic coefficients. Providing a globally optimal solution with low computational resources is a measure of its efficiency. The algorithm thus uses the optimized solution convergence and demonstrates its feasibility.

Particle swarm optimization (PSO) (Lazinica 2009) is one of the most commonly used population-based swarm intelligence and evolutionary techniques for solving global numerical problems. PSO applications are found in practically every scientific field, including engineering optimization. Every year since 1995, the PSO technique has been presented in several studies with many variations. PSO variations are based on individual particle motion through the search space, such as birds or insects. The flocking behavior of birds inspired the original PSO algorithm. This algorithm considers each particle as a solution to an optimization problem. It has two vectors: position and velocity.

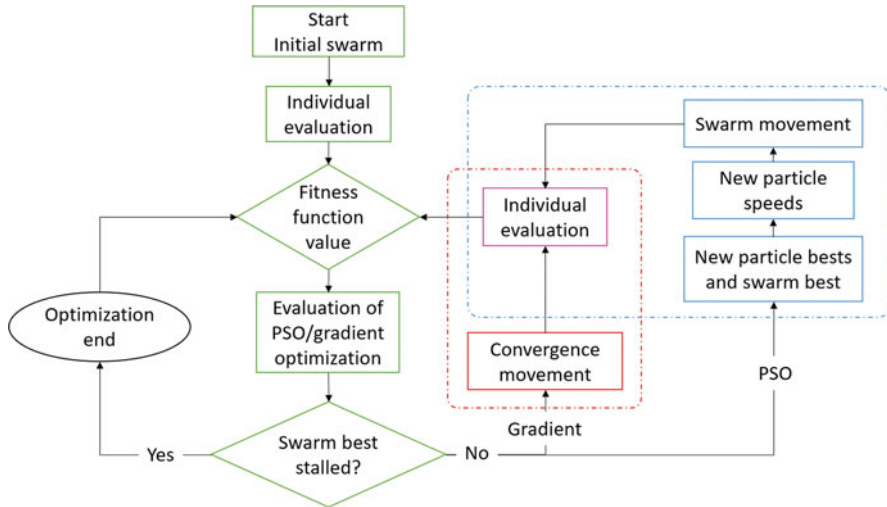


Fig. 7.5 Chart of the PSO algorithm combined with the pattern search algorithm

The position vector contains the values of the function's variables. If a function has two parameters, the particles will have two-dimensional position vectors. Each particle can then move in an n -dimensional search space with n variables.

The second vector (velocity) is used to update a particle's positions. This vector defines the step size for each dimension and particle separately. Instead of using parameters such as "crossovers" and "mutations," PSO algorithms update their solutions by sharing information among the swarm population.

Airfoil shape designers are interested in evolutionary algorithms because of their applicability for modeling discontinuous shape functions, attaining optimal global solutions, and facilitating parallel computing. Gradient-based techniques converge quickly during morphing airfoil optimization but only cover a small portion of the search space, resulting in a local minimum solution rather than a global minimum. Flow discontinuities make finding the gradient of nonlinear flow fields problematic for gradient-based optimizers.

In the proposed PSO-pattern search (PS)-based optimization, a pattern search (PS) method is employed to exploit the parameter's solution space. For each iteration, direct search methods compare a function value in a finite set of trial locations. Direct search approaches do not employ function derivative information but implicitly attempt to create derivative approximations. PS methods are direct search methods that have substantial trial point generation constraints and give convergence for stationary points from arbitrary starting points. PSO-PS investigates the nearest neighbor parameter vectors of the current point and finds a better trajectory. If all the neighbor points fail to produce a reduced value, then the search step is reduced. This process continues until the search step becomes sufficiently small, which ensures the convergence to a local minimum. Pattern search is used to

leverage the parameter solution space in the proposed PSO-PS-based optimization. A hybrid optimizer is used in this study, as shown in Fig. 7.5.

7.3 Discussion of Results

We designed our morphing winglet inspired by the bending behavior of the honeybee abdomen, and 3D-printed a prototype using polyethylene terephthalate glycol (PETG) material. A geometrical model proposed to illustrate the bending behavior of the honeybee abdomen was used for the morphing leading edge. Theoretical analysis of the microstructure of a honeybee abdomen was utilized to investigate its microstructure and motion principles with the aim of depicting a honeybee's landing behavior (Zhao et al. 2017). In the morphing leading-edge winglet, the skin and its compliant mechanisms are connected by three stringers, which help to distribute the forces from the mechanisms to the skin. The morphing structure is attached to the servomechanism, ensuring that the input forces can be applied horizontally, as shown in Fig. 7.6. A servo motor provides the structure motion through a rotating linkage.

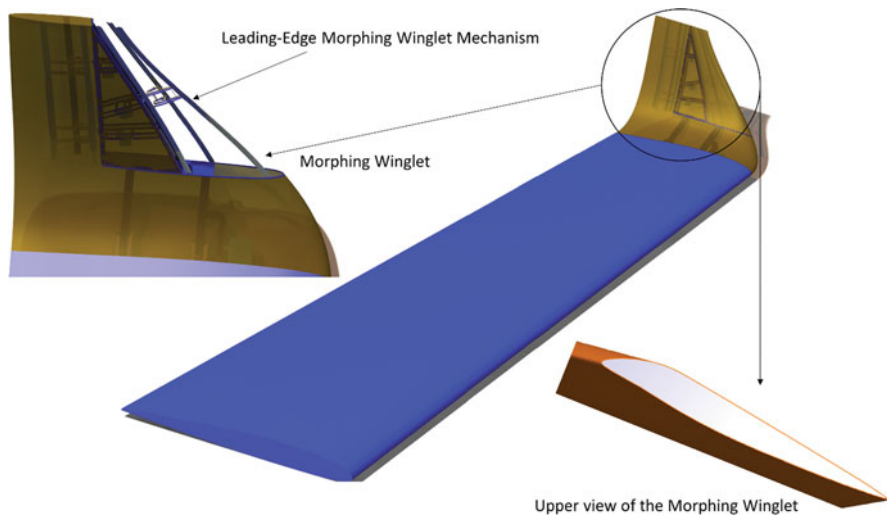


Fig. 7.6 Outline of a morphing winglet concept inspired by the honeybee abdomen's bending mechanism

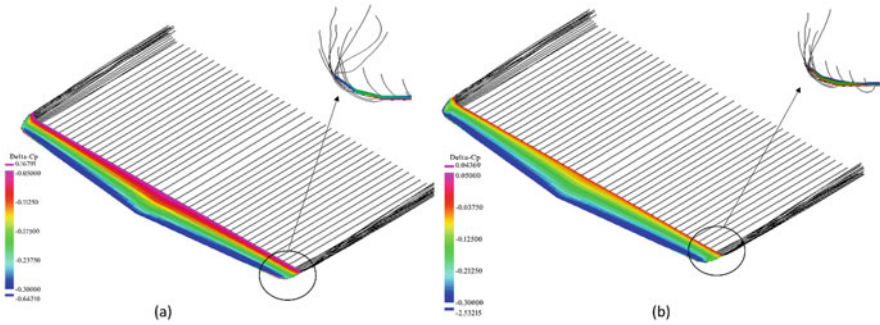


Fig. 7.7 Comparison of the vortices for (a) the reference winglet geometry and (b) the morphing winglet at cruise flight condition

7.3.1 Optimization Results

The aerodynamic optimization considered in this study applies to morphing winglet configurations at two different flight conditions of cruise and climb, for an angle of attack of 2° in cruise and an angle of attack of 6° for climb. Both cases considered a Reynolds number of 2.4×10^6 and a Mach number of 0.1. The design framework uses endurance maximization as an optimization function to enhance the performance of the UAS-S45 over a large part of its flight regime.

The aerodynamic analysis of the winglet suggests that a larger low-pressure area formed on its inboard enhances the section lift coefficients toward the wingtip, explaining why the lift distribution is larger than that of the basic planform geometry. This greater lift distribution reduces the induced drag. Winglets reduce the induced drag by minimizing the size of the wingtip vortices. The wing's lower surface pressure forces air to move toward the wing's tip. Since the wing's upper surface has less air pressure, the air rolls over and swirls around the wingtip. This swirling wind creates a vortex, thus lowering the wing's aerodynamic effectiveness. A "wake" is created when fast-flowing air meets slow-moving air at the wing's tip. Reduced vortex disruption allows for smoother and more efficient aircraft.

The reference winglet and the morphing winglet were compared for cruise flight conditions at an angle of attack of 2° , as shown in Fig. 7.7. Figure 7.7a shows the reference winglet's velocity profiles. The higher streamline concentrations on the reference wing and its winglet tip vortices indicate higher velocities and vorticities, respectively. In Fig. 7.7b, a weaker vortex arises, as indicated by the less-concentrated streamlines. The morphing winglet decreases drag by modifying the tip vortex shape. The morphing winglet tip's vortex structure is similar to that of the reference winglet tip, but there is less twisting around the winglet tip than around the reference wingtip. The vortex core of the reference winglet has a larger radius than that of the morphing winglet.

Figure 7.8 shows a comparison of the reference and morphing winglet vortices for climb flight condition at an angle of attack of 6° . The flow field at the upper surface

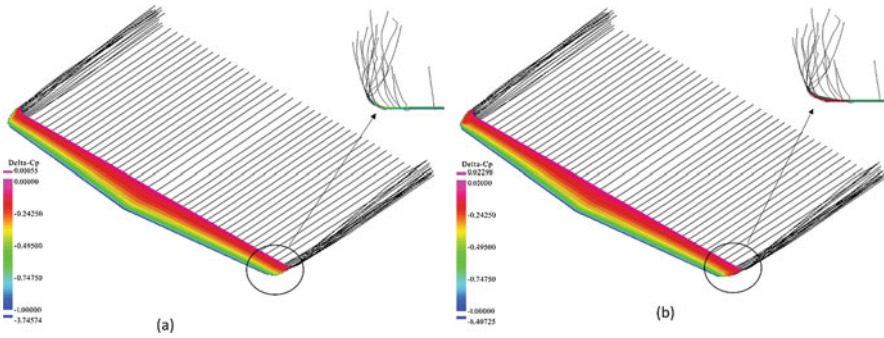


Fig. 7.8 Comparison of the vortices for (a) the reference winglet geometry and (b) the morphing winglet at climb flight conditions

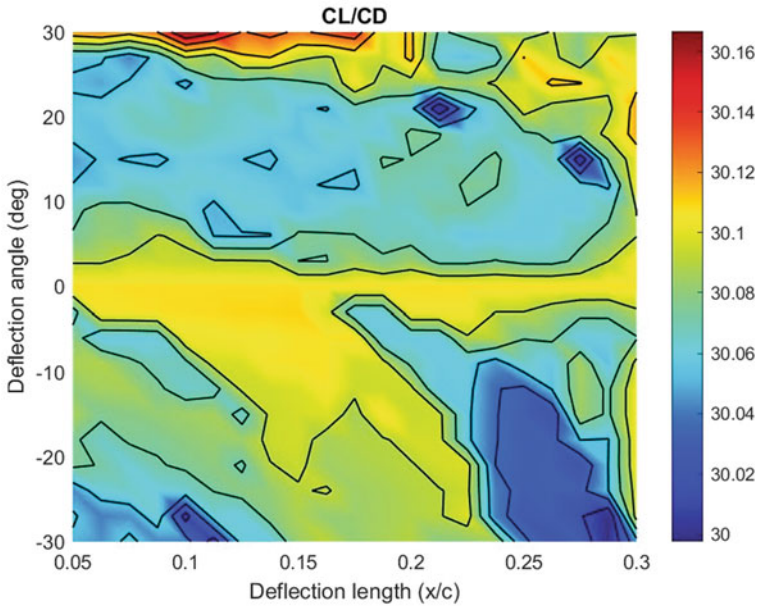


Fig. 7.9 MATLAB plots for the morphing leading edge depicting the C_L/C_D ratio for climb flight conditions

of the wing is affected by the tip vortices formed by the winglets. The vortices will change their shapes with the angle of attack, and the values of the vortices behind the winglets indicate the induced drag. The streamlines are more concentrated on the reference wing, as shown in Fig. 7.8a, indicating higher velocities and vorticities and thus stronger winglet tip vortices. Figure 7.8b shows that the morphing winglet has fewer streamlines, meaning a weaker vortex, as the winglet decreases its drag by modifying the tip's vortex.

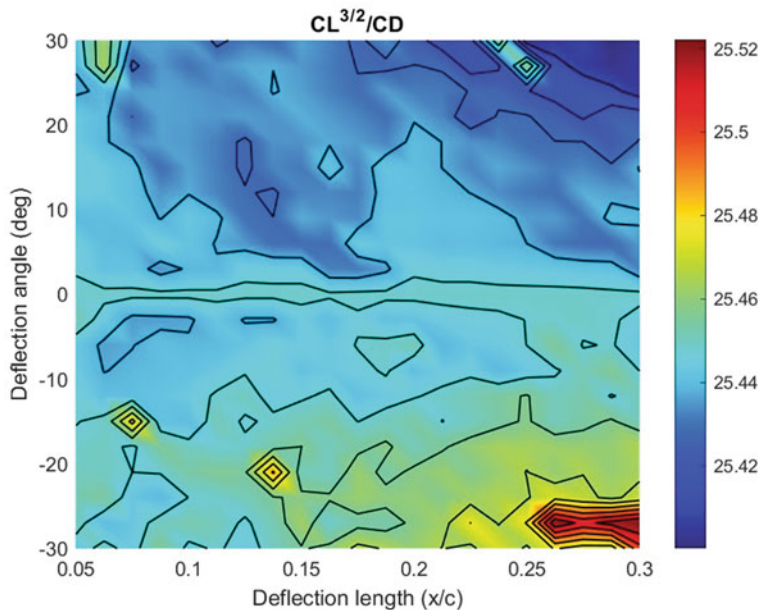


Fig. 7.10 MATLAB plots for the morphing leading edge depicting the $C_L^{3/2}/C_D$ ratio for climb flight conditions

Figures 7.9 and 7.10 show how the angle of the deflection and the length of the deflection segment affect both the C_L/C_D , and the $C_L^{3/2}/C_D$ ratios, respectively. Some significant trends can be noted, such as a small but constant increase in the $C_L^{3/2}/C_D$ values, while the angle of deflection decreases and the deflecting segment size increases, as shown in Fig. 7.10. However, no such trend is present in the C_L/C_D graph (Fig. 7.9), where several locations indicate that a better-than-reference performance can be observed, although they appear to be randomly located. However, small negative deflections seem to positively impact the overall performance of the wing, which suggests an indication of the benefits of the winglet leading-edge deflection. While these trends appear to have a minimal impact on the lift-to-drag ratio, the aircraft's endurance may be affected in a more predictable manner. The deflection values, meanwhile, are high up to 30° ; an analysis of each use case should be performed to determine the feasibility and impact of introducing such a mechanism on an aircraft's weight and power consumption.

Figure 7.11 represents comparisons of the results for the aerodynamic performance of the reference wing with and without a winglet and for a wing with a morphing winglet. The lift coefficients in Fig. 7.11a show that the morphing winglet performed better than the reference winglet and the wing without a winglet. Leading-edge morphing decreases the unfavorable pressure gradient and improves aerodynamic performance by attenuating the leading-edge suction peak. Figure 7.11b depicts the C_L/C_D ratios produced by optimizing the winglet using a leading-edge

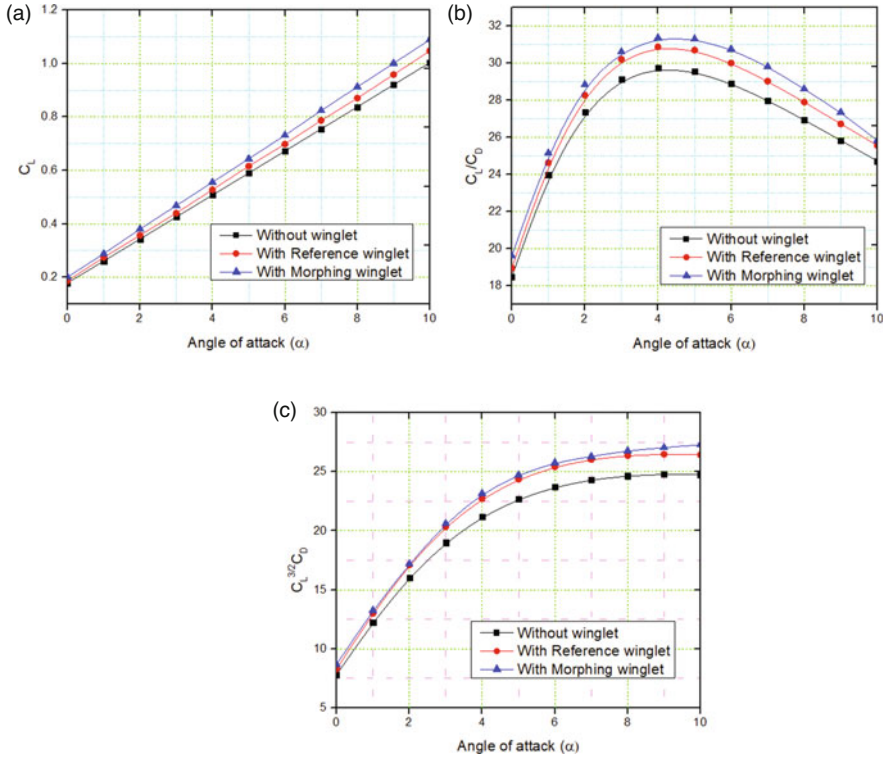


Fig. 7.11 Aerodynamic performance parameter variations of C_L , C_L/C_D , and $C_L^{3/2}/C_D$ vs the angle of attack

morphing method at various angles of attack. The optimized morphing winglet design clearly produces the optimum aerodynamic performance. With a morphing winglet, the wing can reach C_L/C_D values of 28.84, representing a 5.37% increase over its starting value of 27.37 for cruise flight conditions at an angle of attack of 2° . The morphing winglet also outperforms the standard winglet. Figure 7.11c shows the aerodynamic endurance computed for the same three wing designs at various angles of attack and indicates that the endurance is better and virtually the same for the two wing designs with winglets compared to the wing with no winglet.

7.3.2 CFD Simulation Results

We used Computational Fluid Dynamics (CFD) numerical analysis to compare the performance of several winglet types. The impact of the morphing winglet on the aircraft's aerodynamics and performance was assessed, as well as the impact of several types of winglets on wingtip vortex formation, winglet pressure distribution,

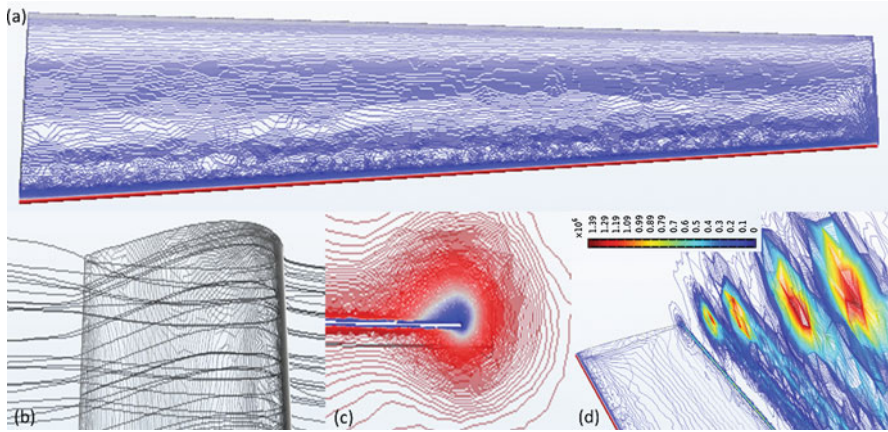


Fig. 7.12 Reference wing without winglet (a) wing geometry, (b) streamlines around the wingtip of the reference wing, (c) high velocity region due to vortices around the wingtip, and (d) effect of the winglet-induced tip vortex structure

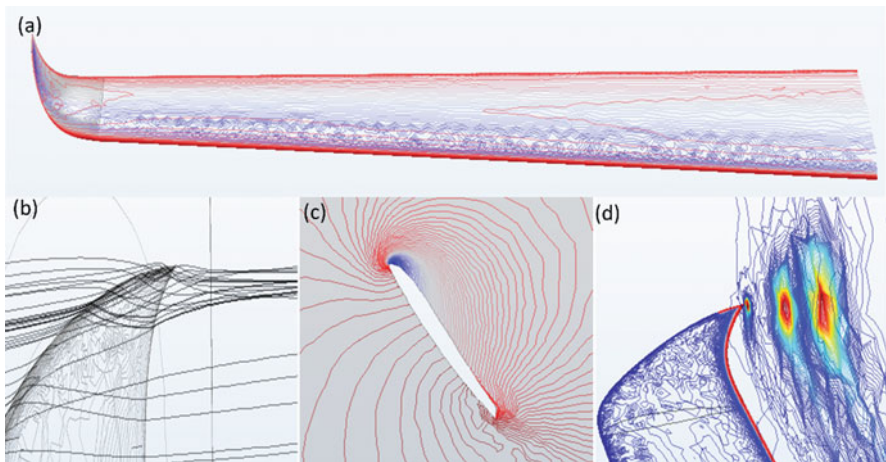


Fig. 7.13 Vortex diffuser winglet (a) wing geometry, (b) streamlines around the wingtip, (c) high velocity region due to vortices around the wingtip, and (d) effect of the winglet-induced tip vortex structure

and streamline distribution. The analysis was done for an angle of attack of 2° . Figures 7.12a, 7.13a, 7.14a, and 7.15a depict the wing geometries of four wingtip shapes.

The data extracted from CFD numerical simulations of flow field structure and vortex formation near the wingtip provides evidence of its increased aerodynamic performance. Figures 7.12b, 7.13b, 7.14b, and 7.15b show the streamlines around the different wingtips along with their associated vortices' sizes and strengths.

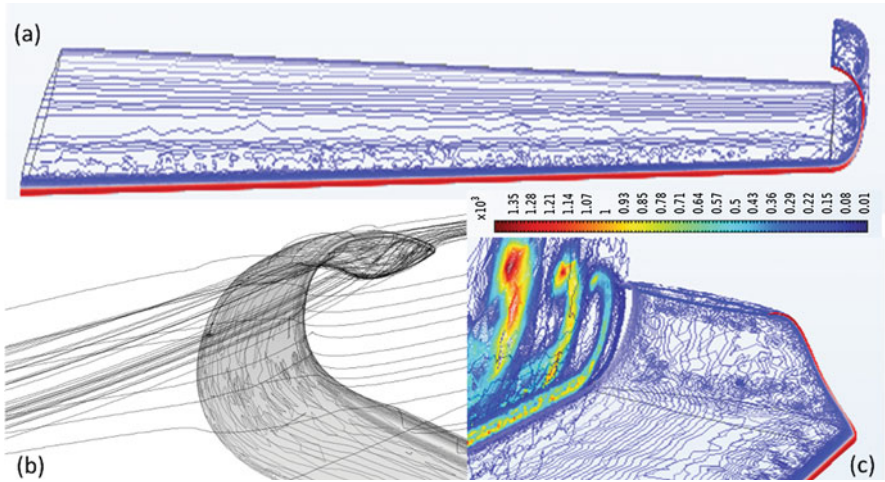


Fig. 7.14 Semi-spiroid winglet (a) wing geometry, (b) streamlines around the wingtip, and (c) effect of the winglet-induced tip vortex structure

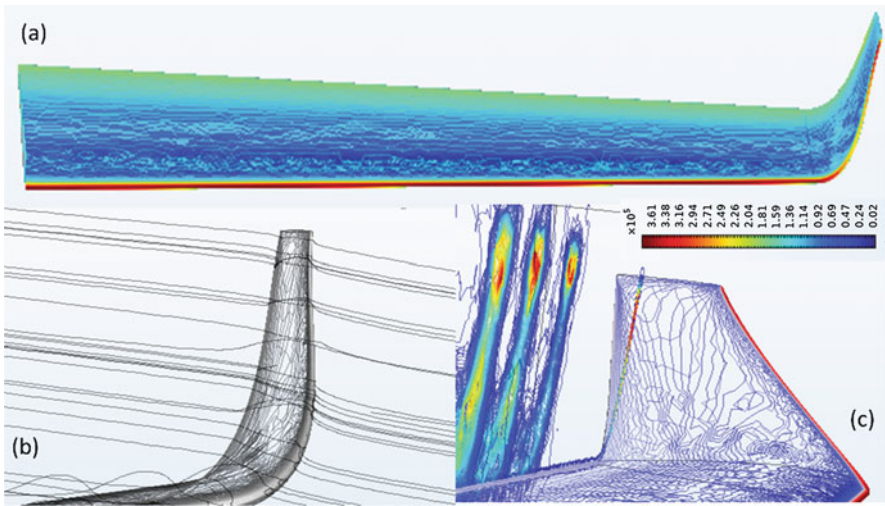


Fig. 7.15 Canted winglet (a) wing geometry, (b) streamlines around the wingtip, and (c) effect of the winglet-induced tip vortex structure

Streamline distribution on the reference wing is more widely distributed compared to that on the winglet shapes, indicating higher velocities and vorticities. The winglet shapes have fewer streamlines, indicating their weaker vortices. Figures 7.12d, 7.13d, 7.14c, and 7.15c show that the winglet reduces the vortex size in cruise conditions. The optimized geometry added the wing with the winglet tip vortices,

thus creating a new vortical structure. The vortex diffuser winglet lowered the tip vortex strength, reducing the induced drag.

The tip vortex structure of the morphing winglet varies according to the morphing optimization results, expressed in terms of the induced drag minimization. The vortex structures and the streamline distributions on the morphing winglets offer a clear explanation of the drag reduction induced by winglet morphing. Furthermore, the pressure distributions in the winglet sections provide additional information by demonstrating the difference between the reference wing without a winglet and the morphing winglet pressure coefficient distributions.

7.4 Conclusion

The objective of this study was to optimize the aerodynamic performance of a morphing winglet for UAS-S45. Particle swarm optimization (PSO) and pattern search (PS) optimization were combined to create a hybrid optimization technique. The optimization function was designed to maximize the C_L/C_D ratio and aerodynamic endurance. Winglet airfoil shapes were parameterized using the modified class shape transformation (CST) approach. The results of hybrid optimization reveal that morphing winglets increased the aerodynamic performance by reducing the drag and by increasing the overall lift and drag coefficients compared to those of an unmorphed winglet. A morphing winglet was compared to a fixed-shape winglet, as well as to a reference wing with no winglet. The optimized winglet's lift coefficients increased with an angle of attack with respect to those of the reference winglet. In addition, the morphing winglet improved the lift-to-drag ratio by up to 10% compared to the reference wing with no winglet. Less drag, better vortex structure, and better pressure distributions were obtained by the use of morphing winglet.

A numerical analysis of different wing geometries was conducted, and the three winglet shapes studied here had the three best performance coefficients. The relative advantage of winglets in terms of lift-to-drag ratio improvement is that they create low-radius tip vortex cores, while the reference (traditional) wing created a large vortex area. Wing vorticity was clearly reduced by introducing diffuser-type winglets and morphing winglets into the UAS-S45 wing, indicating that the use of winglets is an effective method to increase the lift while reducing drag.

Subsonic wind tunnel studies will be conducted in LARCASE's Price-Paidoussis subsonic wind tunnel. This wind tunnel has already been used to evaluate various morphing wing concepts (Communier et al. 2019a, b, 2020; Gabor et al. 2016; Kammegne et al. 2014; Koreanschi et al. 2017, 2016). Additional research was conducted at the LARCASE on morphing winglets for the Cessna Citation X (Ghazi et al. 2020a, b; Segui et al. 2021a; Botez et al. 2019), the CRJ-700 and the UAS-S4 and S45 (Aubeelack and Botez 2019). It is anticipated that these results will explain the flow behavior around a morphing winglet and, as a result, will validate the results of the flow phenomena that occur in its area.

Acknowledgments Special thanks are due to the Natural Sciences and Engineering Research Council of Canada (NSERC) for the Canada Research Chair Tier 1 in Aircraft Modelling and Simulation Technologies funding. We would also like to thank Mr. Oscar Carranza for his support at the Ecole de Technologie Supérieure (ETS), as well as Hydra Technologies' team members Carlos Ruiz, Eduardo Yakin, and Alvaro Gutierrez Prado in Mexico.

References

- Ameduri S, Concilio A (2020) Morphing wings review: aims, challenges, and current open issues of a technology. *Proc Inst Mech Eng Part C J Mech Eng Sci* 237(18). <https://doi.org/10.1177/0954406220944423>
- Arena M, Concilio A, Pecora R (2019) Aero-servo-elastic design of a morphing wing trailing edge system for enhanced cruise performance. *Aerosp Sci Technol* 86:215–235
- Aubeelack H, Botez RM (2019) Simulation study of the aerodynamic force distributions on the Uas-S45 Baalam wing with an upswept blended winglet. *INCAS Bull* 11:21–38
- Barbarino S, Bilgen O, Ajaj RM, Friswell MI, Inman DJ (2011) A review of morphing aircraft. *J Intell Mater Syst Struct* 22:823–877
- Bashir M, Longtin-Martel S, Botez RM, Wong T (2021) Aerodynamic design optimization of a morphing leading edge and trailing edge airfoil—application on the UAS-S45. *Appl Sci* 11:1664
- Bashir M, Longtin Martel S, Botez RM, Wong T (2022a) Aerodynamic design and performance optimization of camber adaptive winglet for the UAS-S45. *AIAA Scitech 2022 Forum*, 1041
- Bashir M, Longtin Martel S, Botez RM, Wong T (2022b) Aerodynamic shape optimization of camber morphing airfoil based on black widow optimization. *AIAA Scitech 2022 Forum*, 2575
- Botez R (2018) Morphing wing, UAV and aircraft multidisciplinary studies at the Laboratory of Applied Research in Active Controls, Avionics and AeroServoElasticity Larcase. *Aerospace Lab* 4:1–11.
- Botez RM (2022) Overview of morphing aircraft and unmanned aerial systems methodologies and results—application on the Cessna Citation X, CRJ-700, UAS-S4 and UAS-S45. *AIAA Scitech 2022 Forum*, 1038
- Botez RM, Molaret P, Laurendeau E (2007) Laminar flow control on a research wing project presentation covering a three year period. *Canadian aeronautics and space institute annual general meeting*
- Botez R, Koreanschi A, Gabor O, Tondji Y, Guezguez M, Kammegne J, Grigorie L, Sandu D, Mebarki Y, Mamou M (2018) Numerical and experimental transition results evaluation for a morphing wing and aileron system. *Aeronaut J* 122:747–784
- Botez RM, Bardela P-A, Bournisien T (2019) Cessna Citation X simulation turbofan modelling: identification and identified model validation using simulated flight tests. *Aeronaut J* 123:433–463
- Büscher A, Radespiel R, Streit T (2006) Modelling and design of wing tip devices at various flight conditions using a databased aerodynamic prediction tool. *Aerosp Sci Technol* 10:668–678
- Céron-Muñoz HD, Cosin R, Coimbra RDF, Correa L, Catalano F (2013) Experimental investigation of wing-tip devices on the reduction of induced drag. *J Aircr* 50:441–449
- Communier D, Botez R, Wong T (2019a) Experimental validation of a new morphing trailing edge system using Price–Païdoussis wind tunnel tests. *Chin J Aeronaut* 32:1353–1366
- Communier D, Le Besnerais F, Botez RM, Wong T (2019b) Design, manufacturing, and testing of a new concept for a morphing leading edge using a subsonic blow down wind tunnel. *Biomimetics* 4:76
- Communier D, Botez RM, Wong T (2020) Design and validation of a new morphing camber system by testing in the price—Païdoussis subsonic wind tunnel. *Aerospace* 7:23

- Concilio A, Dimino I, Pecora R (2021) SARISTU: Adaptive Trailing Edge Device (ATED) design process review. *Chin J Aeronaut* 34:187–210
- Dancila B, Botez R, Labour D (2013) Fuel burn prediction algorithm for cruise, constant speed and level flight segments. *Aeronaut J* 117:491–504
- Dimino I, Pecora R, Arena M, Ameduri S (2019) Effect of hinge elasticity on morphing winglet mechanical systems. *Active and Passive Smart Structures and Integrated Systems XIII*. International Society for Optics and Photonics, 1096711
- Dimino I, Andreutti G, Moens F, Fonte F, Pecora R (2021) Integrated design of a morphing winglet for active load control and alleviation of turboprop regional aircraft. *Appl Sci* 11:2439
- Eguea JP, Catalano FM, Abdalla AM, De Santana LD, Venner CH, Fontes Silva AL (2018) Study on a camber adaptive winglet. 2018 Applied Aerodynamics Conference, 3960
- Eguea JP, Da Silva GPG, Catalano FM (2020) Fuel efficiency improvement on a business jet using a camber morphing winglet concept. *Aerosp Sci Technol* 96:105542
- Eguea JP, Bravo-Mosquera PD, Catalano FM (2021) Camber morphing winglet influence on aircraft drag breakdown and tip vortex structure. *Aerosp Sci Technol* 119:107148
- Elelwi M, Kuitche M, Botez R, Dao T (2020) Comparison and analyses of a variable span-morphing of the tapered wing with a varying sweep angle. *Aeronaut J* 124:1146–1169
- Elham A, Van Tooren MJ (2014) Winglet multi-objective shape optimization. *Aerosp Sci Technol* 37:93–109
- Félix Patrón RS, Berrou Y, Botez R (2014) Climb, cruise and descent 3D trajectory optimization algorithm for a flight management system. *AIAA/3AF Aircraft Noise and Emissions Reduction Symposium*, 3018
- Gabor OS (2015) Validation of morphing wing methodologies on an unmanned aerial system and a wind tunnel technology demonstrator (Ph. D. thesis)
- Gabor OŞ, Koreanschi A, Botez RM, Mamou M, Mebarki Y (2016) Numerical simulation and wind tunnel tests investigation and validation of a morphing wing-tip demonstrator aerodynamic performance. *Aerosp Sci Technol* 53:136–153
- Gamboa P, Vale J, Lau F, Suleman A (2009) Optimization of a morphing wing based on coupled aerodynamic and structural constraints. *AIAA J* 47:2087–2104
- Gavrilović NN, Rašuo BP, Dulikravich GS, Parezanović VB (2015) Commercial aircraft performance improvement using winglets. *FME Trans* 43:1–8
- Ghazi G, Botez RM, Domanti S (2020a) New methodology for aircraft performance model identification for flight management system applications. *J Aerosp Inf Syst* 17:294–310
- Ghazi G, Botez RM, Maniette N (2020b) Cessna Citation X takeoff and departure trajectories prediction in presence of winds. *J Aerosp Inf Syst* 17:659–681
- Grigorie T, Botez R, Popov A (2015) How the airfoil shape of a morphing wing is actuated and controlled in a smart way. *J Aerosp Eng* 28:04014043
- Haddad NE (2015) Aerodynamic and structural design of a winglet for enhanced performance of a business jet
- Hamy A, Murrieta-Mendoza A, Botez R (2016) Flight trajectory optimization to reduce fuel burn and polluting emissions using a performance database and ant colony optimization algorithm
- Heyson HH, Riebe GD, Fulton CL (1977) Theoretical parametric study of the relative advantages of winglets and wing-tip extensions
- ICAO (2019) Aviation's contribution to climate change, environmental report. International Civil Aviation Organisation
- Jones R (1980) Effects of winglets on the induced drag of ideal wing shapes
- Jupp J (2001) Wing aerodynamics and the science of compromise. *Aeronaut J* 105:633–641
- Kammegne MJT, Grigorie TL, Botez RM, Koreanschi A (2014) Design and validation of a position controller in the Price-Paidoussis wind tunnel. In: *IASTED modeling, simulation and control conference*, Innsbruck, Austria, 17–19
- Kammegne MT, Botez R, Grigorie L, Mamou M, Mébarki Y (2019) A new hybrid control methodology for a morphing aircraft wing-tip actuation mechanism. *Aeronaut J* 123:1757–1787

- Khalil EE, Abdelghany ES, Elharriri GM, Abdellatif OE (n.d.) Air craft winglet design and performance: cant angle effect. 14th international energy conversion engineering conference
- Khan S, Grigorie TL, Botez RM, Mamou M, Mébarki Y (2020) Novel morphing wing actuator control-based Particle Swarm Optimisation. *Aeronaut J* 124:55–75
- Koreanschi A, Sugar-Gabor O, Botez RM (2016) Numerical and experimental validation of a morphed wing geometry using Price-Paidoussis wind-tunnel testing. *Aeronaut J* 120:757–795
- Koreanschi A, Gabor OS, Acotto J, Brianchon G, Portier G, Botez RM, Mamou M, Mebarki Y (2017) Optimization and design of an aircraft's morphing wing-tip demonstrator for drag reduction at low speeds, Part II –experimental validation using Infra-Red transition measurement from Wind Tunnel tests. *Chin J Aeronaut* 30:164–174
- Kroo I (2001) Drag due to lift: concepts for prediction and reduction. *Annu Rev Fluid Mech* 33: 587–617
- Kulfan BM (2010) Recent extensions and applications of the ‘CST’ universal parametric geometry representation method. *Aeronaut J* 114:157–176
- Lazinica A (2009) Particle swarm optimization. BoD–Books on Demand
- Liauzun C, Le Bihan D, David J-M, Joly D, Paluch B (2018) Study of morphing winglet concepts aimed at improving load control and the aeroelastic behavior of civil transport aircraft. *Aerospace Lab*:1–15
- Mcdonald RA (2016) Advanced modeling in OpenVSP. 16th AIAA aviation technology, integration, and operations conference, 3282
- Meyran P, Pain H, Botez RM, Laliberté J (2021) Morphing Winglet design for aerodynamic performance optimization of the CRJ-700 aircraft. Part 1 – structural design. *INCAS Bull* 13: 113–128
- Noviello MC, Dimino I, Amoroso F, Pecora R (2019) Aeroelastic assessments and functional hazard analysis of a regional aircraft equipped with morphing winglets. *Aerospace* 6:104
- Oliviu SG, Koreanschi A, Botez RM, Mamou M, Mebarki Y (2016) Analysis of the aerodynamic performance of a morphing wing-tip demonstrator using a novel nonlinear vortex lattice method. 34th AIAA applied aerodynamics conference, 4036
- Pecora R (2021) Morphing wing flaps for large civil aircraft: evolution of a smart technology across the Clean Sky program. *Chin J Aeronaut* 34:13–28
- Rivero AE (2020) Structural and aerodynamic performance of a three-dimensional compliance-based composite camber morphing wing. University of Bristol
- Segui M, Abel FR, Botez RM, Ceruti A (2021a) High-fidelity aerodynamic modeling of an aircraft using OpenFoam–application on the CRJ700. *Aeronaut J* 1–22
- Segui M, Abel FR, Botez RM, Ceruti A (2021b) New aerodynamic studies of an adaptive winglet application on the Regional Jet CRJ700. *Biomimetics* 6:54
- Takenaka K, Hatanaka K, Yamazaki W, Nakahashi K (2008) Multidisciplinary design exploration for a winglet. *J Aircr* 45:1601–1611
- Vasista S, Titze M, Schäfer M, Bertram O, Riemenschneider J, Monner HP (2020) Structural and systems modelling of a fluid-driven morphing winglet trailing edge. *AIAA Scitech 2020 Forum*, 2010
- Whitcomb RT (1976) A design approach and selected wind tunnel results at high subsonic speeds for wing-tip mounted winglets, NASA Technical Note, (No. L-10908)
- Zhao J, Huang H, Yan S (2017) Honey bees (*Apis mellifera ligustica*) swing abdomen to dissipate residual flying energy landing on a wall. *J Appl Phys* 121:094702

Chapter 8

Observer-based Feedback Linearization Control of a Quadrotor Subjected to Sensor Noise



Ahmet Ermeydan and Aziz Kaba

Acronyms

GSA	Gravitational search algorithm
H_∞	H-infinity
LQR	Linear quadratic regulator
PD	Proportional derivative
PID	Proportional, integral, derivative
SNR	Signal-to-noise ratio
UAV	Unmanned aerial vehicle
VAR	Variance

8.1 Introduction

Nowadays, there are many application fields for unmanned aerial vehicles (UAVs) and drones such as surveillance, emergency operations, military applications, and package transportation (Metin and Aygün 2019). In particular, quadrotor becomes popular among researchers due to its hovering capacity and high maneuverability. Quadrotor is a highly nonlinear system and hard to control with linear control methods that operate around an equilibrium point (Zuo 2010). Although linear control techniques such as proportional derivative (PD) (Kıyak 2016), proportional integral derivative (PID) (Ermeydan and Kıyak 2017), linear quadratic regulator (LQR) (Khatoun et al. 2014), and H-infinity (H_∞) (Araar and Aouf 2014) are applied

A. Ermeydan (✉) · A. Kaba
Eskisehir Technical University, Eskisehir, Türkiye
e-mail: aermeydan@eskisehir.edu.tr; azizkaba@eskisehir.edu.tr

to the quadrotor successfully, these control approaches may experience a performance drop when deviating from the equilibrium point (Kendoul 2012).

Recently, nonlinear control techniques have become widespread when it comes to the quadrotor. A PID-like speed controller is proposed by Yazar et al. (2018) for a nonlinear small-scale turbojet engine. Ai and Yu (2019) proposed a flatness-based sliding mode control is proposed for the trajectory tracking problem in a quadrotor in the presence of external disturbances. A backstepping-like feedback linearization method is suggested by Choi and Ahn (2014) for controlling the quadrotor. Köksal et al. (2016) presented a two-level nonlinear control design. An incremental sliding mode fault-tolerant flight controller is proposed by Wang et al. (2019). Xuan-Mung and Hong (2019) presented a new altitude algorithm that consists of nonlinear and linear controllers for quadrotors. A nonlinear PID controller is suggested by Najm and Ibraheem (2019) to stabilize a quadrotor system. To track the position and attitude of a quadrotor, a new control method is proposed by Razmi and Afshinfar (2019). A neural network is used to tune sliding mode controllers in the suggested method. The proposed method obtained better results for both attitude and position tracking in comparison to (Zheng et al. 2014) and (Xiong and Zhang 2017). A robust nonlinear control method is utilized to control the quadrotor's position and orientation (Labbadi and Cherkaoui 2019). A dynamic inversion based nonlinear controller is suggested for quadrotors by Prabhakaran et al. (2015). Nonlinear optimal backstepping control is applied to a quadrotor (Basri et al. 2015).

Literature survey showed that the control of the quadrotor can be insufficient when the dynamics are considered linear. Recent research efforts are shifting toward the nonlinear dynamics and control. Feedback linearization technique as one of the nonlinear controllers can transform the nonlinear plant dynamics to a linear dynamical form by using a proper feedback law (Özbek et al. 2016). In difference to linear controllers, feedback linearization control law is obtained through the exact state transformation rather than the state approximation approach (Gee et al. 1998). So, the nonlinear model of the plant can be converted into a fully or partly linear model with the cancellation of nonlinearities. The application of the feedback linearization control technique into the quadrotor control problem can be found in many research papers. Voos (2009) proposed the nonlinear control of a micro-quadrotor platform by using a feedback linearization technique. Saif (2017) proposed a feedback linearization control law for a tiltable quadrotor under wind gusts scenario. Bonna and Camino (2015) proposed the trajectory tracking control of a quadrotor with feedback linearization technique. Fault-tolerant control application of the feedback linearization approach is proposed by Ghandour et al. (2014) to a quadrotor testbed. Position-tracking control of the quadrotor is proposed by Kuantama et al. (2018) using the feedback linearization linear quadratic regulator (LQR) technique. Quadrotor control using feedback linearization with dynamic extension is proposed by Al-Hiddabi (2009). Attitude and altitude control of a quadrotor with feedback linearization technique is presented by Eltayeb et al. (2019).

Despite the advantages of the feedback linearization technique, the controller operates if all the state parameters are well-defined and do not have any uncertainties (Chen et al. 2016). It is a challenging but an essential task to control the quadrotor in

full degree-of-freedom space since quadrotors are both subjected to internal and external noise sources such as modeling inaccuracies, assumptions, wind gusts, measurement noises, and sensor errors. To overcome these disturbances, the feedback linearization control technique is enhanced with an observer to handle the control of the quadrotor subjected to internal and external disturbances.

Several disturbance-observer-based control techniques are available in the literature Chen et al. (2016). In this chapter, the enhancement of the feedback linearization control method is ensured by particle filter–based observer. The particle filter is a Monte Carlo–based suboptimal algorithm that deals with closed-loop integral problems of the recursive Bayesian estimation (Oh and Kim 2019). Unlike linear observers and simple robust controller structures, the particle filter can handle system nonlinearities and noise with both Gaussian and non-Gaussian distributions (Daroogheh et al. 2018).

Based on the given discussion, the originality of this manuscript is to propose a nonlinear observer–based feedback linearization control method of a quadrotor that solves the integration problems, overcomes the uncertainty issue of the feedback linearization technique, and not only reduces disturbance errors and minimizes sensor errors but also controls the quadrotor with nonlinear dynamics in a wide range of operation regions.

The organization of the chapter is as follows: Nonlinear kinematic and dynamic equations of the quadrotor are derived in Sect. 8.2. The proposed method and theoretical background are given in Sect. 8.3. The main results are covered in Sect. 8.4. Conclusions and discussions are given in Sect. 8.5.

8.2 Quadrotor

Quadrotor is a multicopter that consists of four motors and propellers. The two opposite propeller turn in the same direction and the other two turn in the opposite direction. The speeds of the rotors are equal in a balanced flight (Kose and Oktay 2019).

8.2.1 Euler Transformation

There are different methods for expressing a vector in one axis set in another axis set. Euler transformation is one of these methods. In this transformation, one set of axes is rotated three times to overlap the other. Here, the order of rotation of the axis assembly is important; since the rotation order changes, it leads to a different result (Pamadi 2015).

The inertial reference system is $\mathbf{I} = (x_i, y_i, z_i)$ and the body reference system is $\mathbf{B} = (x_b, y_b, z_b)$. So the following is obtained if \mathbf{I} reference system is rotated around \mathbf{B} reference system with angles ψ , θ , and ϕ sequentially as shown in Fig. 8.1.

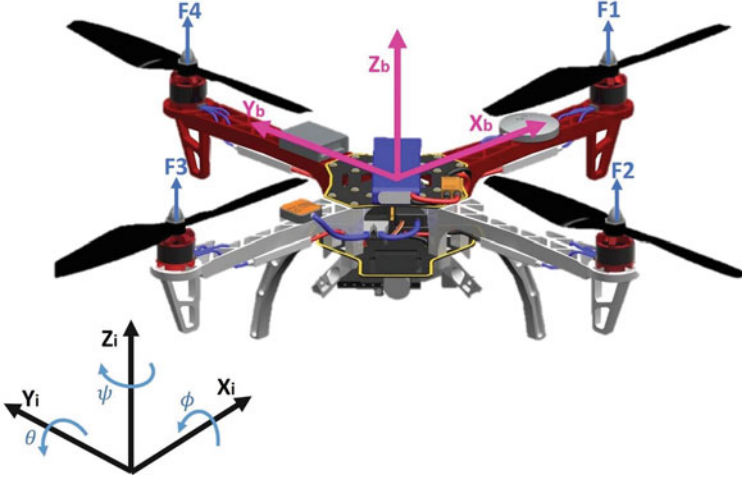


Fig. 8.1 Quadrotor coordinate system

$$R_3(\psi) = [\cos \psi \quad \sin \psi \quad 0 \quad -\sin \psi \quad \cos \psi \quad 0 \quad 0 \quad 0 \quad 1] \quad (8.1)$$

$$R_2(\theta) = [\cos \theta \quad 0 \quad -\sin \theta \quad 0 \quad 1 \quad 0 \quad \sin \theta \quad 0 \quad \cos \theta] \quad (8.2)$$

$$R_1(\phi) = [1 \quad 0 \quad 0 \quad 0 \quad \cos \phi \quad \sin \phi \quad 0 \quad -\sin \phi \quad \cos \phi] \quad (8.3)$$

These matrices are orthogonal matrices and multiplication of the matrices form the following transformation matrix, which moves any vector from **I** reference system to **B** reference system.

$$T_i^b = R_1(\phi)R_2(\theta)R_3(\psi) \quad (8.4)$$

$$\begin{aligned} T_i^b = & [\cos \theta \cos \psi \quad \cos \theta \sin \psi \quad -\sin \theta \quad \sin \theta \sin \phi \cos \psi \\ & -\sin \psi \cos \phi \quad \sin \psi \sin \theta \sin \phi + \cos \psi \cos \phi \quad \sin \phi \cos \theta \quad \sin \theta \cos \phi \cos \psi \\ & + \sin \psi \sin \phi \quad \sin \psi \sin \theta \cos \phi - \cos \psi \sin \phi \quad \cos \phi \cos \theta] \end{aligned} \quad (8.5)$$

It is not possible to measure Euler angles directly in the flight control system. However, P, Q, and R, which are the angular velocities around three axes in the body reference system, can be measured. It is possible to obtain Euler angular velocities by applying a transformation to these angular velocities (Corke 2013).

To move Euler angular velocities from **I** reference system to **B** reference system, the following matrix calculations are performed.

$$[P \ Q \ R] = R_1(\phi)R_2(\theta)[0 \ 0 \ \dot{\psi}] + R_1(\phi)[0 \ \dot{\theta} \ 0] + [\dot{\phi} \ 0 \ 0] \quad (8.6)$$

$$\begin{aligned}
[P \ Q \ R] &= [\cos \theta \ 0 - \sin \theta \ \sin \phi \ \sin \theta \ \cos \phi \ \sin \phi \ \cos \theta \ \cos \phi \ \sin \theta - \sin \phi \ \cos \phi \ \cos \theta] \\
&\times [0 \ 0 \ \dot{\psi}] + [1 \ 0 \ 0 \ 0 \ \cos \phi \ \sin \phi \ 0 - \sin \phi \ \cos \phi] [0 \ \dot{\theta} \ 0] + [\dot{\phi} \ 0 \ 0]
\end{aligned} \tag{8.7}$$

$$[P \ Q \ R] = [1 \ 0 - \sin \theta \ 0 \ \cos \phi \ \sin \phi \ \cos \theta \ 0 - \sin \phi \ \cos \phi \ \cos \theta] [\dot{\phi} \ \dot{\theta} \ \dot{\psi}] \tag{8.8}$$

However, P , Q , and R are generally given, and Euler angular velocities are desired. Therefore, L matrix is defined, and Euler angular velocities can be found using its inverse.

$$L = [1 \ 0 - \sin \theta \ 0 \ \cos \phi \ \sin \phi \ \cos \theta \ 0 - \sin \phi \ \cos \phi \ \cos \theta] \tag{8.9}$$

$$[\dot{\phi} \ \dot{\theta} \ \dot{\psi}] = L^{-1} [P \ Q \ R] \tag{8.10}$$

$$\begin{aligned}
[\dot{\phi} \ \dot{\theta} \ \dot{\psi}] &= [1 \ \sin \phi \ \tan \theta \ \cos \phi \ \tan \theta \ 0 \ \cos \phi - \sin \phi \ 0 \ \sin \phi \ \sec \theta \ \cos \phi \ \sec \theta] \\
&\times [P \ Q \ R]
\end{aligned} \tag{8.11}$$

8.2.2 Equations of Motion

The following assumptions are made while gathering the equations of motion of the quadrotor (Musa 2017).

- Quadrotor is a rigid body.
- The center of gravity of the quadrotor is coincident with the center of the body reference frame.
- The ground effect of the quadrotor is neglected.
- Earth is an inertial reference.

To derive equations of motion according to the Newton–Euler method, it is essential to define forces and torques acting on a quadrotor (He and Zhao 2014). There are four control inputs of a quadrotor, which has six degrees of freedom.

$$u_\phi = l(F_4 - F_2) \tag{8.12}$$

$$u_\theta = l(F_3 - F_1) \tag{8.13}$$

$$u_\psi = d(F_1 - F_2 + F_3 - F_4) \tag{8.14}$$

where l is the distance (m) between the center of gravity of the quadrotor and the center of the propeller, and d is the ratio between the drag and the thrust coefficients of the propeller.

The net moment on the quadrotor is the sum of the moments resulting from the speed differences of the propellers and rotational drag.

$$M_{\text{net}} = M_{\text{quad}} + M_k \quad (8.15)$$

The net moment acting on the quadrotor is equal to the change in angular momentum.

$$M_{\text{net}} = I \frac{d}{dt}(w) + w \times (Iw) \quad (8.16)$$

I_x , I_y , and I_z are moments of inertia, and since the quadrotor is symmetrical along the x and y axes, the product of inertia is zero.

$$M_{\text{net}} = [I_x \dot{P} \ I_y \dot{Q} \ I_z \dot{R}] + [(I_z - I_y)QR \ (I_x - I_z)RP \ (I_y - I_x)PQ] \quad (8.17)$$

Roll, pitch, and yaw inputs are part of the moments on the quadrotor.

$$M_k = [l(F_4 - F_2) \ l(F_3 - F_1) \ d(F_1 - F_2 + F_3 - F_4)] = [u_\phi \ u_\theta \ u_\psi] \quad (8.18)$$

If M_{quad} and M_k are summed and arranged, the following equation is obtained:

$$[\dot{P} \ \dot{Q} \ \dot{R}] = \left[\frac{(I_y - I_z)}{I_x} QR \ \frac{(I_z - I_x)}{I_y} RP \ \frac{(I_x - I_y)}{I_z} PQ \right] + \left[\frac{u_\phi}{I_x} \ \frac{u_\theta}{I_y} \ \frac{u_\psi}{I_z} \right] - \left[\frac{k_r P}{I_x} \ \frac{k_r Q}{I_y} \ \frac{k_r R}{I_z} \right] \quad (8.19)$$

where k_r is the rotational drag coefficient.

A summary of the equations of motion for the rotational subsystem of the quadrotor is given below:

$$\dot{P} = \frac{1}{I_x} [(I_y - I_z)QR + u_\phi - k_r P] \quad (8.20)$$

$$\dot{Q} = \frac{1}{I_y} [(I_z - I_x)RP + u_\theta - k_r Q] \quad (8.21)$$

$$\dot{R} = \frac{1}{I_z} [(I_x - I_y)PQ + u_\psi - k_r R] \quad (8.22)$$

$$\dot{\phi} = P + Q \sin \phi \tan \theta + R \cos \phi \tan \theta \quad (8.23)$$

$$\dot{\theta} = Q \cos \phi - R \sin \phi \quad (8.24)$$

$$\dot{\psi} = Q \sin \phi \sec \theta + R \cos \phi \sec \theta \quad (8.25)$$

8.3 Scheme of the Proposed Method

8.3.1 Input–Output Linearization

We consider the following nonlinear system with n states, m inputs, and m outputs (Freddi 2012):

$$\dot{x} = f(x) + g(x)u = f(x) + \sum_{j=1}^m g_j x u_j \quad (8.26)$$

$$y = [h_1(x), \dots, h_m(x)]^T \quad (8.27)$$

where $x \in R^n$ is the state vector, $u \in R^m$ is the control input, $y \in R^m$ is the output vector, and $f(x), g_1(x), \dots, g_m(x), y$ are smooth vector fields described on an open subset of R^n .

If the system is single input single output (SISO) ($m = 1$), it has a relative degree ρ , $1 \leq \rho \leq n$ in a region $D_0 \subset D$ if

$$L_g L_f^{i-1} h(x) = 0, \quad i = 1, 2, \dots, \rho - 1, L_g L_f^{\rho-1} h(x) \neq 0 \quad \text{for all } x \in D_0 \quad (8.28)$$

If the system is multiple input multiple output (MIMO) ($m \neq 1$), the relative degree definition changes, and the system is said to have a vector relative degree $\{r_1, \dots, r_m\}$ at a point x^0 if:

- The following condition holds for all $1 \leq j \leq m$, for all $k \leq r_i - 1$, for all $1 \leq i \leq m$, and for all x in the neighborhood of x^0 (Freddi 2012)

$$L_g L_f^k h_i(x) = 0 \quad (8.29)$$

- The following matrix is nonsingular at $x = x^0$:

$$M(x) = \begin{bmatrix} L_{g_1} L_f^{r_1-1} h_1(x) \cdots L_{g_m} L_f^{r_1-1} h_1(x) & L_{g_1} L_f^{r_2-1} h_2(x) \cdots L_{g_m} L_f^{r_2-1} h_2(x) & \cdots & L_{g_1} L_f^{r_m-1} h_m(x) \cdots L_{g_m} L_f^{r_m-1} h_m(x) \end{bmatrix} \quad (8.30)$$

The nonlinear system above must hold the conditions below:

- Sum of elements of the vector relative degree $\{r_1, \dots, r_m\}$ must be equal to n .
- The matrix $M(x)$ is invertible.

If these conditions are satisfied, a linearizing control law can be found as follows:

$$u_c(x, w) = \alpha_c(x) + \beta_c(x)w \quad (8.31)$$

where

$$\alpha_c(x) = -M^{-1}(x) \left[L_f^{r_1} h_1(x) \dots L_f^{r_m} h_m(x) \right]^T \quad (8.32)$$

$$\beta_c = M^{-1}(x) \quad (8.33)$$

A diffeomorphism can also be defined as:

$$x_c = \phi_c(x) \quad (8.34)$$

where

$$\phi_c^T = \left[\phi_{c_1}^T(x) \dots \phi_{c_m}^T(x) \right] \quad (8.35)$$

$$\phi_{c_i}^T = \left[h_i(x) L_f h_i(x) \dots L_f^{r_i-1} h_i(x) \right] \quad (8.36)$$

A linear system can be obtained if the diffeomorphism is applied to the nonlinear system.

$$\dot{x} = A_c x_c + B_c w \quad (8.37)$$

where w is linear control law and A_c and B_c represent the canonical Brunowski form.

$$A_c = \text{diag}(A_1 \dots A_m) \quad (8.38)$$

$$B_c = \text{diag}(b_1 \dots b_m) \quad (8.39)$$

where

$$A_i = [0 \ 1 \ 0 \dots 0 \ 0 \ 0 \ 1 \dots 0 \dots \dots 0 \ 0 \ 0 \dots 1 \ 0 \ 0 \ 0 \dots 0] \quad (8.40)$$

$$b_i = [0 \dots 1] \quad (8.41)$$

8.3.2 Control System Structure

Control system consists of two control loops: the inner loop is feedback linearization, and the outer loop is LQR. State variables are selected as follows:

$$x = [x_1 \ x_2 \ x_3 \ x_4 \ x_5 \ x_6] = [\phi \ \theta \ \psi \ P \ Q \ R] \quad (8.42)$$

$x_1, x_2, x_3, x_4, x_5,$ and x_6 are chosen for feedback linearization. The nonlinear system is represented by:

$$x = [x_1 \ x_2 \ x_3 \ x_4 \ x_5 \ x_6] = [\phi \ \theta \ \psi \ P \ Q \ R] \quad (8.43)$$

$$y = [h_1 \ h_2 \ h_3]^T = [x_1 \ x_2 \ x_3]^T \quad (8.44)$$

where

$f(x)$

$$\begin{aligned} & [x_4 + x_5 \sin x_1 \tan x_2 + x_6 \cos x_1 \tan x_2 \ x_5 \cos x_1 \\ & = -x_6 \sin x_1 (x_5 \sin x_1 + x_6 \cos x_1) / \cos x_2 (-k_r x_4 - x_5 x_6 (I_z - I_y)) \\ & / I_x (-k_r x_5 - x_4 x_6 (I_x - I_z)) / I_y (-k_r x_6) / I_z] \end{aligned} \quad (8.45)$$

and

$$g(x) = \left[0 \ 0 \ 0 \ 0 \ 0 \ 0 \ 0 \ 0 \ 0 \ \frac{1}{I_x} \ 0 \ 0 \ 0 \ \frac{1}{I_y} \ 0 \ 0 \ 0 \ \frac{1}{I_z} \right] \quad (8.46)$$

The summation of relative degrees ($r_1 = 2$, $r_2 = 2$, and $r_3 = 2$) equals to the vector relative degree ($r = 6$) that is equal to the number of states. The matrix $\mathbf{M}(x)$ that is nonsingular is calculated as follows:

$$M(x) = \begin{bmatrix} \frac{1}{I_x} \frac{\sin x_1 \tan x_2}{I_y} \frac{\cos x_1 \tan x_2}{I_z} & 0 & \frac{\cos x_1}{I_y} & -\frac{\sin x_1}{I_z} & 0 & \frac{\sin x_1}{I_y \cos x_2} & \frac{\cos x_1}{I_z \cos x_2} \end{bmatrix} \quad (8.47)$$

So, two conditions required for feedback linearization are satisfied. Diffeomorphism converts the state variables in the nonlinear system into the state variables of the new system that is linearized in the feedback linearization method.

$\phi_c(x)$

$$\begin{aligned} & [x_1 \ x_4 + x_6 \cos x_1 \tan x_2 + x_5 \sin x_1 \tan x_2 \ x_2 \ x_5 \cos x_1 \\ & = -x_6 \sin x_1 \ x_3 \frac{(x_5 \cos x_1 + x_5 \sin x_1)}{\cos x_2}] \end{aligned} \quad (8.48)$$

The feedback linearizing law is computed as:

$$u_c(x, w) = \alpha_c(x) + \beta_c(x)w \quad (8.49)$$

where

$$\alpha_c(x) = \left[\begin{array}{l} k_r x_4 + I_z x_5 x_6 - \frac{I_x x_5^2 \sin 2x_1}{2} + \frac{I_y x_6^2 \sin 2x_1}{2} \\ - 2I_x x_5 x_6 \cos x_1 - \frac{k_r x_5 \cos x_2 - I_y x_5^2 \cos x_1 \sin x_2 + 2I_y \cos x_6^2 \cos x_1 \sin x_2 + I_x x_4 x_6 \cos x_2 + a}{\cos x_2} \\ - \frac{(I_z x_5^2 \sin x_1 \sin x_2 - k_r x_6 \cos x_2 + I_z x_4 x_5 \cos x_2 + b)}{\cos x_2} \end{array} \right] \quad (8.50)$$

$$a = I_y x_4 x_6 \cos x_2 - I_z x_4 x_6 \cos x_2 + I_y x_5^2 \cos x_1^3 \sin x_2 - I_y x_6^2 \cos x_1^3 \sin x_2 \quad (8.51)$$

$$b = I_z x_5^2 \cos x_1^2 \sin x_1 \sin x_2 - I_z x_6^2 \cos x_1^2 \sin x_1 \sin x_2 + 2I_z x_5 x_6 \cos x_1^3 \sin x_2 \quad (8.52)$$

$$\beta_c(x) = \begin{bmatrix} I_x & 0 & -I_x \sin x_2 & 0 & I_y \cos x_1 & I_y \cos x_2 \sin x_1 & 0 \\ -I_z \sin x_1 & I_z \cos x_1 & \cos x_2 & & & & \end{bmatrix} \quad (8.53)$$

If the control law is applied, the following linearized system is obtained:

$$\begin{aligned} \dot{x}_c &= A_c x_c + B_c w \\ &= [0 \ 1 \ 0 \ 0 \ 0 \ 0 \ 0 \ 0 \ 0 \ 0 \ 0 \ 0 \ 0 \ 0 \ 1 \ 0 \ 0 \ 0 \ 0 \ 0 \ 0 \ 0 \ 0 \ 0 \ 0 \ 0 \ 0 \ 1 \ 0 \ 0 \ 0 \ 0 \ 0] x_c \\ &\quad + [0 \ 0 \ 0 \ 1 \ 0 \ 0 \ 0 \ 0 \ 0 \ 0 \ 1 \ 0 \ 0 \ 0 \ 0 \ 0 \ 0 \ 1] w \end{aligned} \quad (8.54)$$

Since the system is now linear, a linear control method can be applied. Therefore, linear quadratic regulator (LQR) is preferred because it has easy design and application for linear control of the system. A control law:

$$w = -Kx_c \quad (8.55)$$

is designed by selecting an appropriate K value. This is achieved by choosing Q and R matrices and using MATLAB command `lqr`, where Q and R matrices are given as follows:

$$Q = [100 \ 0 \ 0 \ 0 \ 0 \ 0 \ 0 \ 100 \ 0 \ 0 \ 0 \ 0 \ 0 \ 0 \ 100 \ 0 \ 0 \ 0 \ 0 \ 0 \ 100 \ 0 \ 0 \ 0 \ 0 \ 0 \ 100 \ 0 \ 0 \ 0 \ 0 \ 0 \ 100] \quad (8.56)$$

$$R = [0.01 \ 0 \ 0 \ 0 \ 0.01 \ 0 \ 0 \ 0 \ 0.01] \quad (8.57)$$

In the SISO case, if the dimension of the nonlinear system is not equal to the relative degree, zero dynamics appear. So, the stability of the system depends on the

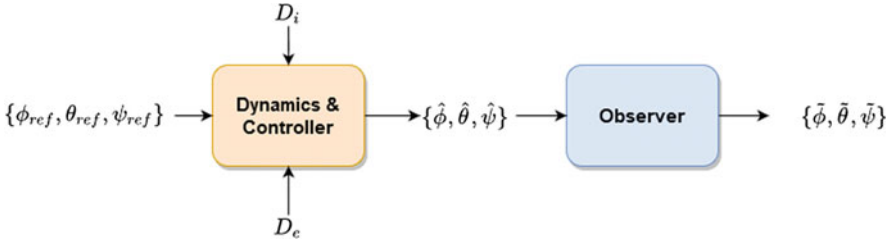


Fig. 8.2 General diagram of the proposed scheme

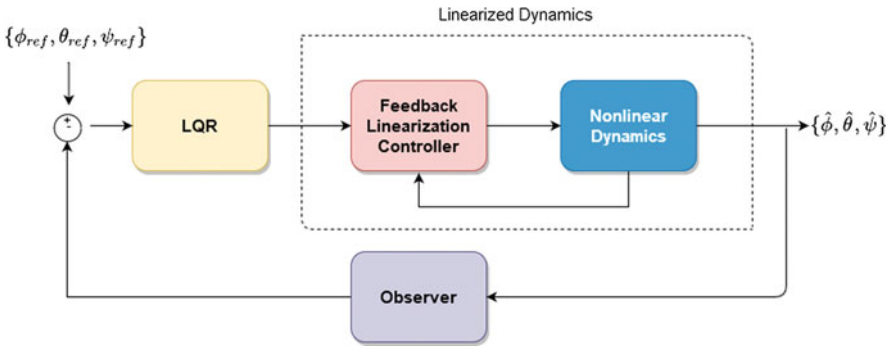


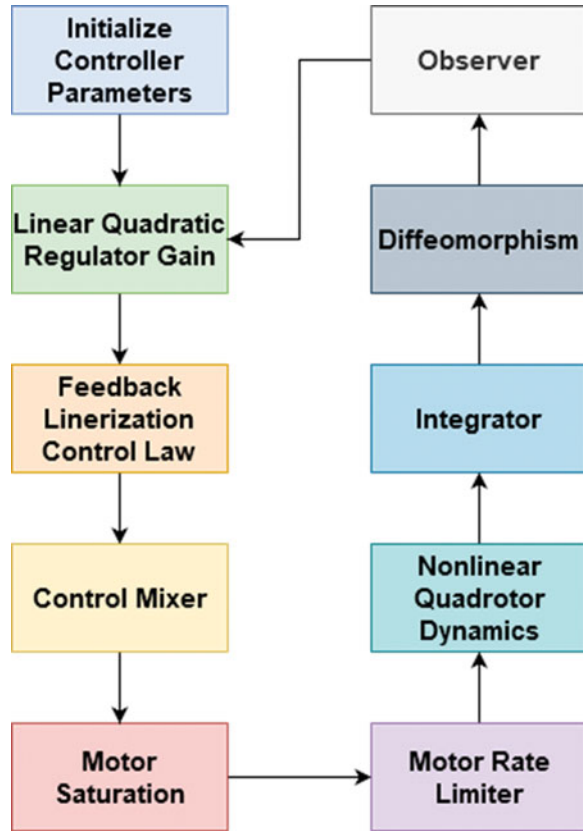
Fig. 8.3 Block diagram of the controller structure

stability of the zero dynamics, but this condition is not valid for MIMO systems. In addition, there are no zero dynamics that appear into the system since relative degree is equal to the dimension of the system. So, since our model is MIMO, it is globally asymptotically stable. Sufficient conditions for the system to be stable can be found in (Seborg and Henson 1996).

The general diagram of the proposed observer-based feedback controller is given in Fig. 8.2. $\{\phi_{ref}, \theta_{ref}, \psi_{ref}\}$ is the reference attitude input. The proposed scheme is based on the quadrotor attitude dynamics given in Eqs. (8.20) and (8.25). The internal disturbance D_i is added to the model since the physical and mathematical modeling of the quadrotor contains unknown errors and uncertainty. The external disturbance D_e is also added due to environmental disturbances and sensor errors. $\{\hat{\phi}, \hat{\theta}, \hat{\psi}\}$ is the set of outputs that contain noise terms. Lastly, $\{\tilde{\phi}, \tilde{\theta}, \tilde{\psi}\}$ is the set of estimated attitude signals of the quadrotor.

The sub-diagram of the dynamics and controller block is given in Fig. 8.3. Nonlinear dynamics are linearized by the feedback linearization controller. Then, LQR controller is designed using the linearized dynamics. The sensor produces noisy $\{\phi, \theta, \psi\}$ states, and reference states are subtracted from these noisy states. The error signal is fed to the LQR controller, which computes the control signal of the linearized system. The feedback linearization controller calculates roll, pitch, and yaw inputs according to LQR output. Nonlinear dynamics generate a state vector that goes to feedback linearization and observer.

Fig. 8.4 Flowchart of the proposed controller



The observer employed in this method is chosen as particle filter. Particle filter is a Monte Carlo–based iterative importance sampling method. Particle filter finds a suboptimal solution to the Bayesian estimation. This suboptimal solution is based on the approximation of the integral terms in the probability density functions. The density functions mentioned before are represented by a vector of random particles and weights. If the number of particle size increases, representation converges to the optimal solution. Particle filter–based scheme is chosen as observer since particle filter has nonlinear framework and can deal with both Gaussian and non-Gaussian distributed noises. Thus, the performance of the proposed controller can be increased and enhanced in real-world scenarios.

The flowchart shown in Fig. 8.4 demonstrates the flow of the proposed controller. First, controller parameters are initialized. Then the loop starts with LQR controller gain. The output of the diffeomorphism is multiplied by LQR gain, and the gain is fed to feedback linearization law. The control mixer produces motor (1–4) inputs from roll, pitch, and yaw inputs. Motor dynamics consist of motor saturation and motor rate limiter. The motor saturation limits motor thrust between 0 N and 5 N. The motor rate limiter restricts the motor rate of thrust by ± 50 N/s. Nonlinear

quadrotor dynamics generate a derivative of the states using motor (1–4) outputs. The integrator integrates the derivative of the state vector to obtain the states to be used in the control system. Diffeomorphism calculates the linearized system state vector that is observed and fed to LQR gain. The loop continues during the simulation time in this way.

8.4 Results and Discussion

The proposed observer-based nonlinear control of the quadrotor is implemented in both MATLAB and Simulink environments. Simulations are carried out for 20 [s] with a discrete time step of 0.1 [s]. The parameters of the nonlinear quadrotor model are given in Table 8.1 (Lanzon et al. 2014), where m is the weight, g is the gravity, (I_x, I_y, I_z) are the moments of inertia, l is the length of the arm, d is the drag coefficient of the propellers, and (k_r, k_t) are rotational and translational drag coefficients. The attitude response of the feedback controller is tested from negative initial angles to positive reference angles for each attitude angle. The initial state vectors are set as $[0, 0, 0]$, $[-\pi/4, -\pi/8, -\pi/12]$ and reference vectors are set as $[\pi/6, \pi/4, \pi/3]$, $[0, 0, 0]$ for first and second scenarios where states are $[\phi, \theta, \psi]$ in [rad], respectively.

8.4.1 Noisy Reference Tracking

Since quadrotors are prone to low-cost and unstable sensor errors, it is an essential task to support the controller with an observer/estimator block. Thus, sensor errors can be eliminated through the observer scheme. To evaluate the sensor noise performance of the proposed method, an internal noise source with a variance of 0.01 [rad²] and an external sensor noise with a variance of 0.02 [rad²] are injected to the attitude states of the quadrotor as disturbances. The disturbances are modeled as Gaussian random variable with zero mean and a total of 0.03 [rad²] variance component. The measured overall variance values of the states are 0.0302 for ϕ ,

Table 8.1 Quadrotor parameters

Variable	Value	Unit
m	0.5	[kg]
g	9.81	[m/s ²]
I_x	5.90E-03	[kg.m ²]
I_y	5.90E-03	[kg.m ²]
I_z	1.16E-03	[kg.m ²]
l	2.55E-01	[m]
d	2.40E-03	[kg.m ²]
kr	1.00E-02	[kg.m ² /s]
kt	1.00E-02	[kg/s]

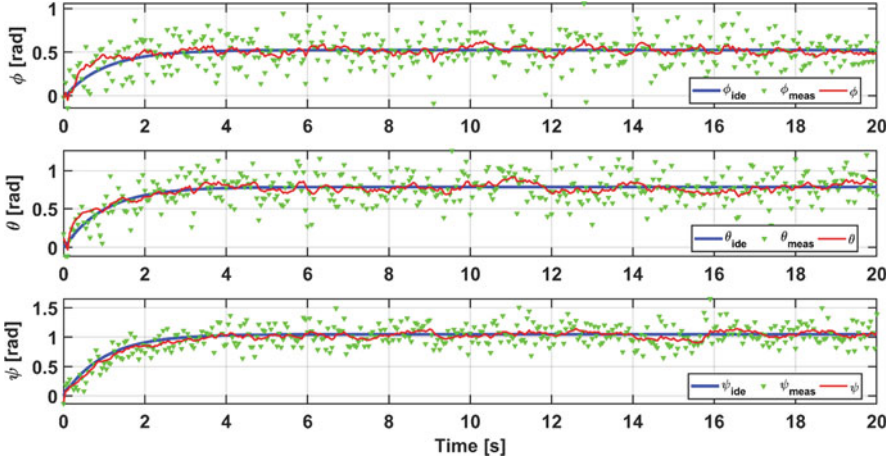


Fig. 8.5 Noisy response of the proposed controller: from 0 [rad] to arbitrary states

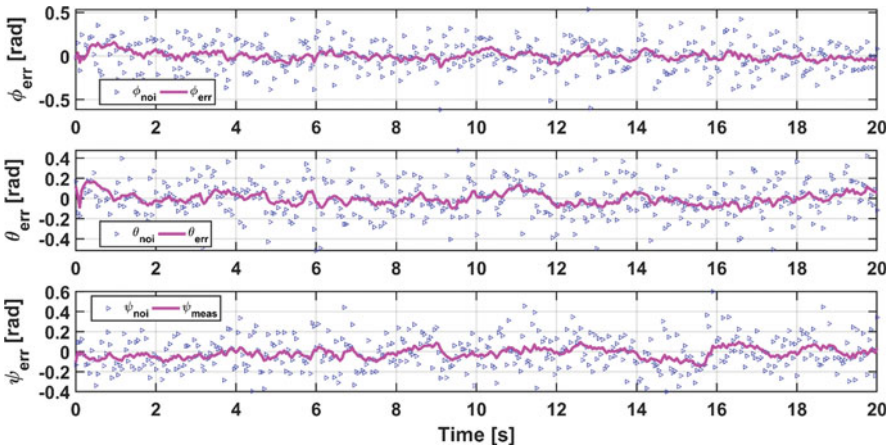


Fig. 8.6 A comparison of sensor noise and error of the proposed method: from 0 [rad] to arbitrary states

0.0327 for θ , and 0.0283 for ψ . The responses of the controller for the first scenario are given in Fig. 8.5 and the error plot is given in Fig. 8.6. The responses of the controller for the second trajectory is given in Fig. 8.7 and the error plot is given in Fig. 8.8. In Fig. 8.5, green points show the measurement of the states subjected to sensor noise, the blue line shows the ideal controller response without any noise component, and, lastly, the red line shows the response of the proposed method under the sensor noise. A comparative analysis of the performance of the proposed method and total noise is seen in Fig. 8.6 where the magenta line denotes the error of the method and blue points show the total error of internal and external disturbances.

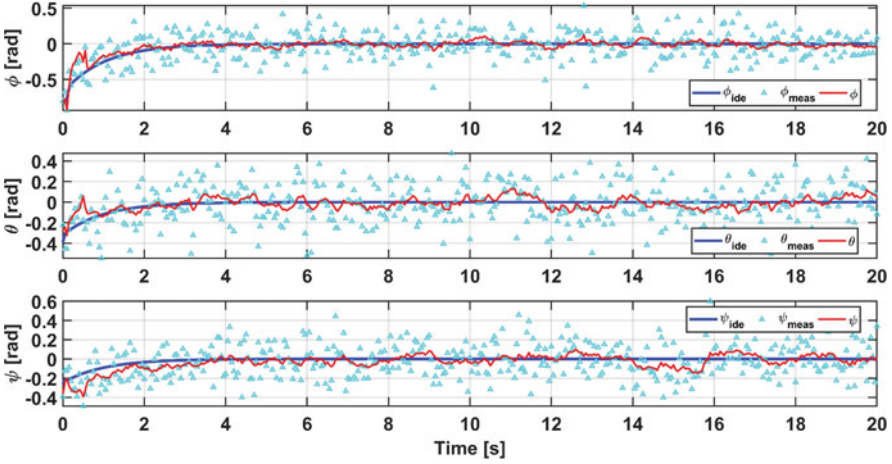


Fig. 8.7 Noisy response of the proposed controller: from arbitrary states to 0 [rad]

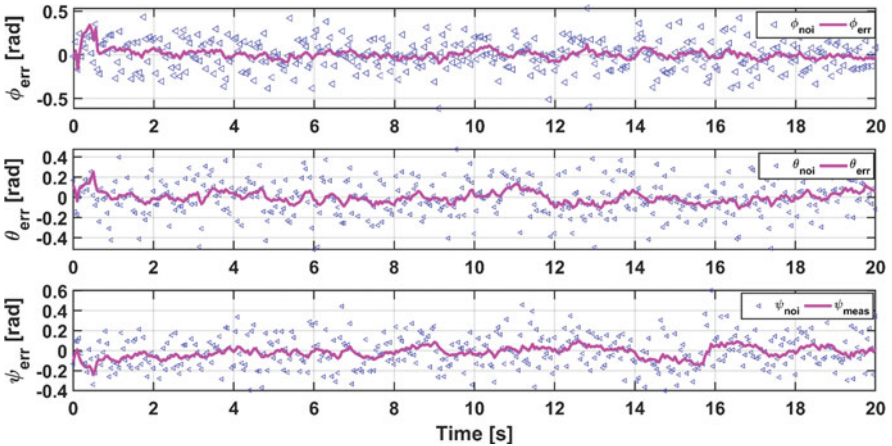


Fig. 8.8 A comparison of sensor noise and error of the proposed method: from arbitrary states to 0 [rad]

The notation is similar for Fig. 8.7 and Fig. 8.8 except sensor noise is given with cyan points for the second scenario. It can be clearly deduced from Figs. 8.5, 8.6, 8.7 and 8.8 that the proposed method is well performed and tracks the reference trajectory even under the sensor noise with a low error ratio for all states.

The statistical analyses of the proposed method under sensor noise are given in Tables 8.2, 8.3, and 8.4 for standard deviation, signal-to-noise ratio (SNR), and absolute error, respectively. The performance of the proposed method is compared against the total noise to show the enhancements of the algorithm. Standard deviations of the errors for all states are seen in Table 8.2 for both trajectories. The

Table 8.2 Standard deviation analysis of the proposed method

	Noise			Method		
	ϕ	Θ	ψ	ϕ	θ	ψ
First trajectory	0.173971	0.181029	0.168277	0.046902	0.055575	0.049403
Second trajectory	0.173971	0.181029	0.168277	0.054185	0.054281	0.054268

Table 8.3 Signal-to-noise ratio analysis of the proposed method

	Noise			Method		
	ϕ	θ	ψ	ϕ	Θ	ψ
First trajectory	9.6586	12.5690	15.5428	20.6373	22.6393	25.5759
Second trajectory	1.3092	0.3413	0.4372	5.7035	1.1488	3.3781

Table 8.4 Absolute error analysis of the proposed method

	Noise			Method		
	ϕ	θ	ψ	ϕ	Θ	ψ
First trajectory	0.6141	0.5173	0.6012	0.1573	0.1710	0.1452
Second trajectory	0.6141	0.5173	0.6012	0.3421	0.2534	0.2428

proposed method is capable of controlling and reducing sensor errors. The standard deviation of the error for the attitude angles are reduced from nearly 0.17 [rad] to nearly 0.05 [rad]. The standard deviation performance of the proposed method is no more than 0.056 [rad], which is approximately reduced three times with respect to the total error. The signal-to-noise ratio analysis of the algorithm is given in Table 8.3. The method is capable of increasing the SNR for all states and trajectories. The SNR is increased as high as 25.5 with the lowest increment of 0.34 to 1.14. Lastly, the absolute error performance of the algorithm is given in Table 8.4. According to the results, the length of the error is reduced from nearly 0.6 [rad] up to 0.145 [rad] with a reduction of four times.

8.5 Conclusion

In this work, an observer-based feedback linearization controller for a quadrotor is proposed to control the nonlinear attitude dynamics subjected to sensor noise. The proposed method is tested for noisy references. Two scenarios are considered: from 0 [rad] to any arbitrary state and from any arbitrary state to 0 [rad] to cover more circumstances. According to the results, the proposed method is capable of tracking the given trajectories for noisy references. Numerical analysis showed that the maximum standard deviation of the error of the proposed method is reduced by three times, signal-to-noise ratio is increased by seven times, and the absolute error is reduced by four times.

The SNR is increased from 0.34 to 1.14, absolute error is reduced from 0.6 [rad] up to 0.145 [rad], and standard deviation is reduced from 0.17 [rad] to 0.05 [rad]. According to the abovementioned results, it can be easily concluded that the proposed controller has good control, estimation, and reference tracking responses regarding internal and external noise sources with a low standard deviation of error, absolute error, and high signal-to-noise ratio statistics, respectively.

References


- Ai X, Yu J (2019) Fixed-time trajectory tracking for a quadrotor with external disturbances: a flatness-based sliding mode control approach. *Aerosp Sci Tech* 89:58–76
- Al-Hiddabi S (2009) Quadrotor control using feedback linearization with dynamic extension. In: *Proceeding of the 6th international symposium on mechatronics and its applications*, Sharjah
- Araar O, Aouf N (2014) Full linear control of a quadrotor UAV, LQ vs H_∞ . In: *UKACC international conference on control*, Loughborough
- Basri MAM, Husain AR, Danapalasingam KA (2015) Nonlinear control of an autonomous quadrotor unmanned aerial vehicle using Backstepping controller optimized by particle swarm optimization. *J Eng Sci Technol* 8(3):39–45
- Bonna R, Camino JF (2015) Trajectory tracking control of a quadrotor using feedback linearization, *Proceedings of the XVII international symposium on dynamic problems of mechanics*, Brazil
- Chen W, Yang J, Guo L, Li S (2016) Disturbance-observer-based control and related methods-an overview. *IEEE Trans Ind Electron* 63(2):1083–1095
- Choi Y-C, Ahn H-S (2014) Nonlinear control of quadrotor for point tracking: actual implementation and experimental tests. *IEEE/ASME Trans Mechatron* 20(3):1179–1192
- Corke P (2013) *Robotics, vision and control: fundamental algorithms in MATLAB*. Springer-Verlag Berlin Heidelberg, Berlin
- Darogheh N, Meskin N, Khorasani K (2018) A dual particle filter-based fault diagnosis scheme for nonlinear systems. *IEEE Trans Control Syst Technol* 26(4):1317–1334. <https://doi.org/10.1109/TCST.2017.2704959>
- Eltayeb A, Rahmat MF, Musa MJ (2019) Feedback linearization and sliding mode control design for quadrotor's attitude and altitude. In: *Proceedings of the IEEE 1st international conference on mechatronics, automation and cyber-physical computer system*
- Ermeydan A, Kiyak E (2017) Fault tolerant control against actuator faults based on enhanced PID controller for a quadrotor. *Aircraft Eng Aerospace Tech* 89(3):468–476
- Freddi A (2012) Model-based diagnosis and control of unmanned aerial vehicles: application to the quadrotor system. *Universita Politecnica Delle Marche, Ancona*
- Gee SS, Lee TH, Tan EG (1998) Adaptive neural network control of flexible joint robots based on feedback linearisation. *Int J Syst Sci* 29:623–635
- Ghandour J, Aberkane S, Ponsart J-C (2014) Feedback linearization approach for standard and fault tolerant control: application to a quadrotor UAV testbed. *J Phys Conf Ser* 570 pp. 1–11
- He Z, Zhao L (2014) A simple attitude control of quadrotor helicopter based on Ziegler-Nichols rules for tuning PD parameters. *Sci World J* 2014:743869. <https://doi.org/10.1155/2014/743869>
- Kendoul F (2012) Survey of advances in guidance, navigation, and control of unmanned rotorcraft systems. *J Field Robotics* 29(2):315–378
- Khatoun S, Gupta D, Das LK (2014) PID & LQR control for a quadrotor: modeling and simulation. In: *2014 international conference on advances in computing, communications and informatics (ICACCI)*, New Delhi
- Kiyak E (2016) Tuning of controller for an aircraft flight control system based on particle swarm optimization. *Aircraft Eng Aerospace Tech* 88(6):799–809

- Köksal N, An H, Fidan B (2016) Two-level nonlinear tracking control of a quadrotor unmanned aerial vehicle. *IFAC-PapersOnLine* 49(17):254–259
- Kose O, Oktay T (2019) Dynamic modeling and simulation of quadrotor for different flight. *Eur J Sci Technol* 15:132–142. <https://doi.org/10.31590/ejosat.546867>
- Kuantama E, Tarca I, Tarca R (2018) Feedback linearization LQR control for quadcopter position tracking. In: *Proceedings of the 5th international conference on control, decision and information technologies*, Thessaloniki
- Labbadi M, Cherkaoui M (2019) Robust adaptive backstepping fast terminal sliding mode controller for uncertain quadrotor UAV. *Aerosp Sci Technol* 93
- Lanzon A, Freddi A, Longhi S (2014) Flight control of a quadrotor vehicle subsequent to a rotor failure. *J Guid Control Dyn* 37(2):580–591. <https://doi.org/10.2514/1.61494>
- Metin EY, Aygün H (2019) Energy and power aspects of an experimental target drone engine at non-linear controller loads. *Energy* 185:981–993
- Musa S (2017) Techniques for quadcopter modeling and design: a review. *J Unmann Syst Technol* 5(3):66–75. <https://doi.org/10.21608/just.2017.543>
- Najm AA, Ibraheem IK (2019) Nonlinear PID controller design for a 6-DOF UAV quadrotor system. *Eng Sci Technol* 22(4):1087–1097
- Oh H, Kim S (2019) Persistent standoff tracking guidance using constrained particle filter for multiple UAVs. *Aerosp Sci Technol* 84:257–264. <https://doi.org/10.1016/j.ast.2018.12.022>
- Özbek NS, Önkol M, Efe MÖ (2016) Feedback control strategies for quadrotor-type aerial robots: a survey. *Trans Inst Meas Control* 38(5):529–554
- Pamadi BN (2015) Performance, stability, dynamics and control of airplanes. *AIAA Education Series*, Reston
- Prabhakaran B, Kothari M, Abhishek (2015) Nonlinear control design for quadrotors, 2015 IEEE Workshop on Computational Intelligence: Theories, Applications and Future Directions (WCID), Kanpur, pp. 1–6
- Razmi H, Afshinfar S (2019) Neural network-based adaptive sliding mode control design for position and attitude control of a quadrotor UAV. *Aerosp Sci Technol* 91:12–27
- Saif A-WA (2017) Feedback linearization control of quadrotor with tilttable rotors under wind gusts. *Int J Adv Appl Sci* 4(10):150–159
- Seborg DE, Henson MA (1996) *Nonlinear process control*. Prentice Hall, Upper Saddle River
- Voos H (2009) Nonlinear control of a quadrotor micro-UAV using feedback-linearization. In: *Proceedings of the 2009 IEEE international conference on mechatronics*, Malaga
- Wang X, Kampen E-J, Chu Q, Lu P (2019) Incremental sliding-mode fault-tolerant flight control. *J Guidance Control Dyn* 42(2)
- Xiong J-J, Zhang G-B (2017) Global fast dynamic terminal sliding mode control for a quadrotor UAV. *ISA Trans* 66:233–240
- Xuan-Mung N, Hong S-K (2019) Improved altitude control algorithm for quadcopter unmanned aerial vehicles. *Appl Sci* 9(10)
- Yazar I, Kıyak E, Çalışkan F, Karakoç TH (2018) Simulation-based dynamic model and speed controller design of a small-scale turbojet engine. *Aircraft Eng Aerospace Tech* 90(2):351–358
- Zheng E-H, Xiong J-J, Luo J-L (2014) Second order sliding mode control for a quadrotor UAV. *ISA Trans* 53(4):1350–1356
- Zuo Z (2010) Trajectory tracking control design with command-filtered compensation for a quadrotor. *IET Control Theory Appl* 4(11):2343–2355

Chapter 9

An Evaluation on Landing Gear Configurations of Fixed-Wing, Rotary-Wing, and Hybrid UAVs



Emre Özbek , Selcuk Ekici, and T. Hikmet Karakoc 

Acronyms

FPV	First-person view
HALE	High-altitude long endurance
MALE	Medium-altitude long endurance
STOL	Short take-off and landing
UAV	Unmanned aerial vehicle
VTOL	Vertical take-off and landing

9.1 A Brief Classification of UAVs

The term ‘UAV’ is used for fixed wing aircraft and the term ‘drone’ for rotary wing UAVs. But this approach should not be followed to keep the order in this technology and UAV science. Fixed wing aircraft generally refers to an aircraft with stationary

E. Özbek (✉)

UAV Technology and Operatorship Program, Eskisehir Technical University, Eskisehir, Türkiye

e-mail: emreozbek@eskisehir.edu.tr

S. Ekici

Igdir University, Igdir, Türkiye

T. H. Karakoc

Faculty of Aeronautics and Astronautics, Eskisehir Technical University, Eskisehir, Türkiye

Information Technology Research and Application Center, Istanbul Ticaret University, Istanbul, Türkiye

e-mail: hkarakoc@eskisehir.edu.tr; thkarakoc@ticaret.edu.tr

wings that has no ability to tilt, morph, and rotate. Fixed wing UAVs are researched for different sizes and operational environments such as micro (Jana et al. 2022), mini (Sharif 2022), tactical (Kapsalis et al. 2022), middle altitude long endurance (MALE) (Panagiotou et al. 2018), and high altitude long endurance (HALE) (Runge et al. 2007). Fixed wing UAVs outshine with their aerodynamic efficiency, and thus, higher flight endurance. But some operational difficulties should be noted such as take-off and landing runway requirements.

Rotary-wing UAVs are a solution to runway requirement with their ability to take off and land on a specific point. This ability paves the way for more operational freedom for the users from the operation territory. A rotary-wing UAV refers to unmanned aircraft which are able to stay airborne by generating lift from a rotating propeller, or in this case, could be referred as a wing. Helicopter and multirotor-type UAVs are the two main types under rotary wing configurations. Although both platform types can perform hovering motion, which fixed wing aircraft cannot, multirotor UAVs are more in demand in the industry. The main reason behind this preference is their ease in pilotage and availability. Quadcopters (Meivel et al. 2016), hexacopters (Park and Cho 2020), and octocopters (Weber et al. 2017) are the most popular rotary wing UAV platforms right now. Although multirotor UAVs offer advantages in terms of pilotage and operational flexibilities, their limited endurance and payload capacity due to battery capacities limit their usage for some advanced operations. When high endurance, heavy payload-carrying capability along with hover capability is required for an operation, helicopter UAVs with internal combustion engines and high blade efficiency due to the longer rotors outshine.

Hybrid UAVs should also be mentioned in this classification as they are the result of a middle ground effort between fixed wing UAVs and rotary wing UAVs. Hybrid UAVs are basically fixed wing aircraft with the ability to take-off and land vertically. They are also referred to as vertical take-off and landing (VTOL) aircraft. Although some VTOL aircraft can perform hover motion (McGonigle et al. 2008), there are some hybrid VTOL aircraft that cannot perform hover motion such as most of the tail-sitter UAVs (Footohi et al. 2019). Hybrid UAVs could be divided into three subgroups such as fixed VTOL UAVs (Jeong et al. 2010), tilt-rotor/tilt-engine UAVs (Dündar et al. 2020), and tail-sitter UAVs (Jung and Shim 2012). Although they require more complex control and design processes, tail-sitter and tilt-rotor UAVs are considered more efficient compared to fixed VTOL UAVs mostly because fixed VTOLs carry unused motors and electronic parts during the cruise flight.

Apart from these three major configuration directions, inflatable UAVs, such as balloons (Lateran et al. 2016), airships (Koska et al. 2017), and aerostats (Pieri et al. 2014), and flapping wing-type UAVs with bird-like (Pan et al. 2017) and bug-like (Geder et al. 2010) design directions should also be mentioned. These applications will not be considered in the following sections due to their lack of landing gear involvement. Figure 9.1 illustrates the previous classification of the mentioned configurations.

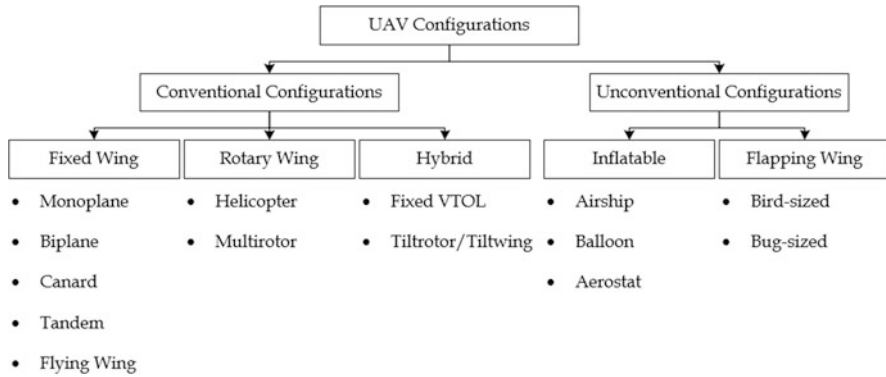


Fig. 9.1 The brief classification of UAV configurations

9.2 UAV Landing Gears

Landing gears of UAVs should be considered as subsystems consisting of components and parts. Although a landing gear subsystem could be composed of only one part in some cases, there are complex systems comprising retraction, braking mechanisms, and their components and parts too. There are many landing gear design selections available for each UAV configuration with specific pros and cons. However, a general definition can be made of the functions. In all landing gear configurations, this subsystem is the part of the aircraft closest to the ground line. The main functions of a landing gear could be summarized as follows:

- The UAV is deployed on it during unassisted take-off and landing methods.
- It protects the payload and other subsystems of the UAV from the ground impact.

Apart from these general functions that are valid for each UAV configuration that uses unassisted take-off and landing methods, there are landing gear subsystem functions that are specific to each UAV configuration. These functions will be explained in the following sections. However, the no-landing gear fixed wing UAVs that use the previously mentioned assisted methods for taking off and landing should be explained first.

9.2.1 Fixed Wing UAVs Without Landing Gears

Assisted take-off methods are used in many UAV operations, particularly in fixed wing UAV configurations to reduce their dependency on runway. Landing gear subsystem comes with a cost to aircraft in terms of weight and drag penalties along with system complexities. If operational requirements could be met by assisted take-off and landing methods, aircraft designers have a tendency to eliminate these

performance penalties from the aircraft. Not using a landing gear increases aircraft's cruise performance and endurance greatly. Since maximizing the cruise performance is the prior design goal for many aircraft designers, landing gear could be seen as a parasitic source of weight and drag in this perspective just after the aircraft is airborne.

Assisted take-off methods are operated using the same principle: making the aircraft airborne with provided external force. These methods can be as simple as hand launching or can be complex systems such as catapults and rocket-assisted take-offs. Hand launching an aircraft is obviously limited by human factors such as height, arm distance, and arm strength. Mini UAVs up to 6.5-kg take-off weight could be accepted as an operational limit considering many field experiences. Another assisted take-off method that could be mentioned here is the usage of catapult systems. Catapult systems can launch an aircraft with the intended force and angle along the track. There are mechanic (Yafei et al. 2020), pneumatic (Siddiqui et al. 2017), hydraulic (Lan-rong and Xiao-chen 2016), and electromagnetic (Li et al. 2014) catapult systems used in different aircraft operations due to the required actuation force and aircraft dimensions.

An exception to that could be kamikaze UAVs. A fixed wing UAV without a landing gear can perform belly landing on a runway or field if available. To increase the operational flexibility, a UAV parachute system (Al-Madani et al. 2018) can be employed with the addition of weight and fuselage interior volume allocation. Apart from belly landings and parachute recovery systems, there are more advanced recovery systems available such as recovery nets (Kim et al. 2013) and recovery winches (Sarigul-Klijn and Sarigulklijn 2016).

In terms of operational flexibility, hand launch take-off and belly landings are most preferred options of mini fixed wing UAVs. In heavier class fixed wing UAV systems, addition of catapults and recovery systems to the operation cycle increases the cost of service. Thus, in micro and mini fixed wing UAV designs, using no landing gear subsystem outshines as a feasible design selection in terms of overall system performance and operational flexibility. However, starting with the tactical fixed wing UAV class, this design choice requires compensations that can increase the cost of the system and bring complexity. Also, it should be noted that higher weight/wing reference area (W/S) ratio can be related with the requirement of a landing gear subsystem.

9.2.2 Fixed Wing UAV Landing Gears

Apart from the previously listed two main functions of landing gears, in fixed wing UAVs that operate using conventional take-off and landing methods, two new functions of landing gear subsystems can be defined:

- Allows the UAV to accelerate on the runway until it performs the take-off rotation
- Allows the UAV to make taxi movements and course correction while runway run

The landing gear subsystem design classification of fixed wing UAVs starts with a distinction that depends on the position of the landing gear during the cruise flight. There are two major options on this topic: fixed landing gears and retractable landing gears. Fixed landing gears are fully deployed in every phase of flight. In contrast, retractable landing gears could be retracted into the aircraft fuselage or wings during the phases in between take-off and landing.

A fixed landing gear, like the fixed wing term, defines a landing gear fixed unit under the aircraft during all flight phases. Fixed landing gears are a great source of drag, thus a limitation for aircraft cruise performance. Additionally, aircraft without landing gear also incur an increase in weight. Fixed landing gears are a selection designers continue with, when the conventional take-off and landing is necessary and the aircraft performance is not the higher merit of configuration selection. Fixed landing gear subsystems are easier to design and use compared to retractable landing gears due to the design and manufacture costs.

Retractable landing gears are used since the 1940s. Retracting the landing gear could be assumed as a shape morphing for aircraft since the shape of the aircraft changes during the flight. Although there are fixed wing UAVs with only retractable front gear, it is expected to minimize the drag by retracting main landing gear too. The retracting mechanisms are complex and costly. Also, they require additional equipment and volume allocation in aircraft fuselage, which can result in additional dimension increase that can lead to an increase in drag too. Usually, landing gears are expected to be stored inside the fuselage as they are retracted. But in some low-wing placement designs, the main landing gear could be stored under the wing (Goraj et al. 2004). The dominant area of retractable landing gear usage in fixed wing UAVs starts with tactical class, MALE class, and HALE class where the project budgets can meet the design complexities and higher performance expectations are required. Figure 9.2 summarizes the landing gear subsystem general configuration selection decision-making process and properties that drive the process.

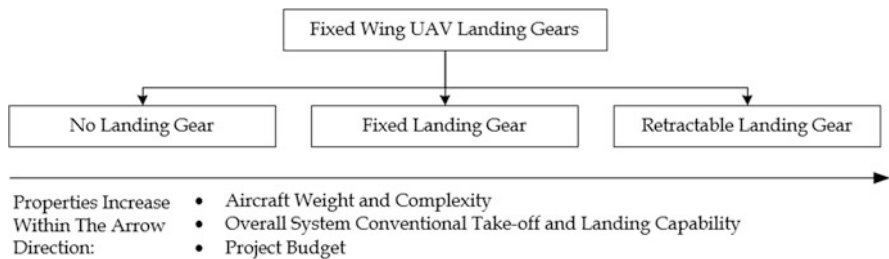


Fig. 9.2 Fixed wing UAV landing gear general configuration decision-making process

The selection of availability and the position during the flight for the landing gear subsystem usually continues with the configuration selection process of landing gear count and position. Although manned aviation and the variety of manned aircraft types require different landing gear configurations such as main single, bicycle, multi-bogey for airliners, cargo aircraft, and quadricycles, the dominant landing gear configurations in fixed wing UAVs are tricycle landing gear configuration and tail gear configuration; both landing gear configurations offer a main landing gear. The difference between the two is the location of the secondary gear. The tricycle configuration has the front secondary gear placement, while the latter places the secondary gear under the empennage section.

Tricycle landing gear placement offers better ground controllability to the aircraft compared to the tail gear configuration during the taxi on the runway. In short take-off and landing (STOL) designs, the tail gear configuration is the aircraft’s wings already placed with an angle to the ground plane at the start of the take-off run. Also, the retraction styles of these two configurations come with a difference. The front gear requires a retracting mechanism inside the front of the fuselage where the payload could be placed. On the other hand, in tail gear configuration designs, the tail gear could be fixed outside of the aircraft as it contributes to the drag lesser due to the smaller tire diameter and strut height. As a side note, the direction control during the take-off usually requires yaw motion around the z-axis. Steering capability of the aircraft can be combined with the rudder deflection for better ground handling. The option of combining the rudder and tail gear mechanically also contributes to overall system multi-functionality. However, the most dominant landing gear placement position for fixed wing UAVs is tricycle with some tail gear designs appearing within the mini fixed UAV platforms. Figure 9.3 details these two dominant fixed wing UAV landing gear positions.

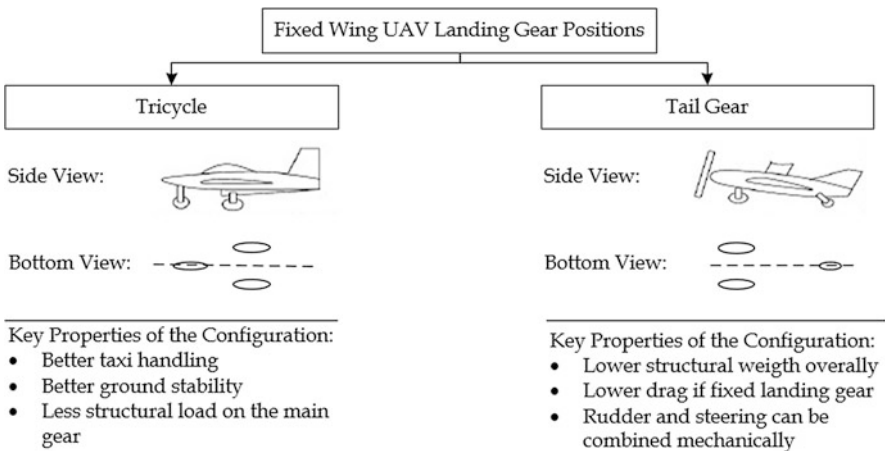


Fig. 9.3 Dominant fixed wing UAV landing gear positions and details

The design process of a fixed wing UAV landing gear subsystem continues with the selection of the components for the design after landing gear general configuration, landing gear number and placement selections. A conventional fixed wing UAV subsystem mainly consists of tyres, struts, shock absorbers. Steering and retracting can be seen as optional. These two mechanisms can also be added to the components if they are enabled.

Tyres of a landing gear:

- Absorbs the shock from the runway during landing
- Transmits acceleration and braking
- Changes or maintains the run direction

The fixed wing UAV landing gear tyres can be filled with air or sponge. Sponge-filled ones are usually preferred in mini-class UAVs. Air-filled tyres are preferred for UAVs in heavier classes. When sizing tyres, their diameter and width are taken into account. Proper sizing of both is important to optimize drag and weight. Generally speaking, for a tricycle configuration, it can be assumed that the nose tyre is about 50–100% the size of the main tyres.

Struts are considered the main structural element of landing gears. A strut connects the UAV landing gear tyre with a fork-like attachment to the fuselage. Two typical strut cross sections are circular and rectangular. Aluminium landing gear struts are generally seen in UAVs as structural stiffness is required for this component. Carbon tubes are also used in mini-class UAVs due to their availability and high strength-to-weight ratio. The height of a strut is usually determined by the ground clearance requirement of the aircraft. In fixed wing UAVs, the lowermost elements are usually propeller blades, externally placed payloads, and inverted tail components in configurations such as inverted V tail and inverted U tail. The typical value of the ground clearance requirement for a fixed wing UAV is about 20 cm from the ground line.

Generally, ‘solid spring’-type shock absorbers are used in unmanned aerial vehicles. Solid spring-type landing gear struts look like the letter ‘C’ when viewed from the front of the aircraft. Oleo-type struts, on the other hand, are a type often encountered in manned aviation and retractable landing gear. The elastic structure in the strut works like a shock absorber and absorbs the shock. From a cost perspective, solid spring is a cheaper component in both designing and manufacturing. Figure 9.4 illustrates the placement of a solid spring-type main landing gear that is designed for the Dorje UAV that has 2.5 kg take-off weight.



Fig. 9.4 Solid spring-type main landing gear placement on Dorje UAV

The steering mechanism is required to change the nose direction of the aircraft while taxiing on the runway. It may not be available in all fixed wing UAVs. In its absence, extra care is taken during the assembly of the main landing gear to ensure that the UAV is proceeding straight on the runway. Although the nose direction can be changed by using the rudder on the runway, the forces produced are limited because the airspeed is quite low. In the tricycle configuration, the front gear provides steering capability while in the tail dragger configuration, the gear under the tail is usually moved in sync with the rudder. Electromechanical units such as servomotors are used to provide this direction change in UAVs.

Apart from the ground clearance of the aircraft, which is directly a function of landing gear height, there are two other dimensions that should be carefully evaluated during the design such as the wheel track and the wheel base. These two parameters affect aircraft landing gear subsystem performance greatly.

Wheel base is the distance between the main landing gear and the secondary landing gear. This distance affects the aircraft's ground controllability, ground stability, and structural load distribution between main and secondary gear components. The design take-off rotation angle must be carefully considered in this parameter selection since this is one of the major contributors to the phenomenon called tail strike during the take-off procedures.

Wheel track is the second effective parameter that must be decided during the sizing process of the landing gear subsystem. Wheel track defines the distance between two main landing gear tyres. This parameter directly affects ground directional handling and tipping phenomena. The wheel track of the main landing gear should be arranged in such a way that the airplane cannot overturn too easily due to wind or ground turn during taxi.

9.2.3 Rotary Wing UAV Landing Gears

Rotary wing UAVs have the ability to take-off and land vertically. Thus, their landing gear subsystems can be regarded as simpler than the fixed wing UAVs both function-wise and in component count. Rotary wing UAV landing gear functions can be described as follows:

- The rotary wing UAV is deployed during take-off and landing procedures.
- The landing gear offers ground clearance for payloads and other subsystems.

The landing gear subsystems of rotary wing UAVs are sometimes addressed with terms such as skids and pods in different sources as the term 'landing gear' usually comes to mind with tyres. The term 'skid' hails from the manned helicopter terminology.

Multirotor UAVs have limited payload placement area under their frame under the centre of gravity location. This inflexibility pushes designers to locate payloads under the frame in the crossing point of arms. Typically, payloads for rotary-wing UAVs are positioned beneath the frame, which is the lowest element of the



Fig. 9.5 Multipurpose helicopter UAV skid design

aircraft. Exception to that is racing multirotor UAVs with forward placed camera as payload as fixed-person view (FPV) piloting and flight training UAVs do not require a payload at all. In these exceptions, UAVs can land on their frames or motor mounts. Apart from these two applications, usually, a ground clearance about 15–20 cm is required between the ground line and the UAV's components or payload.

Rotary wing UAV landing gear subsystems can also be fixed during the flight or can be retracted to the horizontal plane position to increase the gust resistance and visual clearance for the camera. Also, there are landing gear subsystems that could be retracted to the horizontal plane only for modularity reasons to fit in a carrying box. The availability of electromechanical units in the airframe that can perform direction change is the key difference between these configurations.

Helicopter UAV designs usually continue in the same direction with manned helicopter technology. These skids are fixed landing gear subsystems consisting of two solid spring struts that provide the clearance and two longitudinal tracks curved on the edge that connect struts. These strut and track components are usually manufactured from aluminium or carbon fibre materials. The distance between the tracks is also an important consideration for ground structural load distribution such as the wheel track parameter on fixed wing UAV landing gears. Figure 9.5 shows a conventional skid design for a multipurpose helicopter UAV.

In multirotor UAVs, there are fixed and retractable landing gear options. However, the retracting mechanism can be used in-flight or off-flight. The off-flight retraction mechanism does serve as a mere modularity option. Multirotor UAV designers and manufacturers consider modularity and carry box dimensions for their products since it is an important customer expectancy. The in-flight retraction is based on improving the flight stability of the aircraft by decreasing the side cross-sectional area, thus improving the useful camera angles by removing landing gear from the sight. Servomotor included mechanisms are the key difference in the in-flight and off-flight retraction mechanisms.

Apart from helicopter skids, multirotor UAV landing gear configurations are mainly clustered around three design directions. The first direction is usually seen in multirotor UAVs with approximately 0.5–2-kg take-off weights and consisting of

Fig. 9.6 Miniquad multirotor with pod-type rotary wing landing gear

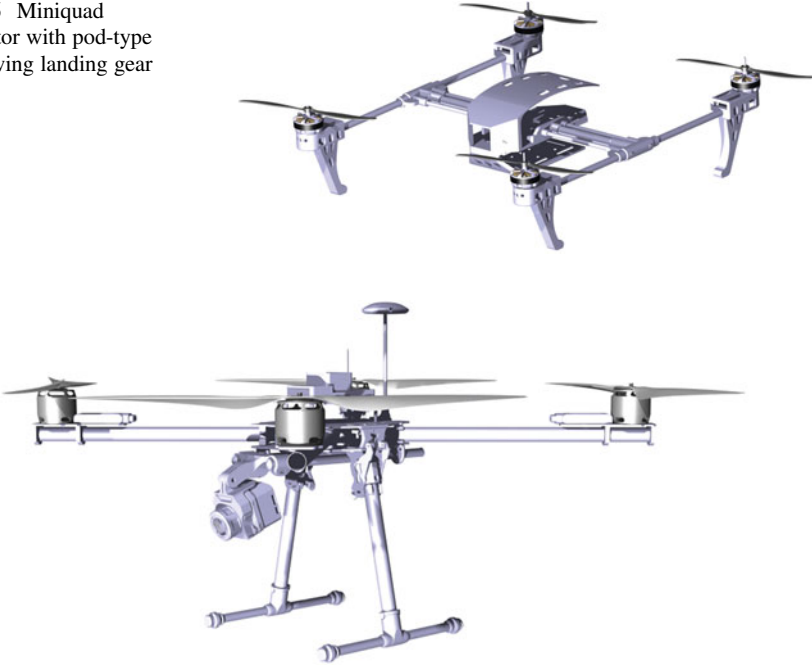


Fig. 9.7 Ace UAV with off-flight T-shaped retractable landing gear

four pod-shaped elements located under each motor mounts. Due to the rarest design choice among the three options (fixed pods, skids and retractable gear) and its low structural load, these pods can be manufactured from three-dimensional thermoplastics or carbon fibre materials. Figure 9.6 shows a multirotor design called Huma Miniquad that weighs around 1.5 kg and uses pods as the landing gear subsystem.

The second design model of the multirotor UAV landing gear consists of two parallel tracks connected to the frame using individual struts. This T-shaped design is usually associated with retractable landing gear units on multirotor UAVs. The root of the strut is connected to the aircraft frame. The off-flight retracted types can be manually retracted for modularity purposes. In-flight retracted types usually have a retraction mechanism consisting of an electromechanical activator and push-pull rods. The Ace UAV design shown in Fig. 9.7 with a 4.5 kg take-off weight is an example for this design direction. Off-flight retraction was enabled for this UAV design to meet packaging volume requirements. T-tube shaped components are usually made of three-dimensional printing thermoplastics, and strut and track printing thermoplastics, and strut and track materials are made of carbon fibre tubes. Optionally, some polymer materials can be implemented to each end of the track in order to reduce ground impact.

The third direction of the multirotor landing gear designs can be described as frame pods. Unlike the first direction, these pods hail from the frame of the multirotor instead of motor mounts which are located at the end of each arm.



Fig. 9.8 Smartquad UAV with pods from fuselage landing gear configuration

These components are essentially curved and connected to each arm root of the multirotor UAV within the frame. These arms are usually manufactured from aluminium milling and three-dimensional printing related to the UAVs' take-off weight. Smartquad UAV design with 6-kg take-off weight shown in Fig. 9.8 employs these curved elements as the landing gear.

9.2.4 Hybrid UAV Landing Gears

Fixed VTOL UAVs and tiltrotor/tiltwing UAVs can be considered as configurations that combine fixed wing and rotary wing designs to benefit from the capabilities of each individual configuration. Fixed wing aircraft excel in flight endurance, while rotary wing platforms can offer VTOL and hover flight capabilities. Landing gear subsystems of these hybrid platforms can vary as expected. A fixed wing UAV landing gear configuration such as fixed tricycle can be integrated to the design of a fixed VTOL UAV if conventional take-off and landing are expected or may be required in some operations. However, if the UAV only performs VTOL operations, then the third direction in the multirotor UAV landing gear can be adapted, which in this case is pods from fuselage.

The usage of fixed wing UAV landing gear configurations adds more drag and weight compared to fuselage pod design. However, conventional take-off and landing could be required in some scenarios; for instance, in the case of vertical motor malfunction in fixed VTOL or tilting mechanism malfunction in a tiltrotor UAV. In these two hybrid UAV configurations, there is a trade-off that the designer has to deal with considering operational limits and performance. Tardis fixed VTOL UAV design in Fig. 9.9 was designed with fixed tricycle landing gear as a result of this trade-off.

Tail-sitter platforms are usually considered as platforms that have no landing gear subsystem. However, in many designs, assisting rods are placed in the tip of the wings or empennage sections as inverted V-shaped structural elements. These components are essentially carbon fibre rods used as landing gear struts that can result in increased drag and weight.



Fig. 9.9 Tardis VTOL UAV with conventional fixed tricycle landing gear

9.3 Conclusion

With the booming UAV industry in both military and civil applications, there are many UAV platforms designed by experienced and inexperienced designers. Landing gears are important subsystems of these systems as they are essential for take-off and landing procedures, which can end up with a loss of system in case of failure. There are many sources in the literature for airplane landing gear design and sizing methodology. Fixed wing UAV designers have been benefitting from these sources. When it comes to the rotary wing UAV platforms and hybrid platforms, even a classification of current landing gear applications was unavailable. In this chapter, the mainly used landing gear configurations were assessed, and design methodology was explained for fixed wing, rotary wing, and hybrid UAV platforms. Unconventional or rare landing gear subsystems were neglected and conventional configurations were discussed. Important selection merits for each configuration were explained to guide design trade-offs.

References

- Al-Madani B, Svirskis M, Narvydas G, Maskeliūnas R, Damaševičius R (2018) Design of automatic drone parachute system with temperature compensation mechanism. *J Adv Transp* 22(1): 100–109
- Dündar Ö, Bilici M, Ünler T (2020) Design and performance analyses of a fixed-wing battery VTOL UAV. *Eng Sci Technol Int J* 23(5):1182–1193
- Footohi P, Bouskela A, Shkarayev SV (2019) Aerodynamic design of long-range VTOL UAV. In: *AIAA Scitech 2019 Forum*, pp 2291
- Geder J, Ramamurti R, Sandberg W, Flynn A (2010) Modeling and control design for a flapping-wing nano air vehicle. In: *AIAA guidance, navigation, and control conference*, p 7556
- Goraj Z, Frydrychewicz A, Świtkiewicz R, Hernik B, Gadomski J, Goetzendorf-Grabowski T et al (2004) High altitude long endurance unmanned aerial vehicle of a new generation – a design challenge for a low cost, reliable and high performance aircraft. *Bull Polish Acad Sci Techn Sci* 52(2):173–194

- Jana, S., Kandath, H., Shewale, M., Dhingra, G., Harish, D. S., & Bhat, M. S. (2022). Design and development of a novel fixed-wing biplane micro air vehicle with enhanced static stability. *CEAS Aeronaut J* 13(2):433–452
- Jeong Y, Shim D, Ananthkrishnan N (2010) Transition control of near-hover to cruise transition of a tail sitter UAV. In: *AIAA atmospheric flight mechanics conference*, pp 7508
- Jung Y, Shim DH (2012) Development and application of a controller for the transition flight of a tail-sitter UAV. *J Intell Robot Syst* 65(1):137–152
- Kapsalis S, Kantourous B, Panagiotou P, Yakinthos K (2022) DOE-based method for aerodynamic, stability and layout optimization of a tactical Blended-Wing-Body UAV. In: *AIAA SCITECH 2022 Forum*, pp 0127
- Kim HJ, Kim M, Lim H, Park C, Yoon S, Lee D et al (2013) Fully autonomous vision-based net-recovery landing system for a fixed-wing UAV. *IEEE/ASME Trans Mech* 18(4):1320–1333
- Koska B, Jirka V, Urban R, Křemen T, Hesslerová P, Jon J et al (2017) Suitability, characteristics, and comparison of an airship UAV with LIDAR for middle-size area mapping. *Int J Remote Sens* 38(8–10):2973–2990
- Lan-rong LIU, Xiao-chen MA (2016) Simulation analysis and experimental research of UAV hydraulic catapult ejection process. *Chin Hydraul Pneumat* 5:65
- Lateran S, Sedan MF, Harithuddin ASM, Azrad S (2016, Oct). Development of an unmanned aerial vehicle (UAV)-based high altitude balloon (HAB) platform for active aerosol sampling. In: *IOP conference series: materials science and engineering* 152(1), p. 012018, IOP Publishing
- Li H, Li X, Li Z (2014, July) Study on a long primary moving-magnet type linear electromagnetic catapult. In: *2014 17th international symposium on electromagnetic launch technology*. IEEE, pp 1–6
- McGonigle AJS, Aiuppa A, Giudice G, Tamburello G, Hodson AJ, Gurrieri S (2008) Unmanned aerial vehicle measurements of volcanic carbon dioxide fluxes. *Geophys Res Lett* 35(6)
- Meivel S, Maguteeswaran R, Gandhiraj N, Srinivasan G (2016) Quadcopter UAV based fertilizer and pesticide spraying system. *Int Acad Res J Eng Sci* 1:8–12
- Pan E, Chen L, Zhang B, Xu W (2017, Aug) A kind of large-sized flapping wing robotic bird: design and experiments. In: *International conference on intelligent robotics and applications*. Springer, Cham, pp 538–550
- Panagiotou P, Fotiadis-Karras S, Yakinthos K (2018) Conceptual design of a blended wing body MALE UAV. *Aerosp Sci Technol* 73:32–47
- Park J, Cho N (2020) Collision avoidance of hexacopter UAV based on LiDAR data in dynamic environment. *Remote Sens* 12(6):975
- Pieri DC, Diaz JA, Bland G, Fladelland MM, Abtahi A, Alan Jr, A, Weber K (2014, Dec) Systematic observations of Volcán Turrialba, Costa Rica, with small unmanned aircraft and aerostats (UAVs): the Costa Rican Airborne Research and Technology Applications (CARTA) missions. In *AGU Fall Meeting Abstracts*, Vol. 2014, pp V41C-4838
- Runge H, Rack W, Ruiz-Leon A, Hepperle M (2007, Sept) A solar powered HALE-UAV for Arctic research. In: *1st CEAS European air and space conference*
- Sarigul-Klijn N, Sarigulklijn M (2016) A novel sea launch and recovery concept for fixed wing UAVs. In: *54th AIAA aerospace sciences meeting*, p 1527. <https://doi.org/10.2514/6.2016-1527>
- Sharif A (2022) Conceptual design and analysis of a fixed wing mini unmanned aerial vehicle for humanitarian assistance operations. In: *AIAA SCITECH 2022 forum*, pp 1504
- Siddiqui BA, Rahman HU, Kumar C, Solen MA, Bashir UD (2017, Feb) Computer-aided modeling and simulation of pneumatic UAV catapult mechanism. In: *7th international mechanical engineering congress*, pp 24–25
- Weber K, Heweling G, Fischer C, Lange M (2017) The use of an octocopter UAV for the determination of air pollutants—a case study of the traffic induced pollution plume around a river bridge in Duesseldorf, Germany. *Int J Environ Sci* 2:63–68
- Yafei LU, Qingyang CHEN, Gaowei JIA, Zheng GUO (2020, Dec) Development and experiment of elastic-rope launcher for small fixed-wing UAVs. In: *2020 3rd world conference on mechanical engineering and intelligent manufacturing (WCMEIM)*. IEEE, pp 654–658

Chapter 10

Non-linear System Identification for UAS Adaptive Control



Sean Bazzocchi and Afzal Suleman

Acronyms

CFD	Computational fluid dynamics
MIAC	Model identification adaptive controller
SID	System identification
SINDy	Sparse identification of non-linear dynamics
UAS	Unmanned aerial system
u	Linear rate on x body axis, m/s
w	Linear rate on z body axis, m/s
q	Pitch angular rate, rad/s
u	Command
X	States
T	Training time, s
k	Harmonic multiplier
t	Time, s
R^2	R -squared fitness value
θ	Pitch angle, rad
Θ	Library of candidate non-linear functions
Ξ	Sparse coefficient matrix
ξ	Sparse coefficient vector
η	Noise magnitude
c	Canard
t	Throttle
$\hat{\cdot}$	Estimated noisy state

S. Bazzocchi (✉) · A. Suleman
University of Victoria, Centre for Aerospace Research, Victoria, BC, Canada
e-mail: seanbazzocchi@uvic.ca; suleman@uvica.ca

10.1 Introduction

The conventional design and tuning method of an autopilot system for unmanned aerial system (UAS) is a highly time-consuming process. This procedure, shown in Fig. 10.1, usually starts with ground-based analysis, such as computational fluid dynamics (CFD) and wind tunnel sessions, to generate the data needed to develop a flight dynamic model (FDM) of a vehicle. After designing or selecting appropriate control laws, the model and controller can then be tested in software-in-the-loop simulations with the goal of tuning control parameters for the desired performance. The controller is then deployed into hardware and the vehicle flight tested while recording all observable states from the sensors. This data is then usually processed to correct the initial FDM allowing for greater precision in a second tuning iteration. The described process needs to be repeated for all new prototypes and when a system goes through any modification that alters the dynamics of the vehicle.

One of the benefits of adaptive controllers is the elimination of this lengthy procedure and automation of the tuning process. However, rapid prototyping and the ability to easily overcome changes in system dynamics are not the only motivations that are driving this research field. As stated by Morelli (Morelli and Grauer 2018), there are several other advantages including:

- Detection and mitigation of failures
- Ability to cope with morphing aerodynamic properties
- Dynamic flight envelope correction
- Exploration of non-linear dynamics for complex aircraft configuration
- Fast generation of a time-varying system model

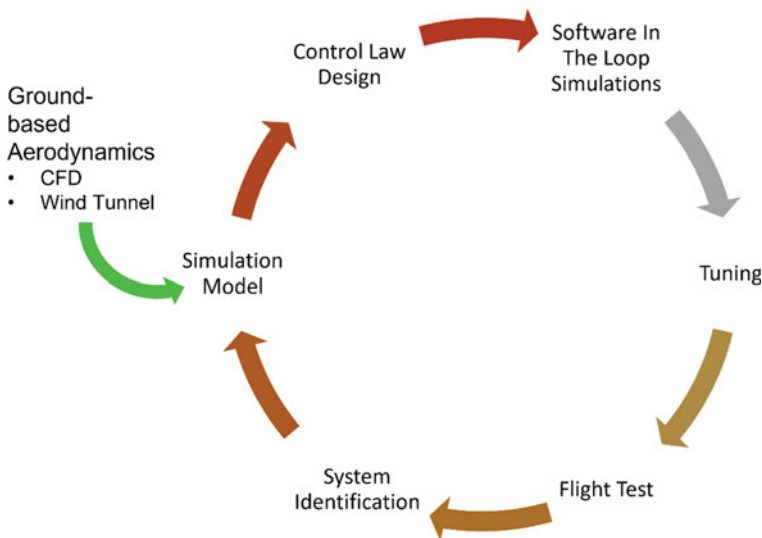


Fig. 10.1 Conventional control design and tuning process

Some of the well-known research laboratories and industries in the aerospace sector are pursuing these objectives, including the US Air Force with project RESTORE, Boeing with project RACE, and NASA with the L2F project (Eugene et al. 2020).

This study first presents an effective architecture to achieve the stated adaptive control benefits, and it next validates a system identification method in the context of a UAS platform developed at the University of Victoria – Centre for Aerospace Research (UVicCfAR).

10.2 Method

There are many different techniques that may be adopted to achieve adaptive control capabilities such as extremum peak-seeking control, adaptive pole placement, model reference adaptive control, reinforcement learning, and self-designing control. However, only the model identification adaptive control (MIAC) method can generate a human-readable, time-varying system model online.

10.2.1 Model Identification Adaptive Control

Figure 10.2 shows the high-level structure of a model identification adaptive controller. It is possible to identify several blocks part of a conventional autopilot system such as the estimator, guidance, and controller. The main difference is the presence of system identification process which collects data from the controller output and state estimator with the goal of generating a near real-time model of the vehicle. This information is then fed to the model-based controller which becomes “adaptive” by virtue of the updating dynamic model. It is also possible to extrapolate model performance parameters from the identified system which can be used to tune the guidance and navigation controller.

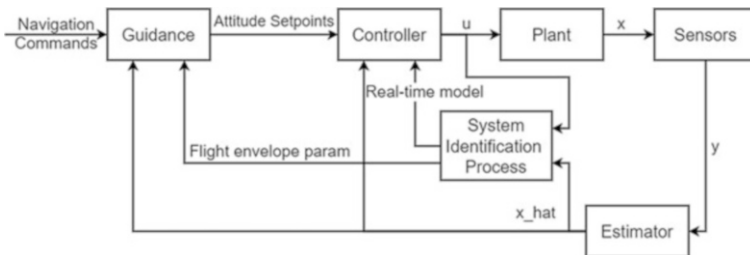


Fig. 10.2 Model identification adaptive controller architecture

One of the main advantages of this type of architecture compared to other data-driven controllers is human readability. This property allows for formal validation of the controller. In other words, it is possible to validate the control behaviour without testing every single condition, something that is not possible with a neural network type of architecture, for example (Van Wesel and Goodloe 2017). Furthermore, the generation of a real-time system identification (SID) model allows for rapid investigation of the system performance and analysis of any changes to the dynamics during flight.

In a real-world application of this controller, other three components would need to be present to complete this architecture: an online simulation of the identified model, a model supervisor, and a control perturbator. The online simulation is needed to generate the state prediction from the predicted model. This can be intelligently obtained from the prediction of an Model Predictive Controller (MPC) reducing the computational power required. The model supervisor compares the predicted state of the identified model with the real states being computed by the estimator. If a discrepancy of a certain amplitude is recorded for a set number of samples, this would trigger the control perturbator and the SID program to start a system identification process. The control perturbator generates and injects the desired perturbation signal on top of the actuator commands coming from the controller.

10.2.2 System Identification Method

The selection and development of the system identification method is crucial since the MIAC is highly dependent on the capability of the SID process to effectively identify the vehicle dynamics.

Nonlinear Autoregressive Moving Average model with exogenous inputs (NARMAX), Eigensystem Realization Algorithm (ERA), Genetic Programming (GP), Neural Network (NN), and Koopman with control are some of the multiple data-driven techniques for SID and control discussed in (Brunton and Kutz 2019), a recommended reference for an overview on machine learning for control. The method selected and employed in this project is the sparse identification of non-linear dynamics (SINDy) (Brunton et al. 2016a). This theory combines sparsity-promoting techniques and machine learning with non-linear dynamical systems to discover governing equations from noisy measurement data. SINDy was published in 2016 and rapidly evolved to SINDyc to include external inputs and feedback control to the system identification process (Brunton et al. 2016b). In 2018, Kaiser demonstrated the capability of SINDy algorithm to perform system identification with limited and noisy data, proving the capability of this technique to be applied online for a control optimization problem (Kaiser et al. 2018). Quade investigated the capability of SINDy by generating a structure for fault detection based on model prediction to trigger the system identification process (Quade et al. 2018). The results from the tests performed on non-linear dynamic systems with

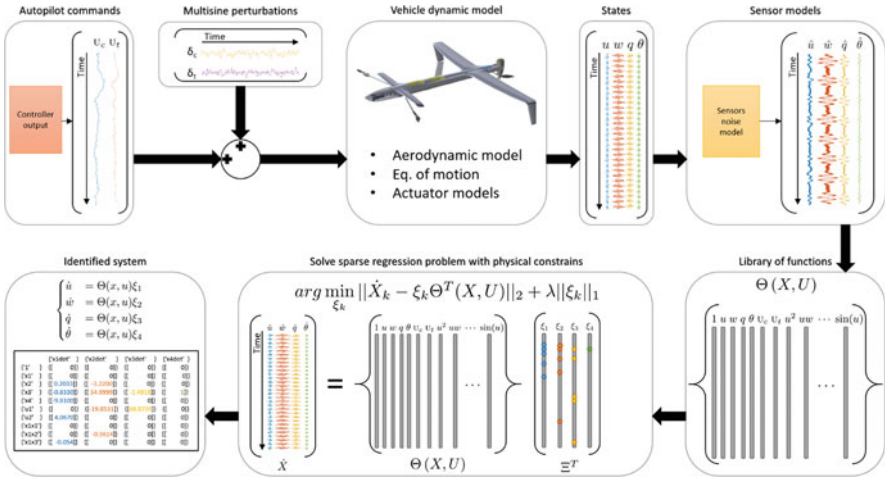


Fig. 10.3 System identification process

discrete and noisy data highlighted the interesting potential of this new theory to be applied in the ongoing aerospace research of an adaptive controller.

The scheme shown in Fig. 10.3 illustrates the high-level system identification process for the longitudinal dynamics (u, w, q, θ) of the Eusphyra aircraft using SINDy. Note that the same study can be performed on the lateral-directional dynamics or both combined.

During forward flight, the longitudinal actuator commands (u_c and u_e) generated by the controller can be perturbed by unique, zero-mean, multi-frequency signals (δ_c and δ_e). This practice ensures that the vehicle dynamics are effectively excited to allow for an effective system identification. In this study, the non-linear flight dynamic model was generated using CFD analysis and coded in Simulink to calculate the system response (X). The calculated true states are then fed into the sensors and estimator models which apply noise to the response depending on the signals' standard deviation. The estimated or noisy states are used to generate the matrix Θ which holds the pool of candidate non-linear equations that may describe the system. It is important to properly select a list of functions that is capable of describing the dynamic system. Ideally, this pool of functions contains all the terms necessary to represent the system but at the same time is small enough to guarantee a convergence to the correct solution. In this case, the library was formed by constants, polynomial terms up to third order, and trigonometric terms. Because only a few terms of the proposed library of functions will be active in each differential equation, a sparse regression problem is formulated to determine the vector of coefficients ξ forming the matrix Ξ .

$$\xi_i = \arg \min_{\hat{\xi}_i} \frac{1}{2} \left\| X'_{i} - \hat{\xi}_i \Theta^T(X, U) \right\|_2^2 + \lambda \left\| \hat{\xi}_i \right\|_1 \quad (10.1)$$

Each column ξ_i is a sparse vector of coefficients determining which terms of Θ are active in the corresponding differential equation:

$$\dot{x}_i = f_i(x) = \Theta(x^T) \xi_i \quad (10.2)$$

The sparsity of the resulting equations can be tuned by the parameter λ , which defines the threshold for the elimination of the small entries (Mangan et al. 2017).

The execution speed of this algorithm depends on the following factors: number of states, number of functions in the library, length of training data, and number of iterations required to obtain a solution to the sparse regression problem that does not present any small entries. In the simulations conducted in this research, the time required to process the solution resulted negligible compared to the time needed to acquire the training data. This is because the solution is calculated only once per buffer of finite-history data set (near real time) instead of recalculating the solution for every new data point continually shifting the buffer (real time).

The convergence of this method is not guaranteed. If the parameter λ is not set correctly or the pool of equations is too vast, the algorithm may terminate with an incorrect non-sparse solution. It is recommended to set as many constraints as possible to contain the dimensions of Θ and reduce the number of differential equations to discover. In this study, it was possible to constrain one of the differential equations (Eq. 10.3) and reduce the size of the pool of candidate functions by computing the angle of attack α and therefore eliminating the need for trigonometric terms (Eq. 10.4).

$$\dot{\theta} = q \quad (10.3)$$

$$\alpha = \tan^{-1} \left(\frac{w}{u} \right) \quad (10.4)$$

10.2.3 Command Perturbation

One of the most important components in the system identification is the correct perturbation of the available actuators. This not only serves the purpose of identifying control effectiveness but also excites the system dynamics across a defined spectrum of frequencies. The amplitude of the perturbations must also be properly set to ensure that the signal-to-noise ratio remains above the usable threshold without endangering the state of the vehicle.

There are several types of perturbation signals that may be used for this purpose, such as singlets, 3-2-1-1, doublets, sinusoids, and chirps. The signal type used in this project are orthogonal, phase-optimized, and multisine inputs (Grauer 2018). The

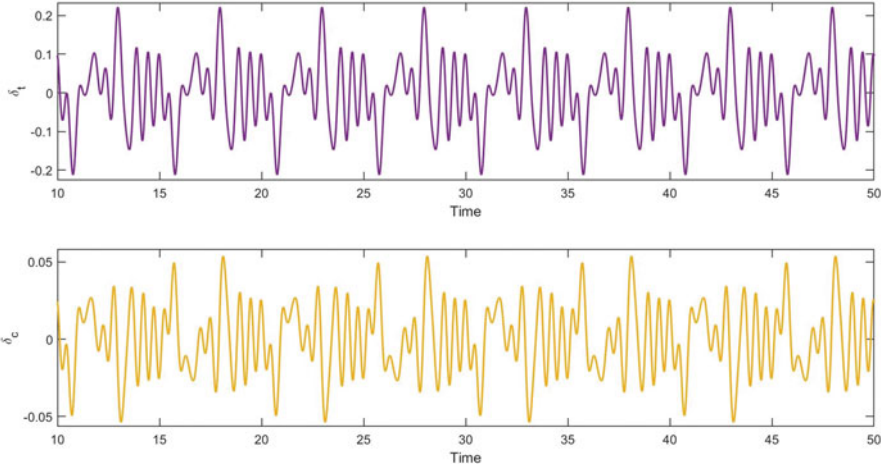


Fig. 10.4 Multisine perturbation

primary benefit of this type of signal is that the orthogonal nature allows simultaneous perturbations of different actuators without correlating responses. These inputs are also effective in generating the steady-state response data needed to estimate frequency responses.

Defining the duration of the excitation T is the first step towards the design of a multisine perturbation. This characterizes the fundamental frequency $1/T$ and by extension the harmonic multiples k/T . Each actuator u_j has a unique subset of multipliers K_j which define the frequency range spanned during excitation. The multisine signal is then generated as a sum of sinusoids as shown in Eq. (10.5).

$$u_j(t) = \sum_{k \in K_j} a_k \sin\left(\frac{2\pi k}{T}t + \phi_k\right) \quad (10.5)$$

The amplitudes a_k are calculated according to the desired power spectra for each input, and the phase angles ϕ_k are optimized to reduce the peak value of the multisine signal to keep the response near the desired flight condition.

An example of the multisine signals generated to perturb the thrust and canard controls is shown in Fig. 10.4. It is possible to observe the multiple overlaid frequencies and the fact that both signals average is zero, which maintains the vehicle states close to the desired set points.

10.3 Results and Discussion

After finding the correct order of magnitude of the tuning parameter λ , it was possible to repeatedly identify the differential equations coded in the FDM with small deviations from the original coefficients. This error can be eliminated by reducing the noise injected through the sensor models under a certain threshold.

To better understand the results obtained from the SID process, the response of the true dynamic system was compared with the simulated response of the discovered model generated from the same control inputs and initial conditions. The graph in Fig. 10.5 displays the simulation results of a model trained with only 5 seconds of dynamic data and a noise-to-signal ratio of 0.01. The vertical dashed line separates the training data (on the left) from the validation data (on the right). Once the training time elapsed, the SID algorithm processes the data and generates a model. The model can then be initialized with the current flight conditions and fed with the same control inputs as the true system.

The goodness of fit of the identified model can then be numerically evaluated with the R-square method.

Even with this short training time, the SID process was capable of generating a model with a minimum of 88% goodness of fit across the four states (u , w , q , θ). It is worth noting that the main deviation of the identified model from the true dynamics in this example is observed on the response of the linear body rate u . The main

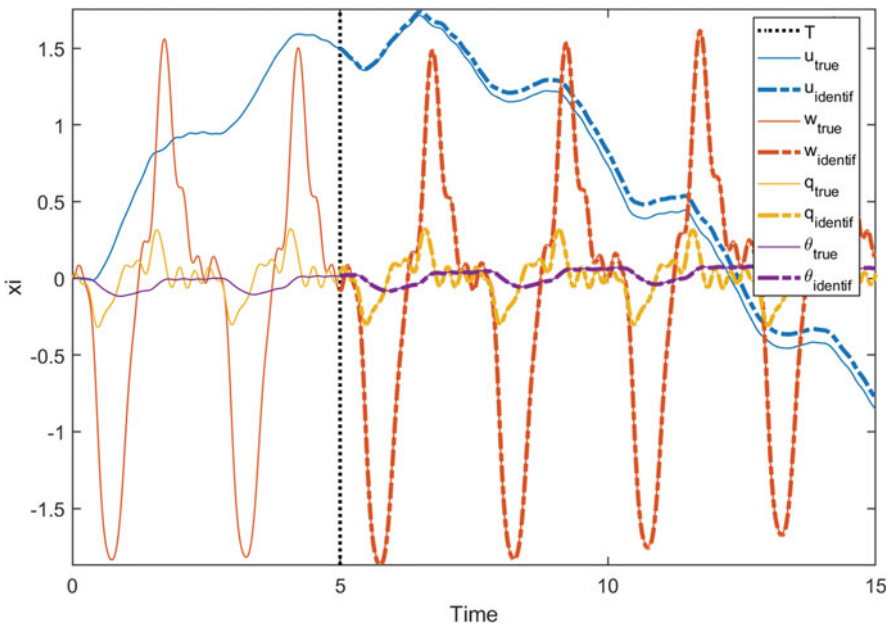


Fig. 10.5 Validation of the identified system

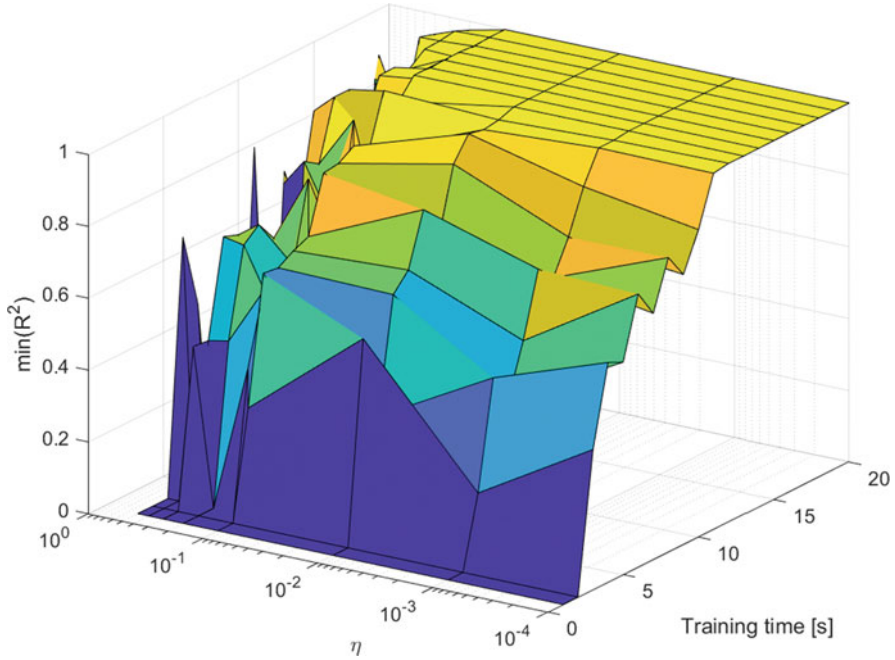


Fig. 10.6 Fitness level in function of noise and training time

contributing factor to this error is the low frequency limit of the perturbation input which is set to be equal or greater than two times the training time T to allow at least two full cycles for each frequency. Increasing the training time T lowers the minimum frequency of the command perturbation allowing improving the identification of the slower dynamics associated with the linear body speed u .

Once the identification problem is set, the main variables that can influence the results are training time T and noise levels. The surface in Fig. 10.6 reports the minimum fitness level of the identified model as a function of the noise level η and training time T . As expected, increasing training time improves the fitness of the identified model. In this study, the vehicles' system dynamics can be correctly identified with training times greater than 9 seconds. On the other hand, increasing the noise-to-signal ratio above 0.5 while holding training time constant significantly reduces the fitness level of the model.

Table 10.1 displays the maximum noise-to-signal ratio, in relation to specific training times, for the SID algorithm to obtain a model with an R-square greater than 80%.

Even with large increases of training data, the maximum tolerable noise to obtain a fitness level of 80% averages around $\eta = 0.64$. This asymptotic trend can be also observed in Fig. 10.7. The yellow-coloured area defines the region in which it is possible to correctly identify the studied system. The curve that outlines this region flattens for $T > 60$ s, therefore for higher levels of noise increasing the training time does not show any substantial improvement in the model fitness.

Table 10.1 Required training time for extreme noise-to-sig-
nal ratios

η	T (s)	R^2 (%)
0.01	5	88
0.22	10	99
0.35	20	98
0.42	30	98
0.53	50	94
0.61	80	86
0.63	120	83
0.63	160	81

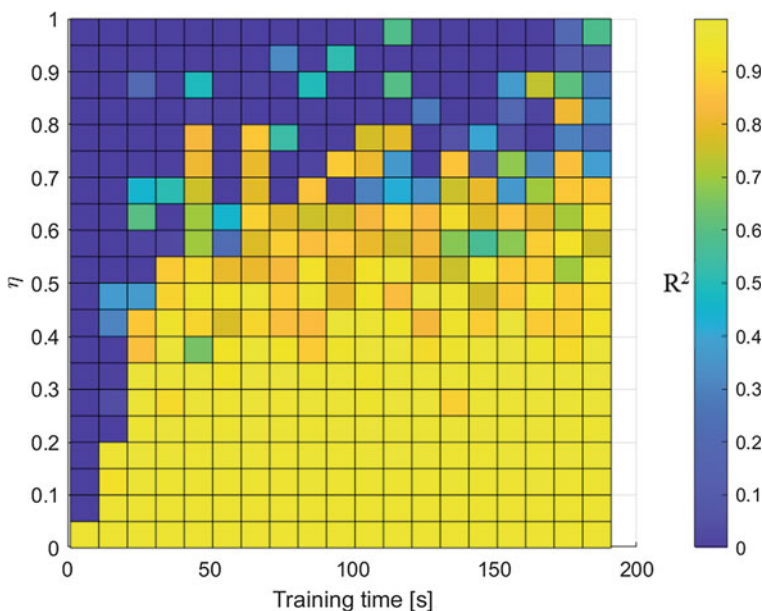


Fig. 10.7 Fitness level distribution for high level of noise and increased training time

It is important to mention that if the training time is increased, the harmonic multipliers K_j should also increase in value to ensure that the higher frequencies are still being excited. Failing to do so results in a degradation of the fitness level.

10.4 Conclusion

The innovation in vehicle configurations and the increase of on-board computational power contribute to the growing interest towards adaptive controllers and data-drive models.

Model identification adaptive controller (MIAC) stands as the preeminent architecture to meet the objectives set in this project, allowing for the exploration of a machine learning technique while maintaining a certain level of verification for the safety of flight.

In this paper, the high-level MIAC structure was presented highlighting the benefits of having a human readable controller. This method heavily relies on the SID process to correctly identify the vehicle dynamics, therefore a significant part of this research focused on the study of an effective technique for online system identification processing. The SINDy method was proven to successfully identify the non-linear dynamics of the flight test vehicle. The results demonstrate the fitness of the identified model in several conditions of noise and training time. Lastly, the analysis of the simulation data established the limit conditions within which the SID process can produce an accurate model.

To conclude, it is worth pointing out the conflicting nature of this type of control theory. The main objective of controller is to suppress perturbations and track the set point in the most actuator-efficient way, while the SID process requires some degree of vehicle perturbation and control actuation in order to generate a dynamic model. The outcomes of this study indicate that it is possible to generate a suitable model from the system identification process described with minimal perturbation. The next steps of this research will be to run the SID process online using real flight data fed from an autopilot in the first instance, and then pair the validated SID algorithm with a model-based controller to close the loop and control the vehicle.

References

- Brunton SL, Kutz JN (2019) Data-driven science and engineering: machine learning. *Dyn Syst Control*. <https://doi.org/10.1017/9781108380690>
- Brunton SL, Proctor JL, Kutz JN, Bialek W (2016a) Discovering governing equations from data by sparse identification of nonlinear dynamical systems. *Proc Natl Acad Sci U S A* 113:3932–3937
- Brunton SL, Proctor JL, Kutz JN (2016b) Sparse identification of nonlinear dynamics with control (SINDy). *IFAC-PapersOnLine* 49:710–715
- Eugene HH, Viken EM, Brandon JM, Croom MA (2020) NASA's learn-to-fly project overview
- Grauer J (2018) Frequency responses estimated with multisine inputs dynamic modeling using output-error parameter estimation based on frequency responses estimated with multisine inputs
- Kaiser E, Kutz JN, Brunton SL (2018) Sparse identification of nonlinear dynamics for model predictive control in the low-data limit. *Proc R Soc A Math Phys Eng Sci*. <https://doi.org/10.1098/rspa.2018.0335>
- Mangan NM, Kutz JN, Brunton SL, Proctor JL (2017) Model selection for dynamical systems via sparse regression and information criteria. *Proc R Soc A Math Phys Eng Sci*. <https://doi.org/10.1098/rspa.2017.0009>
- Morelli EA, Grauer JA (2018) Practical aspects of the frequency domain approach for aircraft system identification. <https://doi.org/10.2514/6.2018-3477>
- Quade M, Abel M, Nathan Kutz J, Brunton SL (2018) Sparse identification of nonlinear dynamics for rapid model recovery. *Chaos* 28:1–10
- Van Wesel P, Goodloe AE (2017) Challenges in the verification of reinforcement learning algorithms NASA STI program . . . in profile. 2017–219628

Chapter 11

Use of Unmanned Aerial Vehicles for Imaging and Remote Sensing



Alpaslan Durmuş and Erol Duymaz

Acronyms

EMS	Electromagnetic spectrum
GNSS	Global navigation satellite system
GPS	Global positioning system
HSI	Hyperspectral imaging
LiDAR	Light detection and ranging
NIR	Near-infrared
RGB	Red green blue
SAR	Synthetic aperture radar
SWIR	Shortwave infrared
UAV	Unmanned aerial vehicle
UV	Ultraviolet
UV–VIS	Visible spectrophotometry
VNIR	Visible and near-Infrared

11.1 Introduction

In recent years, with the rapid development of the economy and society, great changes are constantly occurring in the world. Therefore, it is in great demand to obtain remote sensing data of specific regions and update their geographic information flexibly and quickly. The great flexibility of UAVs can enable new approaches when collecting remote sensing data, for example, integrating real-time mapping and

A. Durmuş (✉) · E. Duymaz
Ostim Technical University, Ankara, Türkiye
e-mail: Alpaslan.durmus@ostimteknik.edu.tr; erol.duymaz@ostimteknik.edu.tr

autonomous navigation. In addition, UAVs are a serious alternative to traditional photogrammetric data capture, especially when targeting mapping applications with high spatial and temporal resolution. UAV-based photogrammetric data acquisition system, control system requires a standard digital camera and a UAV platform. Thus, a UAV-based photogrammetric data acquisition system can be realized at much lower costs compared to digital photogrammetric systems. It is much more appropriate to use UAV systems for photogrammetric data capture, especially in small areas where there is no freedom of movement.

11.2 UAV-Based Imaging Systems

Drone flight control systems consist of a global positioning system (GPS) receiver, an inertial navigation system (INS), and a flight computer that processes data from sensor systems. Flight control cards can perform many functions during flight operations. Operator-controlled and automatic flight can be performed with flight control cards; at the same time, with the autonomous flight modes of the flight control cards, images can be taken on the desired trajectory.

Ground control stations (GCSs) have autopilot software. The software provides an interface that allows the setting of mission parameters such as mission planning, flight altitude, and travel speed based on a map. GCS offers the possibility of adjusting the camera so that images can be taken at preset positions. This is particularly useful for 3D mapping. GCS provides real-time display of flight data such as speed, altitude, and other important system features such as mission safety.

At the same time, the knowledge of experts in image processing and analysis is very important. Commercial geographic information systems (GIS) and remote sensing software are costly. As a result, the interpretation of aerial photography requires technically strong camera technologies, advanced software, and experienced experts.

11.2.1 UAV-Based Imaging Techniques

UAV systems offer more cost-effective alternatives to traditional approaches, as they reduce imaging costs and provide better-quality aerial images. UAV-based remote sensing and image processing are seen as cost-effective alternatives (Wan et al. 2014; Müllerová et al. 2017). Technical developments in UAV systems and reduction in the size of camera systems used as payloads; has expanded the use of UAV systems as remote detection and imaging systems. Traditionally, the acquisition of aerial images by aircraft requires more operating personnel and detailed long-term planning. This situation increases the cost of the process. At the same time, an important feature of the imaging systems in which aircraft are used is that they mostly cover large areas (Bakuła et al. 2019). UAV systems offer much more

economical and fast solutions for monitoring and image acquisition of small- or medium-sized regions (Colomina and Molina 2014). The technical preparation and start-up of a UAV system for imaging can be accomplished in a very short time. High-resolution images are required to detect any object or track its actions over time. With UAV systems, high-resolution image data can be obtained in a short time.

Multi-rotor rotary-wing UAV systems are widely used in imaging systems. In other words, the use of rotary-wing UAV systems for reconnaissance and observation is quite common. It is frequently used successfully as an environmental remote sensing platform in fixed-wing UAV systems or model aircraft (Laliberte et al. 2011; Colomina and Molina 2014). Model airplanes or fixed-wing UAV systems can move at higher speeds as they are aerodynamic systems. At the same time, their useful load-carrying capacity is higher. Fixed-wing systems have more take-off weight with the same thrust and battery pack. In other words, since fixed-wing UAV systems can stay in the air longer, they can take images from wider areas per flight. Fixed-wing UAV systems have simpler aerodynamic and avionic systems. Fixed-wing UAV systems can fly with more affordable maintenance and repair costs.

11.3 Ready-to-Flight Fixed-Wing UAV Systems for Imaging

Today, the importance of UAV-based imaging systems and the diversity of their usage areas are increasing. The use of UAV systems for imaging is increasing rapidly in different fields. UAV-based imaging and monitoring systems are increasingly used in many areas, from their use for security reconnaissance and surveillance to precision agriculture and monitoring of hard-to-reach areas such as pastures (Euchi 2021). In particular, precision agriculture applications are one of the most important application areas of UAV-based imaging systems. Precision farming requires collecting data on air, soil, crop health, and air quality to get more yield from seeds (Reinecke and Prinsloo 2017). The data collected from the field of agriculture provides data for a range of preventive and regulatory practices on the crops to be grown. These agricultural activities can be planting time, irrigation, fertilization, and harvesting. The use of autonomous drones can collect aerial images of a specific area, providing farmers with crucial information about crop health (Yun et al. 2017; Raparelli and Bajocco 2019). The use of unmanned aerial systems (UAS) in precision agriculture applications has increased greatly in recent years. The main reason for this is that UAS can provide farmers with important information regarding crop management. Among the advantages of using UAS is that it can provide low-cost solutions compared to manned aircraft or satellite-based systems. In addition, UAV systems have the advantage of being small and easy to use. In addition, there are ready-to-fly fixed-wing UAV systems developed especially for imaging applications (Finger et al. 2019). These systems offer important advantages to farmers.

The use of customized fixed-wing systems is preferred for imaging with better flight parameters. Companies such as SenseFly, Gatewing, and Trimble offer cost-effective off-the-shelf systems for environmental management. Systems offered by SenseFly, QuestUAV, Gatewing, and Trimble companies also include practical applications. These systems include full autopilot control and camera systems. Fixed UAVs are produced and offered for use by companies such as SenseFly, QuestUAV, and Trimble. This system meets the flight criteria for different conditions. These ready-to-fly fixed-wing UAV systems also offer operators the opportunity to fly more easily. In this context, the different fixed-wing UAV systems optimized for imaging are produced. The most known ready-to-fly fixed-wing UAV system is produced by SenseFly firm. Table 11.1. gives the comparison of SenseFly eBee ready-to-fly fixed-wing UAVs and their imaging systems.

11.3.1 SenseFly eBee

eBee X is the fixed-wing mapping system produced by SenseFly. eBee X can be used easily by operators, and high-resolution images can be obtained with its camera technologies. These systems can be used in different environmental conditions. eBee X can perform operations such as terrain mapping, topographic mapping, city planning, crop mapping, thermal mapping, and environmental monitoring.

11.3.2 SenseFly Camera Technologies

SenseFly S.O.D.A. 3D. It has a 3D 1-inch sensor. Very high-quality images can be obtained for 3D mapping processes. SenseFly S.O.D.A. 3D can work in harmony with Pix4Dmapper software.

SenseFly Aeria X: Aeria X is a compact drone photogrammetry camera with Advanced Photo System tip-C (APS-C) sensor. It provides digital single-lens reflex camera (DSLR) quality images. It provides clear images in all light conditions (“SenseFly Applications” 2022).

SenseFly Duet T: Duet T is a dual-camera thermal mapping system that enables rapid creation of geothermal maps and digital surface models. Duet T includes a high-resolution (640×512 px) thermal infrared camera and SenseFly S.O.D.A with 1-inch sensor red green blue (RGB) camera. The system works in harmony with Pix4Dmapper photogrammetry software (“SenseFly Cameras” 2022).

Table 11.1 Comparison of SenseFly eBee ready-to-fly fixed-wing UAV and imaging systems

	eBee TAC	eBee X	eBee Geo	eBee Ag
Ground sampling distance at 122 m (400 ft)	2.5 cm (1.0 in)/pixel with SenseFly Aeria X	2.5 cm (1.0 in)/pixel with SenseFly Aeria X	2.8 cm (1.1 in)/pixel	2.8 cm (1.1 in)/pixel RGB 11.5 cm (4.5 in)/ pixel multispectral
Absolute horizontal/vertical accuracy	Down to 3 cm (1.2 in)	Down to 3 cm (1.2 in)	Down to 3 cm (1.2 in)	Down to 3 cm (1.2 in)
Absolute horizontal/vertical accuracy	1–5 m (3–16 ft)	1–5 m (3–16 ft)	1–5 m (3–16 ft)	1–5 m (3–16 ft)
Lowest ground sampling distance ¹	1.0 cm (0.4 in)/pixel with SenseFly Aeria X	1.0 cm (0.4 in)/pixel with SenseFly Aeria X	1.1 cm (0.4 in)/pixel	1.1 cm (0.4 in)/pixel
Absolute X, Y, Z accuracy ⁵	1.5 cm (0.6 in)	1.5 cm (0.6 in)	2.5 cm (1 in) RTK only	2.5 cm (1 in) on the SenseFly S.O.D.A. data RTK only
Hardware				
Wingspan	116 cm (45.7 in)	116 cm (45.7 in)	116 cm (45.7 in)	116 cm (45.7 in)
Weight (incl. camera & battery)	1.3–1.6 kg (2.8–3.6 lb) depending on camera and battery	–	1.3 kg (2.2 lb)	1.4–1.6 kg (3–3.5 lb) depending on battery
Electric motor	Low-noise, brushless	Low-noise, brushless	Low-noise, brushless	Low-noise, brushless
Radio link range ³	3 km nominal (up to 8 km)/1.9 mi (up to 5 mi)	3 km nominal (up to 8 km)/1.9 mi (up to 5 mi)	3 km nominal (up to 8 km)/1.9 mi (up to 5 mi)	3 km nominal (up to 8 km) / 1.9 mi (up to 5 mi)
Detachable wings	Yes	Yes	Yes	Yes
Cameras (supplied)	None	None	SenseFly S.O.D.A.	SenseFly Duet M

(continued)

Table 11.1 (continued)

	eBee TAC	eBee X	eBee Geo	eBee Ag
Cameras (optional)	SenseFly S.O.D.A. 3D, SenseFly Aeria X, SenseFly Duet T, SenseFly Duet M, Parrot Sequoia+, SenseFly S.O.D.A., SenseFly Corridor, MicaSense RedEdge MX	SenseFly S.O.D.A. 3D, SenseFly Aeria X, SenseFly Duet T, Parrot Sequoia+, SenseFly S.O.D.A., SenseFly Corridor, MicaSense RedEdge MX	There is no other camera compatible with eBee Geo	There is no other camera compatible with eBee Ag
Global navigation satellite system grade	Survey	Survey	Survey	Survey
Carry backpack dimensions	75 × 50 × 29 cm (30 × 20 × 11 in)	75 × 50 × 29 cm (30 × 20 × 11 in)	75 × 50 × 29 cm (30 × 20 × 11 in)	75 × 50 × 29 cm (30 × 20 × 11 in)
Backpack weight (empty)	4.6 kg (8.8 lb)	4.6 kg (8.8 lb)	4.6 kg (8.8 lb)	4.6 kg (8.8 lb)
Carry case dimensions (optional)	75 × 48 × 33 cm (30 × 19 × 13 in)	75 × 48 × 33 cm (30 × 19 × 13 in)	75 × 48 × 33 cm (30 × 19 × 13 in)	75 × 48 × 33 cm (30 × 19 × 13 in)
Weight (incl. camera & battery)	–	1.3–1.6 kg (2.2–3.6 lb) depending on camera and battery		
Software				
Flight planning & control software (supplied)	eMotion	–	eMotion	eMotion
Automatic 3D flight planning	Incl. in eMotion 3	Incl. in eMotion 3	Incl. in eMotion 3	Incl. in eMotion 3
3D environment	Yes	Yes	Yes	Yes
Photogrammetry software (optional)	Pix4Dmapper/Pix4DCloud/Pix4Dmatic/Pix4Dfields, Agisoft PhotoScan, Esri Drone2Map, DroneDeploy, Trimble Business Center, Autodesk® ReCap™, Bentley ContextCapture	Pix4Dmapper/Pix4DCloud/Pix4Dmatic/Pix4Dfields, Agisoft PhotoScan, Esri Drone2Map, DroneDeploy, Trimble Business Center, Autodesk® ReCap™, Bentley ContextCapture	Pix4Dmapper/Pix4DCloud/Pix4Dmatic/Pix4Dfields, Agisoft PhotoScan, Esri Drone2Map, DroneDeploy, Trimble Business Center, Autodesk® ReCap™, Bentley ContextCapture	Pix4Dmapper/Pix4Dfields, Agisoft PhotoScan, DroneDeploy

	Yes	Yes	No	Yes
Vegetation index calculation (w/optional photogrammetry software)				Yes
Geographic Information System	AutoCAD, ArcGIS, Trimble Business Center, Leica Geo Office, VAGNET Office Tools, ArcGIS, MicroStation, & more	AutoCAD, ArcGIS, Trimble Business Center, Leica Geo Office, VAGNET Office Tools, ArcGIS, MicroStation, & more	AutoCAD, ArcGIS, Trimble Business Center, Leica Geo Office, VAGNET Office Tools, ArcGIS, MicroStation, & more	–
Flight planning & control software (supplied)	–	eMotion	–	–
Operations				
Cruise speed	40–110 km/h (11–30 m/s or 25–68 mph)	40–110 km/h (11–30 m/s or 25–68 mph)	40–110 km/h (11–30 m/s or 25–68 mph)	40–110 km/h (11–30 m/s or 25–68 mph)
Wind resistance	Up to 46 km/h (12.8 m/s or 28.6 mph)	Up to 46 km/h (12.8 m/s or 28.6 mph)	Up to 46 km/h (12.8 m/s or 28.6 mph)	Up to 46 km/h (12.8 m/s or 28.6 mph)
Maximum flight time	Up to 90 minutes depending on camera and battery	Up to 90 minutes depending on camera and battery	Limited to 45 minutes	45 to 55 minutes depending on battery
Endurance extension available (fly more than 60 minutes)	Yes	Yes	No	No
Nominal coverage at 120 m (400 ft) ²	220 ha (~550 ac), with SenseFly S.O.D.A./no endurance extension	220 ha (~550 ac), with SenseFly S.O.D.A./no Endurance Extension	160 ha (~395 ac)	160 ha (~395 ac) with standard battery
Maximum coverage at 120 m (single flight)	500 ha (~1250 ac), with SenseFly S.O.D.A. 3D/endurance extension	500 ha (~1250 ac), with SenseFly S.O.D.A. 3D/endurance extension	–	200 ha (~494 ac) with endurance battery
Max. flight range ⁴	Standard: 37 km (~23 mi) endurance: 55 km (~34 mi)	Standard: 37 km (~23 mi) endurance: 55 km (~34 mi)	30 km (~19 mi)	Standard: 30 km (~19 mi) endurance: 36 km (~22 mi)

(continued)

Table 11.1 (continued)

	eBee TAC	eBee X	eBee Geo	eBee Ag
Post-processed kinematic	Yes	Yes	No	No
Real-time kinematic/virtual base station	Yes	Yes	Yes	Yes
Real-time kinematic/base station unknown point	Yes	Yes	Yes	Yes
Real-time kinematic/base station known point	Yes	Yes	Yes	Yes
Ground control points	Not required	Not required	Not required	Not required
Oblique imagery	Yes with SenseFly S.O.D.A. 3D	Yes with SenseFly S.O.D.A. 3D	No	No
Hand launch	Yes	Yes	Yes	Yes
Landing	Automatic linear landing (5 m/16.4 ft accuracy in 20° angle cone)	Automatic linear landing (5 m/16.4 ft accuracy in 20° angle cone)	Automatic linear landing (5 m/16.4 ft accuracy in 20° angle cone)	Automatic linear landing (5 m/16.4 ft accuracy in 20° angle cone)

11.4 UAV Imaging Systems and Example Applications

Owing to technological development, the use of smartphones and tablets instead of the control unit, availability of GPS, Wi-Fi receivers as well as visible band, multispectral, thermal, hyperspectral, and laser sensors in flight operation at low costs have reduced the production costs of UAVs. Through the minimized hardware solutions in GNSS technology, the positioning of the navigation performed with post-processed kinematic (PPK) GNSS can be done more accurately (Colomina and Molina 2014). The top five sectors in which UAV finds the most common application on a global scale are real estate and construction, photogrammetry (aerial surveying), film/aerial photography, agriculture, and aerial monitoring (tracking). UAV photogrammetry is used in agriculture, mining, aerial photography, and real estate sectors.

Various sensors and cameras are used for aerial and space image acquisition systems. This section focuses on remote sensing tools that may be suitable for micro, mini, and tactical UAV payloads, especially distinguishing between visible band, near-infrared, multispectral, hyperspectral, thermal, laser scanners, and synthetic aperture radar.

11.4.1 *Visible-Band, Near-Infrared, and Multispectral Cameras*

Hyperspectral image detection in remote sensing systems is the measurement of the energy reflected from object (organic/inorganic) surfaces in narrow and contiguous wavelength bands, and the recording and processing of data come from the electromagnetic spectrum. Today, this technology is developing, and its usage areas are becoming widespread; it is used in many fields such as agriculture, military, mining, physics, astronomy, environment, and eye care (De Baerdemaeker et al. 2001). Multispectral images obtained from satellites are frequently used to detect many problems observed in agriculture (Orhan and Yakar 2016; Orhan et al. 2014; Orhan et al. 2019; Kuşak and Küçükali 2019; Çömert et al. 2019).

Today, it is frequently used to obtain multispectral images from UAV systems. UAV systems are suitable for fast data collection and low-cost mapping in small areas (Ahmad et al. 2013). UAV-based spectral imaging offers significant advantages in high-resolution remote sensing applications. However, the number of cameras that can be placed on UAV systems is very limited. The human eye perceives the range 0.4–0.7 μm (400–700 nm) as color. In hyperspectral imaging, this range is usually designed as 0.4–2.5 μm (400–2500 nm). This broad bandgap, which includes the visible, near-infrared, and mid-infrared ranges, is critical for object identification (discrimination). Thus, hyperspectral imaging provides data in spectral bands and wavelengths that the human eye cannot detect, just like other remote sensing techniques (satellite images, multispectral images), providing important information to researchers and growers on different stages of plant cultivation,

plant needs, and yield estimations (Hashimoto 1989). Obtaining the optimal combination of multispectral images is a difficult process (Ishida et al. 2018). Determining the vegetation cover or detecting the problems in the plants is closely related to the resolution of the multispectral camera images obtained. The type of camera used in UAV systems, the flight altitude, and the date the images were acquired greatly affect the resolution of multispectral camera images (Peña et al. 2015). The use of UAVs equipped with thermal, laser, or spectral cameras for modeling, mapping, and monitoring applications in pastures, forests, and agricultural environments shows great advances (Salamí et al. 2014). Agricultural sensor systems used in UAV systems are generally passive systems and use the rays reflected from the sun. The most distinctive feature of hyperspectral receivers is that they have much more bands, unlike multispectral images. However, what makes the sensor of cameras hyperspectral is not so much the number of bands as how narrow and how adjacent the bands are. Also, hyperspectral image detection is the ability to resolve the several hundred spectral bands stated in the region from visible light band to short-wave infrared band.

The visible and near-infrared (VNIR) portion of the electromagnetic spectrum has wavelengths between approximately 400 and 1100 nm (Moseley and Zabierek 2006). VNIR multispectral image cameras have wide applications in remote sensing and imaging spectroscopy (Ben-Dor et al. 1997).

11.4.2 Hyperspectral Cameras

Hyperspectral imaging is used in many fields such as defense, chemical analysis, agriculture, and medical field. With hyperspectral imaging, image data of many narrow wavelengths are obtained from infrared and visible regions, and as a result, separation according to wavelength is provided. The signature created by the luminance values of any pixel selected on the hyperspectral image according to the wavelengths shows a material-specific behavior.

Light and electromagnetic radiation in other forms are generally defined in terms of wavelength. For example, the wavelength of visible light ranges from 400 nm (violet) to 700 nm (red). The amount of light falling on the material and reflecting back from it is proportional to the reflectance coefficient of the material and is generally expressed in percentages. The reflectance spectrum, on the other hand, refers to the reflectance measured at a certain wavelength (or wavelength range) of the substance. Some substances reflect light of certain wavelengths, while others absorb light of the same wavelength. Reflection and absorption patterns in the measured wavelength range are a kind of signature of substances and are used in the detection and classification of substances. For example, terrestrial spectral measurements from high altitudes are widely used to detect aboveground and underground natural resources (Vane and Goetz 1988).

But multispectral remote sensing produces discrete bands and generally has a lower spectral resolution. Therefore, hyperspectral camera sensors provide more detailed data than multispectral sensors, as they acquire the entire spectrum in each

pixel. Unlike visible-spectrum camera developments that reach hundreds of grams of weight and tens of megapixel resolution, the miniaturization process of multispectral and hyperspectral cameras is demanding in terms of optics and sensor calibration.

C-Astral launched a combination of two commercial products in the first quarter of 2013. These two products are in the configuration of fixed-wing UAS Bramor and Rikola Ltd. are small and lightweight hyperspectral cameras developed by (Colomina and Molina 2014).

In industrial applications, hyperspectral camera systems integrated into UAV systems are used in many different areas. These are given below:

- Mining
- Defense and security
- Plant classification
- Precision agriculture and forestry
- Phenotype studies
- Environmental audit
- Water quality and analysis
- Defense and security
- Corrosion and paint analysis

11.4.3 Thermal Imaging

Thermography is used for the process of using sensors to create images of radiation in the infrared (IR) portion of the electromagnetic spectrum (EMS). Radiation is emitted by all objects and objects around us. Radiation includes visible light (which occupies a small portion of EMS) and invisible light wavelengths. The rays in the infrared wavelength are not visible to the human eye but can be felt as radiated heat when their intensity increases. Thermal sensors capture infrared images and enable people to see light beams at wavelengths that they cannot see. After converting the invisible heat radiation emitted or reflected by all objects into an image, regardless of the lighting conditions, it is possible to distinguish between temperatures by assigning them a different color.

A drone equipped with a thermal camera is used in everything from finding missing people to helping firefighters put out a fire. UAV technologies offer low-cost solutions with thermal camera systems in different applications, especially in public safety, industry, and agriculture.

In recent years, there has been noticeable progress in thermal imaging systems miniaturization. For remote reconnaissance, low-weight and small-size thermal camera systems were used in military applications (Kostrzewa et al. 2003). In addition to military applications, these systems are becoming more common in applications such as forest fire monitoring (Rufino and Moccia 2005; Scholtz et al. 2011).

UAV systems equipped with thermal camera systems are becoming more and more common today. DJI is one of the leading companies. DJI has launched the H20T thermal camera systems specially designed for M300 RTK UAV systems.

11.4.4 Laser Scanners

Light detection and ranging (LiDAR) is basically defined as a remote sensing method that uses a laser or light beam for measurement. In the map industry, LiDAR systems are used to measure complex objects or regions. The LiDAR method is also frequently used in the construction industry. LiDAR technology is used in autonomous vehicles. Thus, instantaneous data generation and analysis are made, and vehicles are enabled to move.

Precision is required when photogrammetry and LiDAR (laser scanning) are used together. The expectation of users from LiDAR scanning is to reach precise measurement results. Examples of the use of LiDAR systems are given below. It gives users the option to gain some precision, but it is also difficult to get high resolution (dot density) from airborne LiDAR data.

Laser scanners along with camera systems are widely used in conventional photogrammetry. However, studies have shown that any change in forest structure such as biomass loss due to disease or pruning can be noticed with the help of the data obtained from LiDAR systems (Wallace et al. 2012).

11.4.5 Synthetic Aperture Radar

High-resolution imaging of large areas is required in military systems, environmental monitoring, and mapping of soil resources. In some cases, it may be necessary to take high-resolution images at night or in harsh weather conditions. Synthetic aperture radar (SAR) systems offer operators the opportunity to take high-resolution images in harsh weather conditions. SAR systems take advantage of the long-range propagation characteristics of radar signals to obtain high-resolution images. SAR is complementary to photographic and other optical imaging techniques (“What is sar” 2022). With the SAR system, any terrain can be viewed at any time of the day, in any meteorological condition. SAR technology can provide structured information about the terrain for mineral exploration. Mining is among the important uses of SAR technology. In addition, detecting oil spills on the sea surface, providing information about the sea situation for ships, creating glacier maps, and obtaining information about reconnaissance and target for military intelligence operations are some of the important uses of SAR technology. Progress has been made in the use of synthetic aperture radar (SAR) technology in remote sensing systems. However, continuing problems are observed in the adaptation of UAV systems.

11.5 Results

Remote sensing is a well-known technique for agriculture and environmental analysis. Vegetation or biodiversity control has traditionally been accomplished using aerial and/or satellite imagery, which incurs high costs when precision resolution is required. The UAV is a smaller, cheaper-to-use, and successful system in the remote sensing community. The range of available sensors is expanding in a natural attempt to adapt to smaller platforms where weight and size restrictions apply as opposed to manned aerial platforms, as well as to adapt to user-application needs.

Aerial observation by unmanned platforms has mainly been supported in a military context. Indeed, a small, particularly handheld or hand-launched UAS can provide an army's ground troops with an "overhead" view to avoid potential unseen hazards. In larger UAS categories, large drones provide wide-area surveillance, i.e., border control and restricted area surveillance. UAS has also been used as communication relays to increase battlefield awareness or as decoys to fool the enemy's radars. Near-military, search and rescue, or disaster management missions share many objectives with those previously mentioned (basically providing quick snapshots from an area where no supporting structures can be assumed) and thus can be somewhat classified as intelligence, surveillance, and reconnaissance (ISR) missions.

References

- Ahmad A, Tahar KN, Udin WS, Hashim KA, Darwin N, Hafis M, Azmi SM (2013, Nov) Digital aerial imagery of unmanned aerial vehicle for various applications. In: 2013 IEEE international conference on control system, computing and engineering. IEEE, pp 535–540
- Bakuła K, Ostrowski W, Pilarska M, Szender M, Kurczyński Z (2019) Evaluation and calibration of fixed-wing multisensor UAV mobile mapping system: improved results. *Int Arch Photogramm Rem Sens Spat Inf Sci* 42:189–195
- Ben-Dor E, Inbar Y, Chen Y (1997) The reflectance spectra of organic matter in the visible near-infrared and short wave infrared region (400–2500 nm) during a controlled decomposition process. *Remote Sens Environ* 61(1):1–15
- Colomina I, Molina P (2014) Unmanned aerial systems for photogrammetry and remote sensing: a review. *ISPRS J Photogramm Remote Sens* 92:79–97. <https://doi.org/10.1016/j.isprsjprs.2014.02.013>
- Çömert R, Matci DK, Avdan U (2019) Object based burned area mapping with random forest algorithm. *Int J Eng Geosci* 4(2):78–87. <https://doi.org/10.26833/ijeg.455595>
- De Baerdemaeker J, Munack A, Ramon H, Speckmann H (2001) Mechatronic systems, communication, and control in precision agriculture. *IEEE Control Syst Mag* 21(5):48–70
- Euchi J (2021) Do drones have a realistic place in a pandemic fight for delivering medical supplies in healthcare systems problems? *Chin J Aeronaut* 34(2):182–190
- Finger R, Swinton SM, El Benni N, Walter A (2019) Precision farming at the nexus of agricultural production and the environment. *Ann Rev Resour Econ* 11:313–335
- Hashimoto Y (1989) Recent strategies of optimal growth regulation by the speaking plant concept. In: International symposium on growth and yield control in vegetable production 260, pp 115–122

- Ishida T, Kurihara J, Viray FA, Namuco SB, Paringit EC, Perez GJ et al (2018) A novel approach for vegetation classification using UAV-based hyperspectral imaging. *Comput Electron Agric* 144:80–85
- Kostrzewa J, Meyer WH, Laband S, Terre WA, Petrovich P, Swanson K et al (2003, Sept) Infrared microsensor payload for miniature unmanned aerial vehicles. In: *Unattended ground sensor technologies and applications V*, vol 5090. International Society for Optics and Photonics, pp 265–274
- Kuşak L, Küçükali UF (2019) Outlier detection of land surface temperature: Küçükçekmece region. *Int J Eng Geosci* 4(1):1–7. <https://doi.org/10.26833/ijeg.404426>
- Laliberte AS, Winters C, Rango A (2011) UAS remote sensing missions for rangeland applications. *Geocarto Int* 26(2):141–156. <https://doi.org/10.1080/10106049.2010.534557>
- Moseley T, Zabierek G (2006) *Guidance on the safe use of lasers in education and research*. University of Sheffield and Gus Zabierek, University of Birmingham, sn
- Müllerová J, Bartaloš T, Brůna J, Dvořák P, Vítková M (2017) Unmanned aircraft in nature conservation: an example from plant invasions. *Int J Remote Sens* 38(8–10):2177–2198. <https://doi.org/10.1080/01431161.2016.1264030>
- Orhan O, Yakar M (2016) Investigating land surface temperature changes using Landsat data in Konya, Turkey. *Int Arch Photogramm Rem Sens Spat Inf Sci* 41:B8
- Orhan O, Ekercin S, Dadaser-Celik F (2014) Use of landsat land surface temperature and vegetation indices for monitoring drought in the Salt Lake Basin Area, Turkey. *Sci World J* 2014:142939
- Orhan O, Dadaser-Celik F, Ekercin S (2019) Investigating land surface temperature changes using Landsat-5 data and real-time infrared thermometer measurements at Konya closed basin in Turkey. *Int J Eng Geosci* 4(1):16–27. <https://doi.org/10.26833/ijeg.417151>
- Peña JM, Torres-Sánchez J, Serrano-Pérez A, De Castro AI, López-Granados F (2015) Quantifying efficacy and limits of unmanned aerial vehicle (UAV) technology for weed seedling detection as affected by sensor resolution. *Sensors* 15(3):5609–5626
- Raparelli E, Bajocco S (2019) A bibliometric analysis on the use of unmanned aerial vehicles in agricultural and forestry studies. *Int J Remote Sens* 40(24):9070–9083
- Reinecke M, Prinsloo T (2017) The influence of drone monitoring on crop health and harvest size. In: *2017 1st international conference on next generation computing applications (NextComp)*. IEEE, pp 5–10
- Rufino G, Moccia A (2005) Integrated VIS-NIR hyperspectral/thermal-IR electro-optical payload system for a mini-UAV. In: *Infotech@ Aerospace*, p 7009
- Salamí E, Barrado C, Pastor E (2014) UAV flight experiments applied to the remote sensing of vegetated areas. *Remote Sens* 6(11):11051–11081
- Scholtz A, Kaschwich C, Krüger A, Kufieta K, Schnetter P, Wilkens CS et al (2011) Development of a new multi-purpose UAS for scientific application. *Int Arch Photogramm Rem Sens Spat Inf Sci* 38(1/C22)
- SenseFly Applications. (2022, 10 Feb) <https://www.sensefly.com/industry/surveying-drones-mapping-industry>
- SenseFly Cameras. (2022, 15 Feb) <https://www.sensefly.com/industry/surveying-drones-mapping-industry>
- Vane G, Goetz AF (1988) Terrestrial imaging spectroscopy. *Remote Sens Environ* 24(1):1–29
- Wallace LO, Lucieer A, Watson CS (2012) Assessing the feasibility of UAV-based LiDAR for high resolution forest change detection. In: *The 12th congress of the International Society for Photogrammetry and Remote Sensing*, vol 39, pp 499–504
- Wan H, Wang Q, Jiang D, Fu J, Yang Y, Liu X (2014) Monitoring the invasion of *Spartina alterniflora* using very high resolution unmanned aerial vehicle imagery in Beihai, Guangxi (China). *Sci World J* 2014. <https://doi.org/10.1155/2014/638296>
- What is sar (2022, 12 Jan) <https://www.sandia.gov/radar/pathfinder-radar-isr-and-synthetic-aperture-radar-sar-systems/what-is-sar/>
- Yun G, Mazur M, Pederii Y (2017) Role of unmanned aerial vehicles in precision farming. *Proc Natl Aviat Univ* 1:106–112

Index

A

Adaptive control, 168–177
Aerodynamics, 2, 27, 32–51, 75, 104, 112–130, 154, 168, 181
Airfoils, 34–35, 47, 116–122, 130
All-electric aircraft, 97, 98, 102
Automated external defibrillator (AED), 70, 83, 84, 88
Autonomous UAVs, 99

C

Cardiac arrests, 83
Civilian drones, 1–12, 72
Computational fluid dynamic (CFD), 41–46, 114, 127–130, 168, 171

D

Decision-making, 15, 21, 22, 54, 82, 157
Deep stall landing, 34, 41, 51
Defibrillation, 83
Design and sizing for UAV landing gear, 164
Drones, 1–12, 18, 69–88, 135, 153
Drone services, 5
Drone transportation, 71, 74, 80, 81, 83
Drone trends, 1–12

E

Environmental monitoring, 32–52, 182, 190

F

Feedback linearization, 135–151

H

Healthcare, 8, 70, 75, 80, 82, 85, 88
Hybrid-UAV landing gears, 153–164
Hyperspectral cameras thermal cameras, 25, 69, 78, 189

L

Laser scanners, 69, 187, 190
Low-altitude UAV, 54

M

Morphing surfaces, 119
Morphing wings, 11, 12, 112, 116, 130
Multiple UAV, 53–67
Multi rotor UAV, 58
Multispectral cameras, 187–188

N

Near Infrared Cameras, 187
Noise, 2, 7, 9, 11, 96, 99, 104, 106, 135–151, 171, 174–177

Q

Quadrotor UAV, 85, 135–151

R

Remote data collection, 188

S

Shape optimization, 112–130

Simulation, 12, 40, 43, 47, 51, 54, 57–60,
62–66, 83, 99, 127–131, 147, 168, 170,
172, 174, 177

Solar powered UAV, 32–51

Synthetic Aperture Radar Systems, 187, 190

Systems engineering, 15–29

T

Tip vortex structure, 128–130

Trajectory coordination, 53–67

U

UAV-based imaging, 180–181

UAV classification, 25

UAV landing gear configurations, 161, 163

Unmanned aerial system (UAS), 4, 5, 15–29,
70, 87, 97, 168–177, 181, 189, 191

Unmanned aerial vehicle (UAV), 2, 17, 32, 53,
97, 112, 135, 153

Urban air mobility (UAM), 5, 9, 53, 96–106